

Advances in natural product chemistry: Yunnan university 100th anniversary

Edited by

Wen Chen, Jian-Wei Dong, Ana Figueiras and Siva S. Panda

Published in

Frontiers in Chemistry



FRONTIERS EBOOK COPYRIGHT STATEMENT

The copyright in the text of individual articles in this ebook is the property of their respective authors or their respective institutions or funders. The copyright in graphics and images within each article may be subject to copyright of other parties. In both cases this is subject to a license granted to Frontiers.

The compilation of articles constituting this ebook is the property of Frontiers.

Each article within this ebook, and the ebook itself, are published under the most recent version of the Creative Commons CC-BY licence. The version current at the date of publication of this ebook is CC-BY 4.0. If the CC-BY licence is updated, the licence granted by Frontiers is automatically updated to the new version.

When exercising any right under the CC-BY licence, Frontiers must be attributed as the original publisher of the article or ebook, as applicable.

Authors have the responsibility of ensuring that any graphics or other materials which are the property of others may be included in the CC-BY licence, but this should be checked before relying on the CC-BY licence to reproduce those materials. Any copyright notices relating to those materials must be complied with.

Copyright and source acknowledgement notices may not be removed and must be displayed in any copy, derivative work or partial copy which includes the elements in question.

All copyright, and all rights therein, are protected by national and international copyright laws. The above represents a summary only. For further information please read Frontiers' Conditions for Website Use and Copyright Statement, and the applicable CC-BY licence.

ISSN 1664-8714
ISBN 978-2-8325-2831-0
DOI 10.3389/978-2-8325-2831-0

About Frontiers

Frontiers is more than just an open access publisher of scholarly articles: it is a pioneering approach to the world of academia, radically improving the way scholarly research is managed. The grand vision of Frontiers is a world where all people have an equal opportunity to seek, share and generate knowledge. Frontiers provides immediate and permanent online open access to all its publications, but this alone is not enough to realize our grand goals.

Frontiers journal series

The Frontiers journal series is a multi-tier and interdisciplinary set of open-access, online journals, promising a paradigm shift from the current review, selection and dissemination processes in academic publishing. All Frontiers journals are driven by researchers for researchers; therefore, they constitute a service to the scholarly community. At the same time, the *Frontiers journal series* operates on a revolutionary invention, the tiered publishing system, initially addressing specific communities of scholars, and gradually climbing up to broader public understanding, thus serving the interests of the lay society, too.

Dedication to quality

Each Frontiers article is a landmark of the highest quality, thanks to genuinely collaborative interactions between authors and review editors, who include some of the world's best academicians. Research must be certified by peers before entering a stream of knowledge that may eventually reach the public - and shape society; therefore, Frontiers only applies the most rigorous and unbiased reviews. Frontiers revolutionizes research publishing by freely delivering the most outstanding research, evaluated with no bias from both the academic and social point of view. By applying the most advanced information technologies, Frontiers is catapulting scholarly publishing into a new generation.

What are Frontiers Research Topics?

Frontiers Research Topics are very popular trademarks of the *Frontiers journals series*: they are collections of at least ten articles, all centered on a particular subject. With their unique mix of varied contributions from Original Research to Review Articles, Frontiers Research Topics unify the most influential researchers, the latest key findings and historical advances in a hot research area.

Find out more on how to host your own Frontiers Research Topic or contribute to one as an author by contacting the Frontiers editorial office: frontiersin.org/about/contact

Advances in natural product chemistry: Yunnan university 100th anniversary

Topic editors

Wen Chen — Yunnan University, China

Jian-Wei Dong — Qujing Normal University, China

Ana Figueiras — University of Coimbra, Portugal

Siva S. Panda — Augusta University, United States

Citation

Chen, W., Dong, J.-W., Figueiras, A., Panda, S. S., eds. (2023). *Advances in natural product chemistry: Yunnan university 100th anniversary*. Lausanne: Frontiers Media SA. doi: 10.3389/978-2-8325-2831-0

Table of contents

- 05 Editorial: Advances in natural product chemistry: Yunnan University 100th anniversary
Wen Chen, Jianwei Dong and Siva S. Panda
- 07 Sesquiterpene lactones from *Artemisia vulgaris* L. as potential NO inhibitors in LPS-induced RAW264.7 macrophage cells
Xiang-Yu Chen, Tao Liu, Yu-Ze Hu, Tian-Tian Qiao, Xiu-Juan Wu, Ping-Hua Sun, Chui-Wen Qian, Zhe Ren, Jun-Xia Zheng and Yi-Fei Wang
- 23 Grandifolines A–F, new anti-inflammatory diterpenoid alkaloids isolated from *Delphinium grandiflorum*
Yuanfeng Yan, Hongjun Jiang, Xiaoyan Yang, Zongbao Ding and Tianpeng Yin
- 33 Transition-metal-free approach to quinolines via direct oxidative cyclocondensation reaction of *N,N*-dimethyl enaminones with *o*-aminobenzyl alcohols
Kairui Rao, Zhangmengjie Chai, Pan Zhou, Donghan Liu, Yulin Sun and Fuchao Yu
- 41 Antioxidant and anti-inflammatory activity of constituents isolated from *Dendrobium nobile* (Lindl.)
Hui Lei, Shunmei Zou, Jiafu Lin, Longfei Zhai, Yifeng Zhang, Xiujuan Fu, Siwei Chen, Hong Niu, Feifei Liu, Chunlian Wu and Dan Zhang
- 53 Underexplored bacteria as reservoirs of novel antimicrobial lipopeptides
Tanya Clements-Decker, Megan Kode, Sehaam Khan and Wesaal Khan
- 74 Identification of 6 ω -cyclohexyl-2-(phenylamino carbonylmethylthio)pyrimidin-4(3*H*)-ones targeting the ZIKV NS5 RNA dependent RNA polymerase
Guang-Feng Zhou, Cong-Qiang Xie, Jian-Xia Xue, Jing-Bo Wang, Yu-Zhuo Yang, Chang-Bo Zheng, Rong-Hua Luo, Ren-Hua Yang, Wen Chen, Liu-Meng Yang, Yue-Ping Wang, Hong-Bin Zhang, Yan-Ping He and Yong-Tang Zheng
- 91 Recent applications of dioxinone derivatives for macrocyclic natural product and terpenoid synthesis
Kai Wei, Xinhua Zheng and Hongbin Zhang
- 106 Aryl acrylonitriles synthesis enabled by palladium-catalyzed α -alkenylation of arylacetonitriles with vinyl halides/triflates
Yonggang Jiang, Bijun Wang, Dongxiang Liu, Dazhen Xia, Zhengfen Liu, Liang Li, Guogang Deng and Xiaodong Yang

- 116 **Total synthesis of justicidin B, justicidin E, and taiwanin C: A general and flexible approach toward the synthesis of natural aryl-naphthalene lactone lignans**
Kai Wei, Yucui Sun, Yiren Xu, Wen Hu, Ying Ma, Yi Lu, Wen Chen and Hongbin Zhang
- 125 **Synthesis and anticancer activity of podophyllotoxin derivatives with nitrogen-containing heterocycles**
Meng Yin, Yongsheng Fang, Xiaotong Sun, Minggao Xue, Caimei Zhang, Zhiyun Zhu, Yamiao Meng, Lingmei Kong, Yi Yi Myint, Yan Li, Jingfeng Zhao and Xiaodong Yang



OPEN ACCESS

EDITED AND REVIEWED BY
Michael Kassiou,
The University of Sydney, Australia

*CORRESPONDENCE

Wen Chen,
✉ wenchen@ynu.edu.cn
Jianwei Dong,
✉ jwdongyn@mail.qjnu.edu.cn
Siva S. Panda,
✉ sspanda12@gmail.com

RECEIVED 03 June 2023

ACCEPTED 09 June 2023

PUBLISHED 13 June 2023

CITATION

Chen W, Dong J and Panda SS (2023),
Editorial: Advances in natural product
chemistry: Yunnan University
100th anniversary.
Front. Chem. 11:1234211.
doi: 10.3389/fchem.2023.1234211

COPYRIGHT

© 2023 Chen, Dong and Panda. This is an
open-access article distributed under the
terms of the [Creative Commons
Attribution License \(CC BY\)](#). The use,
distribution or reproduction in other
forums is permitted, provided the original
author(s) and the copyright owner(s) are
credited and that the original publication
in this journal is cited, in accordance with
accepted academic practice. No use,
distribution or reproduction is permitted
which does not comply with these terms.

Editorial: Advances in natural product chemistry: Yunnan University 100th anniversary

Wen Chen^{1*}, Jianwei Dong^{2*} and Siva S. Panda^{3*}

¹Key Laboratory of Medicinal Chemistry for Natural Resource, Ministry of Education, Yunnan Provincial Center for Research and Development of Natural Products, Yunnan Characteristic Plant Extraction Laboratory, School of Pharmacy, Yunnan University, Kunming, China, ²College of Chemistry and Environmental Science, Qujing Normal University, Qujing, China, ³Department of Chemistry and Physics, Augusta University, Augusta, GA, United States

KEYWORDS

natural products, isolation and structural characterization, synthetic method, total synthesis, medicinal chemistry

Editorial on the Research Topic

Advances in natural product chemistry: Yunnan University 100th anniversary

Natural products have played important roles in drug discovery and development as more than 60% drugs are associated with natural products (Newman and Cragg, 2020). Yunnan University (YNU) located in Yunnan Province, China, the kingdom of plants, was founded in 1922 and officially opened in 1923. With this unique regional advantage, many interesting achievements in natural products have been made at YNU. To celebrate the 100th anniversary of YNU, this Research Topic aims to collect the latest developments in Natural Product Chemistry from school fellows of YNU, as well as the researchers who work or are involved in the development of YNU.

This Research Topic presents a Research Topic of reviews and original research articles on isolation and structural characterization of novel natural products (Chen et al., Lei et al., Yan et al., and Clements-Decker et al.), new synthetic approaches towards the key units of natural products (Rao et al. and Jiang et al.), total synthesis of natural products (Wei et al. and Wei et al.), and structure-activity-relationship (SAR) studies on bioactive natural-product-like molecules (Zhou et al., and Yin et al.). Taken overall, 10 contributions including 2 reviews and 8 original research articles comprise this Research Topic.

Chen et al. reported twelve new guaianolide sesquiterpene lactones, along with ten known analogs were isolated from an EtOH extract of the dried aerial parts of *Artemisia vulgaris* L. The isolated sesquiterpenoids dose-dependently exhibited an NO production inhibitory activity, which is better than that of the positive control (dexamethasone). A study on antioxidant and anti-inflammatory activity of constituents isolated from *Dendrobium nobile* (Lindl.) by Lei et al. shows that nineteen compounds, including two new vitamin E homologues, one new sesquiterpene, and two new dendrobines were isolated. New compound aldehyde- α -tocopherol demonstrated significant antioxidant activity compared with ascorbic acid (VC), as well as equal cytotoxic effect against Hela cell lines to cisplatin, indicating its potential application in the pharmaceutical and food industries. Yan et al. found fourteen C₁₉-lycaconitine-type diterpenoid alkaloids, including six new alkaloids, grandifolines A–F, isolated from *Delphinium grandiflorum* L. New alkaloids grandifolines A–C and E possess a characteristic $\Delta^{2,3}$ functional group in the A ring, while grandifolines E and F feature a rare OH-16 substituent.

New alkaloids exhibit potential inhibition activities of NO in LPS-activated RAW 264.7 macrophages. A review conducted by **Clements-Decker et al.** delved into the antimicrobial properties of lipopeptides derived from various bacteria strains. The study sheds light on the structures and recently discovered frameworks of lipopeptide families produced by these bacteria, which possess promising antimicrobial properties. Furthermore, utilizing the genome mining approach, underexplored sources of novel antimicrobial lipopeptides have been uncovered. A detailed understanding of the mode of action and biosynthesis included in the review provides a clear path for the development of potential antimicrobial therapeutics in the future.

Rao et al. reported a new transition-metal-free direct oxidative cyclocondensation reaction. The protocol highlighted the use of readily available *o*-aminobenzyl alcohols and *N,N*-dimethyl enamines as starting materials, thus provided a flexible strategy for the preparation of 3-substituted or 3,4-disubstituted quinolones with broad substrate scope in moderate to excellent yields. The strategy enriched the quinoline synthesis method. **Jiang et al.** reported an effective palladium-catalyzed method for the synthesis of aryl acrylonitriles. This process uses simple and readily available arylacetonitriles and vinyl halides/triflates as raw materials, and the resultant aryl acrylonitriles can undergo a series of useful conversion reactions, such as reduction, hydrolysis and epoxidation.

Wei et al. reported a general strategy for the total synthesis of aryl-naphthalene lactone lignans (NALLs) including junicidins B and E and taiwanin C. Key features of this synthesis include an aryl-alkyl Suzuki cross-coupling, a novel intramolecular cation-induced cyclization, and a base-mediated oxidative aromatization. **Wei et al.** explored the uses of dioxinones in synthesizing macrocyclic natural products and terpenoids. The review highlights the versatility and efficiency of dioxinones as reactive intermediates, making them valuable tools for the synthesis of diverse and complex natural products.

Zhou et al. designed and synthesized a series of anti-ZIKV active compounds, acetylarlyamine-S-DACOs, and conducted in-depth research on the action mechanism of the representative compound through molecular docking analysis and a series of biological experiments. The results confirmed the anti-ZIKV activity at the molecular and protein levels, and discovered that this selected compound targeted ZIKV RNA-dependent RNA polymerase (RdRp). **Yin et al.** created a series of podophyllotoxin derivatives containing nitrogen-containing heterocycles, which may have potential as anticancer drugs. After synthesizing several derivatives, imidazolium salts and triazolium salts were found to be the most effective against different types of human tumor cells. Additionally, experiments on cell cycle and apoptosis revealed that these compounds could trigger G2/M cell cycle arrest and apoptosis in HCT-116 cells.

We hope that this Research Topic could provide an opportunity to school fellows of YNU to introduce their recent research findings in natural product chemistry to the chemical community, which

could also provide an incentive for further scientific collaborations between school fellows of YNU and other researchers in this field.

Author contributions

WC, JD, and SP co-wrote this Editorial. All authors contributed to the article and approved the submitted version.

Funding

This work was supported by grants from Natural Science Foundation of China (22271247 and 22261054), Ling-Jun Scholars of Yunnan Province (202005AB160003), Yunnan Fundamental Research Projects (202201AT070141 and 202207AB110002), Talent Plan of Yunnan Province (YNWR-QNBJ-2018-025), and National Key R&D Program of China (2019YFE0109200), and the Project of Yunnan Characteristic Plant Screening and R&D Service CXO Platform (2022YKZY001).

Acknowledgments

We gratefully acknowledge the editorial and publishing teams at Frontiers for supporting and assisting the Guest Editors in organizing this Research Topic. We are grateful to Prof. Hongbin Zhang (YNU), Prof. Xiaodong Yang (YNU) and Prof. Chengfeng Xia (YNU) for their helpful guidance. We appreciate Prof. Yanping He (YNU), Prof. Fuchao Yu (Kunming University of Science and Technology) and Dr. Guogang Deng (YNU) for their useful discussion. Finally, we thank the Guest Editors Dr. Gildardo Rivera (National Polytechnic Institute, Mexico) and Dr. Anton V. Dolzhenko (Monash University), and the Reviewers of this Research Topic for their invaluable input.

Conflict of interest

The authors declare that the research was conducted in the absence of any commercial or financial relationships that could be construed as a potential conflict of interest.

Publisher's note

All claims expressed in this article are solely those of the authors and do not necessarily represent those of their affiliated organizations, or those of the publisher, the editors and the reviewers. Any product that may be evaluated in this article, or claim that may be made by its manufacturer, is not guaranteed or endorsed by the publisher.

Reference

- Newman, D. J., and Cragg, G. M. (2020). Natural products as sources of new drugs over the nearly four decades from 01/1981 to 09/2019. *J. Nat. Prod.* 83, 770–803. doi:10.1021/acs.jnatprod.9b01285



OPEN ACCESS

EDITED BY

Jian-Wei Dong,
Qujing Normal University, China

REVIEWED BY

Huai Xiao,
Dali University, China
Chunmao Yuan,
Key Laboratory of Chemistry for Natural
Products of Guizhou Province (CAS),
China

*CORRESPONDENCE

Zhe Ren,
rz62@163.com
Jun-Xia Zheng,
junxiazheng@gdut.edu.cn
Yi-Fei Wang,
twang-yf@163.com

[†]These authors have contributed equally
to this work

SPECIALTY SECTION

This article was submitted to Medicinal
and Pharmaceutical Chemistry,
a section of the journal
Frontiers in Chemistry

RECEIVED 20 May 2022

ACCEPTED 30 June 2022

PUBLISHED 01 September 2022

CITATION

Chen X-Y, Liu T, Hu Y-Z, Qiao T-T,
Wu X-J, Sun P-H, Qian C-W, Ren Z,
Zheng J-X and Wang Y-F (2022),
Sesquiterpene lactones from *Artemisia
vulgaris* L. as potential NO inhibitors in
LPS-induced
RAW264.7 macrophage cells.
Front. Chem. 10:948714.
doi: 10.3389/fchem.2022.948714

COPYRIGHT

© 2022 Chen, Liu, Hu, Qiao, Wu, Sun,
Qian, Ren, Zheng and Wang. This is an
open-access article distributed under
the terms of the [Creative Commons
Attribution License \(CC BY\)](#). The use,
distribution or reproduction in other
forums is permitted, provided the
original author(s) and the copyright
owner(s) are credited and that the
original publication in this journal is
cited, in accordance with accepted
academic practice. No use, distribution
or reproduction is permitted which does
not comply with these terms.

Sesquiterpene lactones from *Artemisia vulgaris* L. as potential NO inhibitors in LPS-induced RAW264.7 macrophage cells

Xiang-Yu Chen^{1,2,3,4†}, Tao Liu^{1,2,3,4†}, Yu-Ze Hu⁵,
Tian-Tian Qiao^{1,2,3,4}, Xiu-Juan Wu^{1,2,3,4}, Ping-Hua Sun⁵,
Chui-Wen Qian^{1,2,3,4,6}, Zhe Ren^{1,2,3,4,6*}, Jun-Xia Zheng^{7*} and
Yi-Fei Wang^{1,2,3,4,6*}

¹Department of Cell Biology, College of Life Science and Technology, Jinan University, Guangzhou, China, ²Guangdong Province Key Laboratory of Bioengineering Medicine, Guangzhou, China, ³Guangdong Provincial Biotechnology Drug & Engineering Technology Research Center, Guangzhou, China, ⁴National Engineering Research Center of Genetic Medicine, Guangzhou, China, ⁵College of Pharmacy, Jinan University, Guangzhou, China, ⁶GuangZhou (Jinan) Biomedical Research and Development Center Co., Ltd., Guangzhou, China, ⁷School of Biomedical and Pharmaceutical Sciences, Guangdong University of Technology, Guangzhou, China

Twelve new guaianolide sesquiterpene lactones (**1–12**), along with ten known analogs (**13–22**) were isolated from an EtOH extract of the dried aerial parts of *Artemisia vulgaris* L. The new structures were elucidated via abundant spectroscopic data analyses (HRESIMS, IR, 1D, and 2D NMR), and the absolute configurations of these compounds were determined by X-ray crystallography and ECD calculations. The compounds (**1–22**) were identified as guaiane-type sesquiterpenes with characteristic α -methylene- γ -lactone and α,β -unsaturated carbonyl moieties. All compounds were tested for their inhibitory activity against NO production in lipopolysaccharide-stimulated RAW264.7 macrophages. The isolated sesquiterpenoids dose-dependently exhibited an NO production inhibitory activity by inhibiting the expression of inducible NO oxidase (iNOS) and cyclooxygenase-2 (COX-2) with IC₅₀ values ranging from 1.0 to 3.6 μ M. The inhibitory effect on the NO production of the compounds (**1–4** and **6–22**) is better than that of the positive control (dexamethasone). The different substitutions of compounds on C-8 influence anti-inflammatory effects, as evidenced by the *in silico* analysis of related binding interactions of new compounds (**1–12**) with iNOS.

KEYWORDS

Artemisia vulgaris L., new structures, guaianolide sesquiterpene lactones, anti-inflammatory, *in silico*

1 Introduction

Artemisia vulgaris L. (mugwort), belonging to the family of Asteraceae, is widespread throughout Asia, North America, and Europe (Weston et al., 2005). *A. vulgaris*, as a kind of traditional medicinal plant, has been extensively used for relieving pain and treating gynecological symptoms in folks (Hershoff, 2001; Pires et al., 2009). The chemical constituents of *A. vulgaris* contain mainly polysaccharides, flavonoids, terpenoids, and sterols, showing anti-tumor, anti-inflammatory, hepatoprotective, anti-oxidant, immunomodulatory, anti-allergic, and anti-bacterial activities (Schmid-Grendelmeier et al., 2003; Blagojević et al., 2006; Saleh et al., 2014; Abiri et al., 2018; Soon et al., 2019; Ekiert et al., 2020). Previous phytochemical investigations reported that sesquiterpenoids are among the most critical ingredients of secondary metabolites in the genus *Artemisia* and have strong application values in contemporary medicine, food, and the perfume industry (Duke and Bogenschutz, 1994; Bora and Sharma, 2011; Rasheed et al., 2017; Sundararajan and Kumari, 2017). It is widely known that artemisinin and arglabin are promising potent remedies in the treatment of malaria and cancer (Lone et al., 2015; Kumari et al., 2019). *A. vulgaris* and *Artemisia annua* L. are very similar in many aspects (Funk, 2009). Therefore, *A. vulgaris* is regarded as an abundant producer of biologically effective sesquiterpene lactones, prompting us to select it for a detailed study.

Inflammation is an essential immune response to pathogens, toxins, and local injuries. The beneficial effects in the physiological or acute inflammation might turn deleterious in a persistent or over-inflammatory response. Macrophage is a primary cell type in directing the host's inflammatory and immune processes, and the excessive release of nitric oxide is an essential sign of an inflammatory response. Testing the inhibitory effect of compounds on NO's release in macrophages is an integral approach for revealing novel small molecules with anti-inflammatory activities. Our investigation for architecturally unique and effective chemical constituents from *A. vulgaris* led to the isolation and structural elucidation of 22 compounds, including 12 new sesquiterpenoids. And, all the compounds were assessed for anti-inflammatory effects by LPS-induced RAW264.7 macrophage cells.

2 Materials and methods

2.1 General experimental procedures

UV spectra were attained on a JASCO V-730 spectrophotometer. IR data were obtained on a Nicolet iS50 spectrometer (Thermo Fisher Scientific, United States) using KBr pellets. Optical rotations were measured using a JASCO P-2000 polarimeter at room temperature. HRESIMS spectra were recorded with an AB Sciex Triple-TOF 5600+

apparatus. ECD measurements were conducted on a Chirascan Plus spectrometer (Applied Photophysics, United Kingdom). 1D and 2D NMR spectra were obtained on a Bruker AVANCE III 500 or 600 MHz instruments. Chemical shifts were reported in ppm (δ) with coupling constants (J) in hertz. The residual signals of CDCl_3 were used as references. Single crystal X-ray diffraction (Rigaku Oxford Diffraction Supernova Dual Source) was used to measure the crystal structures. Silica gel (100–200 and 200–300 meshes, Qingdao Marine Chemical Co., Ltd., China), Sephadex LH-20 gel (GE Healthcare, Sweden), YMC ODS-A-HG gel (50 μm , YMC, Japan), and MCI gel (SaiPuRuiSi, Beijing, China) were used to perform column chromatography (CC). Semi-Preparative HPLC was performed on a Wufeng LC-100 apparatus (Shanghai Wufeng Co., Ltd., China) using photodiode array (PDA) UV analysis at 210 nm with a YMC-Pack ODS-A column (250 \times 10 mm, 5 μm , 3 ml/min).

2.2 Plant material

The whole plant of *A. vulgaris* was collected from Tangyin city, Henan Province, China, in May 2018 and authenticated by Yifei Wang (College of Life Science and Technology, Jinan University). A specimen (No. 201805) was deposited in Guangzhou Jinan Biomedicine Research and Development Center, Jinan University.

2.3 Extraction and isolation

After drying and grinding, the plant sample (40.0 kg) of *A. vulgaris* was extracted with 95% EtOH at room temperature (360 L, 3 times) in order to afford a residue (3.6 kg), which was suspended in H_2O and extracted with EtOAc and PE (8 L, 3 times) to get an EtOAc partition and a PE partition, successively. The EtOAc partition (1.1 kg) was applied to the MCI gel column using gradient mixtures (10 \times 150 cm, H_2O -MeOH, 60:40 to 0:100), yielding 9 fractions (Fr. 1–9). Fr. 7 (120.0 g) was subsequently chromatographed on a silica gel column (100–200 mesh, 10 \times 47 cm, EtOAc-PE, from 12:88 to 100:0) to afford five subfractions (Fr. 7.1–7.5). Fr. 7-2 was separated by Sephadex LH-20 column (2 \times 110 cm, MeOH- CH_2Cl_2 , 50:50) to remove pigments and obtain Fr. 7.2.1 and Fr. 7.2.2. Fr. 7.2.2 (5.7 g) was passed through an opening ODS CC (5.0 \times 17.5 cm, H_2O -MeOH, 50:50–100:0), and the afforded fractions were divided into Fr. 7.2.2.1–7.2.2.14, as instructed by the TLC analysis. The 14 fractions were analyzed on the HPLC-MS, and all were identified to be separated on a silica gel column (200–300 mesh, 2.5 \times 5.5 cm) eluted with a stepwise gradient of EtOAc-PE (5:95 to 100:0) in the next step. Subsequently, further isolation of Fr. 7.2.2.10 (503.0 mg) on Si CC provided four subfractions (Fr. 7.2.2.10a–7.2.2.10d). The obtained Fr. 7.2.2.10b (377.0 mg) was purified by semi-preparative HPLC (H_2O -MeCN, 60:40, flow rate: 3.0 ml min⁻¹)

to yield compounds **1** (36.5 mg, t_R = 69.0 min), **2** (22.6 mg, t_R = 74.9 min), and **3** (28.5 mg, t_R = 80.4 min). Fr. 7.2.2.9 (433.0 mg) was subjected to Si CC to obtain four subfractions (Fr. 7.2.2.9a–7.2.2.9d). The obtained Fr. 7.2.2.9b (237.0 mg) was further purified by semi-preparative HPLC (H₂O–MeOH, 40:60, 3.0 ml min^{−1}) to give compounds **7** (12.7 mg, t_R = 42.9 min), **13** (36.9 mg, t_R = 46.8 min), and **4** (27.0 mg, t_R = 49.5 min). Fr. 7.2.2.6 (483.0 mg) was subjected to Si CC to obtain six subfractions (Fr. 7.2.2.6a–7.2.2.6f). The obtained Fr. 7.2.2.6d (55.0 mg) was further purified by semi-preparative HPLC (H₂O–MeCN, 59:41, 3.0 ml min^{−1}) to give compound **18** (13.2 mg, t_R = 50.0 min). Using similar separation procedures, **17** (4.1 mg, t_R = 37.8 min), **6** (26.4 mg, t_R = 39.2 min), and **16** (9.2 mg, t_R = 57.2 min) were obtained from Fr. 7.2.2.6e (149.0 mg). Fr. 7.2.2.7 (452.3 mg) was subjected to Si CC eluted by EtOAc–PE to yield Fr. 7.2.2.7a–7.2.2.7d. Fr. 7.2.2.7b (138.8 mg), which was purified by semi-preparative HPLC (H₂O–MeCN, 55:45, 3.0 ml min^{−1}) to afford compound **15** (10.4 mg, t_R = 53.0 min) and Fr. 7.2.2.7b.1 (19.8 mg). Compound **5** (2.4 mg, t_R = 38.9 min) was further obtained from Fr. 7.2.2.7b.1 by semi-preparative HPLC (H₂O–MeOH, 40:60, 3.0 ml min^{−1}). In a similar way, Fr. 7.2.2.8 (542.1 mg) was treated with an Si CC yielding six sections (Fr. 7.2.2.8a–7.2.2.8f), and finally semi-preparative HPLC (H₂O–MeCN, 59:41, 3.0 ml min^{−1}) to generate compound **14** (18.4 mg, t_R = 51.9 min) from Fr. 7.2.2.8d (100.2 mg). Compound **19** (16.3 mg) was precipitated from Fr. 7.2.2.8e (140.7 mg) in the form of crystals. Fr. 7.2.2.2 (300.1 mg) was then separated on Si CC to give Fr. 7.2.2.2a–7.2.2.2c. Compound **20** (18.0 mg, t_R = 50.0 min) was obtained from Fr. 7.2.2.2b (181.0 mg) and **22** (12.1 mg, t_R = 57.3 min) was obtained from Fr. 7.2.2.2c (31.8 mg) via semi-preparative HPLC (H₂O–MeCN, 71:29, 3.0 ml min^{−1}). Fr. 7.2.2.3 (241.8 mg) was subjected to Si CC to obtain two subfractions (Fr. 7.2.2.3a–7.2.2.3b). Fr. 7.2.2.3b (154.4 mg) was further subjected to semi-preparative HPLC (H₂O–MeCN, 67:33, 3.0 ml min^{−1}) to afford **11** (4.3 mg, t_R = 46.7 min) and **21** (16.9 mg, t_R = 52.1 min). Fr. 7.2.2.4 (204.4 mg) was separated by Si CC to give five subfractions (Fr. 7.2.2.4a–7.2.2.4e), and Fr. 7.2.2.4c (57.3 mg) was purified by semi-preparative HPLC (H₂O–MeCN, 62:38, 3.0 ml min^{−1}), yielding **9** (5.1 mg, t_R = 39.0 min) and **10** (2.8 mg, t_R = 44.7 min). Compound **12** (12.0 mg, t_R = 35.2 min) was obtained from Fr. 7.2.2.4b (77 mg) by semi-preparative HPLC (H₂O–MeCN, 62:38, 3.0 ml min^{−1}). Fr. 7.2.2.5 (370.0 mg) was further subjected to CC over silica gel to yield four subfractions, followed by purification with semi-preparative HPLC (H₂O–MeCN, 60:40, 3.0 ml min^{−1}) to afford **8** (19.8 mg, t_R = 54.6 min).

2.3.1 Artemvulactone H (1)

Colorless oil; $[\alpha]_D^{20}$ + 142 (c 0.125, MeOH); UV (MeOH) λ_{\max} (log ϵ) 208 (3.64) nm; IR (KBr) $\nu_{\max}/\text{cm}^{-1}$: 3,432, 2,925,

1,767, 1,711, 1,643, 1,380, 1,273, 1,229, 1,145, 1,004. ¹H and ¹³C NMR data (Tables 1, 3); HRESIMS m/z 367.1504 [M + Na]⁺ (calcd for C₂₀H₂₄O₅Na, 367.1516).

2.3.2 Artemvulactone I (2)

White powder; $[\alpha]_D^{20}$ + 80 (c 0.251, MeOH); UV (MeOH) λ_{\max} (log ϵ) 206 (3.53) nm; IR (KBr) $\nu_{\max}/\text{cm}^{-1}$: 3,465, 2,968, 1,769, 1,732, 1,660, 1,379, 1,273, 1,242, 1,144, 1,006. ¹H and ¹³C NMR data (Tables 1, 3); HRESIMS m/z 369.1662 [M + Na]⁺ (calcd for C₂₀H₂₆O₅Na, 369.1672).

2.3.3 Artemvulactone J (3)

Colorless oil; $[\alpha]_D^{20}$ + 75 (c 0.525, MeOH); UV (MeOH) λ_{\max} (log ϵ) 207 (3.03) nm; IR (KBr) $\nu_{\max}/\text{cm}^{-1}$: 3,455, 2,959, 1,769, 1,735, 1,659, 1,370, 1,274, 1,245, 1,149, 1,005. ¹H and ¹³C NMR data (Tables 1, 3); HRESIMS m/z 369.1664 [M + Na]⁺ (calcd for C₂₀H₂₆O₅Na, 369.1672).

2.3.4 Artemvulactone K (4)

Colorless oil; $[\alpha]_D^{20}$ + 165 (c 0.387, MeOH); UV (MeOH) λ_{\max} (log ϵ) 206 (3.82) nm; IR (KBr) $\nu_{\max}/\text{cm}^{-1}$: 3,460, 2,958, 1,769, 1,735, 1,655, 1,366, 1,293, 1,264, 1,147, 1,010. ¹H and ¹³C NMR data (Tables 1, 3); HRESIMS m/z 347.1862 [M + H]⁺ (calcd for C₂₀H₂₆O₅, 347.1853).

2.3.5 Artemvulactone L (5)

Colorless oil; $[\alpha]_D^{20}$ + 130 (c 0.132, MeOH); UV (MeOH) λ_{\max} (log ϵ) 216 (3.60) nm; IR (KBr) $\nu_{\max}/\text{cm}^{-1}$: 3,469, 2,940, 1,773, 1,712, 1,640, 1,379, 1,232, 1,157, 1,004. ¹H and ¹³C NMR data (Tables 1, 3); HRESIMS m/z 369.1660 [M + Na]⁺ (calcd for C₂₀H₂₆O₅Na, 369.1672).

2.3.6 Artemvulactone M (6)

White powder; $[\alpha]_D^{20}$ + 113 (c 0.18, MeOH); UV (MeOH) λ_{\max} (log ϵ) 207 (3.65) nm; IR (KBr) $\nu_{\max}/\text{cm}^{-1}$: 3,495, 2,975, 1,772, 1,731, 1,387, 1,268, 1,144, 1,075, 965. ¹H and ¹³C NMR data (Tables 1, 3); HRESIMS m/z 371.1450 [M + Na]⁺ (calcd for C₁₉H₂₄O₆Na, 371.1465).

2.3.7 Artemvulactone N (7)

Colorless oil; $[\alpha]_D^{20}$ + 158 (c 0.15, MeOH); UV (MeOH) λ_{\max} (log ϵ) 208 (3.49) nm; IR (KBr) $\nu_{\max}/\text{cm}^{-1}$: 3,445, 2,925, 1,768, 1,713, 1,646, 1,454, 1,263, 1,235, 1,145, 1,008. ¹H and ¹³C NMR data (Tables 1, 3); HRESIMS m/z 345.1703 [M + H]⁺ (calcd for C₂₀H₂₄O₅, 345.1697).

2.3.8 Artemvulactone O (8)

White powder; $[\alpha]_D^{20}$ + 105 (c 0.215, MeOH); UV (MeOH) λ_{\max} (log ϵ) 207 (3.50) nm; IR (KBr) $\nu_{\max}/\text{cm}^{-1}$: 3,476, 2,934, 1,769, 1,730, 1,658, 1,469, 1,275, 1,250, 1,146, 1,011. ¹H and ¹³C NMR data (Tables 2, 3); HRESIMS m/z 371.1456 [M + Na]⁺ (calcd for C₁₉H₂₄O₆Na, 371.1465).

TABLE 1 ^1H NMR spectroscopic data for compounds 1–7.

No.	1 ^a	2 ^b	3 ^a	4 ^a	5 ^a	6 ^b	7 ^a
	δ_{H} (J in Hz)	δ_{H} (J in Hz)	δ_{H} (J in Hz)	δ_{H} (J in Hz)	δ_{H} (J in Hz)	δ_{H} (J in Hz)	δ_{H} (J in Hz)
2a	2.65, m	2.63, m	2.62, m	2.31, m	2.46, m	1.93, d (15.3)	2.30, m
2b	–	–	–	2.89, d (17.0)	2.93, d (16.8)	2.24, dd (20.6, 9.4)	–
3	5.50, m	5.49, s	5.49, s	5.55, d (1.3)	5.54, s	3.58, s	5.57, s
5	2.85, d (10.7)	2.84, d (10.7)	2.82, d (10.7)	2.67, m	2.71, m	2.37, d (11.2)	2.71, dd (14.4, 5.6)
6	3.98, dd (10.7, 9.2)	3.95, dd (10.7, 9.2)	3.94, dd (10.6, 9.2)	3.88, m	3.87, t (9.7)	3.94, dd (11.0, 9.2)	3.92, dd (10.4, 9.4)
7	3.58, tt (10.2, 3.2)	3.54, tt (9.8, 3.2)	3.51, m	3.28, tt (9.7, 3.2)	2.46, m	3.27, m	3.33, tt (9.7, 3.2)
8	5.42, ddd (10.3, 3.6, 1.6)	5.34, ddd (10.3, 3.8, 1.6)	5.33, ddd (10.3, 3.6, 1.6)	4.94, ddd (10.3, 6.3, 4.9)	4.97, td (9.1, 4.6)	4.96, td (9.9, 2.1)	5.05, ddd (10.5, 6.0, 4.8)
9a	5.50, m	5.42, dd (3.8, 1.2)	5.45, dd (3.6, 1.2)	2.56, dd (13.9, 4.8)	2.57, dd (13.0, 4.5)	2.24, dd (20.6, 9.4)	2.59, dd (14.0, 4.7)
9b	–	–	–	2.67, m	2.71, m	2.58, dd (15.3, 2.6)	2.71, dd (14.4, 5.6)
11	–	–	–	–	2.46, m	–	–
13a	5.68, d (3.0)	5.71, d (3.0)	5.69, d (3.0)	5.63, d (3.0)	1.27, d (6.4)	5.62, d (3.0)	5.63, d (3.0)
13b	6.26, d (3.0)	6.27, d (3.0)	6.27, d (3.0)	6.22, d (3.0)	–	6.23, d (3.0)	6.21, m
14a	1.94, m	1.93, m	1.92, m	5.14, s	5.21, s	5.00, s	5.16, s
14b	–	–	–	5.40, s	5.31, s	5.55, s	5.44, s
15	1.94, m	1.93, m	1.92, m	1.91, m	1.90, d (11.4)	1.66, s	1.94, m
2'	–	2.43, m	2.27, m	2.31, m	–	2.63, m	–
3'a	–	1.50, m	2.15, m	2.15, m	6.17, q (7.3)	1.23, dd (8.7, 7.0)	6.21, m
3'b	6.21, qd (7.3, 1.4)	1.75, dt (13.7, 7.4)	–	–	–	–	–
4'	2.03, m	0.94, t (7.4)	0.99, d (6.6)	1.00, d (7.1)	2.03, d (7.2)	1.23, dd (8.7, 7.0)	2.04, dd (7.3, 1.5)
5'	1.94, m	1.21, d (7.0)	0.99, d (6.6)	1.00, d (7.1)	1.90, d (11.4)	–	1.94, m

^a500 MHz in CDCl_3 .^b600 MHz in CDCl_3 .

2.3.9 Artemvulactone P (9)

Colorless oil; $[\alpha]_{\text{D}}^{20} + 74$ (c 0.38, MeOH); UV (MeOH) λ_{max} (log ϵ) 257 (2.68) nm; IR (KBr) $\nu_{\text{max}}/\text{cm}^{-1}$: 2,942, 1,773, 1,737, 1,688, 1,433, 1,255, 1,197, 1,137, 1,000. ^1H and ^{13}C NMR data (Tables 2, 3); HRESIMS m/z 317.1370 $[\text{M} + \text{H}]^+$ (calcd for $\text{C}_{18}\text{H}_{20}\text{O}_5$, 317.1384).

2.3.10 Artemvulactone Q (10)

White powder; $[\alpha]_{\text{D}}^{20} + 127$ (c 0.18, MeOH); UV (MeOH) λ_{max} (log ϵ) 223 (4.33) nm; IR (KBr) $\nu_{\text{max}}/\text{cm}^{-1}$: 2,944, 1,770, 1,736, 1,629, 1,460, 1,269, 1,183, 1,143, 1,022. ^1H and ^{13}C NMR data (Tables 2, 3); HRESIMS m/z 349.1644 $[\text{M} + \text{H}]^+$ (calcd for $\text{C}_{19}\text{H}_{24}\text{O}_6$, 349.1646).

2.3.11 Artemvulactone R (11)

White powder; $[\alpha]_{\text{D}}^{20} + 103$ (c 0.23, MeOH); UV (MeOH) λ_{max} (log ϵ) 208 (4.38) nm; IR (KBr) $\nu_{\text{max}}/\text{cm}^{-1}$: 3,465, 2,933, 1,761, 1,736, 1,373, 1,274, 1,241, 1,142, 999. ^1H and ^{13}C NMR data (Tables 2, 3); HRESIMS m/z 357.1301 $[\text{M} + \text{Na}]^+$ (calcd for $\text{C}_{18}\text{H}_{22}\text{O}_6\text{Na}$, 357.1309).

2.3.12 Artemvulactone S (12)

White powder; $[\alpha]_{\text{D}}^{20} + 131$ (c 0.18, MeOH); UV (MeOH) λ_{max} (log ϵ) 211 (3.96) nm; IR (KBr) $\nu_{\text{max}}/\text{cm}^{-1}$: 3,328, 2,942, 1,769, 1,642, 1,452, 1,390, 1,253, 1,143, 1,018, 936. ^1H and ^{13}C NMR data (Tables 2, 3); HRESIMS m/z 315.1008 $[\text{M} + \text{H}]^+$ (calcd for $\text{C}_{15}\text{H}_{19}\text{ClO}_5$, 315.0994).

2.4 X-ray crystallographic analyses

All crystals were obtained by recrystallization from MeOH. The X-ray diffraction data of compounds 6, 8, 10, and 12 were collected on an Agilent SuperNova four-circle instrument by means of Cu K α radiation. The structures were solved by direct methods and refined by the full-matrix least-squares process on F^2 using the SHELXTL or the Olex2 software package. X-ray data can be obtained free from the Cambridge Crystallographic Data Centre via <https://www.ccdc.cam.ac.uk/structures/>.

TABLE 2 ^1H NMR spectroscopic data for compounds 8–12.

No.	8 ^a	9 ^a	10 ^a	11 ^a	12 ^b
	δ_{H} (J in Hz)	δ_{H} (J in Hz)	δ_{H} (J in Hz)	δ_{H} (J in Hz)	δ_{H} (J in Hz)
2a	1.94, d (14.9)	—	—	1.94, d (16.0)	3.69, s
2b	2.47, d (15.0)	—	—	2.48, m	—
3	3.55, s	6.20, m	6.04, m	3.56, s	4.11, s
5	2.57, d (11.7)	3.50, m	3.17, m	2.57, d (11.7)	2.47, s
6	3.90, dd (11.7, 8.5)	3.72, t (10.2)	4.72, dd (10.4, 9.5)	3.90, dd (11.7, 8.5)	4.30, dd (11.5, 9.0)
7	3.33, m	3.26, m	3.06, m	3.31, td (11.2, 2.9)	3.52, m
8a	5.31, m	4.93, td (10.6, 2.1)	5.03, td (10.9, 4.0)	5.32, d (12.0)	1.88, dd (15.8, 7.6)
8b	—	—	—	—	2.64, m
9a	5.24, m	2.47, m	2.49, dt (6.8, 3.4)	5.29, s	1.45, m
9b	—	2.71, dd (13.4, 10.9)	1.59, dd (14.4)	—	2.35, ddt (11.5, 7.7)
13a	5.77, d (3.0)	5.65, d (2.9)	5.79, d (2.8)	5.77, d (2.7)	5.47, d (3.3)
13b	6.32, d (3.0)	6.22, d (2.9)	6.31, d (2.8)	6.33, d (2.7)	6.18, d (3.3)
14	1.92, m	2.47, m	1.56, s (14.4)	1.92, s	1.40, s
15	1.72, s	2.34, s	2.29, s	1.72, s	1.75, s
16	—	—	3.24, s	—	—
2'	2.62, m	2.43, d (5.5, 2.8)	2.41, m	2.42, dd (15.0, 7.5)	—
3'	1.22, d (7.0)	1.21, t (7.6)	1.19, t (7.6)	1.20, t (7.5)	—
4'	1.22, d (7.0)	—	—	—	—

^a600 MHz in CDCl_3 .^b500 MHz in CDCl_3 .

2.4.1 Crystal structure determination of compound 6

Crystal data for $\text{C}_{19}\text{H}_{24}\text{O}_6$ ($M = 348.38$ g/mol): orthorhombic, space group $\text{P}2_12_12_1$ (no. 19), $a = 8.6975$ (2) Å, $b = 9.7500$ (2) Å, $c = 20.3304$ (5) Å, $V = 1,724.03$ (7) Å³, $Z = 4$, $T = 170.00$ (10) K, $\mu(\text{Cu K}\alpha) = 0.823$ mm⁻¹, $D_{\text{calc}} = 1.342$ g/cm³, 9,848 reflections measured ($8.698^\circ \leq 2\theta \leq 147.768^\circ$), 3423 unique ($R_{\text{int}} = 0.0325$, $R_{\text{sigma}} = 0.0320$) which were used in all calculations. The final R_1 was 0.0356 ($I > 2\sigma(I)$) and wR_2 was 0.0914 (all data). The goodness of fit on F^2 was 1.047. Flack parameter: -0.04 (9). CCDC 2164101.

2.4.2 Crystal structure determination of compound 8

Crystal data for $\text{C}_{19}\text{H}_{24}\text{O}_6$ ($M = 348.38$ g/mol): orthorhombic, space group $\text{P}2_12_12_1$ (no. 19), $a = 9.34750$ (10) Å, $b = 10.61860$ (10) Å, $c = 17.3505$ (2) Å, $V = 1,722.16$ (3) Å³, $Z = 4$, $T = 179.99$ (10) K, $\mu(\text{Cu K}\alpha) = 0.824$ mm⁻¹, $D_{\text{calc}} = 1.344$ g/cm³, 18,414 reflections measured ($9.766^\circ \leq 2\theta \leq 147.578^\circ$), 3,462 unique ($R_{\text{int}} = 0.0271$, $R_{\text{sigma}} = 0.0160$) which were used in all calculations. The final R_1 was 0.0293 ($I > 2\sigma(I)$) and wR_2 was 0.0776 (all data). The goodness of fit on F^2 was 1.090. Flack parameter: 0.01 (5). CCDC 2164105.

2.4.3 Crystal structure determination of compound 10

Crystal data for $\text{C}_{19}\text{H}_{24}\text{O}_6$ ($M = 348.38$ g/mol): monoclinic, space group $\text{P}2_1$ (no. 4), $a = 8.4422$ (4) Å, $b = 7.1913$ (4) Å, $c = 15.2596$ (6)

Å, $\beta = 99.791$ (4)°, $V = 912.92$ (8) Å³, $Z = 2$, $T = 169.99$ (10) K, $\mu(\text{Cu K}\alpha) = 0.777$ mm⁻¹, $D_{\text{calc}} = 1.267$ g/cm³, 10,067 reflections measured ($5.878^\circ \leq 2\theta \leq 148.026^\circ$), 3411 unique ($R_{\text{int}} = 0.0440$, $R_{\text{sigma}} = 0.0498$) which were used in all calculations. The final R_1 was 0.0445 ($I > 2\sigma(I)$) and wR_2 was 0.1126 (all data). The goodness of fit on F^2 was 1.053. Flack parameter: -0.08 (15). CCDC 2164102.

2.4.4 Crystal structure determination of compound 12

Crystal data for $\text{C}_{15}\text{H}_{19}\text{ClO}_5$ ($M = 314.75$ g/mol): orthorhombic, space group $\text{P}2_12_12_1$ (no. 19), $a = 5.80960$ (10) Å, $b = 14.6880$ (2) Å, $c = 16.6063$ (2) Å, $V = 1417.04$ (4) Å³, $Z = 4$, $T = 200.00$ (10) K, $\mu(\text{Cu K}\alpha) = 2.575$ mm⁻¹, $D_{\text{calc}} = 1.475$ g/cm³, 14,845 reflections measured ($8.036^\circ \leq 2\theta \leq 147.536^\circ$), 2,827 unique ($R_{\text{int}} = 0.0403$, $R_{\text{sigma}} = 0.0232$) which were used in all calculations. The final R_1 was 0.0300 ($I > 2\sigma(I)$) and wR_2 was 0.0760 (all data). The goodness of fit on F^2 was 1.090. Flack parameter: 0.002 (7). CCDC 2164103.

2.5 ECD calculations

Conformational analyses for new compounds were carried out using MOE software with MMFF94s. The obtained stable conformers were optimized at the b3lyp/6-31+g(d) level in the gas phase and further subjected to ECD calculations at cam-b3lyp/6-31+g(d) level in the PCM model of methanol using the

TABLE 3 ^{13}C NMR spectroscopic data for compounds 8–12.

No.	1 ^a	2 ^b	3 ^a	4 ^a	5 ^a	6 ^b	7 ^a	8 ^b	9 ^b	10 ^b	11 ^b	12 ^a
	δ_{C}	δ_{C}	δ_{C}	δ_{C}	δ_{C}	δ_{C}	δ_{C}	δ_{C}	δ_{C}	δ_{C}	δ_{C}	δ_{C}
1	83.3	83.2	83.2	84.7	84.6	82.0	84.8	80.6	133.7	58.4	80.7	85.8
2	46.3	46.1	46.2	46.0	45.8	40.8	46.0	42.2	195.1	205.4	42.3	66.0
3	123.5	123.4	123.4	124.8	124.6	64.5	124.8	63.1	136.2	133.5	63.1	62.2
4	141.8	141.6	141.6	140.7	140.4	67.6	140.9	67.4	169.4	177	67.4	68.7
5	64.2	64.0	64.1	65.1	64.3	61.2	65.3	60.4	51.7	52.6	60.4	59.0
6	78.5	78.4	78.4	79.3	79.1	75.4	79.3	75.4	81.5	78.7	75.5	78.3
7	46.3	46.1	46.1	48.2	54.1	46.5	48.4	48.3	55.2	50.1	48.2	44.4
8	72.3	72.5	72.6	74.1	75.8	73.1	73.9	71.9	69.3	71.1	72.0	31.1
9	123.3	123.0	123.0	36.5	37.4	35.2	36.4	122.2	44.5	45.1	122.3	23.9
10	140.6	141.1	141.0	144.1	144.8	140.7	144.1	138.9	144.8	76.5	139.0	75.8
11	137.2	137.3	137.1	137.1	41.1	136.7	137.2	135.7	136.2	136.2	135.6	140.2
12	169.4	169.4	169.4	169.4	178.1	168.8	169.4	168.7	168.5	169.3	168.7	169.7
13	123.3	123.1	123.2	122.6	15.4	122.8	122.6	124.7	122.0	124.2	124.8	120.3
14	24.6	24.7	24.7	117.7	117.7	118.2	117.6	24.9	21.4	24.4	24.9	28.9
15	17.7	17.7	17.7	17.8	17.8	18.7	17.8	19.8	20.0	20.40	19.8	19.7
16	—	—	—	—	—	—	—	—	—	50.4	—	—
1'	167.1	176.0	172.5	172.4	167.0	176.4	167.0	176.3	173.3	173.6	173.7	—
2'	127.1	41.5	43.6	43.7	127.3	34.4	127.3	34.3	27.8	27.8	27.9	—
3'	140.8	26.6	25.8	25.8	140.1	18.9	140.3	19.2	9.1	9.1	9.1	—
4'	16.14	11.9	22.5	22.6	16.1	19.1	16.0	18.8	—	—	—	—
5'	20.7	16.9	22.6	22.6	20.7	—	20.7	—	—	—	—	—

^a125 MHz in CDCl_3 .^b150 MHz in CDCl_3 .

Gaussian 09 program. The ECD spectra were weighted according to the Boltzmann distributions.

2.6 Cytotoxicity

For the cytotoxicity assay, RAW 264.7 cells were grown in DMEM containing 10% FBS and cultured at 37°C. Then, the cells were seeded in a 96-well plate (1×10^4 cells/well) before the cells were incubated for 24 h in various concentrations of compounds (3.125–200 μM). Cell viability was examined using a CCK8-kit. The CCK8 solution (5 μL) was added to each well and incubated for 1–2 h at 37°C. The OD value at 450 nm was quantified by Graphpad software, and the corresponding 50% cytotoxic concentration (CC_{50}) of the compounds was subsequently obtained.

2.7 Measurement of NO production

The level of accumulated nitrite in the culture media reflected the level of NO using the classic Griess reagent (Beyotime, Jiangsu, China). The RAW264.7 cells were seeded in a 96-well plate with a 6×10^4 cells/ml density for the indicated time. Then,

the cells were pretreated for 1 h with test compounds (0.25–4 μM), followed by stimulation with LPS (1 $\mu\text{g}/\text{mL}$) for 18 h. Finally, 50 μL of the culture supernatant was mixed with an equal amount of the Griess reagent, and the optical densities at 570 nm were read using a microplate reader. The nitric oxide concentration of the samples was calculated according to the standard curve.

2.8 RNA isolation and quantitative real-time PCR

RAW264.7 cells were seeded in a six-well plate (10×10^5 cells/well) for the indicated time. Cells were pretreated with compound 1 (0.5, 1, and 4 μM) for 1 h and then stimulated with LPS (1 $\mu\text{g}/\text{mL}$) for 18 h. Total cellular RNA was extracted with Trizol reagent (TIANGEN, Beijing, China). One microgram of RNA per sample was reverse-transcribed into cDNA using the PrimeScript RT Reagent Kit (TAKARA, Dalian, China). qPCR assays were performed by the CFX96 Touch Real-Time PCR Detection System (Bio-Rad). The following primers were used: iNOS (forward, 5'-AAA CCC CAG GTG CTA TTC CC-3'; reverse, 5'-TGG GTC CTC TGG TCA AAC TC-3'), COX-2 (forward, 5'-ATT CCA AAC CAG CAG ACT CAT A-3'; reverse, CTT GAG

TTT GAA GTG GTA ACC G-3'), and GAPDH (forward, 5'-GTC ATT GAG AGC AAT GCC AG-3'; reverse, 5'-GTG TTC CTA CCC CCA ATG TG-3'). All relative gene expression levels were normalized to the internal reference (GAPDH).

2.9 Western blotting

RAW264.7 cells with the indicated treatment were harvested and treated in a RIPA lysis buffer (Beyotime, Shanghai, China) containing a protease and phosphatase inhibitor cocktail (Beyotime, Shanghai, China) to obtain the lysates. Then, the total proteins were measured using the bicinchoninic acid (BCA) protein assay kit (Beyotime, Shanghai, China) and regulated by a loading buffer and the RIPA lysis buffer. The samples were separated by sodium dodecyl sulfate polyacrylamide gel electrophoresis (SDS-PAGE) and then transferred to polyvinylidene difluoride membranes (Millipore), followed by blocking with 5% non-fat milk. The membranes were incubated with primary antibodies overnight at 4°C, followed by incubation with specific secondary antibodies. Finally, the protein bands were detected using the ImageJ software (Bio-Rad, Hercules, CA, United States).

2.10 Molecular docking

In order to explore the possibility of compounds **1–6** binding to the INOS target, Autodock vina and AutoDockTools-1.5.6 (Vina, 2010; Forli et al., 2016) were used to predict the free binding energy. Autodock vina used the Broyden-Fletcher-Goldfarb-Shanno (BFGS) 19 method to obtain the optimal conformation (Nguyen et al., 2020). First, the three-dimensional structure of INOS (PDB ID:3E6T) was obtained from the Protein Data Bank (<http://www.rcsb.org>) (Burley et al., 2021), whose resolution was 2.5 Å. The three-dimensional structure of compounds **1–6** was built and optimized by ChemDraw Ultra 8.0. Pymol molecular graphics software and AutodockTools-1.5.6 were used to remove ligand, dehydrate, hydrogenate, and charge the target (Liang, 2003; Seeliger and de Groot, 2010). The cubic grid box was calculated by AutoDockTools-1.5.6 positioned at the center of (122.65, 114.0, 36.63) with a spacing of 0.375 Å. All docking parameters were set to default values, but the modes and exhaustiveness were set to 10. The docking results were further analyzed and presented using pymol.

3 Results and discussion

3.1 Structural elucidation of new compounds **1–12**

Artemvulactone H (**1**), obtained as a colorless oil, had a molecular formula of C₂₀H₂₄O₅ deduced from the molecular ion

at m/z 367.1504 ([M + Na]⁺, calcd for 367.1516) in the HRESIMS, indicating nine degrees of unsaturation. The IR absorptions of **1** suggested typical absorption bands for hydroxy (3,432 cm⁻¹), carbonyl (1,767 and 1,711 cm⁻¹), and olefinic (1,643 cm⁻¹) functionalities. The ¹H NMR spectrum (Table 1) of **1** displayed signals for a vinyl methyl observed at δ_H 1.94 (3H, m, H-15), a pair of terminal olefinic protons at δ_H 5.68 (1H, d, J = 3.0 Hz, H-13a), and 6.26 (1H, d, J = 3.0 Hz, H-13b), two oxygenated methines at δ_H 3.98 (1H, dd, 10.7, 9.2 Hz, H-6), and 5.42 (1H, ddd, 10.3, 3.6, 1.6 Hz, H-8). Apart from these data, the ¹³C NMR (Table 3) and DEPT (Supplementary Figure S3) data of **1** with the aid of HSQC analysis exhibited 15 carbon resonances for 2 methyls, 2 methylenes, 6 methines, and 5 quarternary carbons. Comparison of the NMR spectra of **1** (Tables 1, 3) with 1 α -hydroxy-3(4), 9(10), 11(13)-trien-8 α -seneciodyloxyguaia-12,6 α -olide showed that they had a closely relative stereochemistry except for a different ester side chain, indicating that **1** was a characteristic guaiane-type sesquiterpene lactone skeleton (Huang et al., 2010). A mixture of the ¹H NMR spectrum at δ_H 6.21 (1H, qd, 7.3, 1.4 Hz, H-3'), 2.03 (3H, m, H-4'), and 1.94 (3H, m H-5') and the ¹³C NMR spectrum at δ_C 167.1 (C-1'), 127.1 (C-2'), 140.8 (C-3'), 16.14 (C-4'), and 20.7 (C-5') of **1** displayed signals for an angeloyloxy group. The aforementioned conclusion was confirmed again by the correlation of H-3'/H₃-4' in the ¹H-¹H COSY spectrum and the correlations from H-3' to C-1', C-2', and C-4', from H₃-4' to C-2', C-3', and C-5', and from H₃-5' to C-1', C-2', and C-3' in the HMBC. The proton signal at δ_H 5.42 (H-8) disclosed a ³J coupling with the carbonyl carbon signal at δ_C 167.1 (C-1'), indicating the connection of this group to C-8. The ¹H-¹H COSY data revealed two discrete proton spin systems, which were H-5/H-6/H-7/H-8, and H-3'/H₃-4'. The HMBC correlations of H-6, H-7/C-12, H-5/C-6, and C-7 located the lactone group at C-6 and C-7 (Figure 1). Furthermore, the anguloid group and hydroxyl group were located at C-8 and C-1 based on the correlations of H-8 to C-1', H₃-14 to C-1, H-3 to C-1, and H-5 to C-1 in the HMBC experiment.

The relative configuration was determined by the correlations between H-7/H₂-13, H-7/H-5, and H-6/H-8 in the NOESY spectrum (Figure 2). The absolute configuration of **1** was assigned according to the ECD calculations on the arbitrarily chosen enantiomers. Based on the evidence mentioned previously, the stereochemistry of **1** was eventually assigned as 1S,5R,6S,7R,8S.

Artemvulactone I (**2**) was obtained as a white amorphous powder. The molecular formula of **2** (C₂₀H₂₆O₅) was established by the [M + Na]⁺ ion peak at m/z 369.1662 (calcd for 369.1672) in the HRESIMS (Supplementary Figure S18). The existence of hydroxy (3,465 cm⁻¹), carbonyl (1,769 and 1,732 cm⁻¹), and olefinic (1651 cm⁻¹) groups were reflected in the IR spectrum (Supplementary Figure S20). The ¹H/¹³C-NMR (Tables 1, 3), ¹H-¹H COSY, HMQC, and HMBC spectra of **2** were similar to **1**, with a difference in the C-8 substituent. The angeloyloxy group in

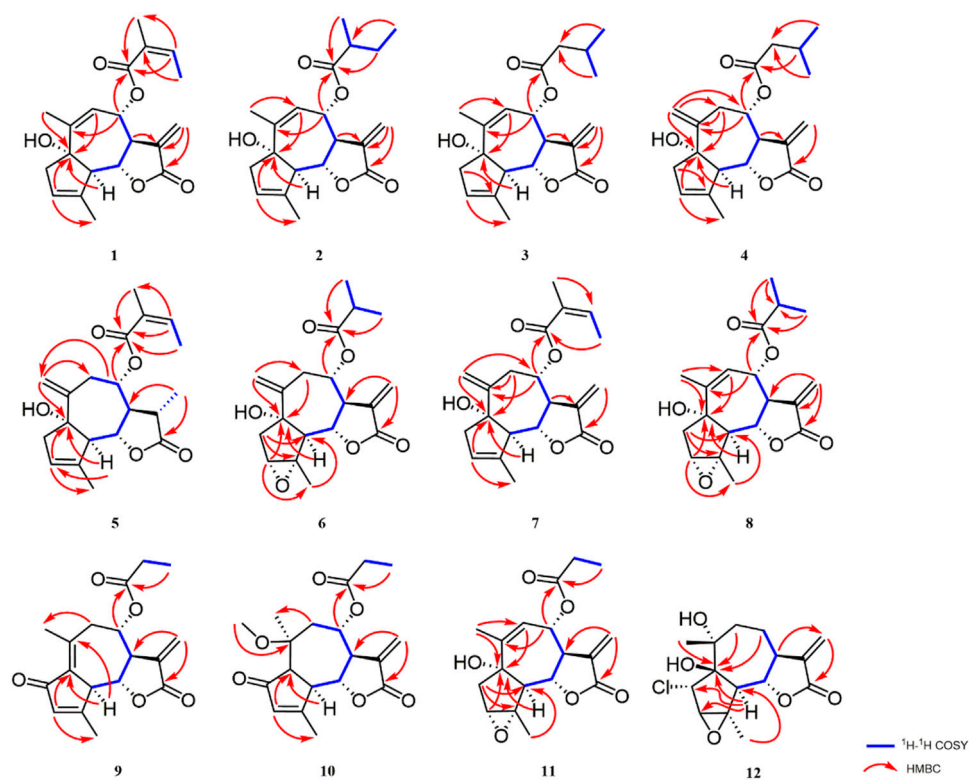


FIGURE 1
Key HMBC and ^1H - ^1H COSY correlations of compounds **1–12**.

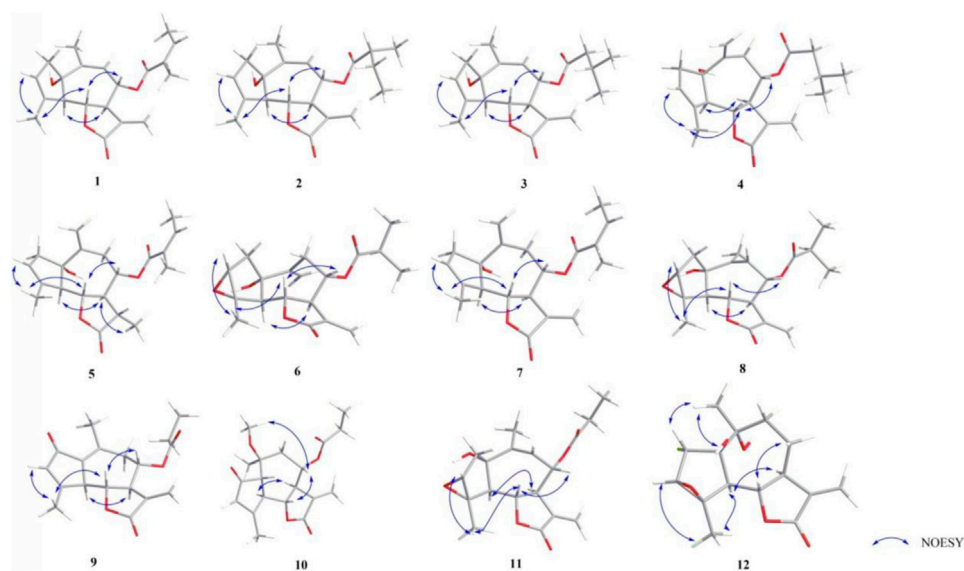


FIGURE 2
NOESY correlations of compounds **1–12**.

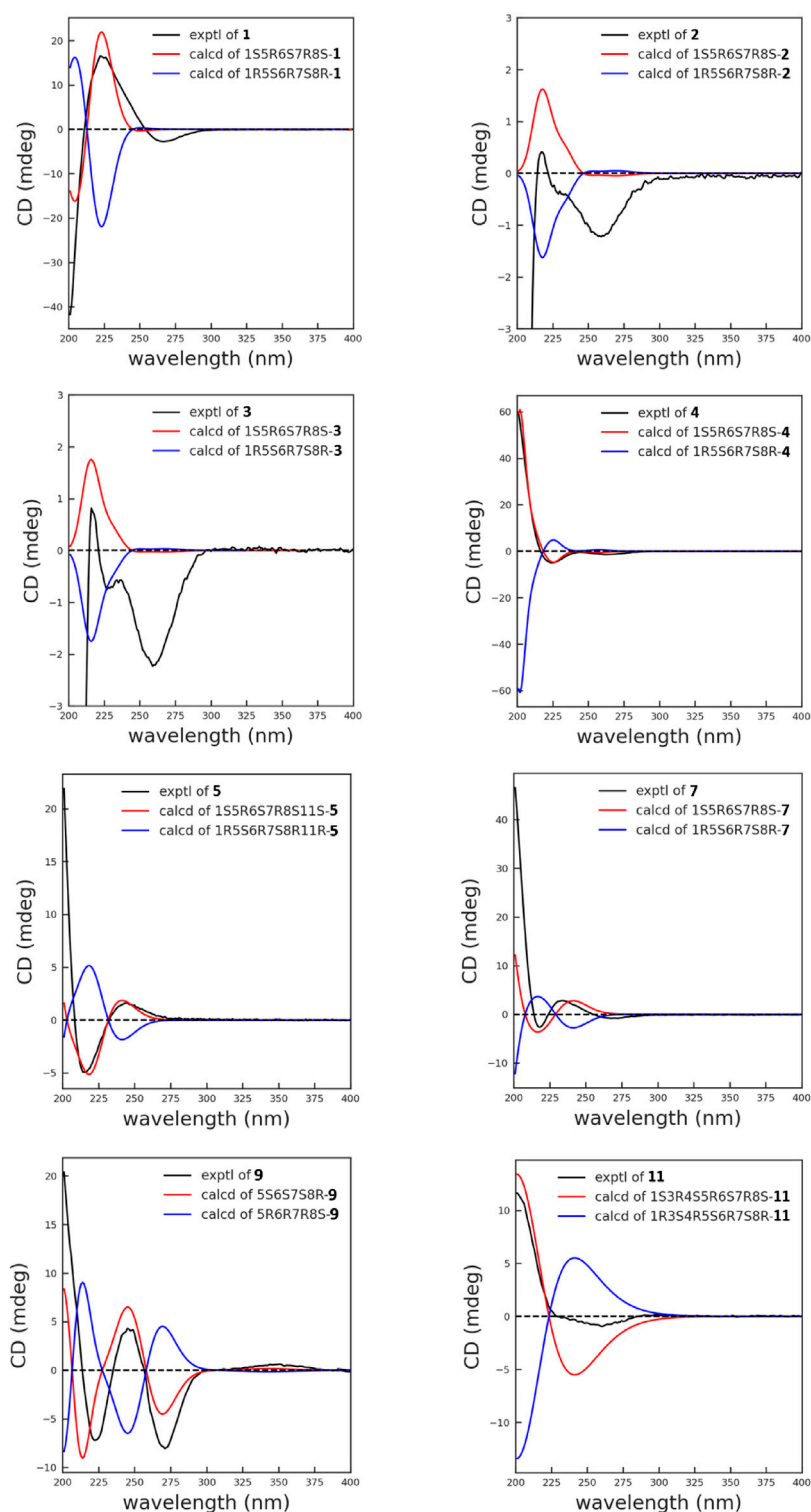


FIGURE 3
Experimental and calculated ECD spectra of compounds **1–5**, **7**, **9**, and **11** in MeOH.

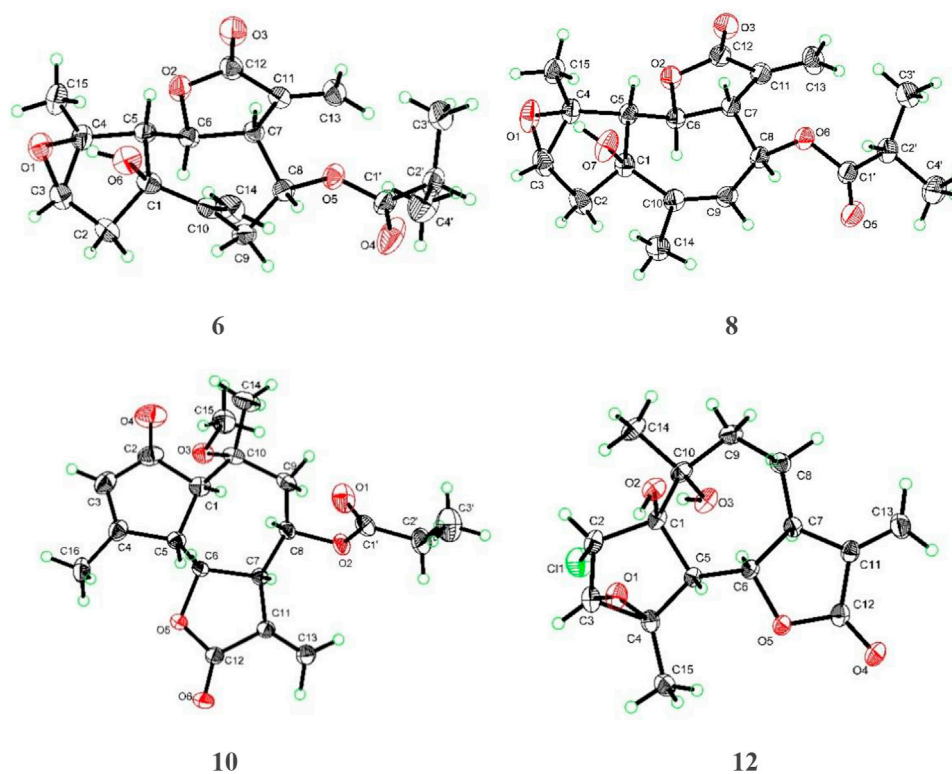


FIGURE 4
X-ray crystallographic analysis of compounds **6**, **8**, **10**, and **12**.

1 was replaced by the 2'-methylbutyryloxy unit in **2**. ^1H NMR signals supported the aforementioned deduction at δ_{H} 2.43 (1H, m, H-2'), 1.50 (1H, m, H-3'a), 1.75 (1H, dt, 13.7, 7.4 Hz, H-3'b), 0.94 (3H, t, 7.4 Hz, H-4'), and 1.21 (3H, d, 7.0 Hz, H-5') and the ^{13}C NMR signals at δ_{C} 176.0 (C-1'), 41.5 (C-2'), 26.6 (C-3'), 11.9 (C-4'), and 16.9 (C-5') of **2**. The absolute configuration of **2** was compared to **1**, which was determined by the NOESY and ECD spectra as shown.

Artemvulactone J (**3**) and Artemvulactone K (**4**) were both obtained as colorless oils and had the same molecular formula of $\text{C}_{20}\text{H}_{26}\text{O}_6$ as that of **2** by HRESIMS. Similar to **2**, their NMR spectra revealed that **3** and **4** also possessed a guaianolide skeleton with characteristic α -methylene- γ -lactone [δ_{H} 5.69 (1H, d, 3.0 Hz, H-13a), 6.27 (1H, d, 3.0 Hz, H-13b), δ_{C} 137.1 (C-11), 169.4 (C-12), 123.2 (C-13)]. The ^1H and ^{13}C NMR spectra of **3** were almost superimposable to those of **2** except for the absence of 2'-methylbutyryloxy moiety. The ^1H NMR signals at δ_{H} 2.27 (2H, m, H-2'), 2.15 (1H, m, H-3'), 0.99 (3H, d, 6.6, H-4'), and 0.99 (3H, d, 6.6, H-5') indicated that **3** has an isovaleryloxy moiety rather than a 2'-methylbutyryloxy group, which was supported by the ^1H - ^1H COSY cross peaks of H_2 -2'/H-3'/H₃-4' (H₃-5') and HMBC spectrum from H-8 to C-1' and H₂-2'/H-3' to C-1'. The 1D NMR spectra of **4** (Tables 1, 3) were very similar to compound **3**, except that a pair of terminal olefinic protons at

δ_{H} 5.14 (1H, s, H-14a) and 5.40 (1H, s, H-14b) in **4**. The relative configurations of compounds **3** and **4** were determined by NOESY correlations and were similar to those of **2**. The 1S,5R,6S,7R,8S absolute configuration of compounds **3** and **4** (Figure 3) was verified based on comparing its ECD spectrum with that of **2**.

Artemvulactone L (**5**) was determined as $\text{C}_{20}\text{H}_{26}\text{O}_5$ by HRESIMS ($[\text{M} + \text{Na}]^+$, m/z 369.1660, calcd for 369.1672). The IR spectrum revealed the presence of hydroxy ($3,469\text{ cm}^{-1}$), carbonyl ($1,773$ and $1,712\text{ cm}^{-1}$), and olefinic ($1,640\text{ cm}^{-1}$) groups. The ^1H and ^{13}C NMR spectra of **5** (Tables 1, 3) were comparable to **1** except for the presence of a pair of terminal olefinic protons at δ_{H} 5.21 (1H, s, H-14a), δ_{H} 5.31 (1H, s, H-14b), and the absence of a terminal double bond at C-13. The HMBC correlation between the proton signal at δ_{H} 4.97 (1H, td, 9.1, 4.6 Hz, H-8) and the carbonyl carbon signal at δ_{C} 167.0 (C-1') demonstrated an angeloyl group attached to C-8 (Figure 1). Finally, the stereochemistry of **5** was determined in a manner similar to that of **1**.

Artemvulactone M (**6**) was determined as $\text{C}_{19}\text{H}_{24}\text{O}_6$ according to the HRESIMS ($[\text{M} + \text{Na}]^+$, m/z 371.1450, calcd for 371.1465). The IR absorption bands at $3,495$, $1,772$, and $1,731\text{ cm}^{-1}$ were marks of hydroxy and carbonyl groups. The ^1H and ^{13}C NMR spectra of **6** were comparable to **4**, but the

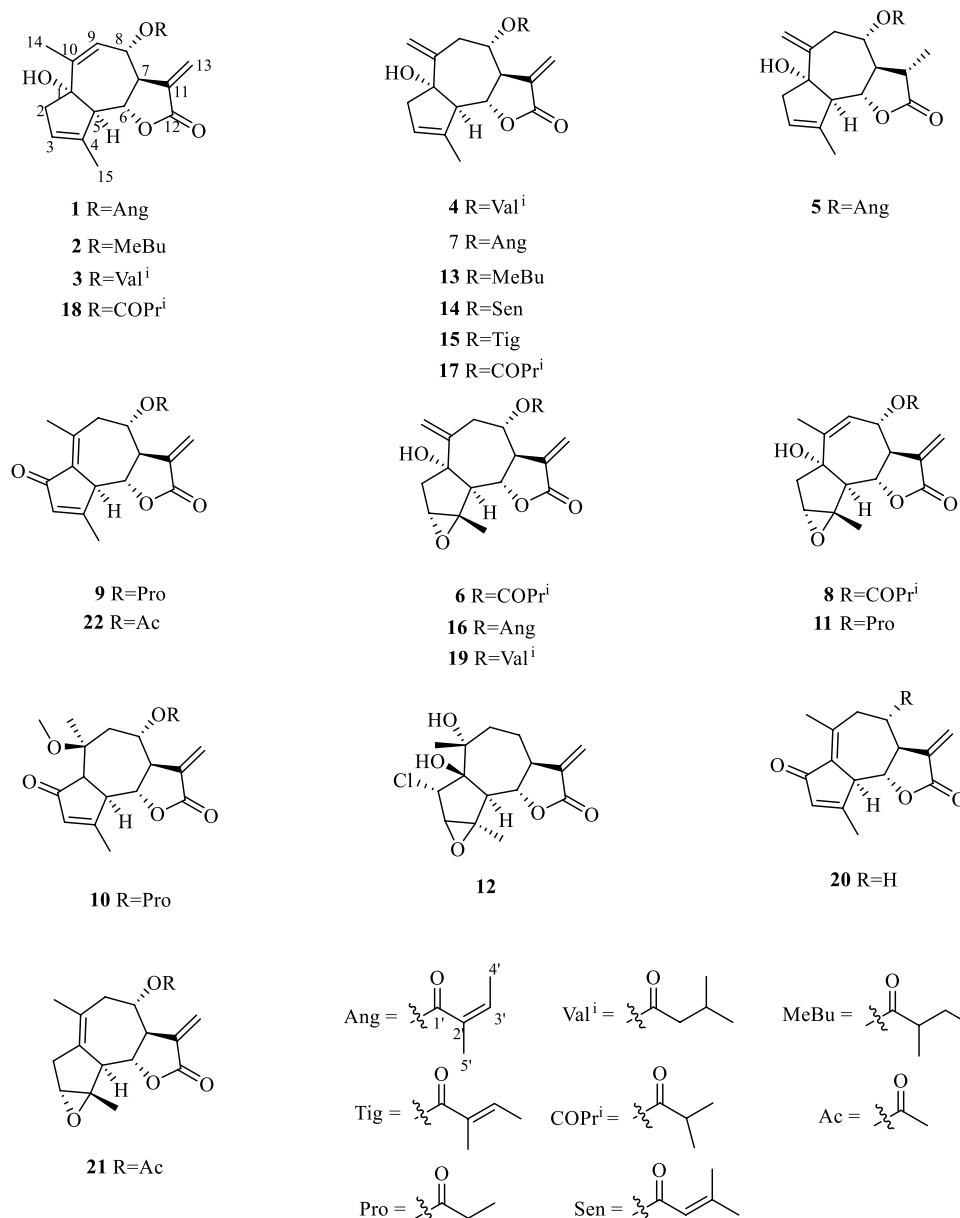


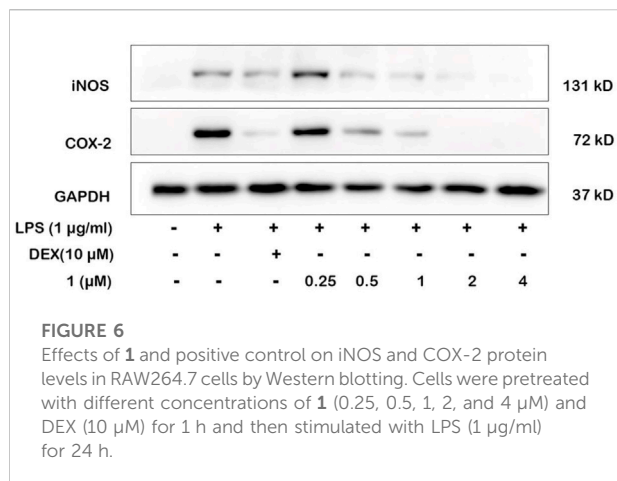
FIGURE 5

Structures of compounds 1–22 isolated from *A. vulgaris*.

isovaleryloxy group is absent. It could be aided by the HMBC correlation between the proton signal at δ_{H} 4.96 (1H, td, 9.9, 2.1 Hz, H-8) and the carbonyl carbon signal at δ_{C} 176.4 (C-1'). In addition, the main difference was ascribed to the absence of a cyclic olefinic bond at C-3 and C-4 in **6**, but an additional ring connected via an oxygen atom. The aforementioned reasoning was based on the correlation of H-2'/H₃-3' (H₃-4') in the ¹H–¹H COSY spectrum and the cross peak from H-2'/H₃-3' (H₃-4') to C-1' in the HMBC spectrum (Figure 1). The single-crystal X-ray diffraction experiment with Cu K α radiation [CCDC,2164101]

confirmed the 2D structure of **6** and defined its absolute configuration as 1S,3R,4S,5R,6S,7R,8S. Therefore, the absolute configuration of compound **6** was established as shown (Figure 4).

Artemvulactone N (**7**) was obtained as a colorless oil. The molecular formula C₂₀H₂₄O₅ was deduced from the HRESIMS at m/z 345.1703 [M + H]⁺ (calcd for 345.1697). The IR spectra revealed that **7** possessed hydroxy, carbonyl, and olefinic groups. In the NMR spectra of **7** (Tables 1, 3), the signals at δ_{H} 5.16 (1H, s, H-14a), 5.44 (1H, s, H-14b), δ_{C} 144.1 (C-10), and 117.6 (C-14)



revealed that a terminal double bond was located at C-10, which was supported by the HMBC correlations from H₂-14 to C-1 and C-8. The NMR spectra of **7** (Tables 1, 3) were very similar to compound **4**, except that the isovaleryloxy substituent at C-8 in **4** was replaced by an angeloyloxy group in **7**. The absolute configuration of 1S,5R,6S,7R,8S was confirmed by the comparison of experimental and calculated ECD spectra (Figure 3).

Artemvulactone O (**8**) gave a molecular formula of C₁₉H₂₄O₆ as defined by the HRESIMS ion at m/z 371.1456 [M + Na]⁺ (calcd for 371.1465). The presence of hydroxy (3,476 cm⁻¹), carbonyl (1,769 and 1,730 cm⁻¹), and olefinic (1,658 cm⁻¹) functionalities was evident from the spectroscopic data. The ¹H and ¹³C NMR spectra of **8** manifested that it was structurally similar to **6**. The main difference was the position of a double bond, which was verified by the HMBC correlations from H₃-14 to C-9 (Figure 1). The absolute configuration of 1S,3R,4S,5R,6S,7R,8S was determined by means of a single crystal X-ray crystallographic diffraction experiment with Cu Kα radiation (CCDC, 2164105, Figure 4).

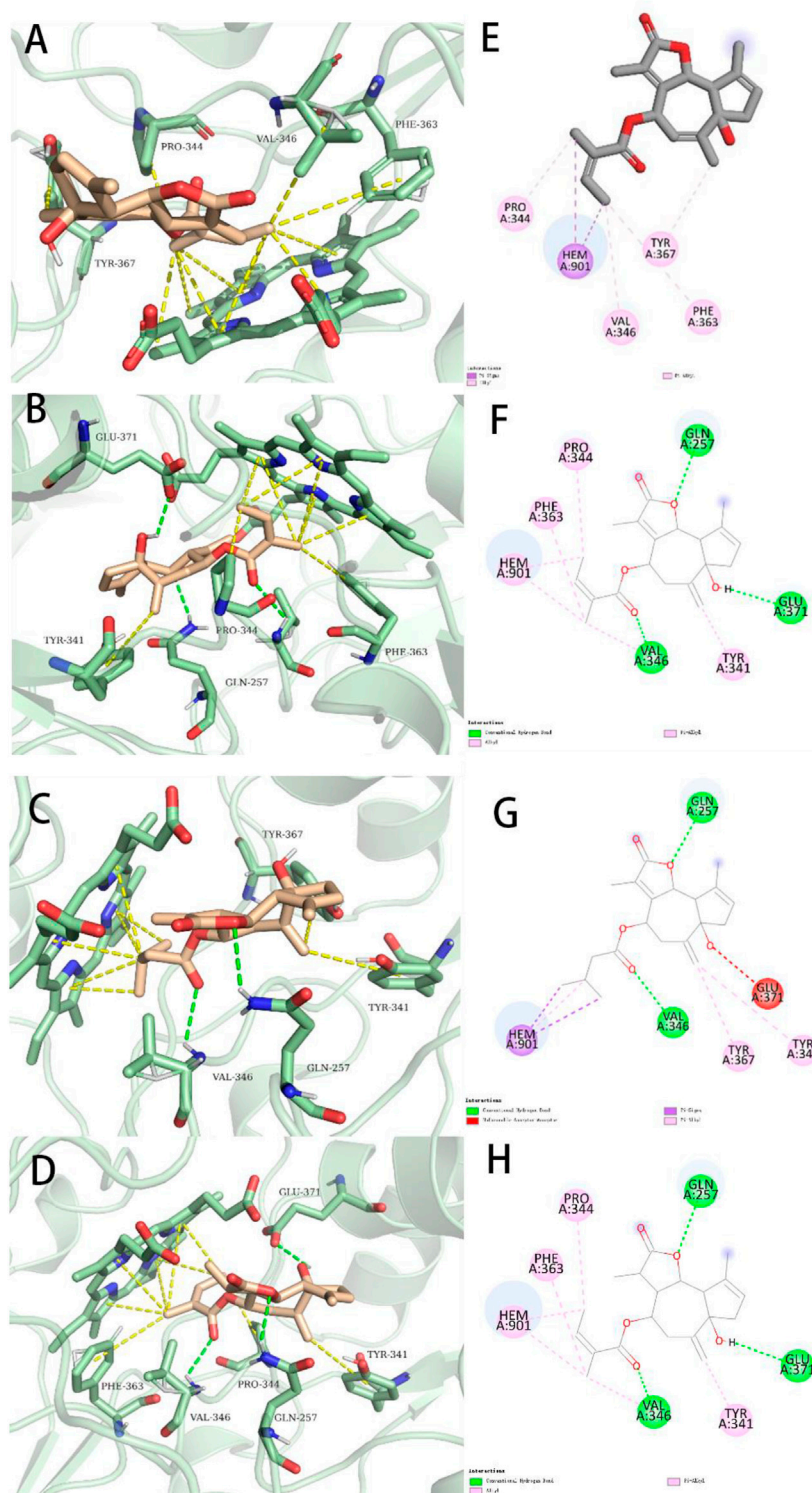
Artemvulactone P (**9**) was isolated as a colorless oil. According to the HRESIMS ([M + H]⁺, m/z 317.1370, calcd for 317.1384) and the 1D NMR spectrum, the molecular formula of **9** was assigned as C₁₈H₂₀O₅. The IR absorption bands at 1,773, 1,737, and 1,673 cm⁻¹ confirmed the existence of carbonyl and olefinic groups, with one less hydroxyl group than compound **1**. Additionally, the propionyl group was attached to oxygen-linked carbon at C-8, which could be demonstrated by the signals at δ_C 173.3 (C-1'), 27.8 (C-2'), and 9.1 (C-3'). In the 1D NMR spectrum, the characteristic signals of methylene [δ_H 2.65 (2H, m, H-2); δ_C 46.3 (C-2)] in **1** were replaced by a carbonyl in **9** at C-2 (δ_C 195.1). Based on the application of the TD-SCF ECD calculation method, the similarity of the calculated ECD spectrum with its experimental spectrum indicated the 5R,6R,7S,8R configuration of **9** (Figure 3).

Artemvulactone Q (**10**) showed the same molecular formula as that of compound **8**. The carbonyl and olefinic groups also existed in the structure of **10**, which were attributable to the IR absorptions at 1,770, 1,736, and 1,629 cm⁻¹. The compound **10** differed from **9** by one more methoxy group and one less cyclic olefinic bond in its chemical structure at C-10. The aforementioned analysis was confirmed by the ¹H-¹H COSY correlations of H-1/H-9/H₃-14/H₃-16 and HMBC correlations from δ_H 3.24 (–OCH₃) to δ_C 76.5 (C-10). The absolute configuration of compound **10** was established based on a single-crystal X-ray crystallographic diffraction experiment with Cu Kα radiation (Figure 4).

Artemvulactone R (**11**) was obtained as a white powder and assigned a molecular formula of C₁₈H₂₂O₆ by HRESIMS and ¹³C NMR data. The IR absorption bands of **11** implied hydroxy, carbonyl, and olefinic groups. The 1D NMR data (Tables 2, 3) revealed a definite structural variation between **11** and **8**. The main difference was that, compound **11** possessed one less methyl group at C-2' [δ_H 2.42 (2H, dd, 15.0, 7.5 Hz, H-2'); δ_C 27.9 (C-2')], which was defined based on the ¹H-¹H COSY

TABLE 4 Cytotoxicity against RAW264.7 cells and NO Inhibition of **1–12** and Dexamethasone toward LPS-Induced RAW264.7 cells (Mean ± SD).

Compound	IC ₅₀ (µM)	CC ₅₀ (µM)	Compound	IC ₅₀ (µM)	CC ₅₀ (µM)
1	1.1 ± 0.1	>10	13	1.5 ± 0.1	>15
2	1.2 ± 0.3	>10	14	1.4 ± 0.2	>15
3	2.8 ± 0.1	>10	15	1.2 ± 0.1	>10
4	3.6 ± 0.1	>20	16	1.1 ± 0.2	>10
5	>10	>100	17	1.5 ± 0.1	>20
6	3.1 ± 0.1	>20	18	1.1 ± 0.1	>20
7	2.1 ± 0.6	>20	19	1.0 ± 0.2	>25
8	3.2 ± 0.1	>20	20	1.8 ± 0.1	>70
9	1.9 ± 0.8	>20	21	1.2 ± 0.2	>20
10	2.1 ± 0.1	>10	22	1.8 ± 0.2	>10
11	1.9 ± 0.4	>15	Dexamethasone	4.3 ± 0.3	—
12	2.7 ± 0.5	>40			

**FIGURE 7**

Representations of lowest energy docking poses of compounds 1 (A), 7 (B), 4 (C), and 5 (D) bound to the iNOS protein (PDB ID:3E6T). Intermolecular interactions between iNOS and compounds 1 (E), 7 (F), 4 (G), and 5 (H) are highlighted by 2-D interaction maps.

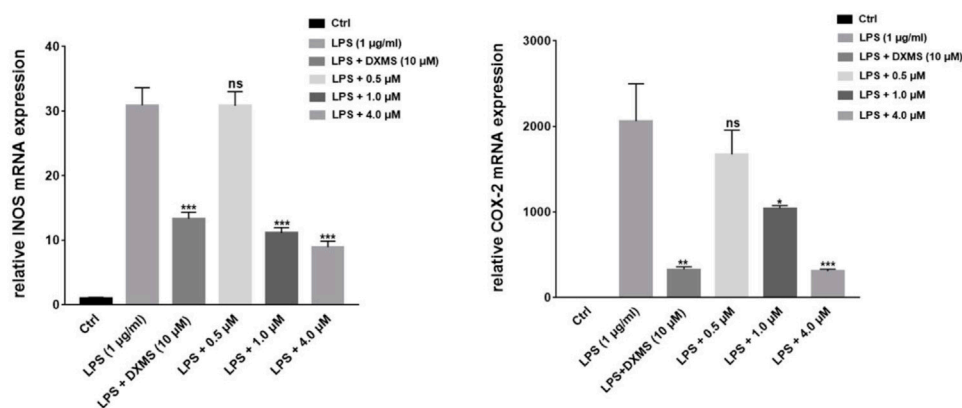


FIGURE 8

Compound 1 on the downregulation of LPS-induced iNOS and COX-2 mRNA expression in RAW264.7 cells. * $p < 0.05$, ** $p < 0.01$, *** $p < 0.001$, compared to the LPS-treated groups.

correlations of H_2-2'/H_3-3' and HMBC correlations from H_3-3' to C-1' and C-2' (Figure 1). The calculated ECD spectrum for the absolute configuration was consistent with the experimental ECD spectrum of compound 11.

Artemvulactone S (12), isolated as a white powder, had the molecular formula of $C_{15}H_{19}ClO_5$, implying six degrees of unsaturation. The IR absorption bands at 3,328, 1,769, and $1,642\text{ cm}^{-1}$ suggested hydroxy, carbonyl, and olefinic groups. The resonances for two methyl singlets at δ_H 1.40 (H_3-14) and 1.75 (H_3-15), a pair of terminal olefinic protons at δ_H 5.47 (1H, d, $J = 3.3\text{ Hz}$, $H-13a$) and 6.18 (1H, d, $J = 3.3\text{ Hz}$, $H-13b$) were observed in the 1H NMR spectrum. The ^{13}C NMR and HSQC spectra revealed that 12 is a sesquiterpene lactone. And the absolute configuration of compound 12 was determined by single crystal X-ray diffraction (Cu K α) (Figure 4).

Additionally, 10 known compounds were isolated and their structures were identified by comparing their physical and spectroscopic data with the reported data (Figure 5). The known compounds were identified as 1 α -hydroxy-8 α -methylbutyroxy-3(4),10(14),11(13)-trienguai-12,6 α -olide (13) (Huang et al., 2010), 1 α -hydroxy-8 α -seneciocyloxy-3(4),10(14),11(13)-trienguai-12,6 α -olide (14) (Huang et al., 2010), 8-epi-Tiglylrupicolin B (15) (Ober et al., 1985), 8-angeloyloxy-1 α -hydroxy-3 α , 4 α -epoxy-5 α , 7 α H-10(14), 11(13)-guaidiene-12,6 α -olide (16) (Jin et al., 2004), 8-epi-isobutyrylrupicolin B (17) (Ober et al., 1984), 8-epi-isobutyrylrupicolin (18) (Ober et al., 1984), 3 α ,4 α -epoxyrupicolin E (19) (Jin et al., 2004), dehydroleucodine (20) (de Heluani et al., 1989), (+)-Arteglinin A (21) (Lee et al., 1971), and Dehydromatricarin (22) (Bohlmann and Zdero, 1978).

TABLE 5 Binding energy, Hydrophobic and Hydrogen bonds formed between INOS (PDB ID:3E6T) and ligands (1–12 and INOS co-crystal ligand 2650707-81-4).

Compound	Binding energy (kcal/mol)	Hydrophobic and Hydrogen bonds
7	−10.2	HEM-901, PHE-363, PRO-344, GLN-257, GLU-371, TYR-341, VAL-346
5	−9.8	HEM-901, PHE-363, PRO-344, GLN-257, GLU-371, TYR-341, VAL-346
4	−9.5	HEM-901, GLN-257, VAL-346, TYR-367, TYR-341
2	−9.3	HEM-901, GLN-257, VAL-346, TYR-367
3	−9.3	HEM-901, GLN-257, VAL-346, TYR-367
6	−9.1	TYR-367, HEM-901, VAL-346, PRO-344, GLN-257
1	−8.9	HEM-901, PRO-344, VAL-346, ASP-376, ARG-362
8	−8.9	ARG-382, ASP-376, VAL-346, TYR-367, HEM-901
11	−8.3	HEM-901, PRO-344, VAL-346, ASP-376, ARG-382
9	−8.2	HEM-901, GLN-257, VAL-346, ARG-260, PRO-344, TYR-367, TYR-341
12	−8.1	TRP-457, GLNN-257, GLU-371, ARG-375
10	−7.6	ARG-260, ARG-375, TYR-367
Dexamethasone	−8.8	ARG-382, ALA-276, HEM-901, TYR-485, TRP-457

3.2 Anti-inflammatory effects for the intervention of NO production in LPS-induced RAW264.7 cells

Inhibition of NO overexpression is an essential indicator for evaluating small molecules with anti-inflammatory activities. Thus, the inhibitory effects of compounds **1–22** on LPS-mediated NO production were tested, and it was found that isolated sesquiterpenoids except compound **5** exhibited a concentration-dependent NO production inhibitory activity with IC₅₀ values ranging from 1.0 to 3.6 μ M (Table 4). It was preliminarily concluded that the isolated compounds had the potential to be developed into anti-inflammatory drugs.

NO production is directly related to the expressions of iNOS and COX-2. We selected the most active compound **1** for gene and protein level verification. The results of experiments demonstrated that compound **1** at 4 μ M reduced more expressions of iNOS and COX-2 than the positive drug (Dexamethasone) in LPS-induced macrophages by quantitative real-time PCR and Western blotting (Figures 6, 7). By comparing the structure and activity of the compounds, we preliminarily summarize the structure–activity relationship of guaiane-type sesquiterpene lactones in inhibiting inflammation: α -methylene- γ -lactone, α,β -unsaturated carbonyl moieties, and the ester side chain at C-8 are critical for cytotoxic activity.

To better compare the binding ability of docking compounds, dexamethasone and INOS were used for redocking. Molecular docking results showed that **1–12** and dexamethasone had a good interaction with the INOS targets by targeting residues in pockets. Figure 8 revealed the predicted geometry of **1**, **7**, **4** and **5** bound to the INOS protein. It was conformable to the results obtained through biological experiments. The free-binding energy and the number of binding residues are shown in Table 5, and that compounds **7**, **5**, and **4** were predicted to possess a stronger association with the protein. Previous research has shown that the type of substituent at C-8 also affects the compound activity: isovaleryloxy > acetyl > angeloyloxy > methylbutyryloxy (Sun et al., 2020). Combined with biological experiments, the hydroxyl group at C-1 was inferred to influence compound activity, and the following trend in activity for the side chain was summarized: angeloyloxy > methylbutyryloxy > isovaleryloxy. The aforementioned information rationalizes the results of molecular docking and biological experiments.

4 Conclusion

In conclusion, in our endeavor to search for anti-inflammatory compounds from *Artemisia vulgaris* L., 12 new and 10 known guaiane-type sesquiterpenoids were isolated and identified, of which compound **1** was the most potent inhibitor on NO release in LPS-stimulated RAW264.7 cells. The biological data confirmed that the expression of inflammatory enzymes of

iNOS and COX-2 was suppressed by **1** in LPS-stimulated RAW264.7 cells. The binding interactions of compound **1** with iNOS also confirmed the conclusion. Further mechanisms need to be further explored. Accordingly, **1** displayed the therapeutic potential for modulating inflammation.

Data availability statement

The datasets presented in this study can be found in online repositories. The names of the repository/repositories and accession number(s) can be found in the article/Supplementary Material.

Author contributions

All authors listed have made a substantial, direct, and intellectual contribution to the work and approved it for publication.

Funding

This work was supported by the Guangdong Province Modern Agricultural Industry Technology System Innovation Team Project (Grant No. 2020KJ142 and 2021KJ142) and the Key Research and Development Plan of Guangzhou (Grant No. 202206010008).

Conflict of interest

Authors C-WQ, ZR, and Y-FW were employed by the company GuangZhou (Jinan) Biomedical Research and Development Center Co., Ltd.

The remaining authors declare that the research was conducted in the absence of any commercial or financial relationships that could be construed as a potential conflict of interest.

Publisher's note

All claims expressed in this article are solely those of the authors and do not necessarily represent those of their affiliated organizations, or those of the publisher, the editors, and the reviewers. Any product that may be evaluated in this article, or claim that may be made by its manufacturer, is not guaranteed or endorsed by the publisher.

Supplementary material

The Supplementary Material for this article can be found online at: <https://www.frontiersin.org/articles/10.3389/fchem.2022.948714/full#supplementary-material>

References

- Abiri, R., Silva, A. L. M., de Mesquita, L. S. S., de Mesquita, J. W. C., Atabaki, N., de Almeida, E. B., Jr, et al. (2018). Towards a better understanding of *Artemisia vulgaris*: Botany, phytochemistry, pharmacological and biotechnological potential. *Food Res. Int.* 109, 403–415. doi:10.1016/j.foodres.2018.03.072
- Blagojević, P., Radulović, N., Palić, R., and Stojanović, G. (2006). Chemical composition of the essential oils of Serbian wild-growing *Artemisia absinthium* and *Artemisia vulgaris*. *J. Agric. Food Chem.* 54 (13), 4780–4789. doi:10.1021/jf060123o
- Bohlmann, F., and Zdero, C. (1978). New sesquiterpenes and acetylenes from *Athanasia* and *Pentzia* species. *Phytochemistry* 17 (9), 1595–1599. doi:10.1016/s0031-9422(00)94650-8
- Bora, K. S., and Sharma, A. (2011). The genus *Artemisia*: A comprehensive review. *Pharm. Biol.* 49 (1), 101–109. doi:10.3109/13880209.2010.497815
- Burley, S. K., Bhikadiya, C., Bi, C., Bittrich, S., Chen, L., Crichlow, G. V., et al. (2021). RCSB protein Data Bank: Powerful new tools for exploring 3D structures of biological macromolecules for basic and applied research and education in fundamental biology, biomedicine, biotechnology, bioengineering and energy sciences. *Nucleic Acids Res.* 49 (D1), D437–D451. doi:10.1093/nar/gkaa1038
- de Heluani, C. S., de Lampasona, M. P., Catalán, C. A., Goedken, V. L., Gutiérrez, A. B., Herz, W., et al. (1989). Guaianolides, heliangolides and other constituents from *Stevia alpina*. *Phytochemistry* 28 (7), 1931–1935. doi:10.1016/s0031-9422(00)97889-0
- Duke, J., and Bogenschutz, M. J. (1994). *Dr. Duke's phytochemical and ethnobotanical databases*. Washington, DC: USDA, Agricultural Research Service.
- Ekiert, H., Pajor, J., Klin, P., Rzepiela, A., Ślesak, H., Szopa, A., et al. (2020). Significance of *Artemisia vulgaris* L. (Common Mugwort) in the history of medicine and its possible contemporary applications substantiated by phytochemical and pharmacological studies. *Molecules* 25 (19), 4415. doi:10.3390/molecules25194415
- Forli, S., Huey, R., Pique, M. E., Sanner, M. F., Goodsell, D. S., Olson, A. J., et al. (2016). Computational protein–ligand docking and virtual drug screening with the AutoDock suite. *Nat. Protoc.* 11 (5), 905–919. doi:10.1038/nprot.2016.051
- Funk, V. A. (2009). *Systematics, evolution, and biogeography of Compositae*. Bratislava, Slovakia: International Association for Plant Taxonomy.
- Hershoff, A. (2001). *Herbal remedies: A quick and easy guide to common disorders and their herbal remedies*. Penguin: Herbal Remedies.
- Huang, Z., Pei, Y., Liu, C., Lin, S., Tang, J., Huang, D., et al. (2010). Highly oxygenated guaianolides from *Artemisia dubia*. *Planta Med.* 76 (15), 1710–1716. doi:10.1055/s-0030-1249957
- Jin, H. Z., Lee, J. H., Lee, D., Hong, Y. S., Kim, Y. H., Lee, J. J., et al. (2004). Inhibitors of the LPS-induced NF- κ B activation from *Artemisia sylvatica*. *Phytochemistry* 65 (15), 2247–2253. doi:10.1016/j.phytochem.2004.06.034
- Kumari, A., Karnatak, M., Singh, D., Shankar, R., Jat, J. L., Sharma, S., et al. (2019). Current scenario of artemisinin and its analogues for antimalarial activity. *Eur. J. Med. Chem.* 163, 804–829. doi:10.1016/j.ejmech.2018.12.007
- Lee, K. H., Matsueda, S., and Geissman, T. A. (1971). Sesquiterpene lactones of *Artemisia*: New guaianolides from fall growth of *A. Douglasiana*. *Phytochemistry* 10 (2), 405–410. doi:10.1016/s0031-9422(00)94057-3
- Liang, M. P. (2003). WebFEATURE: An interactive web tool for identifying and visualizing functional sites on macromolecular structures. *Nucleic Acids Res.* 31 (13), 3324–3327. doi:10.1093/nar/gkg553
- Lone, S. H., Bhat, K. A., and Khuroo, M. A. (2015). Argabin: From isolation to antitumor evaluation. *Chem. Biol. Interact.* 240, 180–198. doi:10.1016/j.cbi.2015.08.015
- Nguyen, N. T., Nguyen, T. H., Pham, T. N. H., Huy, N. T., Bay, M. V., Pham, M. Q., et al. (2020). Autodock vina adopts more accurate binding poses but Autodock4 forms better binding affinity. *J. Chem. Inf. Model.* 60 (1), 204–211. doi:10.1021/acs.jcim.9b00778
- Ober, A. G., Quijano, L., Urbatsch, L. E., and Fischer, N. H. (1984). Guaianolides from *Calea subcordata*. *Phytochemistry* 23 (6), 1289–1292. doi:10.1016/s0031-9422(00)80443-4
- Ober, A. G., Urbatsch, L. E., and Fischer, N. H. (1985). Guaianolides and chromenes from *Calea* species. *Phytochemistry* 24 (4), 795–799. doi:10.1016/s0031-9422(00)84897-9
- Pires, J. M., Mendes, F. R., Negri, G., Almeida, J. M. D., and Carlini, E. A. (2009). Antinociceptive peripheral effect of *Achillea millefolium* L. And *Artemisia vulgaris* L.: Both plants known popularly by brand names of analgesic drugs. *Phytother. Res.* 23 (2), 212–219. doi:10.1002/ptr.2589
- Rasheed, T., Bilal, M., Iqbal, H. M. N., and Li, C. (2017). Green biosynthesis of silver nanoparticles using leaves extract of *Achillea millefolium* L. And *Artemisia vulgaris* L.: Both plants known popularly by brand names of analgesic drugs. *Phytother. Res.* 23 (2), 212–219. doi:10.1002/ptr.2589
- Rasheed, T., Bilal, M., Iqbal, H. M. N., and Li, C. (2017). Green biosynthesis of silver nanoparticles using leaves extract of *Achillea millefolium* L. And *Artemisia vulgaris* L.: Both plants known popularly by brand names of analgesic drugs. *Phytother. Res.* 23 (2), 212–219. doi:10.1002/ptr.2589
- Saleh, A. M., Aljada, A., Rizvi, S. A., Nasr, A., Alaskar, A. S., Williams, J. D., et al. (2014). *In vitro* cytotoxicity of *Artemisia vulgaris* L. essential oil is mediated by a mitochondria-dependent apoptosis in HL-60 leukemic cell line. *BMC Complement. Altern. Med.* 14 (1), 226. doi:10.1186/1472-6882-14-226
- Schmid-Grendelmeier, P., Holzmann, D., Himly, M., Weichel, M., Tresch, S., Rückert, B., et al. (2003). Native Art v 1 and recombinant Art v 1 are able to induce humoral and T cell-mediated *in vitro* and *in vivo* responses in mugwort allergy. *J. Allergy Clin. Immunol.* 111 (6), 1328–1336. doi:10.1067/mai.2003.1495
- Seeliger, D., and de Groot, B. L. (2010). Ligand docking and binding site analysis with PyMOL and Autodock/Vina. *J. Comput. Aided. Mol. Des.* 24 (5), 417–422. doi:10.1007/s10822-010-9352-6
- Soon, L., Ng, P. Q., Chellian, J., Madheswaran, T., Panneerselvam, J., Gupta, G., et al. (2019). Therapeutic potential of *Artemisia vulgaris*: An insight into underlying immunological mechanisms. *J. Environ. Pathol. Toxicol. Oncol.* 38 (3), 205–216. doi:10.1615/jenviroxpatholtoxiconcol.2019029397
- Sun, Y., Ju, Y., Liu, C., Du, K., and Meng, D. (2020). Polyhydroxyl guaianolide terpenoids as potential NF- κ B inhibitors induced cytotoxicity in human gastric adenocarcinoma cell line. *Bioorg. Chem.* 95, 103551. doi:10.1016/j.bioorg.2019.103551
- Sundararajan, B., and Kumari, B. R. (2017). Novel synthesis of gold nanoparticles using *Artemisia vulgaris* L. leaf extract and their efficacy of larvicidal activity against dengue fever vector *Aedes aegypti* L. *J. Trace Elem. Med. Biol.* 43, 187–196. doi:10.1016/j.jtemb.2017.03.008
- Vina, A. (2010). Improving the speed and accuracy of docking with a new scoring function, efficient optimization, and multithreading Trott, Oleg; Olson. *Arthur. J. J. Comput. Chem.* 31 (2), 455–461.
- Weston, L. A., Barney, J. N., and DiTommaso, A. (2005). A review of the biology and ecology of three invasive perennials in New York state: Japanese knotweed (*polygonum cuspidatum*), mugwort (*Artemisia vulgaris*) and pale swallow-wort (*vincetoxicum rossicum*). *Plant and Soil* 277 (1), 53–69. doi:10.1007/s11104-005-3102-x



OPEN ACCESS

EDITED BY

Jian-Wei Dong,
Qujing Normal University, China

REVIEWED BY

Zheng Li,
Jiangsu Normal University, China
Cheng-Ting Zi,
Yunnan Agricultural University, China

*CORRESPONDENCE

Tianpeng Yin,
ytp@zmu.edu.cn

SPECIALTY SECTION

This article was submitted to Medicinal and Pharmaceutical Chemistry, a section of the journal Frontiers in Chemistry

RECEIVED 06 August 2022

ACCEPTED 05 September 2022

PUBLISHED 19 September 2022

CITATION

Yan Y, Jiang H, Yang X, Ding Z and Yin T (2022), Grandifolines A–F, new anti-inflammatory diterpenoid alkaloids isolated from *Delphinium grandiflorum*. *Front. Chem.* 10:1012874. doi: 10.3389/fchem.2022.1012874

COPYRIGHT

© 2022 Yan, Jiang, Yang, Ding and Yin. This is an open-access article distributed under the terms of the [Creative Commons Attribution License \(CC BY\)](https://creativecommons.org/licenses/by/4.0/). The use, distribution or reproduction in other forums is permitted, provided the original author(s) and the copyright owner(s) are credited and that the original publication in this journal is cited, in accordance with accepted academic practice. No use, distribution or reproduction is permitted which does not comply with these terms.

Grandifolines A–F, new anti-inflammatory diterpenoid alkaloids isolated from *Delphinium grandiflorum*

Yuanfeng Yan, Hongjun Jiang, Xiaoyan Yang, Zongbao Ding and Tianpeng Yin*

Department of Pharmacy, Zhuhai Campus of Zunyi Medical University, Zhuhai, Guangdong, China

Delphinium grandiflorum L. (family Ranunculaceae), one of the most important and widely distributed *Delphinium* species, has received considerable interest due to its extremely high medicinal value. The discovery of novel metabolites from *D. grandiflorum* supported and broadened its application as an herbal medicine. In this study, the whole herb of *D. grandiflorum* was phytochemically investigated to obtain fourteen C₁₉-lycaconitine-type diterpenoid alkaloids (**1–14**), including six undescribed alkaloids, grandifolines A–F (**1–6**). The structural elucidation of them was accomplished by detailed spectroscopic analyses, mainly including HR-MS, 1D and 2D NMR (¹H–¹H COSY, NOESY, HMBC and HSQC), and IR spectra. New alkaloids **1–3** and **5** possess a characteristic $\Delta^{2,3}$ functional group in the A ring, while compounds **5** and **6** feature a rare OH-16 substituent. In addition, known compounds **7–12** were isolated from *D. grandiflorum* for the first time. Moreover, according to its medicinal use, new alkaloids **1–6** were estimated for their potential *in vitro* anti-inflammatory effects, and some of them exhibited inhibitory effects on NO production in LPS-activated RAW 264.7 macrophages. Our work enriched the chemical diversity of *D. grandiflorum* and the genus *Delphinium* and presented beneficial information for further investigations.

KEYWORDS

delphinium grandiflorum, ranunculaceae, diterpenoid alkaloid, grandifolines A–F, anti-inflammatory activity

Introduction

The genus *Delphinium* L., which belongs to the tribe *Delphineae* in the family Ranunculaceae, is an important species-rich genus comprising approximately 400 species of annual, biennial, or perennial herbs. *Delphinium* plants prefer cold and humid conditions and are mainly distributed in mountainous regions in the north temperate zone, including Asia, Europe, North America, and sporadically North Africa (Wang, 2019). China is regarded as the distribution center for this genus, as more than half of the confirmed *Delphinium* species were reported to be grown within this country (232 species, 200 endemic), mainly in the high mountain areas in northern Yunnan,

eastern Tibet and western Sichuan (Chen et al., 2009; Wang, 2019). *Delphinium* plants are well-known ornamental plants with a long history around the world (Yin et al., 2020). Many *Delphinium* species, represented by *D. grandiflorum*, *D. elatum*, *Delphinium* × *belladonna*, feature showy flowers with various colors, including white, pink, blue, light blue, violet, purple, and lavender, which are particularly popular worldwide and have been widely cultivated as landscape and potted plants or cut flowers (Ichimura et al., 2009). On the other hand, in many countries and regions, such as China and India, *Delphinium* plants are commonly used as herbal medicines by natives for treating various diseases, mainly traumatic injury, enteritis, rheumatism, headache, toothache, neuralgia, and other kinds of pain. The multiple therapeutic effects of *Delphinium*-derived herbs could be attributed to the abundance of various active ingredients, including diterpenoid alkaloids (DAs), flavonoids, phenolic acids, and volatile oils (Marin, 2011). In particular, DAs, which have been acknowledged as the characteristic ingredients for this genus, have exhibited broad-spectrum biological activities, including analgesic, anti-inflammatory, antiarrhythmic, anticancer, antioxidant, and neuroprotective activities (Thawabteh et al., 2021; Liu et al., 2022). Further exploration and discovery of bioactive DAs with novel structures from *Delphinium* plants could support and broaden their application as medicinal plants.

D. grandiflorum L., one of the best-known *Delphinium* species, is widely distributed in China and other Asian countries, including Mongolia, Korea, and the Russian Far East (Siberia) (Liu et al., 2009; Chen et al., 2017; Xu et al., 2021). This plant has a particularly long history as an ornamental flower and has been cultivated as a horticultural plant in Beijing City of China for hundreds of years. In addition, its roots or whole herbs are used for treating traumatic injury, toothache, and asthma in traditional Chinese medicine (Li et al., 2019). In previous investigations, a number of DAs, mainly C₁₉-lycoctonine-type DAs, have been reported in *D. grandiflorum* (Batbayar et al., 2003; Wang et al., 2021), and some of them possess unprecedented DA skeletons. For example, Chen et al. reported two novel DAs, grandiflodine A and B, from *D. grandiflorum*. The former compound showed a C₁₉-lycaconitine-type DA skeleton with cleavage of N-C19 and C7-C17 bonds and linkage of the N-C7 bond, while the latter represents a rare hetisine-type C₂₀-DA with a broken N-C7 bond (Chen et al., 2017). In addition, two DAs, grandiflonines A and B reported by (Xu et al., 2021), possess an undescribed C₂₀-hetisine-type DA skeleton with an open E ring. These exciting discoveries highlight the significant chemical diversity of DAs in *D. grandiflorum* and promote further in-depth studies on them. Hence, as part of our ongoing research exploring bioactive DAs with novel structures from *Delphinium* plants (Yin et al., 2022), the whole herb of *D. grandiflorum* was phytochemically investigated to afford fourteen C₁₉-lycaconitine-type DAs (1–14), including six undescribed DAs, grandifloines A–F

(1–6) (Figure 1). The structural elucidation was accomplished by detailed spectroscopic analyses, mainly including 1D and 2D NMR, HR-MS, and IR spectra. Moreover, new alkaloids 1–6 were estimated for their potential anti-inflammatory effects in LPS-activated RAW 264.7 macrophages. This paper describes the extraction and isolation, structural elucidation, and activity screening of these compounds.

Materials and methods

General experimental procedures

1D (¹H, ¹³C, and DEPT) and 2D (HSQC, HMBC, ¹H–¹H COSY, and NOESY) NMR spectra were obtained on a Bruker AM-500 spectrometer (Bruker, Germany) in CDCl₃ or CD₃OD (Qingdao Tenglong, China), and TMS was used as an internal reference. IR spectra were scanned on a Nicolet Magna-IR 550 spectrometer (Thermo Nicolet, United States) with KBr pellets. Optical rotations were measured on a Jasco P-1020 digital polarimeter (Jasco, Japan). HR-ESI-MS spectra were obtained on an Agilent 6230 LC/TOF MS spectrometer (Agilent, United States). The prep-HPLC experiment was performed on an Agilent 1260 pump coupled with an analytical preparative ZORBAXSB column (21.2 × 500 m, 5 μm). Silica gel (300–400 mesh, Qingdao Haiyang, China) was used in column chromatography, and Dragendorff's reagent was used in TLC analysis (GF₂₅₄ TLC plates, Qingdao Haiyang, China).

Plant material

Whole herbs of *D. grandiflorum* were gathered in Longhua County of China in December 2020. The voucher specimen (2020-dg-1) identified by Zhang Jun from Kunming GenPHYTech Co., Ltd. is stored at Zunyi Medical University, China.

Extraction and isolation

The whole herbs of *D. grandiflorum* (20 kg) were air-dried, crushed, and then extracted with 95% ethanol three for 3 days at room temperature (three times). The extracted solutions were combined and evaporated under reduced pressure to obtain ethanol extracts (~2 kg), which were completely dissolved in water (2 L) at 70°C, adjusted to pH 1 with HCl and extracted with EtOAc (3 L × 3). After adjusting the acidic aqueous solution to pH 10 with sodium hydroxide, it was extracted with CHCl₃ to obtain the crude alkaloid (320 g).

The crude alkaloid was divided into five fractions (Fr.A–Fr.E) by silica gel CC eluted with a CHCl₃–CH₃OH

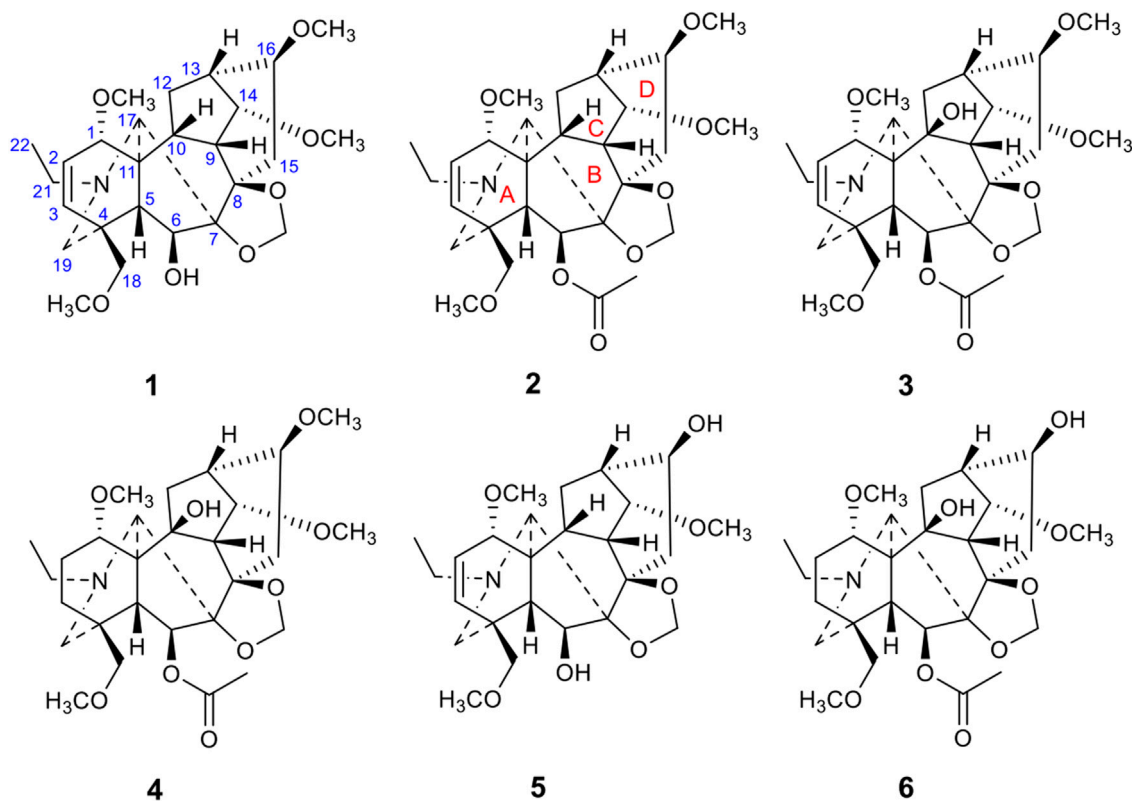


FIGURE 1
The chemical structures of six new diterpenoid alkaloids.

gradient system (100:1 \rightarrow 0:1). Fr.A (5.4 g) was separated by silica gel CC (CHCl_3 - CH_3OH - NH_4OH , 100:1:1) to yield two subfractions (Fr.A1 and Fr.A2). The former subfraction was purified on silica gel CC (CHCl_3 - CH_3OH , 1:1) to afford compound **7** (3 mg), while the latter was purified on silica gel CC (CHCl_3 - CH_3OH - NH_4OH , 100:1:1) to afford compound **2** (168 mg). Fr.B (20.7 g) was further purified by semipreparative HPLC over a ZORBAXSB C_{18} column eluted with petroleum ether-acetone-diethylamine (4:1:1) to obtain compound **1** (7 mg). Further silica gel CC purification of Fr.C (25.3 g) was carried out by elution with CH_3OH - H_2O (30:70 \rightarrow 80:20) to yield four subfractions (Fr.C1–Fr.C4). Subfraction Fr.C1 was separated on silica gel CC (CHCl_3 - CH_3OH - $\text{NH}_3\text{H}_2\text{O}$, 30:1:1) to obtain compounds **5** (5 mg) and **10** (98 mg), while subfraction Fr.C2 was purified by semipreparative HPLC (CH_3OH - H_2O , 65:35, 0.5% NH_4OH) to yield compound **3** (4 mg). Fr.C3 was subjected to silica gel CC (CHCl_3 - CH_3OH - NH_4OH , 100:1:1) to afford two subfractions (SFr.C3-1 and SFr.C3-2). Fr.C3-1 was further separated by silica gel CC (PE-acetone- $\text{NH}_3\text{H}_2\text{O}$, 2:1:1) to afford compounds **8** (6 mg) and **9** (15 mg), and Fr.C3-2 was purified by semipreparative HPLC (CH_3OH - H_2O , 70:30, 0.5% NH_4OH) to afford compounds **6** (7 mg) and **11** (12 mg).

Fr.C4 was separated on a silica gel CC (PE-acetone-diethylamine, 4:1:1) to give two subfractions (Fr.C4-1 and Fr.C4-2), which was purified by semipreparative HPLC (CH_3OH - H_2O , 70:30, 0.5% NH_4OH) to yield compounds **4** (13 mg) and **13** (2 mg). Fr.D (12.9 g) was purified by silica gel CC (PE-acetone- $\text{NH}_3\text{H}_2\text{O}$, 3:1:1) and semipreparative HPLC (CH_3OH - H_2O , 70:30, 0.5% NH_4OH) to afford compound **12** (28 mg). Fr.E (14.1 g) was separated by silica gel CC (CHCl_3 - CH_3OH - NH_4OH , 100:1:1 \rightarrow 220:1:1) along with semipreparative HPLC (CH_3OH - H_2O , 70:30, 0.5% NH_4OH) to afford compound **14** (43 mg).

Grandifoline A (**1**): white powder; IR (KBr, cm^{-1}): 3520, 2917, 2751, 1745, 1675, 1278, 1057, 805; $[\alpha]_D^{22} + 26.0$ ($c = 0.1$, CH_3OH). ^1H and ^{13}C NMR spectral data are shown in [Tables 1, 2](#). HR-ESI-MS m/z 478.2799 $[\text{M}+\text{H}]^+$ (calcd for $\text{C}_{26}\text{H}_{39}\text{NO}_7$, 478.2805).

Grandifoline B (**2**): white powder; IR (KBr, cm^{-1}): 2936, 2881, 1741, 1649, 1452, 1366, 1224, 853; $[\alpha]_D^{22} + 29.8$ ($c = 0.1$, CH_3OH). ^1H and ^{13}C NMR spectral data are shown in [Tables 1, 2](#). HR-ESI-MS m/z 520.2909 $[\text{M}+\text{H}]^+$ (calcd for $\text{C}_{28}\text{H}_{41}\text{NO}_8$, 520.2910).

Grandifoline C (**3**): white powder; IR (KBr, cm^{-1}): 3450, 2933, 2888, 1739, 1674, 1229, 1088, 819; $[\alpha]_D^{22} + 41.26$ ($c = 0.1$,

TABLE 1 ^{13}C NMR (125 MHz) data of compounds 1–6 (compounds 1–4 in CDCl_3 and compounds 5 and 6 in CD_3OD).

Nos	1	2	3	4	5	6
1	80.5 d	80.1 d	76.0 d	77.1 d	81.5 d	78.4 d
2	125.4 d	125.8 d	126.4 d	26.6 t	126.1 d	27.2 t
3	134.6 d	134.6 d	134.2 d	31.5 t	135.6 d	32.5 t
4	39.7 s	40.1 s	39.9 s	37.9 s	40.7 s	39.1 s
5	50.9 d	50.0 d	45.3 d	45.7 d	53.4 d	46.4 d
6	79.5 d	78.4 d	78.8 d	78.7 d	80.0 d	80.0 d
7	92.3 s	91.5 s	91.2 s	91.8 s	93.7 s	93.8 s
8	85.1 s	84.4 s	82.4 s	81.6 s	85.1 s	82.1 s
9	40.3 d	40.0 d	50.7 d	50.5 d	40.5 d	48.8 d
10	47.3 d	47.5 d	84.2 s	84.0 s	49.0 d	83.8 s
11	50.7 s	50.8 s	56.4 s	55.9 s	51.6 s	56.5 s
12	27.9 t	28.1 t	38.5 t	39.2 t	28.5 t	39.3 t
13	38.1 d	38.7 d	38.7 d	38.4 d	43.8 d	42.0 d
14	83.5 d	83.7 d	82.0 d	81.7 d	85.2 d	83.6 d
15	33.7 t	34.4 t	35.2 t	34.9 t	38.5 t	37.8 t
16	82.2 d	82.2 d	81.6 d	81.5 d	73.6 d	73.1 d
17	61.3 d	62.1 d	61.1 d	64.0 d	63.4 d	65.4 d
18	75.9 t	75.9 t	75.9 t	78.4 t	77.2 t	79.6 t
19	54.3 t	53.7 t	53.7 t	53.5 t	55.0 t	54.7 t
21	49.0 t	49.0 t	48.8 t	50.6 t	50.2 t	51.5 t
22	13.1 q	13.1 q	13.0 q	14.0 q	13.2 q	14.1 q
OCH ₂ O	93.2 t	93.8 t	94.4 t	94.1 t	94.3 t	94.7 t
OCH ₃ -1	56.3 q	56.1 q	56.1 q	55.5 q	56.1 q	55.7 q
OCH ₃ -14	58.0 q	57.8 q	57.9 q	57.9 q	58.0 q	58.2 q
OCH ₃ -16	56.5 q	56.4 q	56.3 q	56.4 q		
OCH ₃ -18	59.8 q	59.7 q	59.7 q	59.5 q	59.7 q	59.6 q
OAc-6		170.1 s	169.9 s	170.0 s		171.9 s
		21.8 q	21.8 q	21.8 q		21.6 q

CH_3OH). ^1H and ^{13}C NMR spectral data are shown in Tables 1, 2. HR-ESI-MS m/z 536.2855 $[\text{M}+\text{H}]^+$ (calcd for $\text{C}_{28}\text{H}_{41}\text{NO}_9$, 536.2859).

Grandifoline D (4): white powder; IR (KBr, cm^{-1}): 3515, 2934, 2874, 1739, 1650, 1366, 1090, 852; $[\alpha]_{\text{D}}^{22}$ -16.92 ($c = 0.1$, CH_3OH). ^1H and ^{13}C NMR spectral data are shown in Tables 1, 2. HR-ESI-MS m/z 538.3012 $[\text{M}+\text{H}]^+$ (calcd for $\text{C}_{28}\text{H}_{43}\text{NO}_9$, 538.3016).

Grandifoline E (5): white powder; IR (KBr, cm^{-1}): 3437, 2964, 2824, 1740, 1647, 1397, 1078, 813; $[\alpha]_{\text{D}}^{22}$ +13.8 ($c = 0.1$, CH_3OH). ^1H and ^{13}C NMR spectral data are shown in Tables 1, 2. HR-ESI-MS m/z 464.2643 $[\text{M}+\text{H}]^+$ (calcd for $\text{C}_{25}\text{H}_{37}\text{NO}_7$, 464.2648).

Grandifoline F (6): white amorphous powder; IR (KBr, cm^{-1}): 3467, 2932, 2875, 1741, 1631, 1245, 1054, 852; $[\alpha]_{\text{D}}^{22}$ -37.48 ($c = 0.1$, CH_3OH). ^1H and ^{13}C NMR spectral data are shown in Tables 1, 2. HR-ESI-MS m/z 524.2854 $[\text{M}+\text{H}]^+$ (calcd for $\text{C}_{27}\text{H}_{41}\text{NO}_9$, 524.2859).

NO production in RAW264.7 macrophages

A previously reported method was adopted to evaluate the *in vitro* anti-inflammatory activities of the newly isolated alkaloids (Wang et al., 2019). RAW264.7 cells were plated into 96-well microplates, stimulated with $1\text{ }\mu\text{g/ml}$ LPS, and treated with the alkaloid under test. The nondrug group and L-NMMA-treated group were set as blank and positive controls, respectively. After the macrophages were cultivated overnight, the NO content in the medium and the absorbance of the solution were measured at 570 nm. To exclude the toxic effects of the compound on the cells, MTS was added to the remaining medium to detect cell survival. The inhibition rate on NO generation was calculated by the following equation: inhibition rate (%) = $(\text{OD}_{\text{nondrug group}} - \text{OD}_{\text{sample group}}) / \text{OD}_{\text{nondrug group}} \times 100\%$.

Results and discussion

Structural identification of new compounds

Compound 1, a white powder, exhibited a *pseudo* ion peak at m/z 478.2799 $[\text{M}+\text{H}]^+$ in its HR-MS spectrum, which corresponded to the molecular formula $\text{C}_{26}\text{H}_{39}\text{NO}_7$, with an unsaturation degree of eight. Its ^1H NMR spectrum revealed the existence of an NCH_2CH_3 group (δ_{H} 1.08, t, $J = 7.2$ Hz, 3H), a characteristic *cis*-trisubstituted double bond (δ_{H} 6.03, dd, $J = 9.9$ Hz, 3.6 Hz; 5.95, d, $J = 9.9$ Hz; each 1H), four methoxyl (OCH_3) groups (δ_{H} 3.32, 3.36, 3.38, 3.43, s, each 3H), and a methylenedioxy (OCH_2O) group (δ_{H} 5.08, 5.12, s, each 1H). The ^{13}C NMR spectrum suggested that compound 1 possesses 19 carbons in addition to the NCH_2CH_3 , methoxy, and methylenedioxy groups, including four diagnostic quaternary carbons at δ_{H} 39.7 s, 50.7 s, 85.1 s, and 92.3 s (Yin et al., 2022). Combining the above data with biogenetic considerations implied that compound 1 could be a C_{19} -lycoctonine-type DA (Meng et al., 2017). Seven oxygenated carbons were observed in the ^{13}C NMR spectrum (δ_{C} 75.9 t, 79.5 d, 80.5 d, 82.2 d, 83.5 d, 85.1 s, 92.3 s), in addition to the molecular formula, suggesting an extra OH group in addition to the OCH_3 and OCH_2O groups. According to the HMBC correlations from OCH_3 -1 (δ_{H} 3.32, s) to C-1 (δ_{C} 80.5 d), OCH_3 -14 (δ_{H} 3.43 s) to C-14 (δ_{C} 83.5 d), OCH_3 -16 (δ_{H} 3.38 s) to C-16 (δ_{C} 82.2 d), and OCH_3 -18 (δ_{H} 3.36 s) to C-18 (δ_{C} 75.9 t), four OCH_3 groups were located at C-1, C-14, C-16, and C-18 (Figure 2). The OCH_2O group was placed at C-7 and C-8 as revealed by the long-range correlations from the methylene protons to C-7 and C-8. In addition, on the basis of the HMBC correlation networks from H-6 (δ_{H} 4.28, brs) to C-5 (δ_{C} 50.9 d), C-7 (δ_{C} 92.3 s), and C-11 (δ_{C} 50.7 s), the hydroxyl

TABLE 2 ¹H NMR (500 MHz, δ_H , Mult., J in Hz) data of compounds 1–6 (compounds 1–4 in CDCl₃ and compounds 5 and 6 in CD₃OD).

Nos	1	2	3	4	5	6
1	3.40 d (3.6)	3.42 d (3.5)	3.82 d (3.9)	3.48 m	3.45 d (3.5)	3.59 m
2	6.03 dd (9.9, 3.6)	6.05 dd (10.0, 3.5)	6.10 dd (9.8, 3.9)	a 2.10 m b 2.18 m	5.97 dd (10.0, 3.5)	a 2.10 m b 2.20 m
3	5.95 d (9.9)	5.92 d (10.0)	5.91 d (9.8)	a 1.70 m b 1.41 m	5.91 d (10.0)	a 1.69 m b 1.36 m
4	—	—	—	—	—	—
5	1.83 d (2.2)	1.87 d (2.4)	2.12 d (2.4)	1.83 d (2.4)	1.68 d (2.3)	2.05d (3.7)
6	4.28 brs	5.47 brs	5.51 brs	5.51 brs	4.24 brs	5.50 brs
7	—	—	—	—	—	—
8	—	—	—	—	—	—
9	3.67 t (4.3)	3.53 t (7.2)	3.31 d (5.1)	3.30 d (5.1)	3.81 t (5.1)	3.54 d (5.0)
10	2.23 m	2.23 m	—	—	2.21 m	—
11	—	—	—	—	—	—
12	a 2.21 m b 1.93 m	a 2.25 m b 1.91 m	a 2.82 d (14.9) b 1.84 d (14.9)	a 3.21 t (5.4) b 1.73 t (5.4)	a 2.16 m b 1.91 m	a 2.74 dd (7.3, 8.0) b 1.75 dd (7.3, 8.0)
13	2.40 m	2.38 m	2.56 m	2.53 m	2.22 m	2.37 m
14	3.70 t (5.2)	3.71 t (5.0)	4.13 t (5.7)	4.12 t (4.5)	3.75 t (4.0)	4.24 t (6.0)
15	2.53 dd (14.4, 8.6) 1.88 dd (14.4, 8.6)	2.50 dd (12.8, 6.8) 1.85 dd (12.8, 6.8)	2.52 t (8.1) 1.88 t (8.1)	2.49 t (7.4) 1.83 t (7.4)	2.48 dd (15.0, 7.5) 1.81 dd (15.0, 7.5)	2.51 dd (16.6, 9.1) 1.71 dd (16.6, 9.1)
16	3.26 t (8.4)	3.27 t (9.0)	3.22 t (9.2)	3.19 t (8.9)	3.67 t (8.2)	3.61 t (7.8)
17	3.13 s	3.18 s	3.14 s	3.11 s	3.17 s	3.26 s
18	a 3.31 ABq (9.2) b 3.23 ABq (9.2)	3.30 ABq (8.2) 3.16 ABq (8.2)	a 3.32 ABq (9.5) b 3.21 ABq (9.5)	a 3.21 ABq (9.2) b 3.06 ABq (9.2)	a 3.26 ABq (9.2) b 3.28 ABq (9.2)	a 3.16 ABq (9.2) b 3.06 ABq (9.2)
19	a 2.45 ABq (11.2) b 2.32 ABq (11.2)	a 2.48 ABq (11.5) b 2.44 ABq (11.5)	a 2.51 ABq (8.5) b 2.49 ABq (8.5)	a 2.71 ABq (11.9) b 2.40 ABq (11.9)	a 2.40 ABq (11.6) b 2.31 ABq (11.6)	a 2.73 ABq (11.4) b 2.38 ABq (11.4)
21	a 2.90 m b 2.60 m	a 2.97 m b 2.63 m	a 2.97 m b 2.63 m	a 2.72 m b 2.81 m	a 2.89 m b 2.56 m	a 2.70 m b 2.81 m
22	1.08 t (7.2)	1.07 t (7.1)	1.07 t (7.2)	1.06 t (7.2)	1.03 t (7.0)	1.05 t (7.2)
OCH ₂ O	a 5.12 s b 5.08 s	a 4.95 s b 4.94 s	a 4.97 s 4.96 s	4.94 s 4.92 s	a 5.14 s b 5.01 s	4.88 s 4.86 s
OCH ₃ -1	3.32 s	3.34 s	3.34 s	3.26 s	3.30 s	3.27 s
OCH ₃ -14	3.43 s	3.44 s	3.45 s	3.44 s	3.43 s	3.47 s
OCH ₃ -16	3.38 s	3.36 s	3.35 s	3.33 s		
OCH ₃ -18	3.36 s	3.30 s	3.30 s	3.25 s	3.33 s	3.23 s
OAc-6		2.08 s	2.09 s	2.08 s		2.05 s

group was determined to be connected to C-6 (δ_C 79.5). The double bond was located at C-2 and C-3 based on the ¹H–¹H COSY correlation between H-1 and H-2, which was further confirmed by the HMBC correlations from H-2 to C-1 and C-11 and from H-3 to C-4, C-5, and C-18. Finally, the relative configuration of **1** was deduced from the NOESY experiment (Figure 3). The α -orientation of OCH₃-1 was confirmed by the NOESY correlation between H-1 β and H-10 β , and between H-1 β

and H-12 β . The β -orientation of OH-6 was deduced from the NOESY correlation between H-1 β and H-10 β , and between H-1 β and H-12 β . The orientations of the remaining oxygenated substituents are identical for all lycotonine-type DAs, namely, the α -orientation of OCH₃-14 and the β -orientation of OCH₃-16, OCH₃-18, and OCH₂O (Ablajan et al., 2018). Hence, the structure of **1** was established with the assigned NMR data in Tables 1, 2.

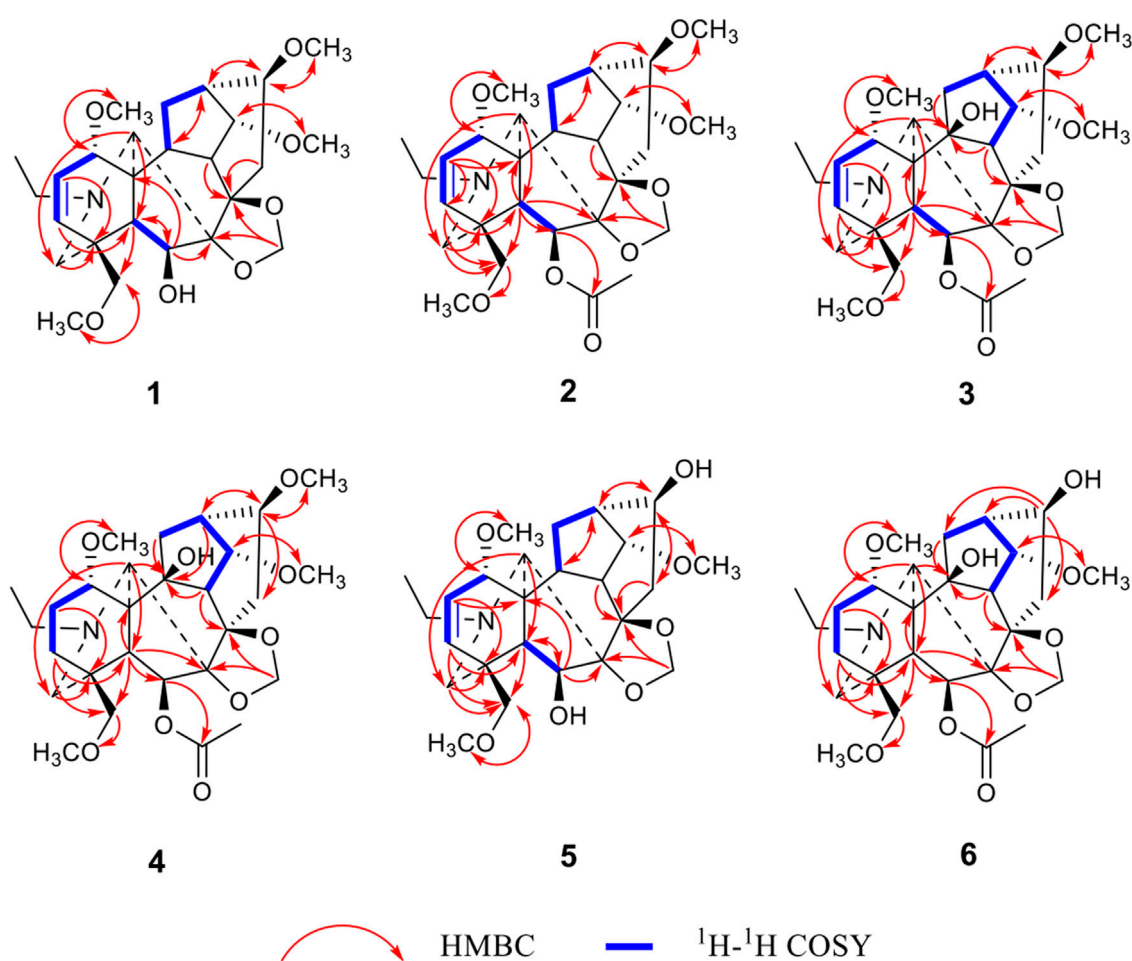


FIGURE 2
Key HMBC and ^1H - ^1H COSY correlations of six new diterpenoid alkaloids.

Compound **2** was afforded as a white powder, and its molecular formula was determined to be $\text{C}_{28}\text{H}_{41}\text{NO}_8$ by HR-MS at m/z 520.2909 $[\text{M}+\text{H}]^+$. A characteristic absorption spectrum for ester carbonyl groups (1741 cm^{-1}) was observed in the IR spectrum. The ^1H NMR spectrum revealed the presence of an NCH_2CH_3 group (δ_{H} 1.03 t, $J = 7.0$ Hz, 3H), four OCH_3 groups (δ_{H} 3.30, 3.34, 3.36, 3.44, s, each 3 H), a *cis*-trisubstituted double bond (δ_{H} 5.92, d, $J = 10.0$ Hz; 6.05, dd, $J = 10.0$ Hz, 3.4 Hz; each 1H), an OCH_2O group (δ_{H} 4.94, 4.95, s, each 1H) and an OAc functional group (δ_{H} 2.08, s, 3H). The above NMR features indicated a C_{19} -lycoctonine-type DA for **2** (Lin et al., 2017). Comparison of NMR data between compounds **2** and **1** (Tables 1, 2) revealed identical substituent patterns. Exceptionally, alkaloid **2** possesses an extra OAc group, which was placed at C-6 according to the HMBC correlation from H-6 to the ester carbonyl carbon (Figure 2). This could be further supported by the fact that H-6 in **2** was significantly shifted downfield from δ_{H} 4.28 in compound **1** to δ_{H} 5.47 due to the substituted effect

(OH \rightarrow OAc). Therefore, the structure of **2** was determined, and its relative configuration was consistent with that of **1**, as revealed by the NOESY experiment (Figure 3). All of the NMR data of **2** were assigned by 2D NMR and are listed in Tables 1, 2.

Compound **3** is a white powder, whose molecular formula was identified as $\text{C}_{28}\text{H}_{41}\text{NO}_9$ by HR-MS at m/z 536.2855 $[\text{M}+\text{H}]^+$. The IR spectrum indicated the existence of hydroxyl (3450 cm^{-1}) and ester (1739 cm^{-1}) groups. Compound **3** displayed characteristic NMR features for a C_{19} -lycoctonine-type DA bearing an NCH_2CH_3 group (δ_{H} 1.07, t, $J = 7.2$ Hz, 3H), an OCH_2O group (δ_{H} 4.96, 4.97, s, each 1H), four OCH_3 groups (δ_{H} 3.30, 3.34, 3.35, 3.45, s, 3H), a *cis*-trisubstituted double bond (δ_{H} 6.10, dd, $J = 9.8$ Hz, 3.9 Hz; 5.91, d, $J = 9.8$ Hz; s, each 1H), and an OAc group (δ_{H} 2.09 s, 3H) (Ping et al., 2007). The NMR data of **3** were highly similar to those of **2** except that the chemical shift of C-10 in compound **3** was shielded downfield with approximately $\Delta\delta_{\text{C}}$ 36. In addition, eight oxygenated carbons (δ_{C} 75.9 t,

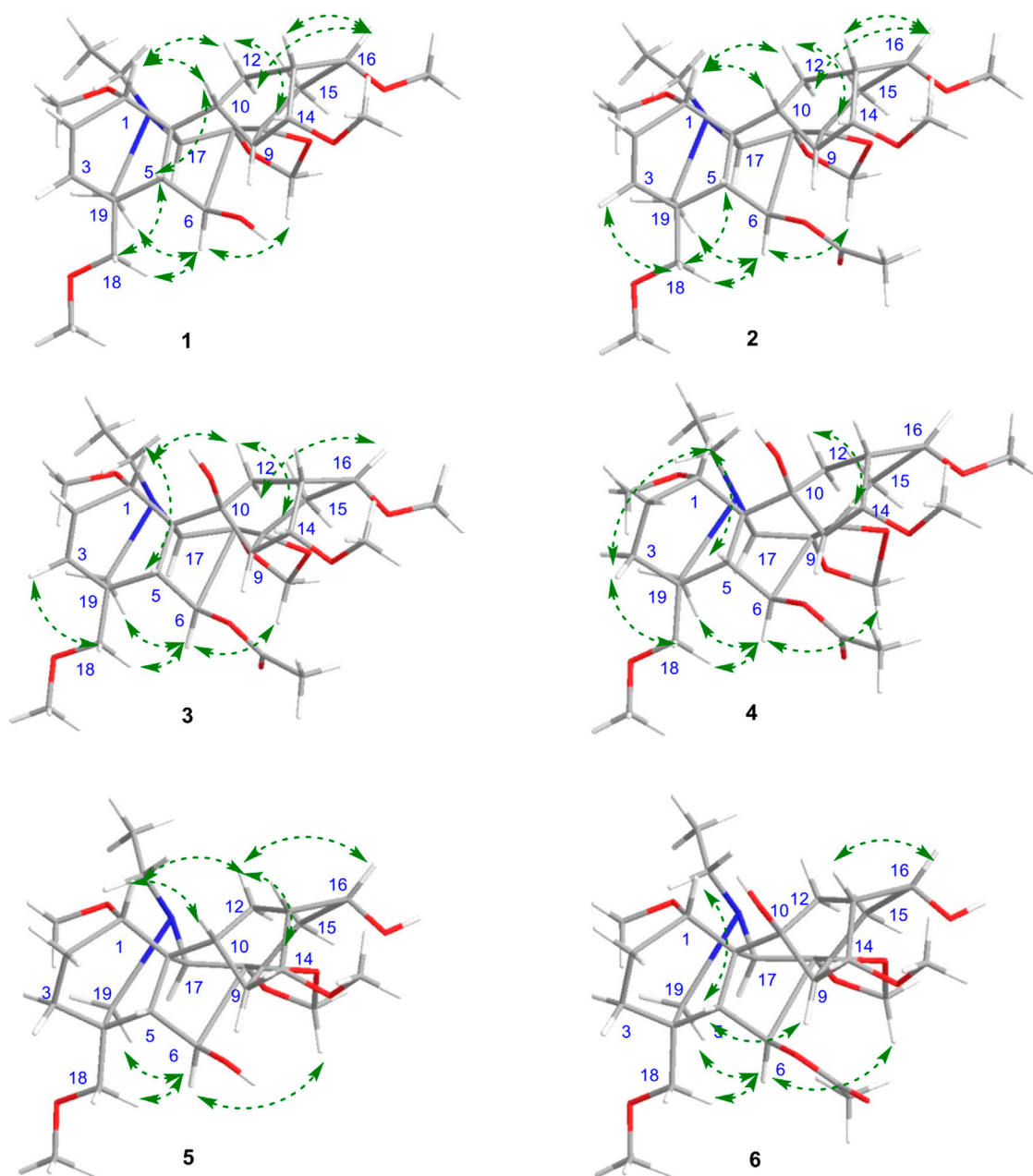


FIGURE 3
Key NOESY correlations of six new diterpenoid alkaloids.

76.0 d, 78.8 d, 81.6 d, 82.0 d, 82.4 s, 84.2 s, 91.2 s) were detected in the ^{13}C NMR spectrum, in combination with the molecular formula, indicating the presence of an extra hydroxyl group in addition to the abovementioned substituents. The hydroxyl group should be positioned at C-10 due to the chemical shift of C-10, which could be further supported by the HMBC correlation networks from H-9, H-12, and H-17 to C-10 (Figure 2). The relative configuration of **3** was also deduced from the NOESY experiment (Figure 3), which was identical

to those of compounds **1** and **2** (Meng et al., 2017). Thus, the structure of compound **3** was determined.

Compound **4** was afforded as a white powder. According to the protonated molecular ion at m/z 538.3012 $[\text{M}+\text{H}]^+$ in the HR-MS spectrum, its molecular formula was identified as $\text{C}_{28}\text{H}_{43}\text{NO}_9$. Analysis of its IR spectrum revealed hydroxyl (3515 cm^{-1}) and ester (1739 cm^{-1}) groups in the structure. In the ^1H NMR spectrum, an NCH_2CH_3 group (δ_{H} 1.06, t, $J = 7.4\text{ Hz}$, 3 H), an OCH_2O group (δ_{H} 4.92, 4.94, s, each 1H), four

OCH₃ groups (δ_{H} 3.25, 3.26, 3.33, 3.44, each 3H), and an OAc group (δ_{H} 2.08 s, 3H) were recognized. Apart from the above groups, compound **4** contains 19 carbons, including five diagnostic quaternary carbons (δ_{C} 37.9, 55.9, 81.6, 84.0, 91.8, s). These data, in combination with biogenetic consideration, suggested a C₁₉-lycoctonine-type DA for **4** (Li et al., 2010). Moreover, a combined analysis of ¹H and ¹³C NMR data suggested that **4** and **3** have similar structures. Correlations between OCH₃-1 (δ_{H} 3.26, s) and C-1 (δ_{C} 77.1 d), OCH₃-14 (δ_{H} 3.44, s) and C-14 (δ_{C} 81.7 d), OCH₃-16 (δ_{H} 3.33, s) and C-16 (δ_{C} 81.5 d), OCH₃-18 (δ_{H} 3.25, s) and C-18 (δ_{C} 78.4 d), and H-6 (δ_{H} 5.51, brs) with C=O (δ_{C} 170.0 s) in the HMBC spectrum confirmed the assignment of four OCH₃ groups and the ester group. A hydroxyl group was placed at C-10 on the basis of the HMBC correlations from H-9 (δ_{H} 3.30, d), H-12 and H-13 (δ_{H} 2.53, m) to C-10 (δ_{C} 83.9) (Figure 2). Based on the long-range correlations of the OCH₂O group with C-7 and C-8, this substituent group was located at C-7 and C-8. Furthermore, in a comparison between **4** and **3** in terms of their molecular formulas and NMR data, one of the most important differences was found to be the lack of the $\Delta^{2,3}$ in **4**. Therefore, its structure was determined and further confirmed by analysing its 2D NMR spectra (Figure 2). Similarly, the orientations for several oxygenated substituents at flexible positions, including OCH₃-1 α and OAc-6 β , were determined by using the NOESY

experiment (Figure 3) (Meng et al., 2017). Thus, the structural elucidation of compound **4** was accomplished.

Compound **5** is a white powder, and its molecular formula was determined to be C₂₅H₃₇NO₇ by HR-MS at m/z 464.2643 [M+H]⁺. The ¹H NMR spectrum showed an NCH₂CH₃ group (δ_{H} 1.03, t, J = 7.0 Hz, 3H), an OCH₂O group (δ_{H} 5.01, 5.14, s, each 1H), three OCH₃ groups (δ_{H} 3.30, 3.33, 3.43, s, each 3H), and a *cis*-trisubstituted double bond (δ_{H} 5.97, dd, J = 10.0 Hz, 3.8 Hz; 5.91, d, J = 10.0 Hz; each 1H). There are nineteen carbons in the ¹³C NMR spectrum of **5** other than the abovementioned groups, including four characteristic quaternary carbons (δ_{C} 40.7, 51.6, 85.2, 93.7). Combining the data presented above with biogenetic considerations suggested that **5** might be a C₁₉-lycoctonine-type DA (Zhang et al., 2016). In addition, seven oxygenated carbons (δ_{C} 73.6 d, 77.2 t, 80.0 d, 81.5 s, 85.1 s, 85.2 d, 93.7 s) were found in the ¹³C NMR spectrum, which corresponded to the molecular formula, implied two extra OH groups in **5**. On the basis of the HMBC correlation networks from H-6 (δ_{H} 4.24, brs) to C-5 (δ_{C} 53.4 d), C-7 (δ_{C} 93.7 s), and C-11 (δ_{C} 51.6 s) and from H-16 (δ_{H} 3.67, t) to C-13 (δ_{C} 43.8 d) and C-15 (δ_{C} 38.5 t), these two hydroxyl groups were determined to connect to C-6 (δ_{C} 80.0) and C-16 (δ_{C} 73.6), respectively. The double bond was located at C-2 and C-3 based on the ¹H-¹H COSY correlation between H-1 and H-2, which was further supported by the HMBC correlations from H-2 to C-1 and C-11 and from H-3 to C-4, C-5, and C-18. Three OCH₃ groups were placed at C-1, C-14, and C-18 on the basis of the HMBC correlations from OCH₃-1 (δ_{H} 3.30, s) to C-1 (δ_{C} 81.5 d), OCH₃-14 (δ_{H} 3.43 s) to C-14 (δ_{C} 85.2 d), and OCH₃-18 (δ_{H} 3.36 s) to C-18 (δ_{C} 59.7 t), respectively. In addition, OCH₂O was located at C-7 and C-8 due to the long-range correlations of the methylene group with C-7 (δ_{C} 91.3 q) and C-8 (δ_{C} 84.2 q) (Figure 2). The relative configurations of OCH₃-1 α and OH-6 β were determined on the basis of the NOESY correlations between H-6 and H-18 and between H-1 and H-10, respectively (Liu et al., 2009). Thus, the structure of compound **5** was determined.

Compound **6** has the molecular formula C₂₇H₄₁NO₉ as determined by the HR-MS experiment (m/z 524.2854 [M+H]⁺), suggesting eight degrees of unsaturation. Its IR spectrum showed the presence of hydroxyl (3467 cm⁻¹) and ester (1741 cm⁻¹) groups. The ¹H NMR spectrum revealed the presence of an NCH₂CH₃ group (δ_{H} 1.05, t, J = 7.2 Hz, 3H), an OCH₂O group (δ_{H} 4.86, 4.88, s, each 1H), an OAc group (δ_{H} 2.05, s, 3H; δ_{C} 21.6 q, 171.9 s), and three OCH₃ groups (δ_{H} 3.23, 3.27, 3.47, s, each 3H). The ¹³C NMR spectrum showed 19 carbons in addition to the aforementioned groups, including four diagnostic quaternary carbons at δ_{C} 39.1, 56.5, 82.1, 93.8, thus revealing a C₁₉-lycoctonine-type DA for **6** (Ablajan et al., 2018). Comparing all of the NMR data of **6** and **5**, it was found that the major difference was the lack of the $\Delta^{2,3}$ group for **6** and an additional ester group and oxygenated carbon (δ_{C} 83.8 s), which can be attributed to an OAc group and

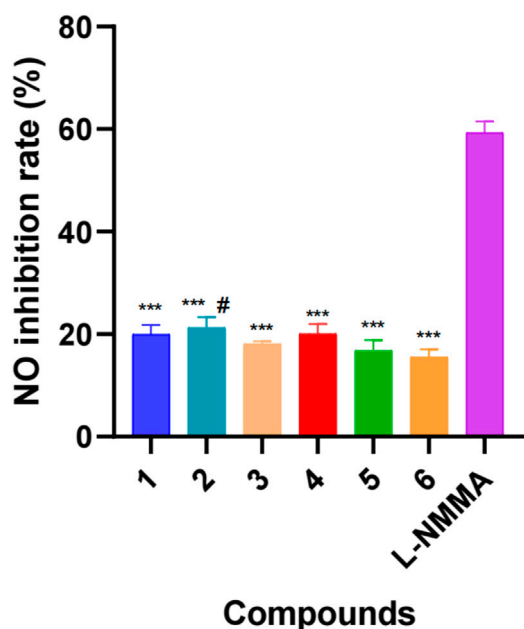


FIGURE 4

Inhibitory effects of six new diterpenoid alkaloids on NO production in LPS-induced RAW264.7 cells. L-NMMA: L-NMMA was used as positive control. Error bars indicate SD, #, $p < 0.05$ vs. compound **6**, ***, $p < 0.001$ vs. L-NMMA.

an OH group. Eight oxygenated carbons (δ_C 73.1 d, 78.4 d, 79.6 d, 80.0 d, 82.1 s, 83.6 d, 83.8 d, 93.8 s) presented in the ^{13}C NMR spectrum also implied the presence of two OH groups along with three OCH_3 groups, an OAc group, and an OCH_2O group in **6** (Xu et al., 2021). The extra OH group could be positioned at C-10 due to the HMBC correlations from H-9 (δ_H 3.54, d) and H-12 (δ_H 1.75, d) to C-10 (δ_C 83.8 s) (Figure 2). Additionally, the HMBC correlation from H-6 (δ_H 5.50, s) to the carbonyl carbon suggested that the OAc group is connected at C-6. Thus, the structure of compound **6** was determined.

The remaining compounds were identified by comparison of the ^1H and ^{13}C NMR data with those in the literature. Finally, they were identified as eight known C_{19} -lycaconitine-type DAs, namely, tatsiensine (**7**) (Wang et al., 2003), deacetyltatsiensine (**8**) (Pelletier et al., 1983), siwanines A and B (**9** and **10**) (Zhang and Ou, 1998), elasine (**11**) (Pelletier et al., 1989), anthriscifoline B (**12**) (Song et al., 2009), brownine (**13**) (Zhou et al., 2005), and lycoctonine (**14**) (Zeng et al., 2007). Among them, compounds **7–12** have not been found in *D. grandiflorum* in previous studies.

Biological activity

Traditionally, *Delphinium* plants have been extensively utilized to treat arthritis and other inflammatory diseases, which implies that their major constituents, namely, diterpenoid alkaloids, possess certain anti-inflammatory activity. It has been reported in previous studies that a certain number of diterpenoid alkaloids, mainly aconitine-type and lycoctonine-type alkaloids, have exhibited *in vitro* anti-inflammatory activity (Shen et al., 2020; Qasem et al., 2022). For example, two typical lycoctonine-type DAs, delbrunine and eldeline, from *D. brunonianum* Royle showed good anti-inflammatory activity in LPS-activated RAW 264.7 cells, which could significantly restrain the elevation of inflammatory factors, including NO, TNF- α (tumor necrosis factor- α), IL-6 (interleukin-6), COX-2 (cyclooxygenase 2), and iNOS (inducible nitric oxide synthase) through NF- κ B signaling pathway (Wang et al., 2010). Another analogous *Delphinium* alkaloid A from *D. giraldii* Diels suppressed the overexpression of the proinflammatory factors TNF- α , IL-6 and IL-8 significantly in LPS-infected Caco2 cells (Liu et al., 2019). Our previous studies also indicated that three aconitine-type DAs, taronenines A, B and D, showed inhibitory effects on the production of IL-6 in LPS-activated RAW 264.7 cells, which exerted IC_{50} values of 29.6, 18.8, and 25.4 $\mu\text{g}/\text{ml}$, respectively (Yin et al., 2018). Accordingly, in the present study, all of the new compounds were screened for their inhibitory activities against NO in LPS-activated RAW 264.7 cells. As a result, all of the isolated new alkaloids exhibited a weak inhibitory effect, exerting an inhibition rate of approximately 20% at a

concentration of 50 μM (Figure 4). This might be attributed to the lack of key pharmacophores responsible for their anti-inflammatory activity, such as aromatic ester groups at C-14 or C-8 (Tang et al., 2022).

Conclusion

DAs have attracted increasing interest due to their complex and diverse structures and bioactivities. In the present study, six previously undescribed C_{19} -lycoctonine-type DAs were isolated and identified from the whole plant of *D. grandiflorum*. New alkaloids **1–3** and **5** possess a characteristic $\Delta^{2,3}$ functional group in the A ring, while compounds **5** and **6** feature a rare OH-16 substituent. In addition, known compounds **7–12** were isolated from *D. grandiflorum* for the first time. The results of our work enriched the chemical diversity of *D. grandiflorum* and the genus *Delphinium* and presented beneficial information for further investigations. Compounds **1–6** only exhibit weak inhibition activities of NO in LPS-activated RAW 264.7 macrophages. The results suggested that the anti-inflammatory effect of *D. grandiflorum* might be attributed to the other DA compounds. Thus, further studies are still needed to elucidate the material basis of *D. grandiflorum* in inflammation-mediated diseases.

Data availability statement

The original contributions presented in the study are included in the article/Supplementary Material, further inquiries can be directed to the corresponding author.

Author contributions

TY conceived and designed the experiments and revised the manuscript. YY isolated the compounds and wrote the original draft. TY carried out structure elucidation. YY, HJ, and XY carried out the experiments and data analyses. ZD collected the plant material. All authors have read and approved the published version of the manuscript.

Funding

This work was financially supported by a grant from the National Natural Science Foundation of China (No. 31860095) and a grant from Chinese Medicine, Ethnic Medicine Science and Technology Research Project of Guizhou Provincial Administration of Traditional Chinese Medicine (No. QZYY-2022-020).

Conflict of interest

The authors declare that the research was conducted in the absence of any commercial or financial relationships that could be construed as a potential conflict of interest.

Publisher's note

All claims expressed in this article are solely those of the authors and do not necessarily represent those of their affiliated

organizations, or those of the publisher, the editors and the reviewers. Any product that may be evaluated in this article, or claim that may be made by its manufacturer, is not guaranteed or endorsed by the publisher.

Supplementary material

The Supplementary Material for this article can be found online at: <https://www.frontiersin.org/articles/10.3389/fchem.2022.1012874/full#supplementary-material>

References

- Ablajan, N., Zhao, B., Xue, W.-J., Ruzi, Z., Zhao, J.-Y., and Aisa, H. A. (2018). Diterpenoid alkaloids from *Delphinium aemulans*. *Nat. Prod. Commun.* 13 (11), 1934578X1801301–1431. doi:10.1177/1934578X1801301104
- Chen, F.-Z., Chen, D.-L., Chen, Q.-H., and Wang, F.-P. (2009). Diterpenoid alkaloids from *Delphinium majus*. *J. Nat. Prod.* 72 (1), 18–23. doi:10.1021/np800439a
- Chen, N.-H., Zhang, Y.-B., Li, W., Li, P., Chen, L.-F., Li, Y.-L., et al. (2017). Grandiflodines A and B, two novel diterpenoid alkaloids from *Delphinium grandiflorum*. *RSC Adv.* 7 (39), 24129–24132. doi:10.1039/c7ra02869e
- Ichimura, K., Shimizu, Y., H., and Goto, R. (2009). Ethylene production by gynoecium and receptacle is associated with sepal abscission in cut *Delphinium* flowers. *Postharvest Biol. Technol.* 52 (3), 267–272. doi:10.1016/j.postharvbio.2008.12.008
- Li, C., Hirasawa, Y., Arai, H., Aisa, H. A., and Morita, H. (2010). A new diterpenoid alkaloid, shawuphine A, from *Delphinium shawurens*. *Heterocycles* 80 (1), 607–612. doi:10.3987/com-09-s(s)20
- Li, G.-Q., Li, Y.-Y., Zhao, Y.-T., Xu, Q.-P., Li, Y.-L., and Wang, G.-C. (2019). Isolation and crystal structure of 4-((2-(methoxycarbonyl)phenyl)amino)-2-methyl-4-oxobutanoic acid from *Delphinium Grandiflorum*, C₁₃H₁₅NO₅. *Z. Krist. New Cryst. Struct.* 234 (3), 521–522. doi:10.1515/ncrs-2018-0517
- Lin, C.-Z., Liu, Z.-J., Zeren-Dawa, B., and Zhu, C.-C. (2017). A new diterpenoid alkaloid isolated from *Delphinium caeruleum*. *Chin. J. Nat. Med.* 15 (1), 45–48. doi:10.1016/s1875-5364(17)30007-9
- Liu, X.-Y., Chen, Q.-H., and Wang, F.-P. (2009). New C₂₀-diterpenoid alkaloids from *Delphinium anthriscifolium* var. *savatierei*. *Helv. Chim. Acta* 92 (4), 745–752. doi:10.1002/hlca.200800376
- Liu, X.-Y., Ke, B.-W., Qin, Y., and Wang, F.-P. (2022). The diterpenoid alkaloids. *Alkaloids. Chem. Biol.* 87, 1–360. doi:10.1016/bs.alkal.2021.08.001
- Marin, C., Ramirez-Macias, I., Lopez-Cspedes, A., Olmo, F., Villegas, N., Diaz, J. G., et al. (2011). *In vitro* and *in vivo* trypanocidal activity of flavonoids from *Delphinium staphisagria* against Chagas disease. *J. Nat. Prod. (Gorakhpur)*. 74 (4), 744–750. doi:10.1021/np1008043
- Meng, X.-H., Guo, Q.-L., Zhu, C.-G., and Shi, J.-G. (2017). Unprecedented C₁₉-diterpenoid alkaloid glycosides from an aqueous extract of "fu zi": Neoline 14-O-L-arabinosides with four isomeric L-anabinosyls. *Chin. Chem. Lett.* 28 (8), 1705–1710. doi:10.1016/j.ccl.2017.04.026
- Pelletier, S. W., Glinski, J. A., Joshi, B. S., and Chen, S.-Y. (1983). The diterpenoid alkaloids of *Delphinium tatsienense* Franch. *Heterocycles* 20 (7), 1347–1354. doi:10.3987/R-1983-07-1347
- Pelletier, S. W., Ross, S. A., and Kulanthaivel, P. (1989). New alkaloids from *Delphinium elatum* L. *Tetrahedron* 45 (7), 1887–1892. doi:10.1016/S0040-4020(01)80053-3
- Ping, T., Chen, D.-L., Chen, Q.-H., Jiang, X.-X., and Wang, F.-P. (2007). Three new C₁₉-diterpenoid alkaloids from *Delphinium laxicosum* var. *pilostachyum*. *Chin. Chem. Lett.* 18 (6), 700–703. doi:10.1016/j.ccl.2007.04.026
- Qasem, A. M. A., Zeng, Z., Rowan, M. G., and Blagbrough, I. S. (2022). Norditerpenoid alkaloids from *aconitum* and *Delphinium*: Structural relevance in medicine, toxicology, and metabolism. *Nat. Prod. Rep.* 39 (3), 460–473. doi:10.1039/D1NP00029B
- Shen, Y., Liang, W. J., Shi, Y. N., Kennelly, E. J., and Zhao, D. K. (2020). Structural diversity, bioactivities, and biosynthesis of natural diterpenoid alkaloids. *Nat. Prod. Rep.* 37 (6), 763–796. doi:10.1039/d0np00002g
- Song, L., Liu, X.-Y., Chen, Q.-H., and Wang, F.-P. (2009). New C₁₉- and C₁₈-diterpenoid alkaloids from *Delphinium anthriscifolium* var. *Chem. Pharm. Bull.* 57 (2), 158–161. doi:10.1248/cpb.57.158
- Tang, Q., Chen, S., Rizvi, S., Qu, J., Kang, W., Wang, S., et al. (2022). Two alkaloids from *Delphinium brunonianum* Royle, their anti-inflammatory and anti-oxidative stress activity via NF-κB signaling pathway. *Front. Nutr.* 8, 826957. doi:10.3389/fnut.2021.826957
- Thawabteh, A. M., Thawabteh, A., Lelario, F., Bufo, S. A., and Scrano, L. (2021). Classification, toxicity and bioactivity of natural diterpenoid alkaloids. *Molecules* 26 (13), 4103. doi:10.3390/molecules26134103
- Wang, F.-P., Chen, Q.-H., and Liu, X.-Y. (2010). Diterpenoid alkaloids. *Nat. Prod. Rep.* 27 (4), 529–570. doi:10.1039/B916679C
- Wang, J.-L., Zhou, X.-L., and Wang, F.-P. (2003). Chemical studies on the diterpenoid alkaloids of *Delphinium giraldii* Diels. *Nat. Prod. Res. Dev.* 15 (6), 498509–499501.
- Wang, J.-P., Shu, Y., Liu, S.-X., Hu, J.-T., Sun, C.-T., Zhou, H., et al. (2019). Expansines A–D: Four unusual isoprenoid epoxycyclohexenones generated by *Penicillium expansum* YJ-15 fermentation and photopromotion. *Org. Chem. Front.* 6 (23), 3839–3846. doi:10.1039/c9qo01076a
- Wang, W. T. (2019). A revision of the genus *Delphinium* (Ranunculaceae) of China (I). *Guihaia* 39 (11), 1425–1469.
- Xu, J.-B., Li, Y.-Z., Huang, S., Chen, L., Luo, Y.-Y., Gao, F., et al. (2021). Diterpenoid alkaloids from the whole herb of *Delphinium grandiflorum*. *L. Phytochem.* 190, 112866. doi:10.1016/j.phytochem.2021.112866
- Yin, T.-P., Hu, X.-F., Mei, R.-F., Shu, Y., Gan, D., Cai, L., et al. (2018). Four new diterpenoid alkaloids with anti-inflammatory activities from *Aconitum taronense* Fletcher et Lauener. *Phytochem. Lett.* 25, 152–155. doi:10.1016/j.phytol.2018.04.001
- Yin, T.-P., Cai, L., and Ding, Z.-T. (2020). An overview of the chemical constituents from the genus *Delphinium* reported in the last four decades. *RSC Adv.* 10 (23), 13669–13686. doi:10.1039/D0RA00813C
- Yin, T.-P., Yu, Y., Liu, Q.-H., Zhou, M.-Y., Zhu, G.-Y., Bai, L.-P., et al. (2022). 2D NMR-based MatchNat dereplication strategy enables explosive discovery of novel diterpenoid alkaloids. *Chin. J. Chem.* 40, 2169–2178. doi:10.1002/cjoc.202200250
- Zeng, L.-G., Chen, D.-L., Wang, F.-P., and Shen, X.-L. (2007). Study on norditerpenoid alkaloids of *Delphinium laxicosum*. *West China J. Pharm. Sci.* 22 (6), 299–300.
- Zhang, J.-F., Dai, R.-Y., Shan, L.-H., Chen, L., Xu, L., Wu, M.-Y., et al. (2016). Iliensines A and B: Two new C₁₉-diterpenoid alkaloids from *Delphinium iliense*. *Phytochem. Lett.* 17, 299–303. doi:10.1016/j.phytol.2016.08.014
- Zhang, S., and Ou, Q. (1998). Norditerpenoid alkaloids from *Delphinium siwanense* var. *Phytochemistry* 48 (1), 191–196. doi:10.1016/S0031-9422(97)00579-7
- Zhou, X., Chen, D., and Wang, F. (2005). Studies on the alkaloids of *Delphinium trifoliatum*. *West China J. Pharm. Sci.* 20 (1), 1–3.



OPEN ACCESS

EDITED BY
Wen Chen,
Yunnan University, China

REVIEWED BY
Jie-Ping Wan,
Jiangxi Normal University, China
Shen Xianfu,
Qujing Normal University, China

*CORRESPONDENCE
Fuchao Yu,
yufuchao05@126.com

[†]These authors have contributed equally to this work

SPECIALTY SECTION
This article was submitted to Medicinal and Pharmaceutical Chemistry, a section of the journal Frontiers in Chemistry

RECEIVED 01 August 2022
ACCEPTED 09 August 2022
PUBLISHED 21 September 2022

CITATION
Rao K, Chai Z, Zhou P, Liu D, Sun Y and Yu F (2022), Transition-metal-free approach to quinolines *via* direct oxidative cyclocondensation reaction of *N,N*-dimethyl enaminones with *o*-aminobenzyl alcohols. *Front. Chem.* 10:1008568. doi: 10.3389/fchem.2022.1008568

COPYRIGHT
© 2022 Rao, Chai, Zhou, Liu, Sun and Yu. This is an open-access article distributed under the terms of the [Creative Commons Attribution License \(CC BY\)](#). The use, distribution or reproduction in other forums is permitted, provided the original author(s) and the copyright owner(s) are credited and that the original publication in this journal is cited, in accordance with accepted academic practice. No use, distribution or reproduction is permitted which does not comply with these terms.

Transition-metal-free approach to quinolines *via* direct oxidative cyclocondensation reaction of *N,N*-dimethyl enaminones with *o*-aminobenzyl alcohols

Kairui Rao[†], Zhangmengjie Chai[†], Pan Zhou[†], Donghan Liu, Yulin Sun and Fuchao Yu*

Faculty of Life Science and Technology, Kunming University of Science and Technology, Kunming, China

A transition-metal-free method for the construction of 3-substituted or 3,4-disubstituted quinolines from readily available *N,N*-dimethyl enaminones and *o*-aminobenzyl alcohols is reported. The direct oxidative cyclocondensation reaction tolerates broad functional groups, allowing the efficient synthesis of various quinolines in moderate to excellent yields. The reaction involves a C(sp³)-O bond cleavage and a C=N bond and a C=C bond formation during the oxidative cyclization process, and the mechanism was proposed.

KEYWORDS

quinolines, *N,N*-dimethyl enaminones, *o*-aminobenzyl alcohols, oxidative cyclocondensation reaction, transition-metal-free

Introduction

Quinolines represent an important class of heterocyclic compounds, which widely occur as a core structural motif in natural products (McCormick et al., 1996; Subbaraju et al., 2004; McCauley et al., 2020), pharmaceuticals (Gorka et al., 2013; Kokatla et al., 2013; Jentsch et al., 2018), functional materials (Tong et al., 2003; Kim et al., 2005; Zhang et al., 2014), organocatalysis or ligands (Biddle et al., 2007; Zhang and Sigman, 2007; Esteruelas et al., 2016), and valuable building blocks (Wan et al., 2016; Duan et al., 2018; Wang et al., 2019; Ankade et al., 2021). Due to their great importance, considerable efforts have been focused on the development of efficient synthetic methods to their structures and modifications over the past years. Classical methodologies (Bharate et al., 2015; Li et al., 2017; Harry et al., 2020), such as Camps, Combes, Conrad-Limpach, Doebner, Friedländer, Knorr, Pfitzinger, Povorov, Skraup synthesis, and others, are known for the construction of quinoline rings; however, these reactions usually suffer from some limitations, such as harsh reaction conditions, tedious workup procedures, and special substrate designs (prefunctionalized anilines). Recently, many elegant strategies toward quinolone rings, such as using new building blocks (Jin et al., 2016; Tiwari et al., 2017; Wu et al., 2017; Trofimov et al., 2018) and multicomponent reactions (Chen et al., 2018; Wang

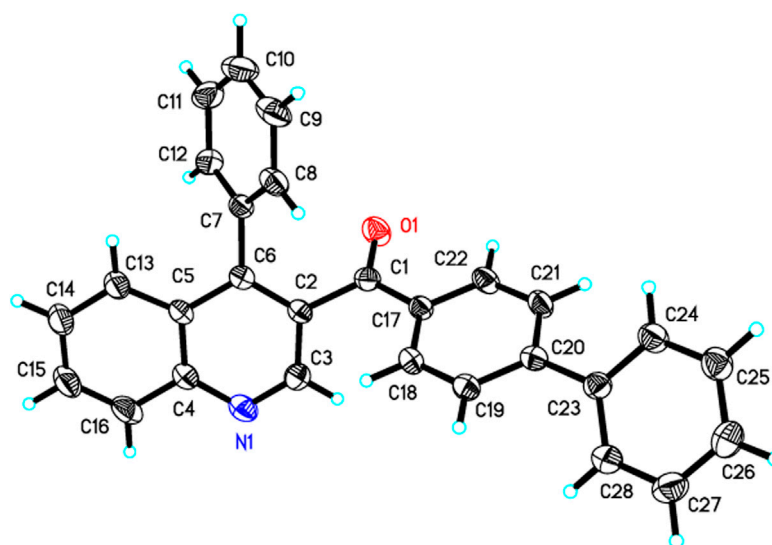
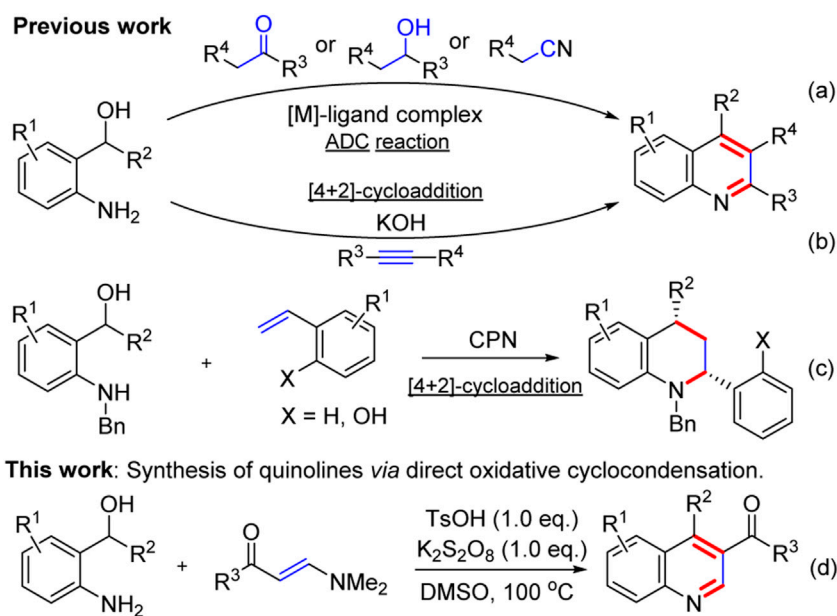


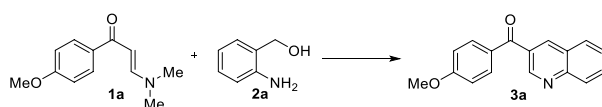
FIGURE 1
X-ray diffraction structure of 3j.



SCHEME 1
Synthesis of quinolines from *o*-aminobenzyl alcohols.

et al., 2018; Zhao et al., 2019; Yang and Wan., 2020), have been developed to construct substituted quinolines. Despite these advances, the development of easy and efficient approaches for the construction of substituted quinolines remains to be explored.

Recently, *o*-aminobenzyl alcohols are versatile intermediates which have attracted increasing attention in organic synthesis owing to their high reactivity in the construction of *N*-heterocycles (Makarov et al., 2018; Wang et al., 2018; Xie et al., 2018; Yang and Gao., 2018), especially

TABLE 1 Optimization of the reaction conditions.^{a,b}

Entry	Acid [eq.]	Oxidant [eq.]	Solvent	T [°C]	Yield [%] ^b
1	AcOH (1.0)		DMSO	100	n.d. ^c
2	PivOH (1.0)		DMSO	100	n.d. ^c
3	ZnCl ₂ (1.0)		DMSO	100	n.d. ^c
4	TFA (1.0)		DMSO	100	25
5	CSA (1.0)		DMSO	100	15
6	TsOH (1.0)		DMSO	100	32
7	TsOH (1.0)	Oxone (1.0)	DMSO	100	68
8	TsOH (1.0)	TBHP (1.0)	DMSO	100	37
9	TsOH (1.0)	Fe ₂ O ₃ (1.0)	DMSO	100	46
10	TsOH (1.0)	AgNO ₃ (1.0)	DMSO	100	59
11	TsOH (1.0)	DDQ (1.0)	DMSO	100	32
12	TsOH (1.0)	<i>m</i> -CPBA (1.0)	DMSO	100	40
13	TsOH (1.0)	K₂S₂O₈ (1.0)	DMSO	100	82
14	TsOH (1.0)	K ₂ S ₂ O ₈ (1.0)	DMF	100	53
15	TsOH (1.0)	K ₂ S ₂ O ₈ (1.0)	Toluene	100	27
16	TsOH (1.0)	K ₂ S ₂ O ₈ (1.0)	MeCN	reflux	58
17	TsOH (1.0)	K ₂ S ₂ O ₈ (1.0)	1,4-Dioxane	100	38
18	TsOH (1.0)	K ₂ S ₂ O ₈ (1.0)	EtOH	reflux	62
19	TsOH (1.0)	K ₂ S ₂ O ₈ (1.0)	H ₂ O	100	59
20	TsOH (0.5)	K ₂ S ₂ O ₈ (1.0)	DMSO	100	54
21	TsOH (1.5)	K ₂ S ₂ O ₈ (1.0)	DMSO	100	79
22	TsOH (1.0)	K ₂ S ₂ O ₈ (0.5)	DMSO	100	51
23	TsOH (1.0)	K ₂ S ₂ O ₈ (1.5)	DMSO	100	81
24	TsOH (1.0)	K ₂ S ₂ O ₈ (1.0)	DMSO	80	28
25	TsOH (1.0)	K ₂ S ₂ O ₈ (1.0)	DMSO	120	67

The bold values is designed to highlight the optimal reaction conditions.

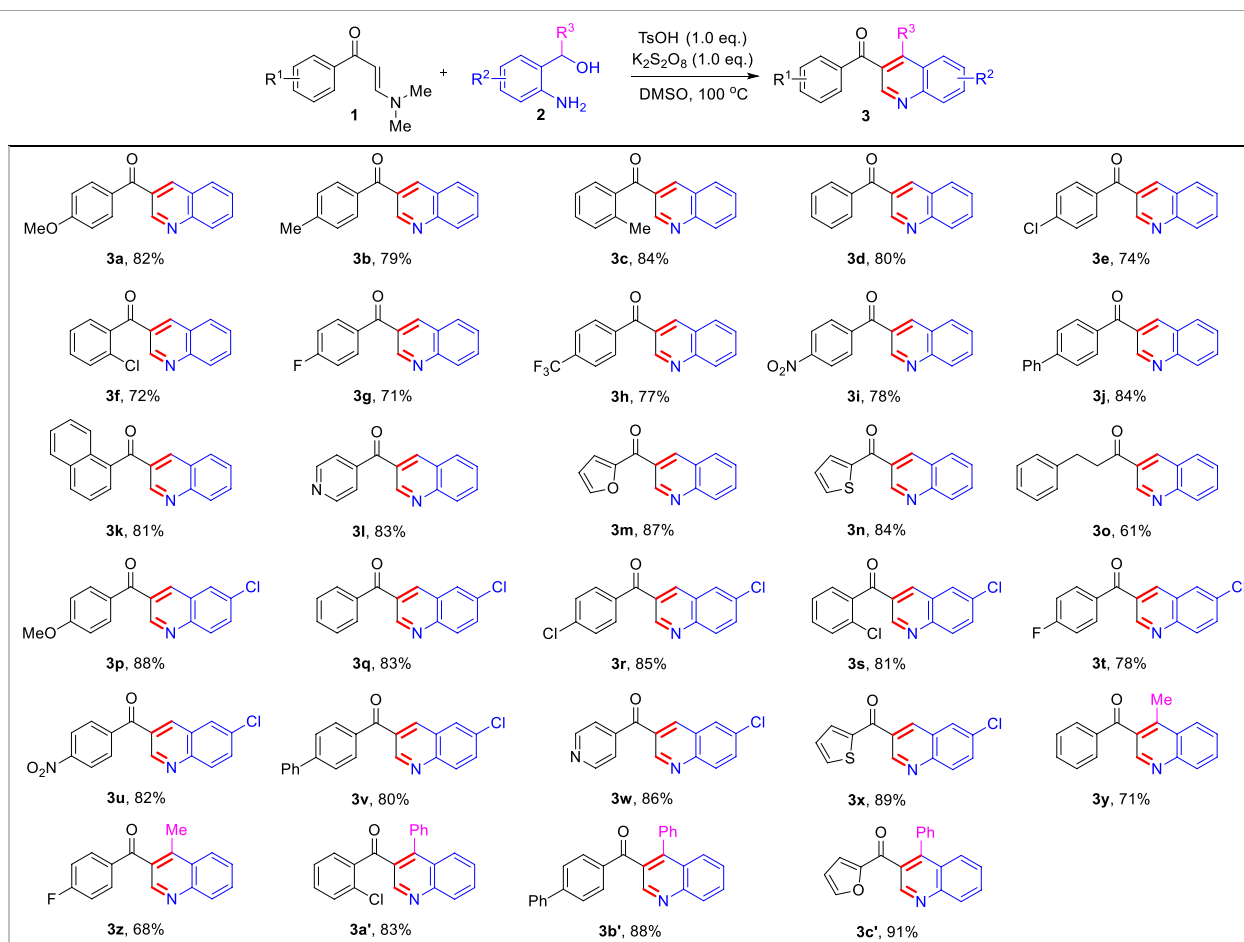
^aReaction conditions: **1a** (0.5 mmol) and **2a** (0.5 mmol) in 3.0 ml solvent for 1.0 h.

^bIsolated yields.

^cNot detected.

quinolines. In this regard, two strategies have been developed to construct the quinoline framework from *o*-aminobenzyl alcohols: acceptorless dehydrogenative coupling (ADC) reactions and [4 + 2]-cycloaddition reactions. The types of ADC reactions of *o*-aminobenzyl alcohols with ketones or secondary alcohols or nitriles to the construction of quinolines by the release of H₂ and H₂O as only by-products have been well-developed (Scheme 1). However, such attractive synthetic strategies required expensive transition-metal (TM) pincer complexes, such as Ir (Wang et al., 2016; Genc et al., 2019), Ru (Maji et al., 2018; Wan et al., 2019), Ni (Das et al., 2018; Das et al., 2018; Singh et al., 2018), Mn (Mastalir et al., 2016; Barman et al., 2018; Das et al., 2019), Cu (Tan et al., 2018), or Re (Wei et al., 2019) complexes. In addition, aza-*ortho*-quinone methides (aza-*o*-QMs), *in situ* generated from *o*-aminobenzyl alcohols as short-lived and

highly reactive diene species, have been extensively investigated and applied in organic synthesis (Huang and Kang., 2017; Mei et al., 2017; Lee et al., 2019; Wang et al., 2021). In 2016, a KOH-promoted regioselective synthesis of quinolones *via* [4 + 2]-cycloaddition of aza-*o*-QMs with internal alkynes was disclosed by Verma and co-workers (Saunthwal et al., 2016) (Scheme 1b). In 2018, Shi and co-workers established chiral phosphoramidate catalytic asymmetric [4 + 2]-cycloaddition of aza-*o*-QMs with *o*-hydroxystyrenes to afford chiral tetrahydroquinolines (Li et al., 2018) (Scheme 1c). This [4 + 2]-cycloaddition protocol enriched the partners of aza-*o*-QMs to construct quinolones. In spite of these powerful works, there is still a demand for new protocols for generation of quinolines from *o*-aminobenzyl alcohols. As our ongoing interest in quinoline synthesis (Lu et al., 2017; Zhou et al., 2018) and enaminone

TABLE 2 Scope of substrates.^{a,b}

^aReaction conditions: *N,N*-dimethylenaminones **1** (0.5 mmol), aryl methyl ketones **2** (0.5 mmol), TsOH (0.5 mmol), and K₂S₂O₈ (0.5 mmol) in 3.0 ml DMSO at 100 °C for 1.0 h.

^bIsolated yields.

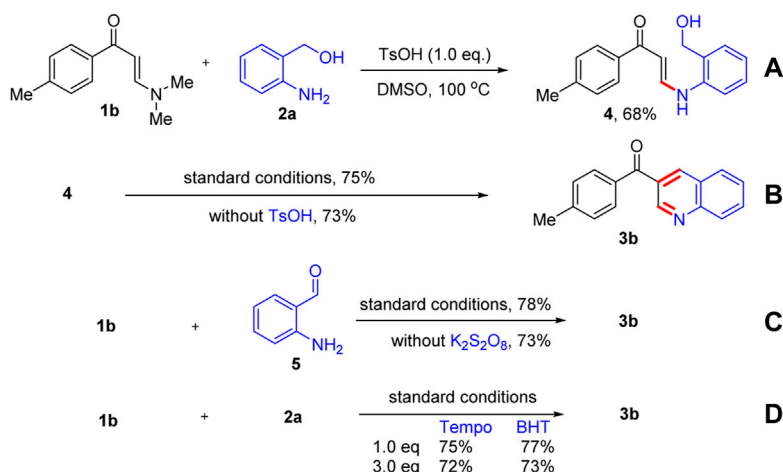
chemistry (Yu et al., 2011; Yu et al., 2013; Xu et al., 2016; Zhou et al., 2017; Fu et al., 2020; Chen et al., 2021; Huang and Yu., 2021; Yu et al., 2021; Zhang et al., 2021; Fu et al., 2022; Liu et al., 2022; Ying et al., 2022), herein, we report a transition-metal-free direct oxidative cyclocondensation strategy of *o*-aminobenzyl alcohols with *N,N*-dimethyl enaminones to synthesize 3-substituted or 3,4-disubstituted quinoline derivatives in moderate to excellent yields (Scheme 1d).

Results and discussion

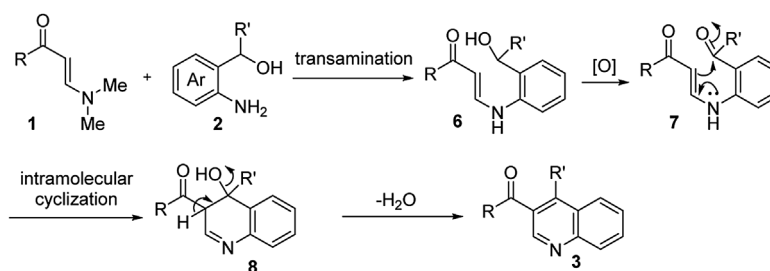
Our investigation started with the reaction of readily available *N,N*-dimethyl enaminone **1a** with *o*-aminobenzyl alcohol **2a** as model substrates in (Table 1). We carried out the model reaction in the presence of AcOH in DMSO at 100°C, but the desired product **3a** was not obtained (entry 1). Various acids were screened, such as pivalic acid (PivOH), ZnCl₂, trifluoroacetic acid (TFA), 10-camphorsulfonic acid (CSA),

and *p*-toluenesulfonic acid (TsOH), which suggested that TsOH was the most suitable acid for this reaction in 32% yield. A series of oxidants show positive effects for the reaction (entries 7–13). To our delight, K₂S₂O₈ was found to be the most effective one to give the desired quinolone **3a** for greatly increasing the yield to 82% (entry 13). Further experiments showed that DMSO was the first choice for solvents; other solvents, such as DMF, toluene, MeCN, 1,4-dioxane, EtOH, and water, were inferior (entries 14–19). With respect to the acid and oxidant loading, 1.0 equiv of TsOH and 1.0 equiv of K₂S₂O₈ were found to be optimal (entries 20–23). The reaction temperature was also screened, and the results showed that 100°C was still with giving the best yield (entries 24–25).

Under the optimized reaction conditions, we next investigated the substrate scope of this direct oxidative cyclocondensation reaction (Table 2). A wide range of *N,N*-dimethyl enaminones **1** bearing different substituents could be used in this transformation. For example,



SCHEME 2
Control experiments.



SCHEME 3
Proposed mechanism.

N,N-dimethyl enaminones bearing electron-rich (4-OMe, 4-Me, and 2-Me), electron-neutral (4-H), halogenated (4-Cl, 2-Cl, and 4-F), and electron-deficient (4-CF₃ and 4-NO₂) groups at the aryl ring were tolerated, affording the corresponding 3-substituted quinoline products in good to excellent yields (71–84%, **3a–3i**). Subsequently, 4-biphenyl and 1-naphthyl *N,N*-dimethyl enaminones were also well compatible with the reaction, giving the expected product in excellent yields (81–84%, **3j–3k**). Furthermore, various heteroaryl *N,N*-dimethyl enaminones, including 4-pyridyl, 2-furanyl, and 2-thienyl, were well tolerated in this reaction, affording the corresponding products in excellent yields (83–87%, **3l–3n**). The phenylethyl enammine worked well for the reaction, furnishing the corresponding quinoline product **3o** in 61% yield. The *o*-aminobenzyl alcohol scope was also examined. Bearing halogenation (5-Cl) was well tolerated on the phenyl ring of the *o*-aminobenzyl

alcohols, furnishing the corresponding 3-substituted quinoline products in good to excellent yields (78–89%, **3p–3x**). Notably, 1-(*o*-aminobenzyl) ethanol and *o*-aminobenzhydrol were also employed, affording 3,4-disubstituted quinolines in moderate to excellent yields (68–91%, **3y–3c'**). Moreover, the structure of **3j** was unambiguously confirmed by X-ray crystallographic analysis (CCDC 1846910, **Figure 1**).

To further understand the reaction mechanism, some control experiments were carried out, and the results are presented in **Scheme 2**. When *N,N*-dimethyl enaminone **1b** was reacted with *o*-aminobenzyl alcohol **2a** in the absence of K₂S₂O₈, the *N*-aryl enaminone intermediate product **4** was obtained in 68% yield by a transamination process (**Scheme 2**). Next, product **3b** was obtained in 75% yield by the intramolecular cyclization reaction of intermediate **4** under optimized reaction conditions. However, the intramolecular

cyclization reaction could also proceed smoothly without the addition of TsOH, affording product **3b** in 73% yield (Scheme 2). When *N,N*-dimethyl enaminone **1b** was reacted with 2-aminobenzaldehyde **5** under the standard conditions or in the absence of K₂S₂O₈, product **3b** was, respectively, isolated in 78 and 73% yields (Scheme 2). Additionally, the reaction was unaffected completely by adding the radical inhibitors Tempo and BHT (Scheme 2). These results revealed that *N*-aryl enaminone **4** and 2-aminobenzaldehyde **5** were important intermediates for this reaction, and the reaction was not a free-radical process.

Based on the above results and previous studies (Zhou et al., 2018), a possible mechanism for this transformation is proposed (Scheme 3). *N,N*-dimethyl enaminones **1** reacted with *o*-aminobenzyl alcohols **2** promoted by TsOH to furnish the *N*-aryl enaminone intermediate **6** via a transamination process. Next, intermediate **6** underwent K₂S₂O₈-assisted oxidation to form the ketone intermediate **7**, which was then converted into intermediate **8** through intramolecular cyclization reaction. Finally, quinolone products **3** were obtained via elimination of a molecule of H₂O and oxidative aromatization.

Conclusion

In conclusion, we have developed a concise protocol for the synthesis of 3-substituted or 3,4-disubstituted quinolines with moderate to excellent yields using readily available *N,N*-dimethyl enaminones and *o*-aminobenzyl alcohols promoted by TsOH/K₂S₂O₈. This direct oxidative cyclocondensation reaction enriched the quinoline synthesis method from *o*-aminobenzyl alcohols.

Data availability statement

The original contributions presented in the study are included in the article/Supplementary Materials; further inquiries can be directed to the corresponding author.

References

- Ankade, S. B., Shabade, A. B., Soni, V., and Punji, B. (2021). Unactivated alkyl halides in transition-metal-catalyzed C–H bond alkylation. *ACS Catal.* 11, 3268–3292. doi:10.1021/acscatal.0c05580
- Barman, M. K., Jana, A., and Majia, B. (2018). Phosphine-free NNN-manganese complex catalyzed alkylation of ketones with primary alcohols and Friedländer quinoline synthesis. *Adv. Synth. Catal.* 360, 3233–3238. doi:10.1002/adsc.201800380
- Bharate, J. B., Vishwakarma, R. A., and Bharate, S. B. (2015). Metal-free domino one-pot protocols for quinoline synthesis. *RSC Adv.* 5, 42020–42053. doi:10.1039/c5ra07798b
- Biddle, M. M., Lin, M., and Scheidt, K. A. (2007). Catalytic enantioselective synthesis of flavanones and chromanones. *J. Am. Chem. Soc.* 129, 3830–3831. doi:10.1021/ja070394v
- Chen, L., Huang, R., Kong, L.-B., Lin, J., and Yan, S.-J. (2018). Facile route to the synthesis of 1,3-diazahetero-cycle-fused [1,2-a]quinoline derivatives via cascade reactions. *ACS Omega* 3, 1126–1136. doi:10.1021/acsomega.7b01856
- Chen, X.-B., Huang, S.-T., Li, J., Yang, Q., Yang, L., and Yu, F. (2021). Highly regioselective and chemoselective [3+3] annulation of enaminones with *ortho*-fluoronitrobenzenes: Divergent synthesis of aposafranones and their *N*-oxides. *Org. Lett.* 23, 3032–3037. doi:10.1021/acs.orglett.1c00710
- Das, J., Singh, K., Vellakkaran, M., and Banerjee, D. (2018). Nickel-catalyzed hydrogen-borrowing strategy for α -alkylation of ketones with alcohols: A new route to branched gem-bis(alkyl) ketones. *Org. Lett.* 20, 5587–5591. doi:10.1021/acs.orglett.8b02256

Author contributions

FY designed the project. KR, ZC, PZ, DL, and YS performed the experiments. FY supervised the work and prepared the manuscript. All authors contributed to the article and approved the submitted version.

Funding

This research was financially supported by the National Natural Science Foundation of China (21961018), the Natural Science Foundation of Yunnan Province (201901T070302 and 202202AG050008), and the Plan of Funding Outstanding Young Talents of Yunnan Province.

Conflict of interest

The authors declare that the research was conducted in the absence of any commercial or financial relationships that could be construed as a potential conflict of interest.

Publisher's note

All claims expressed in this article are solely those of the authors and do not necessarily represent those of their affiliated organizations or those of the publisher, the editors, and the reviewers. Any product that may be evaluated in this article or claim that may be made by its manufacturer is not guaranteed or endorsed by the publisher.

Supplementary material

The Supplementary Material for this article can be found online at: <https://www.frontiersin.org/articles/10.3389/fchem.2022.1008568/full#supplementary-material>

- Das, K., Mondal, A., Pal, D., and Srimani, D. (2019). Sustainable synthesis of quinazoline and 2-aminoquinoline via dehydrogenative coupling of 2-aminobenzyl alcohol and nitrile catalyzed by phosphine-free manganese pincer complex. *Org. Lett.* 21, 3223–3227. doi:10.1021/acs.orglett.9b00939
- Das, S., Maiti, D., and Sarkar, S. D. (2018). Synthesis of polysubstituted quinolines from α -2-aminoaryl alcohols via Nickel-catalyzed dehydrogenative coupling. *J. Org. Chem.* 83, 2309–2316. doi:10.1021/acs.joc.7b03198
- Duan, Y., Liu, Y., and Wan, J.-P. (2018). Copper-catalyzed one-pot *N*-acylation and C5–H halogenation of 8-aminoquinolines: The dual role of acyl halides. *J. Org. Chem.* 83, 3403–3408. doi:10.1021/acs.joc.8b00068
- Esteruelas, M. A., Larramona, C., and Onate, E. (2016). Osmium-mediated direct C–H bond activation at the 8-position of quinolines. *Organometallics* 35, 1597–1600. doi:10.1021/acs.organomet.6b00264
- Fu, L., Xu, W., Pu, M., Wu, Y., Liu, Y., and Wan, J.-P. (2022). Rh-Catalyzed [4 + 2] annulation with a removable monodentate structure toward iminopyranes and pyranones by C–H annulation. *Org. Lett.* 24, 3003–3008. doi:10.1021/acs.orglett.2c00912
- Fu, L., Xu, Z., Wan, J.-P., and Liu, Y. (2020). The domino chromone annulation and a transient halogenation-mediated C–H alkenylation toward 3-vinyl chromones. *Org. Lett.* 22, 9518–9523. doi:10.1021/acs.orglett.0c03548
- Genc, S., Arslan, B., Gulcemal, S., Gunnaz, S., Cetinkaya, B., and Gulcemal, D. (2019). Iridium(I)-catalyzed C–C and C–N bond formation reactions via the borrowing hydrogen strategy. *J. Org. Chem.* 84, 6286–6297. doi:10.1021/acs.joc.9b00632
- Gorka, A. P., Dios, A., and Roepe, P. D. (2013). Quinoline drug–heme interactions and implications for antimalarial cytostatic versus cytotoxic activities. *J. Med. Chem.* 56, 5231–5246. doi:10.1021/jm400282d
- Harry, N. A., Ujwaldev, S. M., and Anilkumar, G. (2020). Recent advances and prospects in the metal-free synthesis of quinolines. *Org. Biomol. Chem.* 18, 9775–9790. doi:10.1039/d0ob02000a
- Huang, H., and Kang, J. Y. (2017). Organocatalytic phosphorylation of *in situ* formed o-quinone methides. *Org. Lett.* 19, 5988–5991. doi:10.1021/acs.orglett.7b03019
- Huang, J., and Yu, F. (2021). Synthesis-Stuttgart, 587–610. doi:10.1055/s-0040-1707328Recent advances in organic synthesis based on *N*, *N*-dimethyl enamines. *Synthesis*.
- Jentsch, N. G., Hart, A. P., Hume, J. D., Sun, J., McNeely, K. A., Lama, C., et al. (2018). Synthesis and evaluation of aryl quinolines as HIV-1 integrase multimerization inhibitors. *ACS Med. Chem. Lett.* 9, 1007–1012. doi:10.1021/acsmchemlett.8b00269
- Jin, H., Tian, B., Song, X., Xie, J., Rudolph, M., Rominger, F., et al. (2016). Gold-catalyzed synthesis of quinolines from propargyl silyl ethers and anthranil through the umpolung of a gold carbene carbon. *Angew. Chem. Int. Ed.* 55, 12688–12692. doi:10.1002/anie.201606043
- Kim, J. I., Shin, I.-S., Kim, H., and Lee, J.-K. (2005). Efficient electrogenerated chemiluminescence from cyclometalated Iridium(III) complexes. *J. Am. Chem. Soc.* 127, 1614–1615. doi:10.1021/ja043721x
- Kokatla, H. P., Sil, D., Malladi, S. S., Balakrishna, R., Hermanson, A. R., Fox, L. M., et al. (2013). Exquisite selectivity for human toll-like receptor 8 in substituted furo [2, 3-*c*]quinolines. *J. Med. Chem.* 56, 6871–6885. doi:10.1021/jm400694d
- Lee, A., Zhu, J. L., Feoktistova, T., Brueckner, A. C., Cheong, P. H.-Y., and Scheidt, K. A. (2019). Carbene-catalyzed enantioselective decarboxylative annulations to access dihydrobenzoxazinones and quinolones. *Angew. Chem. Int. Ed.* 58, 5941–5945. doi:10.1002/anie.201900600
- Li, L.-Z., Wang, C.-S., Guo, W.-F., Mei, G.-J., and Shi, F. (2018). Catalytic asymmetric [4+2] cycloaddition of *in situ* generated o-quinone methide imines with o-hydroxystyrenes: Diastereo- and enantioselective construction of tetrahydroquinoline frameworks. *J. Org. Chem.* 83, 614–623. doi:10.1021/acs.joc.7b02533
- Li, Y., Cao, X., Liu, Y., and Wan, J.-P. (2017). Regioselective three-component synthesis of 2, 3-disubstituted quinolines via the enaminone modified Povarov reaction. *Org. Biomol. Chem.* 15, 9585–9589. doi:10.1039/c7ob02411h
- Liu, D., Lu, X., Zhang, Q., Zhao, Y., Zhang, B., Sun, Y., et al. (2022). Facile approach to multifunctionalized 5-alkylidene-3-pyrrolin-2-ones via regioselective oxidative cyclization of 2, 4-pentanediones with primary amines and sodium sulfonates. *Org. Chem. Front.* 9, 4078–4084. doi:10.1039/d2qo00473a
- Lu, L., Zhou, P., Hu, B., Li, X., Huang, R., and Yu, F. (2017). An improved Pfitzinger reaction: Eco-efficient synthesis of quinaldine-4-carboxylates by TMSCl-mediated. *Tetrahedron Lett.* 58, 3658–3661. doi:10.1016/j.tetlet.2017.08.014
- Maji, M., Chakrabarti, K., Paul, B., Roy, B. C., and Kundua, S. (2018). Ruthenium(II)-NNN-pincer-complex-catalyzed reactions between various alcohols and amines for sustainable C–N and C–C bond formation. *Adv. Synth. Catal.* 360, 722–729. doi:10.1002/adsc.201701117
- Makarov, A. S., Uchuskin, M. G., and Gevorgyan, V. (2018). Intramolecular palladium-catalyzed oxidative amination of furans: Synthesis of functionalized indoles. *J. Org. Chem.* 83, 14010–14021. doi:10.1021/acs.joc.8b02470
- Mastalir, M., Glatz, M., Pittenauer, E., Allmaier, G., and Kirchner, K. (2016). Sustainable synthesis of quinolines and pyrimidines catalyzed by manganese PNP pincer complexes. *J. Am. Chem. Soc.* 138, 15543–15546. doi:10.1021/jacs.6b10433
- McCauley, E. P., Smith, G. C., and Crews, P. (2020). Unraveling structures containing highly conjugated pyrrolo[4, 3, 2-de]quinoline cores that are deficient in diagnostic proton NMR signals. *J. Nat. Prod.* 83, 174–178. doi:10.1021/acs.jnatprod.9b01111
- McCormick, J. L., McKee, T. C., Cardellina, J. H., II, and Boyd, M. R. (1996). HIV inhibitory natural products. 26. Quinoline alkaloids from *Euodia roxburghiana*. *J. Nat. Prod.* 59, 469–471. doi:10.1021/np960250m
- Mei, G.-J., Zhu, Z.-Q., Zhao, J.-J., Bian, C.-Y., Chen, J., Chen, R.-W., et al. (2017). Brønsted acid-catalyzed stereoselective [4+3] cycloadditions of ortho-hydroxybenzyl alcohols with *N*, *N*-cyclic azomethine imines. *Chem. Commun.* 53, 2768–2771. doi:10.1039/c6cc09775h
- Saunthwal, R. K., Patel, M., and Verma, A. K. (2016). Metal- and protection-free [4+2] cycloadditions of alkynes with azadienes: Assembly of functionalized quinolines. *Org. Lett.* 18, 2200–2203. doi:10.1021/acs.orglett.6b00817
- Singh, K., Vellakkaran, M., and Banerjee, D. (2018). A nitrogen-ligated nickel-catalyst enables selective intermolecular cyclisation of β - and γ -amino alcohols with ketones: Access to five and six-membered *N*-heterocycles. *Green Chem.* 20, 2250–2256. doi:10.1039/c8gc00318a
- Subbaraju, G. V., Kavitha, J., Rajasekhar, D., and Jimenez, J. I. (2004). Jusbetonin, the first indolo[3, 2-*b*]quinoline alkaloid glycoside, from *Justicia betonica*. *J. Nat. Prod.* 67, 461–462. doi:10.1021/np030392y
- Tan, D.-W., Li, H.-X., Zhu, D.-L., Li, H.-Y., Young, D. J., Yao, J.-L., et al. (2018). Ligand-controlled copper(I)-catalyzed cross-coupling of secondary and primary alcohols to α -alkylated ketones, pyridines, and quinolines. *Org. Lett.* 20, 608–611. doi:10.1021/acs.orglett.7b03726
- Tiwari, D. K., Phanindrudu, M., Wakade, S. B., Nanubolu, J. B., and Tiwari, D. K. (2017). Functionalization of saturated ketones with anthranils via Cu-catalyzed sequential dehydrogenation/aza-Michael addition/annulation cascade reactions in one-pot. *Chem. Commun.* 53, 5302–5305. doi:10.1039/c7cc01195d
- Tong, H., Wang, L., Jing, X., and Wang, F. (2003). Turn-on conjugated polymer fluorescent chemosensor for fluoride ion. *Macromolecules* 36, 2584–2586. doi:10.1021/ma0258612
- Trofimov, B. A., Belyaeva, K. V., Nikitina, L. P., Mal'kina, A. G., Afonin, A. V., Ushakov, I. A., et al. (2018). Transition metal-free one-pot double C–H functionalization of quinolines with disubstituted electron-deficient acetylenes. *Chem. Commun.* 54, 5863–5866. doi:10.1039/c8cc03269f
- Wan, J.-P., Li, Y., and Liu, Y. (2016). Annulation based on 8-aminoquinoline assisted C–H activation: An emerging tool in *N*-heterocycle construction. *Org. Chem. Front.* 3, 768–772. doi:10.1039/c6qo00077k
- Wan, X.-M., Liu, Z.-L., Liu, W.-Q., Cao, X.-N., Zhu, X., Zhao, X.-M., et al. (2019). NNN pincer Ru(II)-catalyzed dehydrogenative coupling of 2-aminoarylmethanols with nitriles for the construction of quinazolines. *Tetrahedron* 75, 2697–2705. doi:10.1016/j.tet.2019.03.046
- Wang, B.-Q., Zhang, C.-H., Tian, X.-X., Lin, J., and Yan, S.-J. (2018). Cascade reaction of isatins with 1, 1-enediamines: Synthesis of multisubstituted quinoline-4-carboxamides. *Org. Lett.* 20, 660–663. doi:10.1021/acs.orglett.7b03803
- Wang, H.-Q., Ma, W., Sun, A., Sun, X.-Y., Jiang, C., Zhang, Y.-C., et al. (2021). (4 + 2) cyclization of aza-o-quinone methides with azlactones: Construction of biologically important dihydroquinolinone frameworks. *Org. Biomol. Chem.* 19, 1334–1343. doi:10.1039/d0ob02388d
- Wang, J., Zhou, R., Zhuang, S., and Wu, A. (2018). Acid-mediated four-component tandem cyclization: Access to multifused 1, 3-benzoxazine frameworks. *Tetrahedron* 74, 7283–7289. doi:10.1016/j.tet.2018.10.059
- Wang, R., Fan, H., Zhao, W., and Li, F. (2016). Acceptorless dehydrogenative cyclization of o-aminobenzyl alcohols with ketones to quinolines in water catalyzed by water soluble metal-ligand bifunctional catalyst [Cp*₂(6', 6'-(OH)₂bpy)(H₂O)] [OTf]₂. *Org. Lett.* 18, 3558–3561. doi:10.1021/acs.orglett.6b01518
- Wang, Y., Dong, B., Wang, Z., Cong, X., and Bi, X. (2019). Silver-catalyzed reduction of quinolines in water. *Org. Lett.* 21, 3631–3634. doi:10.1021/acs.orglett.9b01055
- Wei, D., Dorcet, V., Darcel, C., and Sortais, J.-B. (2019). Synthesis of quinolines through acceptorless dehydrogenative coupling catalyzed by Rhodium PN(H)P complexes. *ChemSusChem* 12, 3078–3082. doi:10.1002/cssc.201802636

- Wu, X., Geng, X., Zhao, P., Zhang, J., Gong, X., Wu, Y.-D., et al. (2017). I_2 -Promoted Povarov-type reaction using 1, 4-dithane-2, 5-diol as an ethylene surrogate: Formal [4 + 2] synthesis of quinolines. *Org. Lett.* 19, 1550–1553. doi:10.1021/acs.orglett.7b00361
- Xie, F., Chen, Q.-H., Xie, R., Jiang, H.-F., and Zhang, M. (2018). MOF-derived nanocobalt for oxidative functionalization of cyclic amines to quinazolinones with 2-aminoarylmethanols. *ACS Catal.* 8, 5869–5874. doi:10.1021/acscatal.8b01366
- Xu, H., Zhou, B., Zhou, P., Zhou, J., Shen, Y., Yu, F., et al. (2016). Insights into the unexpected chemoselectivity in brønsted acid catalyzed cyclization of isatins with enaminones: Convenient synthesis of pyrrolo[3, 4-c]quinolin-1-ones and spirooxindoles. *Chem. Commun.* 52, 8002–8005. doi:10.1039/c6cc02659a
- Yang, B., and Gao, S. (2018). Recent advances in the application of Diels–Alder reactions involving o-quinodimethanes, aza-o-quinone methides and o-quinone methides in natural product total synthesis. *Chem. Soc. Rev.* 47, 7926–7953. doi:10.1039/c8cs00274f
- Yang, L., and Wan, J.-P. (2020). Ethyl lactate-involved three-component dehydrogenative reactions: Biomass feedstock in diversity-oriented quinoline synthesis. *Green Chem.* 22, 3074–3078. doi:10.1039/d0gc00738b
- Ying, J., Liu, T., Liu, Y., and Wan, J.-P. (2022). Base-promoted annulative difluoromethylation of enaminones with $\text{BrCF}_2\text{CO}_2\text{Et}$ toward 2, 2-difluorinated 2, 3-dihydrofurans. *Org. Lett.* 24, 2404–2408. doi:10.1021/acs.orglett.2c00671
- Yu, F., Huang, R., Ni, H., Fan, J., Yan, S., and Lin, J. (2013). Three-component stereoselective synthesis of spirooxindole derivatives. *Green Chem.* 15, 453–462. doi:10.1039/c2gc36552a
- Yu, F., Yan, S., Hu, L., Wang, Y., and Lin, J. (2011). Cascade reaction of isatins with heterocyclic ketene amins: Synthesis of imidazopyrrolo-quinoline derivatives. *Org. Lett.* 13, 4782–4785. doi:10.1021/ol201783d
- Yu, Q., Liu, Y., and Wan, J.-P. (2021). Metal-free $\text{C}(\text{sp}^2)$ -H perfluoroalkylsulfonylation and configuration inversion: Stereoselective synthesis of α -perfluoroalkylsulfonyl E-enaminones. *Chin. Chem. Lett.* 32, 3514–3517. doi:10.1016/j.ccl.2021.04.037
- Zhang, B., Liu, D., Sun, Y., Zhang, Y., Feng, J., and Yu, F. (2021). Preparation of thiazole-2-thiones through TBPB-promoted oxidative cascade cyclization of enaminones with elemental sulfur. *Org. Lett.* 23, 3076–3082. doi:10.1021/acs.orglett.1c00751
- Zhang, Y., and Sigman, M. S. (2007). Palladium(II)-catalyzed enantioselective aerobic dialkoxylolation of 2-propenyl phenols: A pronounced effect of copper additives on enantioselectivity. *J. Am. Chem. Soc.* 129, 3076–3077. doi:10.1021/ja070263u
- Zhang, Z., Shi, Y., Pan, Y., Cheng, X., Zhang, L., Chen, J., et al. (2014). Quinoline derivative-functionalized carbon dots as a fluorescent nanosensor for sensing and intracellular imaging of Zn^{2+} . *J. Mat. Chem. B* 2, 5020–5027. doi:10.1039/c4tb00677a
- Zhao, P., Wu, X., Zhou, Y., Geng, X., Wang, C., Wu, Y.-D., et al. (2019). Direct synthesis of 2, 3-diaroyl quinolines and pyridazino[4, 5-b]quinolines via an I_2 -promoted one-pot multicomponent reaction. *Org. Lett.* 21, 2708–2711. doi:10.1021/acs.orglett.9b00685
- Zhou, P., Hu, B., Li, L., Rao, K., Yang, J., and Yu, F. (2017). $\text{Mn}(\text{OAc})_3$ -Promoted oxidative Csp^3 -P bond formation through Csp^2 - Csp^2 and P-H bond cleavage: Access to β -ketophosphonates. *J. Org. Chem.* 82, 13268–13276. doi:10.1021/acs.joc.7b02391
- Zhou, P., Hu, B., Rao, K., Li, L., Yang, J., Gao, C., et al. (2018). Chemoselective synthesis of *N*-aryl-enaminones and 3-aryl quinolines via temperature and amount of catalyst synergistic control. *Synlett* 29, 519–524. doi:10.1055/s-0036-1590950
- Zhou, P., Hu, B., Wang, Y., Zhang, Q., Li, X., Yan, S., et al. (2018). Convenient synthesis of quinoline-4-carboxylate derivatives through the $\text{Bi}(\text{OTf})_3$ -catalyzed domino cyclization/esterification reaction of isatins with enaminones in alcohols. *Eur. J. Org. Chem.* 2018, 4527–4535. doi:10.1002/ejoc.201800734
- Zhou, P., Hu, B., Zhao, S., Zhang, Q., Wang, Y., Li, X., et al. (2018). An improved Pfitzinger reaction for the direct synthesis of quinoline-4-carboxylic esters/acids mediated by TMSCl . *Tetrahedron Lett.* 59, 3116–3119. doi:10.1016/j.tetlet.2018.07.006



OPEN ACCESS

EDITED BY
Wen Chen,
Yunnan University, China

REVIEWED BY
Maria Pina,
Faculty of Pharmacy- University of
Coimbra, Portugal
Tao Feng,
South-Central University for
Nationalities, China

*CORRESPONDENCE
Dan Zhang,
zhangdan@swmu.edu.cn
Chunlian Wu,
wcl_xj@163.com
Hui Lei,
leihui-2008@163.com

[†]These authors have contributed equally
to this work

SPECIALTY SECTION
This article was submitted to Medicinal
and Pharmaceutical Chemistry,
a section of the journal
Frontiers in Chemistry

RECEIVED 07 July 2022
ACCEPTED 29 August 2022
PUBLISHED 04 October 2022

CITATION
Lei H, Zou S, Lin J, Zhai L, Zhang Y, Fu X,
Chen S, Niu H, Liu F, Wu C and Zhang D
(2022), Antioxidant and anti-
inflammatory activity of constituents
isolated from *Dendrobium*
nobile (Lindl.).
Front. Chem. 10:988459.
doi: 10.3389/fchem.2022.988459

COPYRIGHT
© 2022 Lei, Zou, Lin, Zhai, Zhang, Fu,
Chen, Niu, Liu, Wu and Zhang. This is an
open-access article distributed under
the terms of the [Creative Commons
Attribution License \(CC BY\)](#). The use,
distribution or reproduction in other
forums is permitted, provided the
original author(s) and the copyright
owner(s) are credited and that the
original publication in this journal is
cited, in accordance with accepted
academic practice. No use, distribution
or reproduction is permitted which does
not comply with these terms.

Antioxidant and anti-inflammatory activity of constituents isolated from *Dendrobium nobile* (Lindl.)

Hui Lei^{1*†}, Shunmei Zou^{1†}, Jiafu Lin², Longfei Zhai³,
Yifeng Zhang¹, Xiujuan Fu¹, Siwei Chen¹, Hong Niu¹, Feifei Liu⁴,
Chunlian Wu^{5*} and Dan Zhang^{1*}

¹School of Pharmacy, Southwest Medical University, Luzhou, Sichuan, China, ²School of Pharmacy, Chengdu University, Chengdu, Sichuan, China, ³Antibiotics Research and Re-evaluation Key Laboratory of Sichuan Province, Sichuan Industrial Institute of Antibiotics, Chengdu University, Chengdu, Sichuan, China, ⁴School of Life Sciences, Jiangsu Normal University, Xuzhou, Jiangsu, China, ⁵Key Laboratory of Southwest China Wildlife Resources Conservation (China West Normal University), Ministry of Education, Nanchong, Sichuan, China

Dendrobium nobile (Lindl.) have long been used as herbal tea and a traditional herbal medicine to treat Alzheimer's disease (AD). In the current study, nineteen compounds (**1–19**), including two new vitamin E homologues (**1–2**), one new sesquiterpene (**6**), and two new dendrobines (**7, 8**), were isolated and identified from stems of *Dendrobium nobile*. Their structures were elucidated on the basis of NMR, ¹³C NMR calculation, and DP4⁺ probability analyses. The absolute configurations of new compounds were determined by electronic circular dichroism (ECD) data analysis. Antioxidant, anti-inflammatory, and cytotoxic activities of isolated compounds were evaluated. Among them, compound **2** demonstrated significant antioxidant activity compared with ascorbic acid (VC), while compounds **2** and **4** also exhibited an equal effect to positive control cisplatin. This study on the biological activity of the new vitamin E homologues from *Dendrobium nobile* may indicate its potential application in the pharmaceutical and food industries.

KEYWORDS

Dendrobium nobile Lindl., chemical constituents, antioxidant, anti-inflammatory activities, structure-activity relationship

Introduction

Dendrobium plants (Orchidaceae) are mainly distributed throughout Asia and the Pacific islands. There are 81 species of *Dendrobium* in China, mostly distributed in the South of the Tsinling Mountains of China (Zheng et al., 2018; Wang, 2021a). Owing to their well-known nutritional value and medicinal properties, the genus *Dendrobium* (Orchidaceae) have attracted interest in many health products and pharmaceutical fields (Teixeira da Silva and Ng, 2017). The species *Dendrobium nobile* Lindl, an edible, ornamental, and also a medicinal plant, is one of the four well-known plant sources

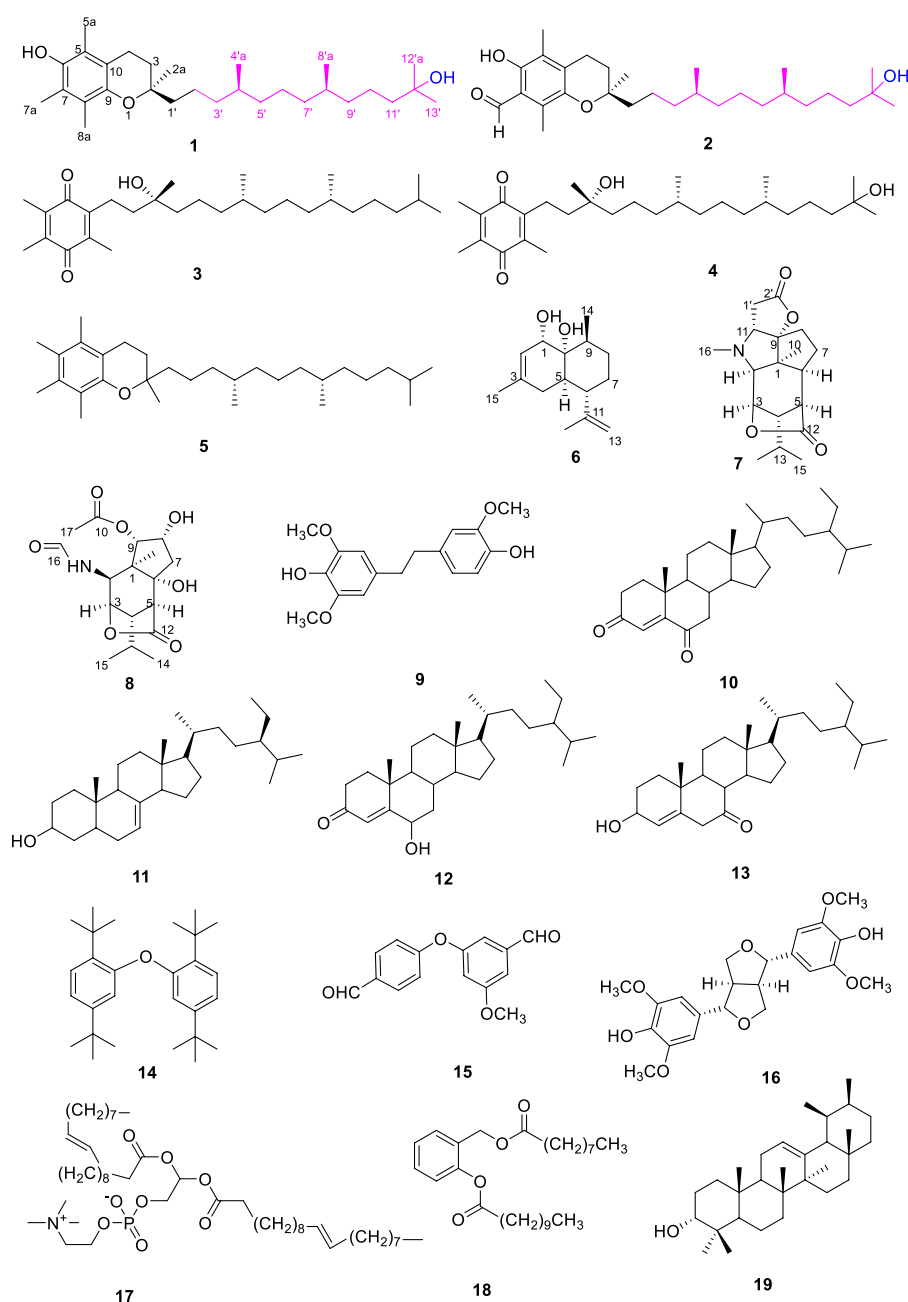


FIGURE 1
Structures of compounds 1–19.

of “Shi Hu”, mainly distributed in southwest China, as Sichuan, Guizhou, and Yunnan (Wang, 2021b). Abundant bioactive constituents of this plant have been previously obtained, including sesquiterpenes (Ling et al., 2021), phenanthrene, bibenzyl derivatives (Cheng et al., 2020), glucosides (Zhao et al., 2001), and alkaloids (Liu and Zhao, 2003). In order to further reveal and utilize the potential value of *Dendrobium nobile* as an industrial crop used in the pharmaceutical and

food industries, we conducted the current study. As a result, nineteen compounds (1–19) (Figure 1), including two new vitamin E homologues (1–2), one new sesquiterpene (6), and two new dendrobines (7, 8), were isolated and identified from the stems of *D. nobile*. In addition, the antioxidant, anti-inflammatory, and anti-tumour activities of the compounds (1–19) were evaluated. These outstanding properties of *Dendrobium nobile* will better expand its applications in

antioxidant, anti-inflammatory, and anti-tumour activities area, especially in the field of pharmaceuticals and food industries.

Materials and methods

General experimental procedures

Optical rotations were measured on an AntonPaar MCP500 polarimeter. IR spectra were performed on a Shimadzu IR spectrometer with KBr disk. HRESIMS were used for a Bruker maXis TOF-Q mass spectrometer. Bruker DRX-500 spectrometer was used to measure the NMR spectra. The UV spectra were recorded on a Shimadzu UV-2600 PC spectrometer. Silica gel (100–200 mesh, 200–300 mesh, Qingdao, China), YMC*GEL ODS-A (S-50 μ m, 12 nm) (YMC Co., Ltd., Kyoto, Japan), Sephadex LH-20 (GE, Sweden) were used for column chromatography. Semipreparative HPLC was used for ODS column (YMC-ODS-A). CD spectra were performed on a Biologic MOS-450 spectra polarimeter.

Plant material

The stems of *Dendrobium nobile* were provided by the Chengming Shihu Industrial Development in October, 2020. The sample was botanically identified by Prof. Dan Zhang. A voucher specimen (No. GFM20201024) has been deposited at the Processing and Preparation Laboratory of Traditional Chinese Medicine, Southwest Medical University (Luzhou, China).

Extraction and isolation

The air-dried stems (2 kg) of *Dendrobium nobile* were crushed and extracted with 95% EtOH (4 \times 20 L, 3 days each). After the solvent was evaporated under reduced pressure. The extract (172.6 g) was subjected to column chromatography (CC) over MCI resin and eluted with EtOH-H₂O (50, 70, 90 and 100%, v/v), to obtain four fractions (Fr.1- Fr.4).

Fr. 1 (62.6 g) was subjected to silica gel column chromatography with gradient elution using methylene chloride/methanol (40:1 to 0:1, v/v) to give eleven subfractions (Fr. 1-1 and Fr.1-11). Fr. 1-2 (1.9 g) was separated by silica gel column with petroleum ether/ethyl acetate (from 15:1 to 0:1, v/v) to yield Fr.1-2-1~Fr.1-2-10. Fr.1-2-2 was analyzed by TLC, and the preparation condition was dichloromethane: acetone = 40:1 to obtain compound **16** (6.9 mg). Compound **17** (t_R = 25 min, 47.3 mg) and compound **18** (t_R = 32 min, 13.7 mg) were purified from Fr.1-2-3, using HPLC (MeOH/H₂O, 55:45, v/v). Fr.1-2-4 was isolated by HPLC (MeOH/H₂O, 55:45, v/v) to obtain compound **19** (t_R = 45 min, 23.7 mg).

TABLE 1 ¹H and ¹³C NMR (600 MHz) data for **1** and **2** in CDCl₃.

No.	1		2	
	δ_C , type	δ_H (J in Hz)	δ_C , type	δ_H (J in Hz)
1	—	—	—	—
2	74.5, C	—	75.2, C	—
3	31.6, CH ₂	1.78, m	30.8, CH ₂	1.82, m
4	20.8, CH ₂	2.60, t (6.9)	18.4, CH ₂	3.03, t (6.8)
5	118.6, C	—	124.2, C	—
6	144.5, C	—	155.8, C	—
7	121.1, C	—	114.5, C	—
8	122.6, C	—	138.4, C	—
9	145.5, C	—	144.0, C	—
10	117.4, C	—	117.6, C	—
1'	39.7, CH ₂	1.53, m	39.5, CH ₂	1.55, m
2'	21.0, CH ₂	1.39, m	20.9, CH ₂	1.40, m
3'	37.6, CH ₂	1.27, m	37.6, CH ₂	1.26, m
4'	32.8, CH	1.39, m	32.8, CH	1.39, m
5'	37.5, CH ₂	1.27, m	37.4, CH ₂	1.26, m
6'	24.5, CH ₂	1.06, m	24.5, CH ₂	1.06, m
7'	37.4, CH ₂	1.07, m	37.4, CH ₂	1.08, m
8'	32.7, CH	1.39, m	32.7, CH	1.39, m
9'	37.4, CH ₂	1.07, m	37.4, CH ₂	1.08, m
10'	21.8, CH ₂	1.30, m	21.8, CH ₂	1.30, m
11'	44.3, CH ₂	1.43, m	44.3, CH ₂	1.43, m
12'	71.2, C	—	71.1, C	—
13'	29.3, CH ₃	1.25, m	29.7, CH ₃	1.25, m
Me-2a	23.8, CH ₃	1.23, m	23.7, CH ₃	1.23, s
Me-5a	11.3, CH ₃	2.11, s	11.3, CH ₃	2.15, s
Me-7a	12.3, CH ₃	2.16, s	194.0, C	10.20, s
Me-8a	11.8, CH ₃	2.14, s	13.2, CH ₃	2.17, s
Me-4'a	19.7, CH ₃	0.85, d (6.6)	19.7, CH ₃	0.85, d (6.6)
Me-8'a	19.7, CH ₃	0.86, d (6.6)	19.7, CH ₃	0.86, d (6.3)
Me-12'a	29.2, CH ₃	1.18, m	29.3, CH ₃	1.26, m

Fr. 2 (6.2 g) was isolated into five subfractions (Fr. 2-1 and Fr.2-5) through silica gel column chromatography with gradient elution using petroleum ether/ethyl acetate (30:1 to 0:1, v/v). Compound **15** (5.9 mg) was purified from Fr. 2-3, and the preparation condition was dichloromethane: acetone (40:1).

Fr. 3 (29.7 g) was separated by silica gel column chromatography with gradient elution using petroleum ether/ethyl acetate (30:1 to 0:1, v/v) to produce nine subfractions (Fr. 3-1 and Fr.3-9). Fr. 3-1 was analyzed by TLC, and further purified by preparative TLC with dichloromethane/acetone (40:1) to afford compounds **3** (6.2 mg) and **4** (7.1 mg). Fr. 3-2 (599 mg) was fractionated into four subfractions (Fr. 3-2-1 and Fr.3-2-4) by silica gel column chromatography with gradient elution using petroleum ether/ethyl acetate (15:1 to 0:1, v/v). Fr. 3-2-4 was separated by Sephadex LH-20 column and purified by PTLC

TABLE 2 ^1H and ^{13}C NMR (600 MHz) data for 6-8 in CDCl_3 .

NO.	6		7		8	
	δ_{C} , type	δ_{H} (J in Hz)	δ_{C} , type	δ_{H} (J in Hz)	δ_{C} , type	δ_{H} (J in Hz)
1	68.9, CH	4.13, d (4.8)	54.5, C	—	49.4, C	—
2	122.0, CH	5.38, d (6.0)	68.7, CH	2.90, s	50.5, CH	4.49, d (10.3)
3	128.7, C	—	79.1, CH	4.93, m	82.1, CH	4.44, d (4.5)
4	37.4, CH_2	2.59, m, 1.96, m	51.2, CH	2.17, m	53.0, CH	2.18, m
5	46.8, CH	1.93, m	43.5, CH	2.25, m, 2.19, m	48.1, CH	3.01, d (4.3)
6	49.7, CH	2.47, dd (12.0, 3.6)	43.7, CH	2.51, m, 2.44, m	77.6, C	—
7	32.2, CH_2	1.45, m	36.0, CH_2	2.20, m, 1.90, m	56.2, CH_2	3.58, m
8	32.0, CH_2	1.71, m	30.4, CH_2	2.34, m	64.0, CH	3.71, m
9	42.6, CH	1.75, m	104.8, C	—	79.3, CH	4.85, s
10	72.0, C	—	25.7, CH_3	1.35, s	170.1, C	—
11	148.4, C	—	69.5, CH	3.57, d (6.0)	24.9, CH_3	1.29, s
12	19.1, CH_3	1.71, s	178.8, C	—	174.8, C	—
13	111.0, CH_2	4.75, d (12.0)	24.9, CH	1.81, m	26.6, CH	2.20, m
14	15.2, CH_3	1.12, d (6.5)	20.5, CH_3	0.99, s	21.8, CH_3	1.08, d (5.6)
15	23.8, CH_3	1.72, s	21.2, CH_3	0.98, s	20.5, CH_3	1.01, d (6.0)
16	—	—	35.6, CH_3	2.57, m	161.3, CH	8.25, s
17	—	—	—	—	21.4, CH_3	2.24, s
1'	—	—	33.4, CH_2	2.43, s	—	—
2'	—	—	175.9, C	—	—	—

with petroleum ether/ethyl acetate (3:1) to obtain compounds **5** (9.3 mg) and **6** (5.9 mg). Fr. 3–5 (1.7035 g) was eluted with silica gel column chromatography using petroleum ether/ethyl acetate (10:1 to 0:1, v/v) and was further separated by PTLC and Sephadex LH-20 (MeOH) to obtain compounds **8** (15.2 mg), **9** (6.4 mg), and **10** (3.6 mg). Fr. 3-5-4 was successively subjected to silica gel CC (dichloromethane/acetone, 40:1) and PTLC to get compounds **11** (5.6 mg) and **7** (18.9 mg). Fr.3-7 was prepared by both silica gel column chromatography and PTLC to obtain compound **12** (9.3 mg). Fr.3-8 was prepared by silica gel column chromatography and PTLC to obtain compound **13** (12.8 mg). Fr.3-9 was prepared by silica gel column chromatography and PTLC to obtain compound **14** (5.4 mg).

Fr. 4 (16.3 g) was chromatographed using silica gel CC and eluted by petroleum ether/ethyl acetate (30:1 to 0:1, v/v) to provide six subfractions (Fr. 4-1 and Fr.4–6). Fr. 4-3 was further fractionated through Sephadex LH-20 (MeOH) as well as PTLC (dichloromethane/acetone, 40:1) to obtain compounds **1** (5.1 mg) and **2** (4.0 mg).

12'-hydroxy- α -tocopherol (**1**)

Yellow oil; $[\alpha]_{\text{D}}^{25}$ -2.1 (c 0.1, MeOH); UV (MeOH) λ_{max} (log ϵ) 290 (2.64) nm; IR (film)vmax 3430, 2970, 1760, 1450, 1360, 1218, 1190, 1118, 1080, 990, cm^{-1} ; ^1H NMR and ^{13}C NMR data, see Table 1; HRESIMS m/z 445.3638 $[\text{M}-\text{H}]^-$ (calcd for $\text{C}_{29}\text{H}_{49}\text{O}_3$, 445.3690).

Aldehyde- α -tocopherol (**2**)

Yellow oil; $[\alpha]_{\text{D}}^{25}$ -1.4 (c 0.1, MeOH); UV (MeOH) λ_{max} (log ϵ) 297 (4.32) nm; IR (film)vmax 3409, 2960, 1745, 173, 1650, 1558, 1460, 1380, 1260, 1060, 940 cm^{-1} ; ^1H NMR and ^{13}C NMR data, see Table 1; HRESIMS m/z 459.3425 $[\text{M}-\text{H}]^-$ (calcd for $\text{C}_{29}\text{H}_{47}\text{O}_4$, 459.3483).

Hydroxy-(+)-epicubenol (**6**)

White amorphous solid; $[\alpha]_{\text{D}}^{25}$ +42 (c 0.2, MeOH); IR (film)vmax 3340, 2968, 2896, 1460, 1381, 1058, 1012, 896 cm^{-1} ; ^1H NMR and ^{13}C NMR data, see Table 2; HRESIMS m/z 219.1745 $[\text{M}+\text{H}-\text{H}_2\text{O}]^+$ (calcd for $\text{C}_{15}\text{H}_{23}\text{O}$, 219.1702).

Dendroterpene F (**7**)

White solid; $[\alpha]_{\text{D}}^{25}$ -15.9 (c 0.1, MeOH); CD (MeOH) λ_{max} ($\Delta\epsilon$) 230 (3.15), IR (film)vmax 3440, 2950, 2862, 1780, 1590, 1460, 1383, 1240, 1040 cm^{-1} ; ^1H NMR and ^{13}C NMR data, see Table 2; HRESIMS m/z 320.1941 $[\text{M}+\text{H}]^+$ (calcd for $\text{C}_{18}\text{H}_{26}\text{NO}_4$, 320.1947).

Dendroterpene G (**8**)

White solid; $[\alpha]_{\text{D}}^{25}$ +12.4 (c 0.20, MeOH); CD (MeOH) λ_{max} ($\Delta\epsilon$) 219 (3.45), IR (film)vmax 3420, 2980, 1780, 1678, 1505, 1380, 1243, 1024 cm^{-1} ; ^1H NMR and ^{13}C NMR data, see Table 2; HRESIMS m/z 354.1565 $[\text{M}-\text{H}]^-$ (calcd for $\text{C}_{17}\text{H}_{24}\text{NO}_7$, 354.1601).

ECD calculations

The calculations of compounds (1–2, 7–8) were achieved using Gaussian 16. At the B3LYP/6–311+G (d,p) level, ECD calculations were chosen for the optimized conformations. And finally, the ECD spectra were obtained by SpecDis version 1.63 software.

Antioxidant activity assays

The DPPH radical scavenging activity was performed according to a previously described method.³⁰ Briefly, a series of various concentrations of the samples (200, 100, 50, 25 μ M) were mixed with DPPH (0.2 mM) in a 96-well microplate. After that, the absorbance of the mixture to react was measured at 517 nm. Percentages of the free radical-scavenging capacity of all the compounds (1–19) were calculated with the following equation:

$$\text{Scavenging rate (\%)} = (A_0 - A_1)/A \times 100 \quad (1)$$

A_0 and A_1 respectively represent the absorbance of the control and the samples. The ascorbic acid was the positive control in this assay. All the results were the averages of triplicate measurements. The IC_{50} values were calculated by Graphpad prism 7.0 statistic software.

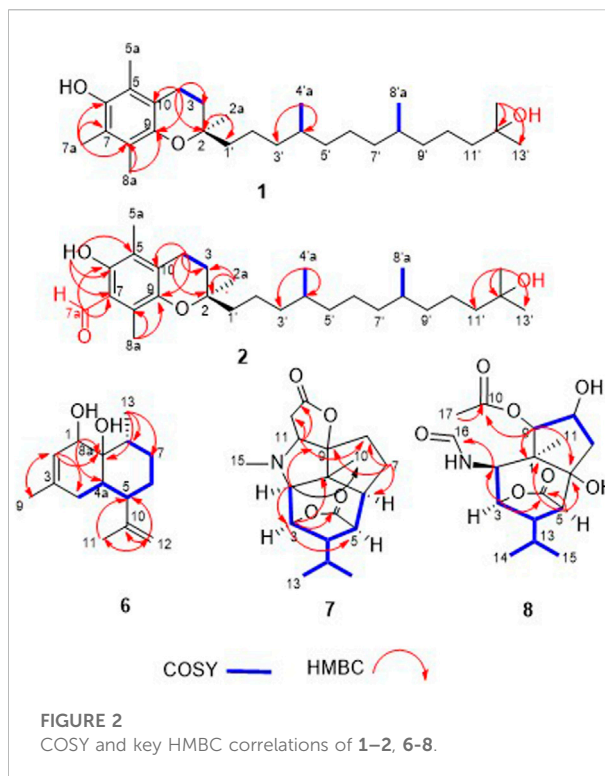
Inhibition of NO production assays

The RAW 264.7, Hela, and HepG2 cells were obtained from Southwest Medical University, and cultured in DMEM medium with 10% FBS, 2 mM glutamine, 100 U/mL of penicillin, and 100 μ g/mL of streptomycin at 37°C under 5% CO₂ atmosphere. The cytotoxicities of compounds (1–19) against the cell lines including RAW 264.7, Hela, and HepG2 cells were determined by the MTT method as previously reported (Lei et al., 2021). The RAW 264.7 cells were plated in six-well plates with 1×10^6 cell/well. After 24 h, the cells were pretreated with compounds 1–19 (33 μ M) for 2 h. The Griess method was used to detect NO production as previously described.

Results and discussion

Identification of compounds

Compound 1 was obtained as a yellow oil. Its molecular formula was assigned as C₂₉H₅₀O₃ by the HRESIMS at m/z 445.3638 [M–H][–]. The ¹H NMR data (see Supplementary Figure S2 in Supplementary Material) of compound 1 revealed the presence of eight methyl signals at 0.85 (d, J = 6.6 Hz, Me-



4'a), 0.86 (d, J = 6.3 Hz, Me-8'a), 1.18 (m, Me-7a), 1.18 (m, Me-12'a), 1.25 (m, Me-13'), 1.23 (m, Me-2a), 2.11 (s, Me-5a), 2.16 (s, Me-7a), 2.14 (s, Me-8a), two methylenes at δ_H 2.60 (t, J = 6.9 Hz, H-4), 1.78 (m, H-3), and other overlapped protons (Table 1). Meanwhile, the ¹³C NMR data (see Supplementary Figure S3 in Supplementary Material) showed 29 carbon signals corresponding to eight methyls, eleven methylenes, two methines carbons, and four oxygenated carbons, including two olefinic carbon, and four quaternary carbons. The similarity of NMR features of compound 1 with α -tocopherol suggested it was a vitamin E derivative (Fiorentino et al., 2009), with the only difference being the presence of the additional oxygenated carbons at C-12' (δ_C 71.2), which was supported by the HMBC (see Supplementary Figure S5 in Supplementary Material) correlation from H-13' (δ_H 1.25) to C-12'a (δ_C 29.2), C-11' (δ_C 44.3), and C-12' (δ_C 71.2). Furthermore, HMBC correlations between H-4 (δ_H 2.60) and C-3 (δ_C 31.6), C-2 (δ_C 74.5), C-9 (δ_C 145.5), and C-10 (δ_C 117.4) and between H-2a (δ_H 1.23) and C-1' (δ_C 39.7), C-2 (δ_C 74.5), and C-3 (δ_C 31.6) reconfirmed that the side chain located at C-2 (Figure 2). In addition, the relative stereochemistry of compound 1 was deduced based on NMR data and NOESY experiment (see Supplementary Figure S7 in Supplementary Material). The configuration of C-2, C-4'a, and C-8'a at the side chain of compound 1 was determined by comparing the ¹³C NMR data with the related compound, α -tocopherol and α -tocomonoenol (Fiorentino et al., 2009) (Kyeong-Hwa et al.,

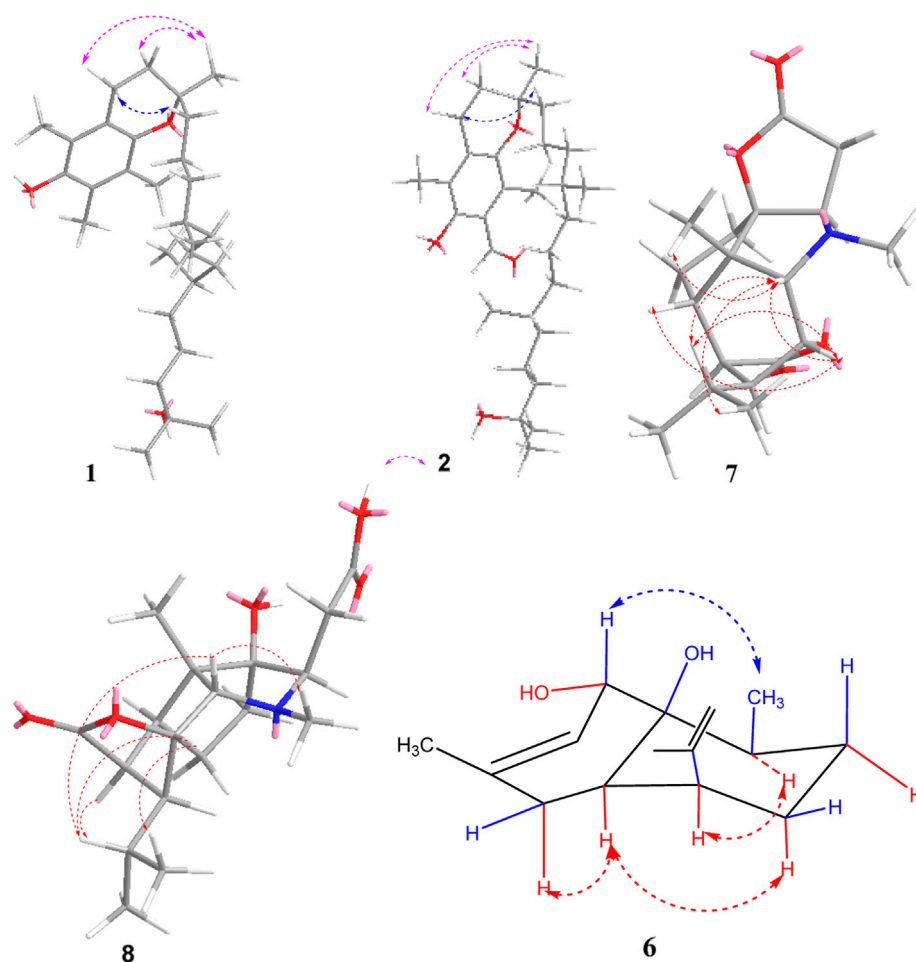


FIGURE 3
Key NOESY correlations of compounds 1–2, 6–8.

2013). The observed NOESY correlations from H-3/H-2a to H-4 α (they were in the same plane), from H-1' β to H-4 β , demonstrated that the chirality (C-2) of the compound **1** was *R* (Figure 3). In order to confirm the configuration of **1**, the calculated NMR chemical shifts of four possible diastereomers, (2*R*, 4'*aR*, 8'*aS*)-**1a**, (2*R*, 4'*aS*, 8'*aS*)-**1b**, (2*R*, 4'*aR*, 8'*aR*)-**1c**, and (2*R*, 4'*aS*, 8'*aR*)-**1d**, were obtained by DP4⁺ probability analysis at the PCM/mPW1PW91/6–31+G (d,p) level (see Supplementary Figure S42 in Supplementary Material). As shown in Figure 4, DP4⁺ analysis suggested that (2*R*, 4'*aS*, 8'*aR*)-**1d** was the most likely candidate with 98.26% probability. Meanwhile, the CD spectrum of compound **1** showed a negative Cotton effect at 183 nm and a positive Cotton effect at 208 nm suggesting the 2*R*, 4'*aS*, and 8'*aR* configuration in compound **1** (Figure 5). Hence compound **1** was determined and named 12'-Hydroxy- α -tocopherol.

Compound **2** was obtained as a yellow oil, of which the molecular formula was assigned to be C₂₉H₄₈O₄ by ¹³C NMR

data and HRESIMS *m/z* 459.3425 [M-H][−]. It is found that the ¹H and ¹³C NMR spectroscopic data of compound **2** (Table 1) were similar to those of compound **1**, indicating that compound **2** was also an α -tocopherol derivative, with the major difference being the absence of a methyl signal at C-7, while the presence of one additional aldehyde group (δ_{H} 10.20, δ_{C} 194.0) in compound **2**. This conclusion was confirmed by the HMBC (see Supplementary Figure S12 in Supplementary Material) correlations from H-7a to C-7 (δ_{C} 114.5), C-6 (δ_{C} 155.8), and C-8 (δ_{C} 138.4). On the basis of the similar chemical shifts and the biosynthetic pathway, we suggest that compounds **1** and **2** had the same relative configurations for C-2, C-4'a, and C-8'a. Furthermore, the observed NOESY (see Supplementary Figure S14 in Supplementary Material) correlations of compound **2** also supported the above deductions (Figure 3). The absolute configurations of compound **2** was determined by comparison of the CD spectrum. As well, the CD spectrum of compound **2** had a similar Cotton effect to those of compound **1** (Figure 5).

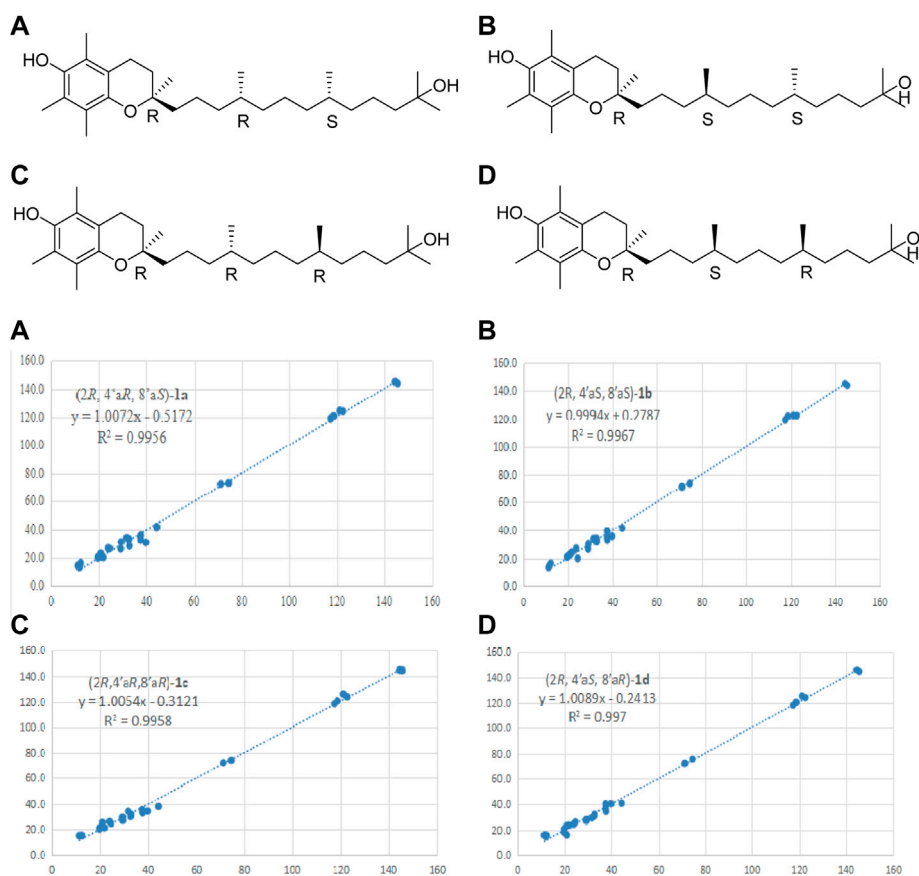


FIGURE 4

Linear regression fitting of computed ^{13}C -NMR chemical shifts of the calculated configuration of compound **1** with the experimental values.

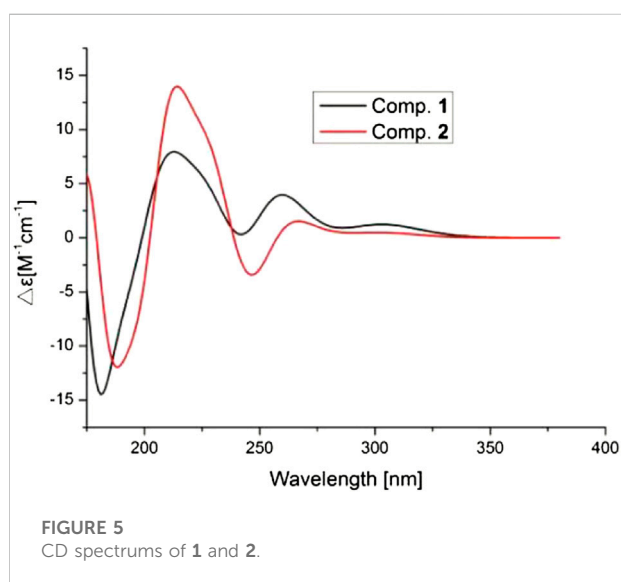


FIGURE 5

CD spectra of **1** and **2**.

Therefore, the structure of compound **2** was determined as 2*R*, 4'*aS*, and 8'*aR*, and named 7-aldehyde- α -tocopherol.

The molecular formula of compound **6** was assigned to be $\text{C}_{15}\text{H}_{24}\text{O}_2$ on the basis of the HRESIMS spectrum at m/z 219.1745 $[\text{M}+\text{H}-\text{H}_2\text{O}]^+$ and ^{13}C NMR data. Additionally, a detailed analysis of its ^1H NMR data (Table 2) exhibited the existence of three olefinic protons at δ_{H} 5.38 (1H, s, H-2) and 4.75 (2H, d, $J = 12.0$, H-13), three methyl signals at δ_{H} 1.72 (3H, s, H₃-15), 1.71 (3H, br. s, H₃-12), and 1.12 (3H, d, $J = 6.5$, H-14). The ^{13}C NMR spectrum of compound **6** exhibited 15 carbon signals, which were assigned to three methyl groups, four methylenes, four methines, two quaternary carbons, and two oxygenated carbons. The ^1H and ^{13}C NMR data of compound **6** suggested that it was very similar to a related sesquiterpene, decalin triol (Kawatsura et al., 1997), except for the presence of signals for an additional olefinic proton group (δ_{H} 5.38, δ_{C} 122.0), a methyl group (δ_{H} 1.72, δ_{C} 23.8), and the lack of signals for a hydroxy group. HMBC (see Supplementary Figure S19 in Supplementary

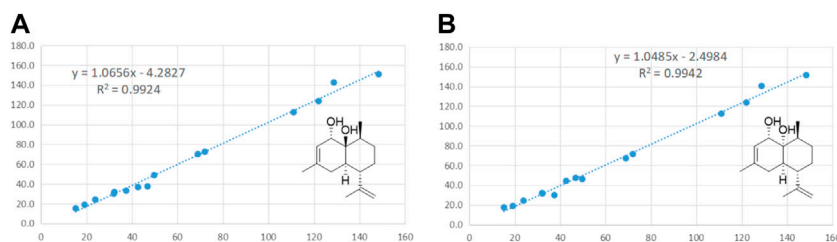


FIGURE 6

Linear regression fitting of computed ^{13}C -NMR chemical shifts of the calculated configuration of compound **6** with the experimental values.

Material) correlations between H-2 (δ_{H} 5.38) and C-15 (δ_{C} 23.8), C-4 (δ_{C} 37.4), and C-10 (δ_{C} 72.0) and between H-15 (δ_{H} 1.72) and C-4 (δ_{C} 37.4), C-2 (δ_{C} 122.0), and C-3 (δ_{C} 128.7) reconfirmed that the methyl group located at C-3. The NOESY (see Supplementary Figure S21 in Supplementary Material) correlations from H-1 to H₃-13 and H-4 α , from H-4 α to H-5, and from H-5 to H-9 indicated that H-1, H₃-14, H-6, and H-4 α were on the same side, while H-5 and H-9 located on the opposite side (Figure 3). To further confirm the configuration of compound **6**, the theoretical NMR calculations and DP4+ probability were performed. The ^{13}C NMR chemical shifts of **6a** and **6b** were calculated at the PCM/mPW1PW91/6-31+G (d,p) level. According to the DP4+ probability analyses, **6b** was the most likely candidate with 99.99% probability. Accordingly, the configuration of **6** was established (Figure 6). Therefore, compound **6** was determined to be 1-hydroxy-(+)-epicubenol.

Compound **7** was obtained as a white amorphous powder. Its molecular formula, $\text{C}_{18}\text{H}_{25}\text{NO}_4$, was established on the HRESIMS (m/z 320.1941 $[\text{M}+\text{H}]^+$). The ^1H NMR spectrum (Table 2) of compound **7** displayed resonances attributed to four methyl groups at δ_{H} 0.98 (3H, s, H₃-15), δ_{H} 0.99 (3H, s, H₃-14), δ_{H} 1.35 (3H, s, H₃-10), and δ_{H} 2.57 (3H, m, H₃-16), as well as an oxymethine groups at 4.93 (m, H-3). The ^{13}C NMR spectrum of compound **7** displayed 18 carbon signals, which were assigned to four methyl groups, three methylenes, seven methines, four

quaternary carbons, including an oxygenated quaternary carbon, two carbonyl, and an quaternary carbon center. The above data suggested that compound **7** was very similar to those of (–)-(1*R*,2*S*,3*R*,4*S*,5*R*,6*S*,9*S*,11*R*)-11-carboxymethyldendrobin (Meng et al., 2017), which was an analogue of dendrobin (Wang et al., 1985; Cassayre and Zard, 1999). The major difference was due to the presence of signals of the oxygenated quaternary carbon (δ_{C} 104.8) and the lactone bridge (C2'-C9) in compound **7**, instead of one methine in (–)-(1*R*,2*S*,3*R*,4*S*,5*R*,6*S*,9*S*,11*R*)-11-carboxymethyldendrobin, which was supported by the HMBC (see Supplementary Figure S26 in Supplementary Material) correlations from H-2 (δ_{H} 2.90) to C-9 (δ_{C} 104.8), C-3 (δ_{C} 79.1), C-11 (δ_{C} 69.5), C-1 (δ_{C} 54.5), and C-10 (δ_{C} 25.7), from H-7 (δ_{H} 1.90) to C-9 (δ_{C} 104.8), C-1 (δ_{C} 54.5), C-5 (δ_{C} 43.5), and C-8 (δ_{C} 30.4), from H-1' (δ_{H} 2.43) to C-2' (δ_{C} 175.9), C-9 (δ_{C} 104.8), and C-11 (δ_{C} 69.5) (Figure 2). In the NOESY spectrum (see Supplementary Figure S28 in Supplementary Material), the key correlations of H-2 with H₃-14, H-10, and H-13, of H-3 with H-13, H-2, and H-6 suggested that these protons were co-facial. The relative configuration of **7** was determined as 1*R*,2*S*,3*R*,4*S*,5*R*,6*S*,11*R*. The absolute configuration of the (–)-(1*R*,2*S*,3*R*,4*S*,5*R*,6*S*,9*S*,11*R*)-11-carboxymethyldendrobin was determined using CD spectrum and synthetic product (Meng et al., 2017) (Cassayre and Zard, 1999). With

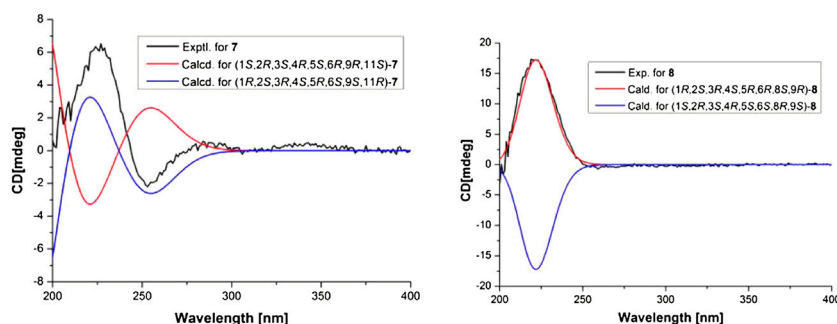
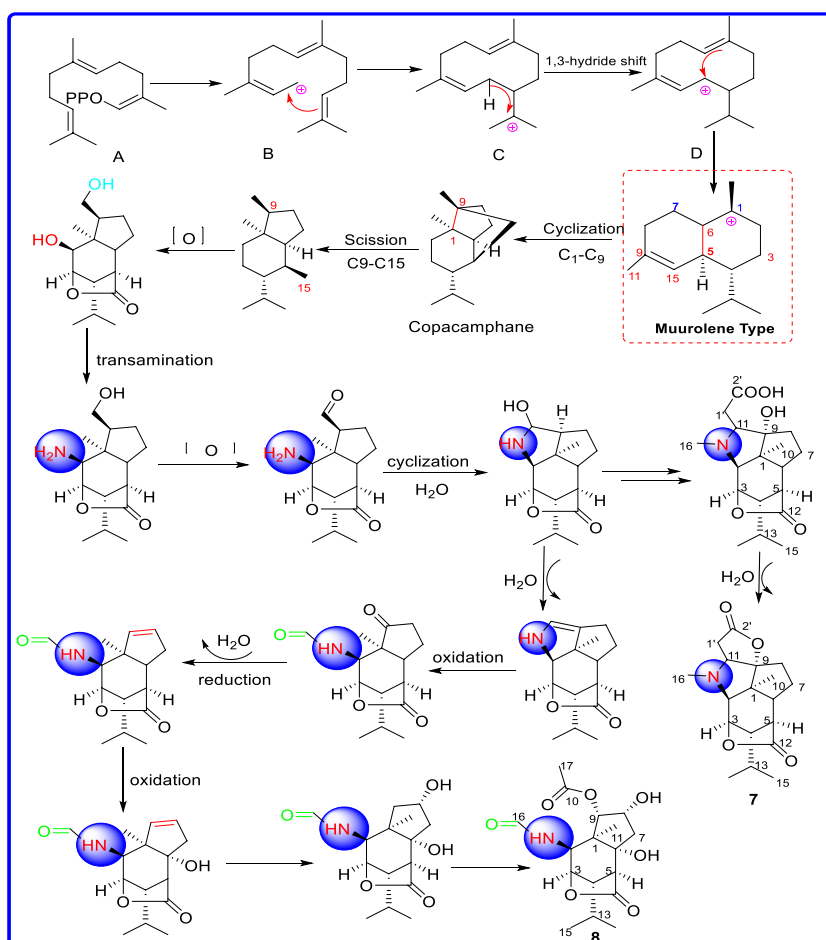


FIGURE 7

Comparison between calculated and experimental ECD spectra of **7** and **8**.



SCHEME 1
Plausible biosynthetic pathway of compounds **7** and **8**.

comparison to the ^{13}C NMR data of both compounds, compound 7 possessed the same relative configuration as the known compound. In order to determine the absolute configurations of 7, the electronic circular dichroism (ECD) spectrum of 7 was carried out. As a result, the calculated spectrum of (1R,2S,3R,4S,5R,6S,9S,11R)-7 matched well with the experimental data (Figure 7), indicating absolute configuration of 7, to be 1R,2S,3R,4S,5R,6S,9S,11R. Thus, compound 7 was established and named dendroterpene F.

The molecular formula of compound **8** was assigned to be C₁₇H₂₅NO₆ on the basis of HRESIMS. And detailed analysis of the NMR data (Table 2) (see Supplementary Figure S32 in Supplementary Material) of compound **8** implied that it was very similar to those of dendroterpene B (Wang et al., 2019). However, the major difference was that one additional ester carbonyl carbon (δ_C 170.1) was present while a double bond was absent in compound **8**, indicating that the double bond was reduced to methines. And the key NOESY (see Supplementary

Figure S37 in Supplementary Material) correlations of H-2 with H₃-11, H-13, of H-3 with H₃-15, H-13, and of H-5 with H-13 suggested the relative configuration was 1*R*, 2*S*, 3*R*, 4*S*, 5*R*, 6*R*, 8*S*, 9*R* (**Figure 3**). Meanwhile, the similar chemical shifts of compound **8** suggested it had the same configurations for C-1, C-2, C-3, C-4, C-5, and C-11 as dendroterpene B, the absolute configuration of which was determined by single crystal X-ray diffraction. Given that both compound **8** and dendroterpene B were isolated from the congeneric species, the absolute configuration of the former was deduced as 1*R*, 2*S*, 3*R*, 4*S*, 5*R*, 6*R*, 8*S*, and 9*R*. Then this assignment was confirmed by the calculated ECD spectrum of (1*R*, 2*S*, 3*R*, 4*S*, 5*R*, 6*R*, 8*S*, 9*R*)-**8** (**Figure 7**). Thus, the structure of compound **8** was finally elucidated and named dendroterpene F.

By comparing NMR data with the previous report, the structures of isolated compounds (**3-5**, **9-19**) were identified as: α -tocopherolquinone (**3**) (Yan et al., 2015), 2-(3,15-dihydroxy-3,7,11,15-tetramethylhexadecyl)-3,5,6-trimethyl-2,5-

TABLE 3 DPPH free-radical-scavenging of compounds 1–19^a.

Sample	DPPH inhibition rate (%)	IC ₅₀ (μmol/L)
1	43.21	—
2	90.02	59.13 ± 2
3	15.88	—
4	18.82	—
5	4.19	—
6	10.34	—
7	18.62	—
8	8.84	—
10	6.22	—
11	36.17	—
12	2.78	—
13	2.45	—
17	2.45	—
18	2.45	—
19	80.36	363.77 ± 3
Ascorbic acid	90.69	101.67 ± 0.2

^aCompounds that are not shown in this table did not exhibit activity.

cyclohexadiene-1,4-dione (4) (Yan et al., 2015), dl- α -tocopherol (5) (Ghelf et al., 2019), mascatilin (9) (Majumder and Sen, 1987), stigmast-4-ene-3, 6-dione (10) (Shen et al., 2002), (3 β ,5 α ,20R,24R)-ster-7-en-3-ol (11) (Jaha et al., 1995), stigmast-4-en-6 β -ol-3-one (12) (Niu et al., 2001), 7-keto- β -sitosterol (13) (Yu et al., 2007), 2, 2'-oxybis (1, 4)-di-tert-butylbenze (14) (Cao et al., 2020), 3-(4'-formylphenoxy)-4-methoxybenzaldehy-de (15) (Cao et al., 2020), (+)-syringaresinol (16) (Wang et al., 2009), 1,2-di-O-9Z-octadecenoyl-sn-glycero-3-phosphorylcholine (17) (Kwon et al., 2003), methyl 2-nonanoate-3-undecanoate-cyclohexyl-1,4-diene ester (18) (Li and Xu, 2018), eqi- α -amyrin (19) (Albert and Duilio, 2005).

Plausible biosynthetic pathway of compounds 7 and 8

From a biosynthetic perspective, characterized by a picrotoxane carbon skeleton with polycyclic and seven contiguous stereocenters, dendrobines are derived from the same precursor, copacamphane. First, the copacamphane are presumably derived from farnesyl pyrophosphate (FPP) through 1,3-hydride shift, cyclization, reduction, dehydration, and oxygenation to form the core skeleton. Then copacamphane may be transformed via the break-off of carbon-carbon bonds at C (9)~C (15) to form picrotoxane, followed by subsequent transamination, oxidation, cyclization, and methyltransferase at C (2)~C (9) to produce compound 7, which successively undergoes dehydration, oxidation, acetylation to provide compound 8 (Scheme 1).

TABLE 4 Inhibition of NO production with IC₅₀ values of compounds 17 and 19^a.

Sample	IC ₅₀ (μmol/L)
17	36.70 ± 2
19	19.47 ± 1
Dexamethasone	17.46 ± 2

^aCompounds that are not shown in this table did not exhibit activity.

TABLE 5 Cytotoxic (IC₅₀ in μM) Activities of Compounds 1–4^a.

Sample	IC ₅₀ (HepG2)/μM	IC ₅₀ (Hela)/μM
1	>100	—
2	51.28 ± 3	18.71 ± 3
3	19.75 ± 1	—
4	37.06 ± 2	19.51 ± 1
Cisplatin	6.58 ± 3	14.93 ± 1

^aCompounds that are not shown in this table did not exhibit activity.

Biological activities

Antioxidant activity

DPPH assays are common methods to evaluate the antioxidant capacity of compounds, thus the antioxidant capacity of compounds 1–19 were evaluated by DPPH assays (Table 3). As a result, the DPPH radical scavenging assay showed that compound 2 (IC₅₀ = 59.13 ± 2 μM) had a stronger efficiency than that of the positive control (ascorbic acid, VC) (IC₅₀ = 101.67 ± 0.2 μM), while compound 19 (IC₅₀ = 363.77 ± 3 μM) exhibited potent antioxidant activity as compared with the ascorbic acid.

Inhibition of NO production

To evaluate the activities of the isolated compounds, compounds 1–16 were tested by examining their ability to inhibit NO production in LPS-stimulated RAW 264.7 macrophage cells. The test activities showed that compounds 17 and 19 exhibited inhibition of NO production with IC₅₀ values of (19.47 ± 1 μM) and (36.7 ± 2 μM), respectively (Table 4). In addition, compounds 17 and 19 did not exhibit cytotoxic. Therefore, these two compounds might serve as potential lead drug to develop NO inhibitors.

Cytotoxicity activity

The cytotoxic activities of compounds (1–19) against Hela and HepG2 cells were evaluated by MTT assay (Table 5). However, Only compounds 2 and 4 exhibited cytotoxic effects against Hela cell lines with the IC₅₀ values of with IC₅₀ of

($18.71 \pm 3 \mu\text{M}$) and ($19.51 \pm 1 \mu\text{M}$), which were comparable to positive control cisplatin ($14.93 \pm 1 \mu\text{M}$). In addition, compounds **2**, **3**, and **4** showed inhibitory activity against HepG2 cells with IC_{50} of ($51.28 \pm 3 \mu\text{M}$), ($19.75 \pm 1 \mu\text{M}$) and ($37.06 \pm 2 \mu\text{M}$), respectively, and cisplatin was used as positive controls ($6.58 \pm 3 \mu\text{M}$). Unfortunately, the remained compounds did not show obvious cytotoxicity.

In addition, comparison of the structural characteristics among these compounds, the structure activity relationship is discussed. Compound **2** displayed higher antioxidant activity than compound **1**, which may be due to the additional aldehyde group at C-7 in **2**, which was in agreement with a previous report (Fiorentino et al., 2009). This result might indicate that the aldehyde group is an important functional group that can increase antioxidant capacity. Comparing with the antioxidant activity compound **2**, compound **3** was inactive, which indicated the side chain group at C-2 for the compounds **2** and **3**, were not essential for antioxidant activities.

Conclusion

As a popular cash crop and a traditional herbal medicine, the extract of *D. nobile* Lindl. has been reported to possess antioxidant, anti-tumour, and anti-inflammatory activities. However, the chemical constituents and biological activities of *Dendrobium nobile* have not been elucidated yet. Therefore, in our current study, chemical composition of the extract of *Dendrobium nobile* was isolated and analyzed. Nineteen compounds, including five new compounds (**1–2**, **6–8**) and fourteen known compounds (**3–5**, **9–19**). Antioxidant tests indicated that compound **2** displayed significant antioxidant activity, while compound **19** displayed weak antioxidant activity compared with ascorbic acid (VC). Meanwhile, compound **2** possessed the aldehyde group, which might be an important functional group for antioxidant ability. Besides, the structure-activity relationships (SARs) of tested compounds also suggested that the aldehyde group may play an important role in DPPH radical scavenging. These results implied that the structural variation of vitamin E analogues significantly affected the bioactivity. In addition, compounds **2** and **4** also exhibited an equal effect to positive control cisplatin. Therefore, this research provided a reliable support for *Dendrobium nobile* as potential application in the pharmaceutical and food industries.

Additionally, increasing evidence suggests that oxidative stress plays an important role in the pathogenesis of Alzheimer's disease (AD) (Guidi et al., 2006). Thus, the inhibition of oxidative stress could be a feasible treatment against Alzheimer's disease (AD). Fortunately, studies have shown that natural antioxidants

could exert positive effects against oxidative stress-induced chronic metabolic diseases (Xu et al., 2015). As an important source of natural antioxidants, the *Dendrobium nobile* has attracted much attention in the treatment of AD (Yan et al., 2015). Interestingly, compound **19** not only exhibited antioxidant activity, but also displayed inhibition of NO production, while did not exhibit cytotoxic. The result is consistent with the results reported in the previous literature (Nie et al., 2020). Antioxidant and anti-inflammatory activities are associated with a series of signaling pathways, which may interact with each other in the pathological process of AD (Nie et al., 2020). Therefore, compound **19** might serve as potential lead drug to treat Alzheimer's disease (AD). Findings from this current study provide insights on the phytochemical constituents and significant antioxidant activities of *Dendrobium nobile*, which are critical for the further development for its applications in Alzheimer's disease (AD).

Data availability statement

The original contributions presented in the study are included in the article/Supplementary Material, further inquiries can be directed to the corresponding authors.

Author contributions

HL and SZ performed the extraction, isolation and identification, and wrote the manuscript. JL and LZ contributed to the collection and identification the stems of *Dendrobium nobile*. YZ, XF, and SC contributed to this work by bioassay experiments. HN and FL accomplished the ECD calculation. CW and DZ performed revised the manuscript. All authors have read and agreed to the published version of the manuscript.

Funding

This work was supported in part by grants from National Natural Science Foundation of China (No. 31900293), 2019 Ministry of Education "Chunhui Plan" Cooperative Scientific Research Project (No. 131) and the Fundamental Research Funds of China West Normal University (19B038), the Open Project of Sichuan Industrial Institute of Antibiotics, Chengdu University (ARRLKF20-04), "Student's Platform for Innovation and Entrepreneurship Trainig Program" (S202110632258), (201910632030), (2019036). Basic Scientific Research Fund of Southwest Medical University (2021ZKQN104, 2021CXYY03).

Conflict of interest

The authors declare that the research was conducted in the absence of any commercial or financial relationships that could be construed as a potential conflict of interest.

Publisher's note

All claims expressed in this article are solely those of the authors and do not necessarily represent those of their affiliated

organizations, or those of the publisher, the editors and the reviewers. Any product that may be evaluated in this article, or claim that may be made by its manufacturer, is not guaranteed or endorsed by the publisher.

Supplementary material

The Supplementary Material for this article can be found online at: <https://www.frontiersin.org/articles/10.3389/fchem.2022.988459/full#supplementary-material>

References

- Albert, E., and Duilio, A. (2005). Revisited after 50 years: The stereochemical interpretation of the biogenetic isoprene rule for the triterpenes. *Helv. Chim. Acta* 88, 3011–3050. doi:10.1002/hlca.200590245
- Cao, J., Yang, J. N., Zhou, X. Q., Zhang, Y. Y., Zhu, X. Y., Yue, R. M., et al. (2020). Chemical constituents of *Psychotria hainanensis*. *Chem. Nat. Compd.* 56, 533–534. doi:10.1007/s10600-020-03081-4
- Cassayre, J., and Zard, S. Z. (1999). A short synthesis of (–)-dendrobine. *J. Am. Chem. Soc.* 121, 6072–6073. doi:10.1021/ja990707p
- Cheng, L., Guo, D. L., Zhang, M. S., Hu, L. L., Fu, S. B., Deng, Y., et al. (2020). Dihydrophenanthrofurans and bisbibenzyl derivatives from the stems of *Dendrobium nobile*. *Fitoterapia* 143, 104586. doi:10.1016/j.fitote.2020.104586
- Fiorentino, A., Mastellone, C., D'abrosca, B., Pacifico, S., Scognamiglio, M., Cefarelli, G., et al. (2009). δ -Tocomenonol: A new vitamin E from kiwi (*Actinidia chinensis*) fruits. *Food Chem.* 115, 187–192. doi:10.1016/j.foodchem.2008.11.094
- Ghelf, M., Maddalena, L. A., Stuart, J. A., Atkinson, J., Harroun, T. A., and Marquardt, D. (2019). Vitamin E-inspired multi-scale imaging agent. *Bioorg. Med. Chem. Lett.* 29, 107–114. doi:10.1016/j.bmcl.2018.10.052
- Guidi, I., Galimberti, D., Lonati, S., Novembrino, C., Bamonti, F., Tirittico, M., et al. (2006). Oxidative imbalance in patients with mild cognitive impairment and Alzheimer's disease. *Neurobiol. Aging* 27, 262–269. doi:10.1016/j.neurobiolaging.2005.01.001
- Jaha, N., Ahmed, W., and Malik, A. (1995). New steroidal glycosides from *mimusops elengi*. *J. Nat. Prod. (Gorakhpur)*. 58, 1244–1247. doi:10.1021/np50122a014
- Kawatsura, M., Kishi, E., Kito, M., Sakai, T., Shirahama, H., and Matsuda, F. (1997). Hydroxyl-directed stereocomplementary pinacol cyclizations mediated by SmI₂. *Synlett* 1997 (SI), 479–480. doi:10.1055/s-1997-6153
- Kwon, H. C., Jung, I. Y., Cho, S. Y., Cho, O. R., Yang, M. C., Lee, S. O., et al. (2003). Phospholipids from *Bombycis corpus* and their neurotrophic effects. *Arch. Pharm. Res.* 26, 471–477. doi:10.1007/bf02976865
- Kyeong-Hwa, S., Lee, D., Nam, T., Kim, D., Lee, D., Kim, E., et al. (2013). New tocopherol analogue with radical-scavenging activity from the peels of citrus *unshiu* Marcovich. *J. Korean Soc. Appl. Biol. Chem.* 56, 747–750. doi:10.1007/s13765-013-3230-6
- Lei, H., Bi, X. X., Lin, X. P., She, J. L., Luo, X. W., Niu, H., et al. (2021). Heterocornols from the sponge-derived fungus *Pestalotiopsis heterocornis* with anti-inflammatory activity. *Mar. Drugs* 19, 585. doi:10.3390/md19110585
- Li, Q. H., and Xu, D. P. (2018). Chemical constituents of pumpkin seeds against benign prostatic hyperplasia. *Nat. Prod. Res. Dev.* 30, 978–982. doi:10.16333/j.1001-6880.2018.6.011
- Ling, H. C., Gu, R. H., and Qin, L. K. (2021). Research progress on chemical constituents and pharmacological effects of *Dendrobium nobile*. *Chin. Traditional Herb. Drugs* 52, 7693–7708. doi:10.7501/j.jissn.0253-2670.2021.24.032
- Liu, Q. F., and Zhao, W. M. (2003). A new dendrobine-type alkaloid from *Dendrobium nobile*. *Chin. Chem. Lett.* 14, 278–279.
- Majumder, P. L., and Sen, R. C. (1987). Moscatilin, a bibenzyl derivative from the orchid *Dendrobium moscatum*. *Phytochemistry* 26, 2121–2124. doi:10.1016/S0031-9422(00)81777-X
- Meng, C. W., He, Y. L., Peng, C., Ding, X. J., Guo, L., and Xiong, L. (2017). Picrotoxane sesquiterpenoids from the stems of *Dendrobium nobile* and their absolute configurations and angiogenesis effect. *Fitoterapia* 121, 206–211. doi:10.1016/j.fitote.2017.07.017
- Nie, X. Q., Chen, Y., Li, W., and Lu, Y. L. (2020). Anti-aging properties of *Dendrobium nobile* Lindl.: From molecular mechanisms to potential treatments. *J. Ethnopharmacol.* 257, 112839. doi:10.1016/j.jep.2020.112839
- Niu, X. M., Li, S. H., Peng, L. Y., Lin, Z. W., Rao, G. X., and Sun, H. D. (2001). Constituents from *Limonia crenulata*. *J. Asian Nat. Prod. Res.* 3, 299–311. doi:10.1080/10286020108040370
- Shen, C. C., Syu, W. J., Li, S. Y., Lin, C. H., Lee, G. H., and Sun, C. M. (2002). Antimicrobial activities of naphthazarins from *Arnebia euchroma*. *J. Nat. Prod. (Gorakhpur)*. 65, 1857–1862. doi:10.1021/np010599w
- Teixeira da Silva, T. J. A., and Ng, T. B. (2017). The medicinal and pharmaceutical importance of *Dendrobium* species. *Appl. Microbiol. Biotechnol.* 101, 2227–2239. doi:10.1007/s00253-017-8169-9
- Wang, H., Zhao, T., and Che, C. T. (1985). Dendrobine and 3-hydroxy-2-oxodendrobine from *Dendrobium nobile*. *J. Nat. Prod.* 48, 796–801. doi:10.1021/np50041a014
- Wang, L. Q., Zhao, Y. X., Zhou, L., and Zhou, J. (2009). Lignans from *gnetum montanum* Markgr. f. megalocarpua. *Chem. Nat. Compd.* 45, 424–426. doi:10.1007/s10600-009-9325-y
- Wang, P., Chen, X., Wang, H., Huang, S. Z., Cai, C. H., Yuan, J. Z., et al. (2019). Four new picrotoxane-type sesquiterpenes from *Dendrobium nobile* Lindl. *Front. Chem.* 7, 812–818. doi:10.3389/fchem.2019.00812
- Wang, Y. H. (2021a). Traditional uses and pharmacologically active constituents of *Dendrobium* plants for dermatological disorders: A review. *Nat. Prod. Bioprospect.* 11, 465–487. doi:10.1007/s13659-021-00305-0
- Wang, Y. H. (2021b). Traditional uses, chemical constituents, pharmacological activities, and toxicological effects of *Dendrobium* leaves: A review. *J. Ethnopharmacol.* 270, 113851. doi:10.1016/j.jep.2021.113851
- Xu, J., Ji, F. F., Sun, X. C., Cao, X. R., Li, S., Ohizumi, Y. S., et al. (2015). Characterization and biological evaluation of diterpenoids from *Casearia graveolens*. *J. Nat. Prod. (Gorakhpur)*. 78, 2648–2656. doi:10.1021/acs.jnatprod.5b00583
- Yan, X. T., Lee, S. H., Li, W., Jang, H. D., and Kim, Y. H. (2015). Terpenes and sterols from the fruits of *Prunus mume* and their inhibitory effects on osteoclast differentiation by suppressing tartrate-resistant acid phosphatase activity. *Arch. Pharm. Res.* 38, 186–192. doi:10.1007/s12272-014-0389-2
- Yu, B. C., Yang, M. C., Lee, K. H., Kim, K. H., and Lee, K. R. (2007). Norsesquiterpene and steroid constituents of *Humulus japonicus*. *Nat. Prod. Sci.* 13, 332–336.
- Zhao, W. M., Ye, Q. H., Tan, X. J., Jiang, H. L., Li, X. Y., Chen, K. X., et al. (2001). Three new sesquiterpene glycosides from *Dendrobium nobile* with immunomodulatory activity. *J. Nat. Prod.* 64, 1196–1200. doi:10.1021/np0102612
- Zheng, S. G., Hu, Y. D., Zhao, R. X., Yan, S., Zhang, X. Q., Zhao, T. M., et al. (2018). Genome wide researches and applications on *Dendrobium*. *Planta* 248, 769–784. doi:10.1007/s00425-018-2960-4



OPEN ACCESS

EDITED BY

Siva S. Panda,
Augusta University, United States

REVIEWED BY

Piyush Baindara,
University of Missouri, United States
David Cole Stevens,
University of Mississippi, United States

*CORRESPONDENCE

Wesaal Khan,
wesaal@sun.ac.za

SPECIALTY SECTION

This article was submitted to Medicinal and Pharmaceutical Chemistry, a section of the journal Frontiers in Chemistry

RECEIVED 23 August 2022

ACCEPTED 13 September 2022

PUBLISHED 05 October 2022

CITATION

Clements-Decker T, Kode M, Khan S and Khan W (2022), Underexplored bacteria as reservoirs of novel antimicrobial lipopeptides. *Front. Chem.* 10:1025979. doi: 10.3389/fchem.2022.1025979

COPYRIGHT

© 2022 Clements-Decker, Kode, Khan and Khan. This is an open-access article distributed under the terms of the [Creative Commons Attribution License \(CC BY\)](#). The use, distribution or reproduction in other forums is permitted, provided the original author(s) and the copyright owner(s) are credited and that the original publication in this journal is cited, in accordance with accepted academic practice. No use, distribution or reproduction is permitted which does not comply with these terms.

Underexplored bacteria as reservoirs of novel antimicrobial lipopeptides

Tanya Clements-Decker¹, Megan Kode², Sehaam Khan¹ and Wesaal Khan^{2*}

¹Faculty of Health Sciences, University of Johannesburg, Doornfontein, South Africa, ²Department of Microbiology, Faculty of Science, Stellenbosch University, Stellenbosch, South Africa

Natural products derived from microorganisms play a prominent role in drug discovery as potential anti-infective agents. Over the past few decades, lipopeptides produced by particularly *Bacillus*, *Pseudomonas*, *Streptomyces*, *Paenibacillus*, and cyanobacteria species, have been extensively studied for their antimicrobial potential. Subsequently, daptomycin and polymyxin B were approved by the Food and Drug Administration as lipopeptide antibiotics. Recent studies have however, indicated that *Serratia*, *Brevibacillus*, and *Burkholderia*, as well as predatory bacteria such as *Myxococcus*, *Lysobacter*, and *Cystobacter*, hold promise as relatively underexplored sources of novel classes of lipopeptides. This review will thus highlight the structures and the newly discovered scaffolds of lipopeptide families produced by these bacterial genera, with potential antimicrobial activities. Additionally, insight into the mode of action and biosynthesis of these lipopeptides will be provided and the application of a genome mining approach, to ascertain the biosynthetic gene cluster potential of these bacterial genera (genomes available on the National Center for Biotechnology Information) for their future pharmaceutical exploitation, will be discussed.

KEYWORDS

lipopeptides, antimicrobial activity, biosynthesis, antibiotics, genome mining, antiSMASH

Introduction

Microbial natural products are valuable sources of structurally diverse, antimicrobial compounds; many of which are currently implemented as therapeutic agents (Genilloud, 2014; Challinor and Bode, 2015). However, microbial resistance to several classes of commercial antimicrobials has compromised the successful treatment of infectious diseases, resulting in significant morbidity and mortality rates worldwide (Genilloud, 2014; Murray et al., 2022). There is thus an urgent need to not only discover new lead antimicrobial classes that effectively combat multidrug-resistant pathogens, but to integrate innovative approaches and technologies into antimicrobial drug discovery (Genilloud, 2014). A prominent class of microbial natural products that has gained

interest over the last several decades, due to their potent bioactive properties, is lipopeptides (Patel et al., 2015).

Structurally, lipopeptide antibiotics are characterised by a core hydrophilic head-group of amino acids considered as the peptide moiety, linked to a hydrophobic fatty acid (FA) chain, resulting in their amphiphilic nature (Cochrane and Vederas, 2016; Reynolds et al., 2018). A wide variety of lipid chains has been observed, including variation in their chain length, configuration, and degree of unsaturation, while variation in the peptide moiety is due to the change in amino acid composition, which may be cyclic or linear (Burgard et al., 2017; Reynolds et al., 2018). This variation in the structural diversity of lipopeptides results in a broad range of beneficial biological properties, including antibacterial, antiviral, antifungal, antitumor and immunomodulator activities (Patel et al., 2015).

The isolation and characterisation of amphotycin (produced by a *Streptomyces canus* strain) over 60 years ago, then pioneered the usage of lipopeptides as antibiotics (Heinemann et al., 1953; Reynolds et al., 2018). Subsequently, the class of lipopeptides expanded, where prospecting for new lipopeptides primarily focused on exploiting a relatively small group of bacterial genera, including *Streptomyces*, *Bacillus*, *Pseudomonas*, *Paenibacillus*, and cyanobacteria (Patel et al., 2015; Li et al., 2021a). In 2003, the cyclic lipopeptide antibiotic, daptomycin (also called Cubicin®), produced by *Streptomyces roseosporus*, was approved by the Food and Drug Administration for the treatment of serious skin and soft tissue infections, and in 2006, for the treatment of methicillin-resistant *Staphylococcus aureus* (*S. aureus*; MRSA) bacteraemia (Strieker and Marahiel, 2009; Cochrane and Vederas, 2016). Moreover, several different lipopeptides, such as tsushimycin, daptomycin and surfactin, amongst others, have also shown promise as antiviral drug candidates against the coronavirus, SARS-CoV-2 (Chowdhury et al., 2021; De Vries et al., 2021).

Recently, several bacterial genera such as *Serratia*, *Brevibacillus* and *Burkholderia*, have emerged as underexplored sources of novel antimicrobial lipopeptides (Etzbach et al., 2014; Burgard et al., 2017; Ganley et al., 2018; Li et al., 2018; Sang et al., 2019; Ning et al., 2021). For example, four species within the *Serratia* genus, including *Serratia marcescens* (*S. marcescens*), *Serratia plymuthica* (*S. plymuthica*), *Serratia ureilytica* (*S. ureilytica*), and *Serratia surfactantifaciens* (*S. surfactantifaciens*), have been reported as lipopeptide producers, with serrawettin W1 (also referred to as serratamolide), serrawettin W2 or stephensiolides families, produced by various strains (Kuo et al., 2012; Menezes et al., 2021; Clements-Decker et al., 2022). Strains of *Brevibacillus laterosporus* (*B. laterosporus*) and *Brevibacillus brevis* (*Br. brevis*) also produce several lipopeptide families, such as tauramamides, bogorols, brevibacillins, brevilaterins, brevicidines, laterocidines, relacidines, brevistin and surfactin (Barsby et al., 2006; Desjardine et al., 2007; Wang et al., 2010;

Yang et al., 2016; Li et al., 2018, 2020a, 2020b; Ning et al., 2021). Moreover, *Burkholderia* species have emerged as promising lipopeptide producers, as several species within the genus [including *Burkholderia ambifaria* (*B. ambifaria*), *Burkholderia pseudomallei* (*B. pseudomallei*), *Burkholderia plantarii* (*B. plantarii*), *Burkholderia gladioli* (*B. gladioli*), and *Burkholderia glumae* (*B. glumae*)] produce burkholdines, icosalides, haereogladins, haereoglumins, haereogladiodins, haereoplantins, burriogladins, burrioglumins, burriogladiodins, burrioplantins, malleipeptins and glidopeptins families (Tawfik et al., 2010; Biggins et al., 2014; Dose et al., 2018; Niehs et al., 2018; Thongkongkaew et al., 2018; Wang et al., 2018; Yoshimura et al., 2020; Chen et al., 2021).

Predatory bacteria have also been recognised as natural factories of bioactive compounds, as their lifestyle depends on the production of various enzymes and secondary metabolites to naturally invade and consume specific prey microorganisms as a nutrient source (Rosenberg and Varon, 1984; Herencias et al., 2020; Sester et al., 2020; Atterbury and Tyson, 2021). Certain predatory bacterial genera, such as *Myxococcus*, *Cystobacter*, and *Lysobacter*, have then been identified to produce lipopeptides during secondary metabolism (Herrmann et al., 2017; Yan et al., 2018; Yue et al., 2022). For example, one of the most extensively studied lipopeptides produced by *Myxococcus* species [including *Myxococcus virescens* (*M. virescens*), *Myxococcus xanthus* (*M. xanthus*) and an unclassified *Myxococcus* sp.], are the myxochromides, whilst cystomanamides from *Cystobacter* species [including *Cystobacter fuscus* (*C. fuscus*)], have also been structurally elucidated (Etzbach et al., 2014). In addition, *Lysobacter* have recently been highlighted as a promising source of lipopeptides, as various species within the genus [including *Lysobacter enzymogenes* (*L. enzymogenes*), *Lysobacter antibioticus* (*L. antibioticus*), *Lysobacter capsica* (*L. capsica*) and an unclassified *Lysobacter* sp.] were reported as lipopeptide producers, with WAP-8294A, WBP-29479A1, lysocin and tripropeptin families described (Sang et al., 2019; Arlt et al., 2021).

Genetically, these lipopeptide classes are primarily synthesised non-ribosomally during secondary metabolism by complex enzymes known as non-ribosomal peptide synthetases (NRPSs) and polyketide synthases (PKSs) that are encoded by large biosynthetic gene clusters (BGCs) (Aleti et al., 2015). Although a recent report has identified ribosomally synthesised lipopeptides (Hubrich et al., 2022), this review will primarily focus on lipopeptides synthesised non-ribosomally. The development of high-throughput whole genome sequencing technology has made it possible to identify new BGCs within genomic data and thus putatively predict structures of their associated chemical products (Kreutzer and Nett, 2012; Aleti et al., 2015). This circumvents the need to rely on bioactive-guided screening assays for the discovery of novel compounds and has subsequently promoted a paradigm shift in

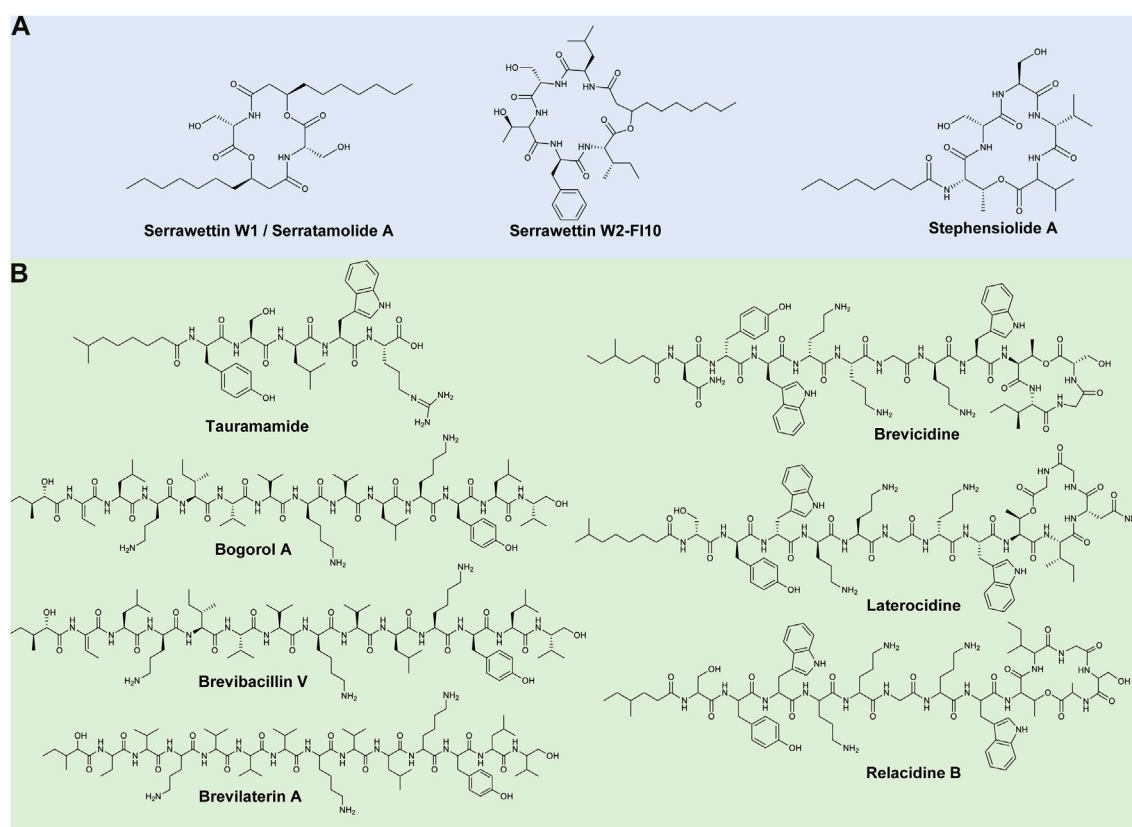


FIGURE 1

Representative lipopeptides produced by (A) *Serratia* and (B) *Brevibacillus* species. The structural information was obtained from the PubChem database (<https://pubchem.ncbi.nlm.nih.gov/>), as well as the corresponding references provided in-text. The structures were subsequently drawn in ChemDraw Ultra version 12.0.

natural product research (Kreutzer and Nett, 2012; Aleti et al., 2015). Moreover, advances in next generation sequencing have contributed to the surge of genome sequences available in public databases. Therefore, genome mining in combination with available web-based tools used for metabolite prediction, such as antibiotics and Secondary Metabolite Analysis Shell (antiSMASH), can be employed to reveal uncharacterised secondary metabolites, including lipopeptides, within the genomes of relatively unexploited bacterial genera (Aleti et al., 2015).

This review thus highlights the antimicrobial lipopeptides produced by members of the *Serratia*, *Brevibacillus*, *Burkholderia*, *Myxococcus*, *Cystobacter*, and *Lysobacter* genera that have been described to date and their subsequent antimicrobial activity and mode of action. In addition, a global genome mining approach, based on the antiSMASH web tool, was applied for the exploration of lipopeptide BGCs within the genomes of the six selected bacterial genera as available on the National Center for Biotechnology Information (NCBI) database, highlighting the various species as underexplored sources for new lipopeptide families.

Antimicrobial lipopeptides: Production by underexplored bacterial genera

Serratia

Members of the *Serratia* genus are Gram-negative, facultative anaerobes and belong to the Enterobacteriaceae family (Grimont and Grimont, 2015). The genus is comprised of 23 validly published species (available at: <https://lpsn.dsmz.de/genus/serratia>) that occur ubiquitously in water, soil, plants, insects, and marine environments (Cristina et al., 2019). Although originally considered non-pathogenic saprophytic bacteria, certain species within this genus, such as *S. marcescens*, *Serratia fonticola* (*S. fonticola*), and *S. plymuthica*, have been implicated as important nosocomial pathogens (Carrero et al., 1995; Cristina et al., 2019; Hai et al., 2020). *Serratia* species do, however, have a notable secondary metabolism, as they can produce a wide range of antimicrobial natural products, such as the well-known red pigment called prodigiosin, whilst also

showing promise as lipopeptide producers (Clements et al., 2019). To date, three lipopeptide families, as well as numerous analogues of these lipopeptides families, have been discovered, including serrawettin W1 (also referred to as serratomolide), serrawettin W2, and stephensioides (Figure 1A).

Serratomolide was first discovered by Wasserman et al. (1961), after it was produced by a *Serratia* strain, and was later isolated from a *S. marcescens* strain where the lipopeptide was referred to as serrawettin W1 (Matsuyama et al., 1985) (Figure 1A). This lipopeptide has a peptide moiety of two amino acid residues (i.e., Ser-Ser) linked to two C₁₀ fatty acid chains (Figure 1A) (Matsuyama et al., 1985). Numerous analogues of this compound have been identified, which are produced by pigmented and non-pigmented *S. marcescens*, *S. ureilytica*, and *S. plymuthica* strains (as well as a *Serratia liquefaciens* strain that was reclassified as a *S. marcescens* strain), that vary based on the length and saturation/unsaturation of the fatty acid moiety and can be cyclic or open-ring structures (Eberl et al., 1999; Labbate et al., 2007; Dwivedi et al., 2008; Kuo et al., 2012; Clements et al., 2021; Menezes et al., 2021). Serratomolides exhibit promising activity against Gram-positive bacteria, such as *Enterococcus faecalis*, *Mycobacterium* spp. and MRSA (Dwivedi et al., 2008; Kadouri and Shanks 2013; Clements et al., 2021).

Serrawettin W2 is a cyclic lipopeptide family produced by *S. marcescens* and *S. surfactantfaciens*. The peptide moiety is comprised of five amino acids (i.e., Leu-Ser-Thr-Phe-Ile) attached to a C₁₀ fatty acid chain, now referred to as serrawettin W2-FI10 (Figure 1A) (Matsuyama et al., 1986; Clements-Decker et al., 2022). Analogues of serrawettin W2 (i.e., sw-1–sw-4 and sw-6–sw-8) were putatively identified and differed based on amino acid substitutions (first, second or fifth amino acid positions) (Su et al., 2016). Similarly, Motley et al. (2017) elucidated the structures of three new analogues (i.e., W4–W6) with varying fatty acyl chain lengths and amino acid compositions (fourth or fifth amino acid positions). The serrawettin W2 family was recently expanded, and the nomenclature clarified, as 16 new analogues (such as W2-YV8, W2-Fl8, W2-FV10, W2-FL12:1, etc.) were isolated from a *S. marcescens* strain (Clements-Decker et al., 2022), which differed based on position of the final two amino acids and varying fatty acid chain length and saturation/unsaturation (Clements-Decker et al., 2022). Serrawettin W2 analogues have also exhibited promising activity against Gram-positive bacteria, such as MRSA [minimum inhibitory concentration (MIC) of 4 µg/ml] and *Enterococcus faecium* (*E. faecium*) (MIC of 15.6 µg/ml) and Gram-negative bacteria, such as *Pseudomonas aeruginosa* (*P. aeruginosa*) (Su et al., 2016; Heise et al., 2019; Clements-Decker et al., 2022). Serrawettin W3 was originally partially characterised as its own lipopeptide family and contained a fatty acid chain (dodecanoic acid) and five amino acids, including Thr, Ser,

Val, Leu and Ile (Matsuyama et al., 1986). However, Clements-Decker et al. (2022) has since suggested that W3 is an analogue of serrawettin W2-FI10 based on metabolomics and genome mining analysis.

Stephensioides are a cyclic lipopeptide family produced by various *Serratia* sp. (Ganley et al., 2018). Stephensioidide A is comprised of a peptide moiety of five amino acids of Thr-Ser-Ser-Val-Val attached to a C₈ fatty acid chain (Matsuyama et al., 1986) (Figure 1A). Analogues (stephensioides B–K) of this compound were identified, varying in the final two amino acids residues and length and saturation/unsaturation of the fatty acid chain (Ganley et al., 2018). Moreover, these lipopeptides exhibit promising activity against Gram-positive bacteria, such as *Bacillus subtilis* (*B. subtilis*) [half-maximal inhibitory concentration (IC₅₀) of 15 µg/ml], as well as antiparasitic activity against *Plasmodium falciparum* (IC₅₀ of 14 µg/ml) (Ganley et al., 2018).

Brevibacillus

Members of the *Brevibacillus* genus are rod-shaped, Gram-positive or Gram-variable firmicutes that belong to the Paenibacillaceae family (De Vos et al., 2011; Panda et al., 2014). The endospore-forming *Brevibacillus* species were genetically reclassified as a distinct genus from the *Bacillus brevis* (*B. brevis*) cluster in 1996 (Ray et al., 2020), and now consists of 29 validly published species (available at: <https://lpsn.dsmz.de/genus/brevibacillus>). Members of this genus are widely distributed in nature, occurring in soil, plants, aquatic environments, intestinal tracts of insects, and animals (Panda et al., 2014; Yang and Yousef, 2018). Although certain *Brevibacillus* species can cause infections in immunocompromised individuals, such as *Br. brevis* and *B. laterosporus*, they are rarely implicated as human pathogens (Parvez et al., 2009; Curtis et al., 2020). *Brevibacillus* species are also well-known producers of antimicrobial peptides, such as gramicidins and tyrocidines (Yang and Yousef, 2018), while members of this genus have shown promise as lipopeptide producers. Eight lipopeptide families have been identified, including tauramamides, bogorols, succilins, brevibacillins, brevilaterins, brevicidines, laterocidines and relacidines. A *Br. brevis* strain was then found to produce surfactin, a lipopeptide commonly isolated from *Bacillus* species (Wang et al., 2010). Additionally, Singh et al. (2021) identified an iturin-like lipopeptide with a structure of FA-Asp-Asp-His-Ser-Ala-Gly-Thr from *Brevibacillus* sp. GI9. Moreover, a *Br. brevis* strain (previously *B. brevis*) was found to produce an acylpeptide, namely brevistin, with a structure of FA-Thr-Dab-Asp-Gly-Asn-Asp-Gly-Trp-Ile-Dab-Phe (where Dab refers to diaminobutanoic acid) in 1975, while no recent information on this antimicrobial lipopeptide have been reported and it will thus not be discussed in this review (Shoji et al., 1976).

Tauramamide is a linear lipopeptide produced by a marine *B. laterosporus* strain (Desjardine et al., 2007) and is comprised of five amino acid residues (i.e., Tyr-Ser-Leu-

Trp-Arg) linked to a C₆ fatty acid chain (Figure 1B). Homologues of tauramamide were also elucidated and resulted from the addition of methyl or ethyl esters (Desjardine et al., 2007). Tauramamide and tauramamide ethyl ester exhibit potent activity (MIC of 0.1 µg/ml) against *Enterococcus* sp., while tauramamide ethyl ester has also been reported to display weak activity against *Candida albicans* (*C. albicans*) (Desjardine et al., 2007).

Bogorols, brevicacillins and brevilaterins are structurally similar, linear lipopeptide families produced by *B. laterosporus* strains (Barsby et al., 2001, 2006; Yang et al., 2016; Ning et al., 2021). All three lipopeptide families consist of 13 amino acids linked to a C₆-fatty acid chain, which differ based on the peptide moiety. Bogorol A, brevicacillin and brevilaterin A have peptide sequences of Dhb-Leu-Orn-Ile-Val-Val-Lys-Val-Leu-Lys-Tyr-Leu-valinol, Dhb-Leu-Orn-Ile-Ile-Val-Lys-Val-Val-Lys-Tyr-Leu-valinol, and Aba-Val-Orn-Val-Val-Val-Lys-Val-Leu-Lys-Tyr-Leu-valinol, respectively (Figure 1B) (Barsby et al., 2001, 2006; Yang et al., 2016; Ning et al., 2021). Analogues of bogorol A have been identified (bogorol B-E, B-JX, I-L), differing based on amino acid substitutions (amino acid positions of 2–5 and 9) (Barsby et al., 2006; Jiang et al., 2017; Li et al., 2020a). Succinylated bogorols (addition of a succinyl group to the third amino acid residue in bogorols I–L), named succilins, have additionally been identified (Li et al., 2020a). Moreover, Singh et al. (2021) identified a bogorol-like lipopeptide with a structure of Dhb-Tyr-Orn-Ile-Val-Val-Lys-Val-Leu-Asp-Val-Glu from *Brevibacillus* sp. SKDU10. In comparison, three analogues of brevicacillin have been identified, namely brevicacillin V, 2V, and I, and differ based on amino acid substitutions (amino acid positions of 4, 5, and 8) (Wu et al., 2019; Zhao et al., 2021). Finally, analogues of brevilaterin A (i.e., B-E, X, V1–V6) have been identified and differ based on amino acid substitutions (amino acid positions of 2–4, and 6) (Ning et al., 2021; Chen et al., 2022). All three families display potent activity against Gram-positive bacteria, such as *S. aureus* strains (MICs of 1–5 µg/ml) (Barsby et al., 2006; Ning et al., 2021; Zhao et al., 2021) as well as moderate activity against Gram-negative bacteria, such as *Escherichia coli* (*E. coli*) (MICs of 16–75 µg/ml) (Barsby et al., 2006; Zhao et al., 2021; Chen et al., 2022). The antifungal activity of these lipopeptide families has additionally been reported (Yang et al., 2016; Jiang et al., 2017; Wu et al., 2019, 2021; Ning et al., 2021; Chen et al., 2022).

Brevicidines are partially cyclised lipopeptides produced by *B. laterosporus* strains (Li et al., 2018). Brevicidine is comprised of 12 amino acids (i.e., Asn-Tyr-Trp-Orn-Orn-Gly-Orn-Trp-Thr-Ile-Gly-Ser), with the final four amino acids cyclised via a lactone bond and linked to a fatty acyl chain (i.e., 4-methyl-hexanoyl) (Figure 1B) (Li et al., 2018; Hermant et al., 2021). An analogue, namely brevicidine B, was then identified by Zhao and Kuipers (2021) and contained a single amino acid substitution (Tyr² to Phe²). The brevicidines exhibit potent activity against Gram-negative pathogens, such as *E. coli* and

Klebsiella pneumoniae (MICs of 0.25–4 µg/ml), amongst others (Zhao and Kuipers, 2021). Brevicidine also exhibits moderate activity against *B. subtilis* (MIC of 32 µg/ml), while brevicidine B displayed potent activity against vancomycin-resistant *Enterococcus* (VRE) and MRSA strains (MICs of 2–8 µg/ml) (Li et al., 2018; Zhao and Kuipers, 2021).

Laterocidine and relacidines (A and B) are partially cyclised lipopeptides produced by *B. laterosporus* strains (Li et al., 2018; 2020b). Both lipopeptide families have 13 amino acids with the final five amino acids cyclised via a lactone bond, linked to a fatty acyl chain (i.e., 7-methyl-octanoyl or 4-methyl-hexanoyl) (Li et al., 2018; Hermant et al., 2021). These lipopeptides differ based on the peptide moiety, where laterocidine has a peptide sequence of Ser-Tyr-Trp-Orn-Orn-Gly-Orn-Trp-Thr-Ile-Asn-Gly-Gly (Figure 1B), while relacidine A has a peptide sequence of Ser-Tyr-Trp-Orn-Orn-Gly-Orn-Trp-Thr-Ile-Gly-Ser-Gly. Relacidine B varies from A based on a single amino acid substitution of Gly¹³ to Ala¹³ (Figure 1B). Laterocidine and relacidines have exhibited promising activity against Gram-negative bacteria, such as *Xanthomonas campestris* (*X. campestris*), *E. coli* and *P. aeruginosa*, with MICs of 0.25–8 µg/ml recorded (excluding laterocidine against *X. campestris*, where the MIC of was not tested) (Li et al., 2018; 2020b). However, moderate or no activity was observed against Gram-positive bacteria (Li et al., 2018; 2020b).

Burkholderia

The Gram-negative *Burkholderia* genus is comprised of 34 validly published species (available at: <https://lpsn.dsmz.de/genus/burkholderia>) and belongs to the Burkholderiaceae family (Garrity et al., 2005). *Burkholderia* species are widely distributed in aquatic and soil niches, while also associating with eukaryotic hosts such as plants, fungi, animals, and humans (Coenye and Vandamme, 2003; Kunakom and Eustáquio, 2019). In particular, members of the *Burkholderia cepacia* (*B. cepacia*) complex, *Burkholderia thailandensis* (*B. thailandensis*), *Burkholderia pickettii*, *B. gladioli*, *B. pseudomallei*, and *Burkholderia mallei* (*B. mallei*) have been implicated as opportunistic human pathogens (Fernández et al., 1996; Graves et al., 1997; Srinivasan et al., 2001; Chang et al., 2017; Kunakom and Eustáquio, 2019). *Burkholderia* species have relatively large genome sizes, split up into three chromosomes and large plasmids, which contain BGCs encoding for diverse secondary metabolites, such as the lipopeptide families (Esmaeel et al., 2016). The lipopeptide families that have been discovered and characterised from *Burkholderia* species include burkholdines, icosalides, haereogladins, haereoglumins, haereogladiodins, haereoplantins, burriogladins, burrioglumins, burriogladiodins, burrioplantins, malleipeptins, and glidopeptins. Lipopeptides from *Paraburkholderia* species, such as holrhizin and rhizomide, as well as lipoglycopeptides (such as cepacine

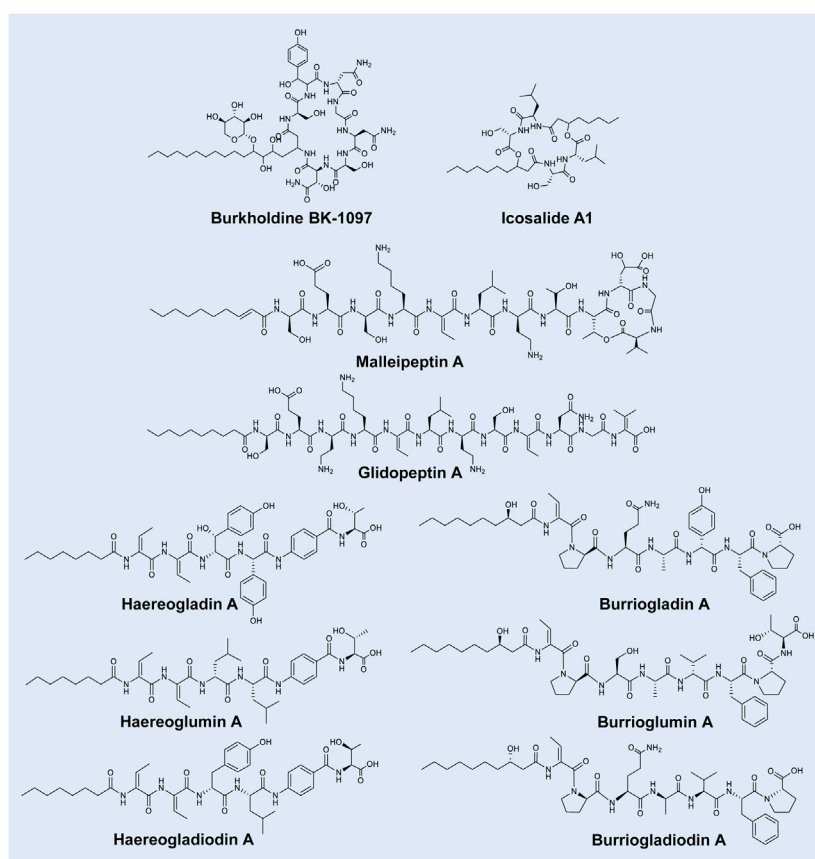


FIGURE 2

Representative lipopeptides produced by *Burkholderia* species. The structural information was obtained from the PubChem database (<https://pubchem.ncbi.nlm.nih.gov/>), as well as the corresponding references provided in-text. The structures were subsequently drawn in ChemDraw Ultra version 12.0.

from *B. cepacia*) will however, not be discussed in this review (Niehs et al., 2018; Wang et al., 2018).

Burkholdines are cyclic lipopeptides primarily produced by *B. ambifaria* and are comprised of a peptide moiety of Asn-Ser-Asn-Gly-Asn-Tyr-Ser attached to a fatty acid chain (referred to as Bk-1097; Figure 2) (Lu et al., 2009; Tawfik et al., 2010; Ellis et al., 2012). Analogues of Bk-1097 have since been identified (i.e., Bk-1229, Bk-1119, Bk-1213 and Bk-1215) and differ based on an additional xylose attached to the fatty acid chain (a cyclic glyco-lipopeptide) or amino acid substitutions (Lu et al., 2009; Ellis et al., 2012; Lin et al., 2012). The five burkholdines have been shown to exhibit promising antifungal properties, particularly against *Saccharomyces cerevisiae*, *C. albicans* and *Aspergillus niger* (MICs of 0.1–31 µg/ml) (Tawfik et al., 2010; Lin et al., 2012).

Icosalides are a family of cyclic two-tailed depsipeptides reportedly produced by a fungal *Aureobasidium* sp. (Boros et al., 2006). Dose et al. (2018) then isolated a *B. gladioli*

strain capable of producing these lipopeptides. Thus, the origin of icosalides was deliberated by Dose et al. (2018), who speculated that the icosalide-positive *Aureobasidium* culture may have contained an associated bacterial icosalide producer in or on the hyphae. Nonetheless, the structures of the icosalides (analogues of A1, A2 and B) were described as containing a peptide moiety of Leu-Ser-Ser-Leu (varying in D/L-configuration) attached to two fatty acid chains (that may vary in length of C₈ and C₁₀) (Figure 2) (Dose et al., 2018; Jenner et al., 2019). Boros et al. (2006) then found that icosalide A1 exhibits promising antibacterial activity against *Streptococcus pyogenes* (MICs of 8–16 µg/ml). In addition, icosalide A1 displayed activity against *Bacillus thuringiensis* (MIC of 12.5 µg/ml) and *E. faecium* (MIC of 16 µg/ml) (Dose et al., 2018; Jenner et al., 2019).

Malleipeptins are partially cyclised lipopeptides produced by *B. pseudomallei* strains (Biggins et al., 2014). Malleipeptin A is comprised of a peptide moiety of 12 amino acids

(i.e., Ser-Glu-Ser-Lys-Thr-Leu-Dab-Thr-Thr-Glu-Gly-Ile, where Dab refers to 2,4-diaminobutyric acid) cyclised between the final four amino acids, linked to a fatty acid chain (Figure 2). Malleipeptin B differs from A based on a substitution in the twelfth amino acid position (Biggins et al., 2014). The same lipopeptide was independently described by Esmaeel et al. (2016) following the exploration of the genomes of 48 *Burkholderia* strains and was subsequently named burkholdermycin. Glidopeptin A is a linear lipopeptide from a *Burkholderia* DSM7029 strain with structural similarity to malleipeptin and is comprised of 12 amino acids (i.e., Ser-Glu-Dab-Lys-Dhb-Leu-Dab-Ser-Dhb-Asn-Gly-Dhv; where Dhb refers to dehydrobutyryne and Dhv refers to dehydrovaline) linked to a fatty acid chain (decanoic acid) (Figure 2) (Wang et al., 2018). Weak inhibition activities (100 µg/ml) were observed for glidopeptin A against *S. aureus* and *B. subtilis* (Wang et al., 2018), while the antimicrobial activity of malleipeptins/burkholdermycin is currently unknown.

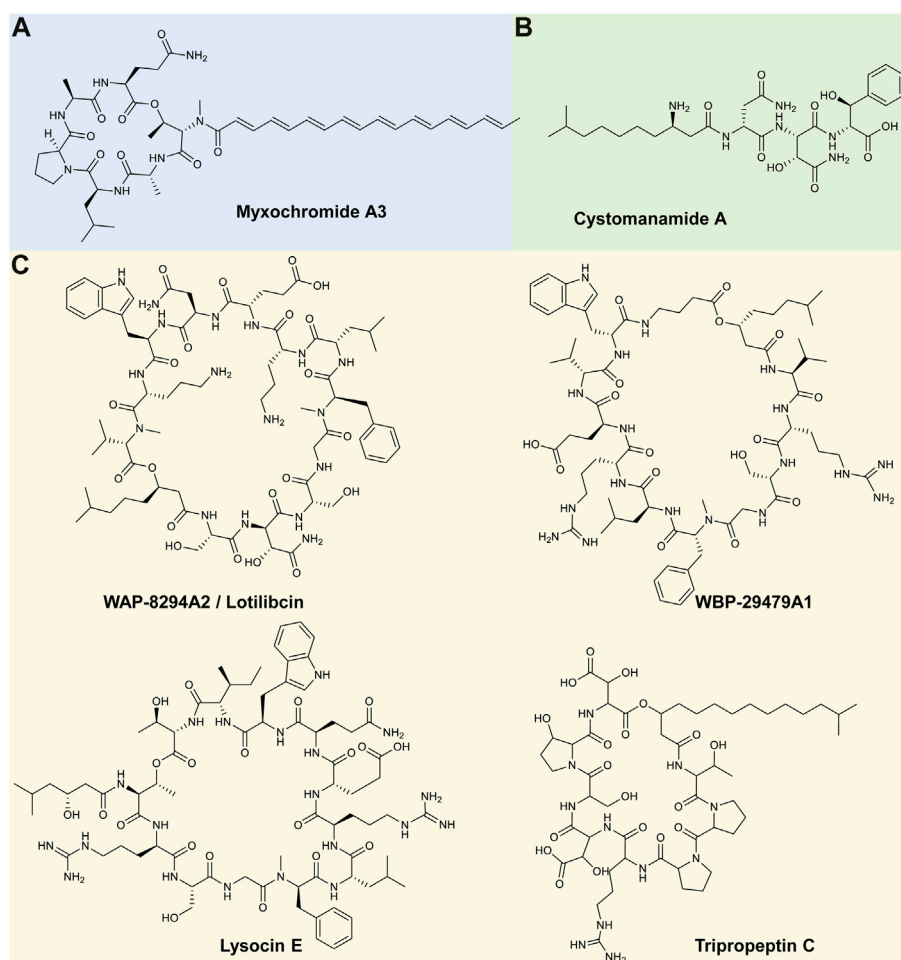
The “haereo” families of lipopeptides are comprised of the structurally similar haereogladiins, haereoglumins, haereogladiodins and haereoplantins. Haereogladiins and haereoglumins are linear lipopeptide families isolated from *B. gladioli* pv. *agaricicola* and *B. glumae* strains, respectively (Thongkongkaew et al., 2018). Haereogladin A is comprised of a peptide moiety of Dhb-Dhb-βHtyr-pHpg-PABA-Thr (where βHtyr refers to β-Hydroxytyrosine, pHpg refers to p-hydroxyphenyl glycine and PABA refers to p-amino benzoate) linked to an octanoic acid (Figure 2). Analogues (B–E) of this lipopeptide differ based on the change of βHtyr to Tyr and the presence or absence of the final amino acid (i.e., Thr) (Thongkongkaew et al., 2018). The structurally similar haereoglumin A is comprised of a peptide moiety of Dhb-Dhb-Leu-Leu-PABA-Thr linked to an octanoic acid (Figure 2). An analogue (haereoglumin B) of this lipopeptide was additionally characterised, which differed from A based on the absence of the final two residues (PABA and Thr) (Thongkongkaew et al., 2018). More recently, Chen et al. (2021) identified haereogladiodin A produced by *B. gladioli* which was comprised of a peptide moiety of Dhb-Dhb-Tyr-Leu-PABA-Thr linked to an octanoic acid, while B is comprised of Dhb-Dhb-Tyr linked to an octanoic acid (Figure 2). Structurally similar haereoplantins were then recently discovered from *B. plantarii* (Yoshimura et al., 2020). Haereoplantin A is comprised of Dhb-Dhb-(β-OH-Leu)-Hpg-PABA-Thr linked to octanoic acid. Analogues (B–H) varied in the acyl group or amino acid positions (3 or 4 or the lack of Thr) (Yoshimura et al., 2020; Li et al., 2021b). Haereogladiins and haereoglumins were evaluated for biological activity against several bacterial and fungal strains, such as MRSA, VRE, *P. aeruginosa* and *C. albicans*, amongst others; however, no activity was observed (Thongkongkaew et al., 2018). Similar results were reported by Chen et al. (2021) for haereogladiodin A and B, while the antimicrobial activity of haereoplantins is unknown.

The “burrio” families of lipopeptides consists of the structurally similar burriogladiins, burrioglumins, burriogladiodins and burrioplantins. Burriogladiins and burrioglumins are linear lipopeptide families first isolated from *B. gladioli* pv. *agaricicola* and *B. glumae* strains, respectively (Thongkongkaew et al., 2018). Burriogladin A is comprised of a peptide moiety of Pro-Phe-pHpg-Ala-Glu-Pro-Dhb linked to a fatty acid chain (β-hydroxydecanoic acid) (Figure 2) (Thongkongkaew et al., 2018). In comparison, burrioglumin A is comprised of a peptide moiety of Dhb-Pro-Ser-Ala-Val-Phe-Pro-Thr linked to β-hydroxydecanoic acid (Figure 2). An analogue (burrioglumin B) of this lipopeptide was additionally characterised, which differed from A based on a substitution of Val⁵ with Leu⁵. More recently, Chen et al. (2021) discovered burriogladiodins produced by *B. gladioli*. Burriogladiodin A is comprised of a peptide moiety of Dhb-Pro-Gln-Ala-Val-Phe-Pro linked to β-hydroxydecanoic acid (Figure 2), while burriogladiodin B has a peptide moiety of Dhb-Pro-Gln-Ala-Val-Phe-Pro-Thr. Additional analogues of burriogladiodin (C–H) were identified, that differ from B based on the amino acid substitutions and/or the absence of one or both final two residues (Chen et al., 2021). Burrioplantin A was also recently discovered from *B. plantarii* (Yoshimura et al., 2020), with a structure of Dhb-Pro-Ser-Ala-Hpg-Phe-Pro-Homoserine linked to β-hydroxydecanoic acid (Yoshimura et al., 2020). The antimicrobial potential of these lipopeptides is still currently unknown, despite efforts to test burriogladiins and burriogladiodins against selected Gram-negative and Gram-positive bacteria (Thongkongkaew et al., 2018; Chen et al., 2021).

Antimicrobial lipopeptides: Production by underexplored predatory bacterial genera

Myxococcus

The Gram-negative, rod-shaped *Myxococcus* genus belongs to the Myxococcaceae family (Chambers et al., 2020), with seven validly published species identified to date (available at: <https://lpsn.dsmz.de/genus/myxococcus>). This genus is ubiquitous in soil environments and has been isolated from various climates, including temperate zones, tropical rain forests, arctic tundra and deserts, amongst others (Mohr, 2018). Like other myxobacteria, these predators can move in co-ordinated swarms by gliding over solid surfaces; however, under nutrient-deficient conditions, they can form fruiting bodies in which myxospores are produced (Mohr, 2018). Although *Myxococcus* species produce a wide range of secondary metabolites and hydrolytic enzymes (i.e., proteases, lipases, peptidases, and glycoside hydrolases) that assist in the lysis and degradation of their prey organisms, which include Gram-negative and Gram-positive bacteria as well as fungi, their potential lipopeptide

**FIGURE 3**

Representative lipopeptides produced by (A) *Myxococcus* species, (B) *Cystobacter* species and (C) *Lysobacter* species. The structural information was obtained from the PubChem database (<https://pubchem.ncbi.nlm.nih.gov/>), as well as the corresponding references provided in-text. The structures were subsequently drawn in ChemDraw Ultra version 12.0.

production has been relatively underexplored (Burgard et al., 2017). Currently, one lipopeptide family has been characterised from this genus, namely the myxochromide lipopeptides (Hu et al., 2021).

The myxochromides are a group of cyclic depsipeptides that contain an unsaturated polyketide chain (Ohlendorf et al., 2008). Myxochromides were originally described by Wenzel et al. (2005) and were produced by a myxobacterium *Stigmatella aurantiaca* strain (producing analogues of S₁₋₃) and by a *M. virescens* strain (producing the myxochromide A analogue). Myxochromide A is a lipohexapeptide containing a peptide moiety of Thr-Ala-Leu-Pro-Ala-Gln linked to a heptaenoic acid (Wenzel et al., 2005). A follow up study by Wenzel et al. (2006) further identified a *M. xanthus* strain that could produce myxochromide analogues (A₂₋₄), which have the same peptide core as myxochromide A but differ in the

polyketide chain (Figure 3A) (Wenzel et al., 2006; Ohlendorf et al., 2008). In 2008, the myxochromide B subgroup was elucidated from a *Myxococcus* sp. strain (Ohlendorf et al., 2008), where myxochromide B₃ was found to share a similar peptide sequence as myxochromide A; however, myxochromide B₃ contained an additional Leu residue (Ohlendorf et al., 2008; Burgard, 2017). Burgard et al. (2017) further reported on the isolation of four novel myxochromides types, namely the C, D, S-Abu and S-di-Abu subgroups. The C subgroup of myxochromides had a similar peptide structure to the A-type myxochromides but without the Ala residue between the Pro and Glu residues, while the D and S subgroups myxochromides were produced by *Hyalangium*, *Cystobacterineae* sp. or *Stigmatella* species (Burgard et al., 2017). The myxochromide S₁₋₃ and B₃ were tested against Gram-positive (such as *S. aureus*) and

Gram-negative bacteria (such as *E. coli*); however, no activity has been observed to date (Wenzel et al., 2005; Ohlendorf et al., 2008; Burgard et al., 2017).

Cystobacter

The Gram-negative *Cystobacter* genus is comprised of seven validly published species (available at: <https://lpsn.dsmz.de/genus/cystobacter>) and although previous taxonomic studies have indicated that this genus belongs to the Archangiaceae family, a recent study by Waite et al. (2020) proposed its reclassification as a member of the Myxococcaceae family, within the Myxococcales order. These myxobacteria are ubiquitous in soil environments and similar to *Myxococcus* species, *Cystobacter* utilise gliding motility to move over surfaces, and are also able to form spore-filled fruiting bodies when subjected to unfavourable conditions (Akbar et al., 2017; Treuner-Lange et al., 2017). However, the *Cystobacter* fruiting bodies differ in morphology to those of the *Myxococcus* genus, and are shiny, spherical and held within a slime matrix, whereas the latter are characterised by haystack-shaped cell aggregates (Treuner-Lange et al., 2017). *Cystobacter* species have a relatively large genome size, thus enabling them to produce a vast range of secondary metabolites, including bacteriocins, polyketides, lantipeptides and microcins (Saadatpour and Mohammadipanah, 2020). Although their potential lipopeptide production has been relatively underexplored (Burgard et al., 2017), one lipopeptide family, namely the cystomanamide lipopeptides, has been characterised (Etzbach et al., 2014).

The cystomanamides are a family of four structurally similar linear lipopeptides isolated from *C. fuscus* MCy9118 (Etzbach et al., 2014). Cystomanamide A contains a peptide moiety of Asn-(β -OH-Asn)-(β -OH-Phe) linked to a fatty acid chain (i.e., 3-amino-9-methyldecanoic acid) (Figure 3B) (Etzbach, 2015). Analogues (B–D) have been identified and differ from cystomanamide A based on the addition of a Tyr and glyceric acid residues (B), fructose (C) or the addition of fructose and substitution of β -OH-Phe with Phe (D). Similar to the myxochromides produced by *Myxococcus*, to date the cystomanamides have not been reported to exhibit any antimicrobial activity (Etzbach et al., 2014; Herrmann et al., 2017).

Lysobacter

The Gram-negative *Lysobacter* genus belong to the Xanthomonadaceae family (Christensen and Cook, 1978) and are currently comprised of 67 validly published species (available at: <https://lpsn.dsmz.de/genus/lysobacter>). *Lysobacter* species have frequently been detected in soil, rhizosphere and

freshwater environments and their micro-predatory activity against various Gram-negative and Gram-positive bacteria, fungi, yeasts and even nematodes, has been reported (Hayward et al., 2010; De Bruijn et al., 2015). Moreover, *Lysobacter* species have been recognised as “peptide production specialists” (Panthee et al., 2016). The majority of the *Lysobacter* species have BGCs encoding for approximately 15 secondary metabolites, including NRPSs, NRPS hybrids, lantipeptides, bacteriocins, terpenes, amongst others (Panthee et al., 2016). Moreover, several lipopeptides that exhibit antimicrobial activity have been identified.

The WAP-8294A lipopeptide family was first isolated from a *Lysobacter* sp. WAP-8294 strain and numerous analogues (such as A1, A2, A4, Ax8, Ax9, and Ax13, etc.) of this lipopeptide have since been isolated from several *Lysobacter* sp. (Kato et al., 1997; Chen et al., 2019). This family of lipopeptides consists of at least 19 closely related cyclic lipodepsipeptides, where WAP-8294A2 was identified as the major compound produced (Harada et al., 2001). The WAP-8294A2 has a peptide moiety of 12 amino acids [peptide sequence of Ser-Asn-Ser-Gly-(Nme-Phe)-Leu-Orn-Glu-Asn-Trp-Orn-(NmeVal)], linked to a fatty acid chain (3-hydroxyl-7-methyloctanoic acid) (Figure 3C) (Zhang et al., 2011). Other members of this complex contain a similar scaffold structure but differ in their fatty acid component (Chen et al., 2019). Recently, new analogues of WAP-8294A were identified (AZ1–AZ4, AZ6, and AZ7) from a *L. enzymogenes* OH11 strain, where the structures differed from A2 in one amino acid residue or the length of the fatty acid chain (Zhu et al., 2022). Due to its potent antimicrobial activity against MRSA, WAP-8294A2 (also referred to as Lotilibcin) underwent phase I/II clinical trials by aRigen Pharmaceuticals in 2009 (Gómez Expósito et al., 2015; Yue et al., 2022). Currently, stage II clinical trials, for the topical application treatment of Gram-positive bacterial infections, are underway (Dijksteel et al., 2021).

A new cyclic lipopeptide, named WBP-29479A1, was discovered utilising genome mining analysis and was isolated from *L. antibioticus* ATCC 29479 (Sang et al., 2019). The peptide structure of this compound is comprised of Val-Arg-Ser-Gly-(Nme-Phe)-Leu-Arg-Glu-Val-Trp-Aba (where Aba refers to aminobutyric acid) (Figure 3C). This compound also exhibited strong antimicrobial activity against MRSA (MICs of 0.25–2 μ g/ml) and *Staphylococcus epidermis* (MIC \leq 0.25 μ g/ml) (Yue et al., 2022).

Lysocins were isolated from *Lysobacter* sp. RH2180-5, and currently nine congeners have been discovered (Hamamoto et al., 2015; Panthee et al., 2016). The primary cyclic lipodepsipeptide identified in this family was named lysocin E and has a peptide moiety of 12 amino acid residues [Thr-Arg-Ser-Gly-(Nme-Phe)-Leu-Arg-Glu-Gln-Trp-Ile-Thr], with an ester linkage to the fatty acid chain (3-OH-5-Me-hexanoic acid) (Figure 3C) (Hamamoto et al., 2015). Although similar in their amino acid sequence to other cyclic lipopeptides such as WAP-8294A2 and WBP-29479A1, the fatty acid of the lysocins does not form part of the cyclic system (Yue et al., 2022). Derivatives of

lysocins (A–I) have been shown to differ in the length of the fatty acid chain, and in the methylation of Phe in the fifth position (Panthee et al., 2016). While lysocin E contains Ile in the 11th position, lysocin B contains Val in this position (Panthee et al., 2016). Lysocin E has exhibited the most potent antimicrobial activity, specifically against MRSA, where an MIC of 4 µg/mL has been reported. However, activity has also been reported against methicillin-resistant and methicillin-susceptible *Staphylococcus simulans*, *Staphylococcus haemolyticus* and *Staphylococcus pseudintermedius*, as well as *B. subtilis*, *Bacillus cereus* and *Listeria monocytogenes* (*L. monocytogenes*) (Hamamoto et al., 2015).

The tripropeptins are a family of lipopeptide antibiotics that were first isolated from *Lysobacter* sp. strain BMK333-48F3. One of the major components identified from this strain was tripropeptin C (TPPC) that has a structure of eight amino acids [peptide sequence of (*allo*-Thr)-Pro-Pro-Arg-(*threo*-β-OHAsp)-Ser-(*trans*-3-OH-Pro)-(threo-β-OHAsp)] linked to a fatty acid chain (13-methyl-3-hydroxy-tetradecanoic acid) (Figure 3C) (Hashizume et al., 2011). Several derivatives of tripropeptin have been identified, each differing in the length of the fatty acid chain (Hashizume et al., 2011). Tripropeptin C is reported to exhibit the most potent antimicrobial activity against MRSA, penicillin-resistant *Streptococcus pneumoniae* and VRE (Arlt et al., 2021; Yue et al., 2022).

Mechanism of action

The mode of action of numerous lipopeptides is to primarily target the cell membrane of bacteria and fungi (Balleza et al., 2019). Various factors, such as electrostatic interactions and hydrophobicity, play an important role in the interaction of the lipopeptide with the cell membrane, and subsequent lipopeptide insertion into the membrane bilayer (Balleza et al., 2019). This results in membrane disruption (caused by pore formation or membrane solubilisation) and affects the barrier properties of the membrane (such as ion leakage), leading to cell death (Balleza et al., 2019). In the current review, despite the promising antimicrobial activity exhibited by several *Burkholderia*, *Myxococcus* and *Cysobacter* lipopeptides, the mode of action of these lipopeptides has not been extensively explored. Similarly, while serrawettin W2 analogues and stephensolides produced by *Serratia* species exhibit potent antimicrobial activity, the mode of action of these lipopeptides is currently unknown. Moreover, while Deol et al. (1973) found that 10 µg/ml of serratomolide A produced by *Serratia* species increased the rate of movement of K⁺ and H⁺ ions across the cell membrane of *S. aureus*, with no membrane permeability or cell growth inhibition detected at this lipopeptide concentration; limited information exists on the mode of action of serratomolides. Contrastingly, the mode of action of

lipopeptides produced by *Brevibacillus* and *Lysobacter* species has been investigated and will be discussed in this review.

With the exception of tauramamides, the antimicrobial mechanisms of action of several lipopeptides produced by *Brevibacillus* species have been described. For example, Li et al. (2020a) investigated the mode of action of bogorol K against *S. aureus* and *X. campestris*. This lipopeptide was then found to target the cell membrane of both Gram-negative and Gram-positive bacteria by forming pores within the membrane and causing the leakage of intracellular material. In contrast, brevibacillin first binds to the lipoteichoic acid (LTA) of *S. aureus* and lipopolysaccharides (LPS) of *Salmonella typhimurium* before interacting with the cell membrane and increasing membrane permeability, resulting in the leakage of intracellular material and leading to cell death (Yang et al., 2017; Wu et al., 2021). The mode of action of brevilaterin B was also investigated and it was found to cause membrane depolarisation of *L. monocytogenes*, while liposome analysis (model membranes) confirmed that brevilaterin B integrates into the lipid bilayer and increases membrane permeability, causing leakage of intracellular material (Liu et al., 2020). Similarly, mode of action studies revealed that brevicidine B increases membrane permeability of *S. aureus*, while causing membrane depolarisation (interfering with the proton motive force) in *E. coli* (Zhao and Kuipers, 2021). In comparison, relacidine B was found to bind to the LPS of *X. campestris* but was unable to form pores in the membrane (Li et al., 2020b). Rather, it affected the oxidative phosphorylation process of cells and diminished ATP biosynthesis (Li et al., 2020b). The laterocidines were similarly found to associate with the LPS, while no significant membrane disruption was observed against *E. coli* (Li et al., 2018). Li and co-authors (2018) thus suggested that this lipopeptide could have multiple targets and recommended additional in-depth mechanism studies.

The mechanism of action of lipopeptides produced by *Lysobacter* species, including WAP-8294A2, WBP-29479A1, lysocin E and TPPC, has been determined. Specifically, the mode of action of WAP-8294A2, WBP-2947A1 and lysocin E was revealed to cause bacterial cell membrane disruption in a menaquinone-dependent manner (Hamamoto et al., 2015; Itoh et al., 2018; Sang et al., 2019). Menaquinone is an essential component involved in electron transfer within the respiratory chain. In comparison, the potent antimicrobial activity of TPPC has been attributed to the inhibition of phosphatase activity, which is crucial for the peptidoglycan biosynthesis process. More specifically, TPPC forms a complex with undecaprenyl pyrophosphate in the presence of calcium ions and, thus interfering with the lipid cycle of the cell wall synthesis (Hashizume et al., 2011). It has also been reported that TPPC is able to potentiate and re-sensitise MRSA to beta (β)-lactam antibiotics, further indicating this compound's promise as an effective antimicrobial agent (Hashizume et al., 2015).

TABLE 1 Summary of the known PKS-NRPS BGCs identified from *Serratia*, *Brevibacillus*, and *Burkholderia* species.

Lipopeptide	Producing genus	Gene name	No. of NRPS modules	NRPS domains	Peptide sequence	Reference(s)
Serrawettin W1	<i>Serratia</i>	<i>swrW</i>	1	C ₁ -A ₁ -PCP ₁ -TE	Ser	Li et al. (2005)
Serrawettin W2	<i>Serratia</i>	<i>swrA</i>	5	(C-A-PCP) ₁₋₅ -TE	Leu-Ser-Thr-Phe-X	Su et al. (2016), Clements-Decker et al. (2022)
Stephensiolide	<i>Serratia</i>	<i>sphA</i>	5	(C-A-PCP) ₁₋₅ -TE	Thr-Ser-Ser-Val-Ile/Val	Ganley et al. (2018)
Tauramamide	<i>Brevibacillus</i>	<i>tau</i>	5	(C-A-PCP-E) ₁ -(C-A-PCP) ₂ - (C-A-PCP-E) ₃ -(C-A-PCP) ₄₋₅ -TE	Phe/Trp-Ser-Leu-Phe/Trp-Phe/Arg	Dejong et al. (2016)
Bogorol	<i>Brevibacillus</i>	<i>bogA-F</i> ; <i>bogJ</i>	13	(C-A-PCP) ₁₋₂ -(C-A-PCP-E) ₃ - (C-A-PCP) ₄₋₆ -(C-A-PCP-E) ₇ - (C-A-PCP) ₈₋₁₀ -(C-A-PCP-E) ₁₁ - (C-A-PCP) ₁₂₋₁₃ -TD-TE	Dhb-Leu/Val-Orn/Lys-Ile/Val- Val/Ile-Val-Lys-Val-Leu-Lys- Tyr-Leu-Val	Dejong et al. (2016), Li et al. (2020a)
Bogorol-like lipopeptide	<i>Brevibacillus</i>	Not provided	13	Domain information not provided	Dhb-Tyr-Orn-Ile-Val-Val-Lys- Val-Leu-Asp-Val-Glu	Singh et al. (2021)
Brevibacillin	<i>Brevibacillus</i>	<i>brvA-E</i>	13	(C-A-PCP) ₁₋₂ -(C-A-PCP-E) ₃ - (C-A-PCP) ₄₋₆ -(C-A-PCP-E) ₇ - (C-A-PCP) ₈₋₁₀ -(C-A-PCP-E) ₁₁ - (C-A-PCP) ₁₂₋₁₃ -TD-TE	Dhb-Leu-Orn-Val/Ile-Val/Ile- Val-Lys-Val/Ile-Val-Lys-Tyr- Leu-Val	Zhao et al. (2021)
Brevilaterin	<i>Brevibacillus</i>	<i>bre260-261</i> ; <i>bre265-270</i>	13	(C-A-PCP) ₁₋₂ -(C-A-PCP-E) ₃ - (C-A-PCP) ₄₋₆ -(C-A-PCP-E) ₇ - (C-A-PCP) ₈ -(C-A-PCP-E) ₉ - (C-A-PCP) ₁₀ -(C-A-PCP-E) ₁₁ - (C-A-PCP) ₁₂₋₁₃ -TD-TE	Thr-Leu/Met/Val/Ile-Orn/Lys- Ile/Val/Leu-Val/Ile-Val/Ile-Lys/ Orn-Val/Ile-Val/Leu-Lys/Orn- Tyr/Val/Ile-Leu/Val-Val	Han et al. (2022)
Brevicidine	<i>Brevibacillus</i>	<i>breA-E</i>	12	(C-A-PCP-E) ₁₋₄ -(C-A-PCP) ₅₋₆ - (C-A-PCP-E) ₇ -(C-A-PCP) ₈₋₁₂ -TE	Asn-Phe/Tyr-Tyr/Trp-Orn- Orn-Gly-Orn-Tyr/Trp-Thr-Ile- Gly-Ser	Li et al. (2018), Zhao and Kuipers (2021)
Laterocidine	<i>Brevibacillus</i>	<i>latA-E</i>	13	(C-A-PCP-E) ₁₋₄ -(C-A-PCP) ₅₋₆ - (C-A-PCP-E) ₇ -(C-A-PCP) ₈₋₁₃ -TE	Ser-Phe/Tyr-Tyr/Trp-Orn- Orn-Gly-Orn-Tyr-Thr-Ile-Asn- Gly-Gly	Li et al. (2018)
Relacidine	<i>Brevibacillus</i>	<i>rlcA-E</i>	13	(C-A-PCP-E) ₁₋₄ -(C-A-PCP) ₅₋₇ - (C-A-PCP-E) ₈₋₉ -(C-A-PCP) ₁₀₋₁₃ -TE	Ser-Phe-Tyr-Orn-Orn-Gly- Orn-Tyr-Thr-Ile-Gly-Ser-Gly	Li et al. (2020b)
Icosalide	<i>Burkholderia</i>	<i>icoS</i>	4	(C-A-PCP) ₁₋₂ -(C-C-A-PCP) ₃ - (C-A-PCP) ₄ -TE	Leu-Ser-Ser-Leu	Dose et al. (2018), Jenner et al. (2019)
Malleipeptin/ Burkhomycin	<i>Burkholderia</i>	<i>mpnB-E</i>	12	(C-A-PCP) ₁₋₁₂ -TE ₁ -TE ₂	Ser-Glu-Ser-Lys-Thr/Dhb-Leu- Dab-Thr-Thr-Glu/hGlu-Gly- Val/Ile	Biggins et al. (2014)
Glidopeptin	<i>Burkholderia</i>	<i>glpA-H</i>	12	(C-A-PCP) ₁₋₁₂ -TE ₁ -TE ₂	Ser-Glu-Dab-Lys-Thr/Dab- Leu-Dab-Ser-Thr/Dhb-Asn- Gly-Val/Dhv	Wang et al. (2018)
Holrhizin	<i>Burkholderia</i>	<i>holA</i>	6	(C-A-PCP) ₁₋₆ -TE	Val-Phe-Glu-Ile-Ala-Ile	Niehs et al. (2018)
Haereogladin	<i>Burkholderia</i>	<i>hgdA</i>	5/6	(C-A-PCP) _{1-5/6} -TE	Dhb-Dhb-(β-Htyr/Tyr)-pHpg- PABA-Thr/H ₂ O	Thongkongkaew et al. (2018)
Haereoglumin	<i>Burkholderia</i>	<i>hgmC</i>	5/6	(C-A-PCP) _{1-5/6} -TE	Dhb-Dhb-Leu-Leu-PABA- Thr/H ₂ O	Thongkongkaew et al. (2018)
Haereogladiodin	<i>Burkholderia</i>	<i>hgddC</i>	5/6	(C-A-PCP) _{1-5/6} -TE	Dhb-Dhb-Tyr-Leu-PABA- Thr/H ₂ O	Chen et al. (2021)
Haereoplatin	<i>Burkholderia</i>	<i>hptC</i>	5/6	(C-A-PCP) ₁₋₃ -(C-A-PCP-E) ₄ - (C-A-PCP) _{5/6} -TE	Dhb-Dhb-(β-OH-Leu)-Hpg- PABA-Thr	Yoshimura et al. (2020)
Burriogladin	<i>Burkholderia</i>	<i>bgdA-B</i>	6/7	(C-A-PCP) _{1-6/7} -TE	Dhb-Pro-Glu-Ala-pHpg-Phe- Pro-Thr/H ₂ O	Thongkongkaew et al. (2018)
Burrioglumin	<i>Burkholderia</i>	<i>bgmA</i>	7	(C-A-PCP) ₁₋₇ -TE	Pro-Ser-Ala-Val/Leu-Phe- Pro-Thr	Thongkongkaew et al. (2018)
Burriogladiodin	<i>Burkholderia</i>	<i>bgddA</i>	7/8	(C-A-PCP) _{1-7/8} -TE	Dhb-Pro-Glu-Ala-Val/Ala/Ile/ Leu-Phe-Pro-Thr/H ₂ O	Chen et al. (2021)
Burrioplatin	<i>Burkholderia</i>	<i>bptE</i>	7/8	(C-A-PCP) ₁ -(C-A-PCP-E) ₂₋₄ - (C-A-PCP) ₅ -(C-A-PCP-E) ₆ - (C-A-PCP) _{7/8} -TE	Dhb-Pro-Ser-Ala-pHpg-Phe- Pro-Homoserine	Yoshimura et al. (2020)

TD, terminal reductase.

Biosynthesis of lipopeptides

Generally, lipopeptides are biosynthesised via enzymatic machinery encoded by a hybrid PKS and NRPS system (Kunakom and Eustáquio, 2019). The NRPS and PKS megaenzymes are arranged in an assembly line, where a set of catalytic domains are grouped into modules that incorporate monomers through sequential condensation (Burgard, 2017; Kunakom and Eustáquio, 2019). The PKSs are derived from fatty acid synthases and use a wide range of starter and extender units for fatty acid biosynthesis, which originate from the primary carbon metabolism (Burgard, 2017; Kunakom and Eustáquio, 2019). In general, fatty acids are synthesised via decarboxylative Claisen-type condensation of short-chain acetyl-CoA (most common starter unit) and are typically extended with malonyl-CoA or methylmalonyl-CoA (Burgard et al., 2017; Kunakom and Eustáquio, 2019). The acyl-transferase (AT) is responsible for the selection and transfer of the acetyl-CoA starter unit and extender unit (i.e., malonyl-CoA) to the acyl-carrier protein (ACP). The acetyl-CoA bound to ACP is then elongated by β -ketoacyl synthase (KS), which catalyses decarboxylative Claisen-type condensations to form C-C bonds between the starter and extender units, resulting in a β -ketoacyl still bound to the ACP. The growing ACP-bound acyl chain can then be processed by a set of reductive enzymes, including a ketoreductase (KR), a dehydratase (DH) and an enoylreductase (ER). The KR can catalyse the conversion of β -ketoacyl functionality to β -hydroxy compounds. Thereafter, the DH can catalyse the loss of water from β -hydroxy compounds and result in the formation of a C=C bond in the growing fatty acid chain (β -enoyl compounds). Finally, the β -enoyl compounds can be reduced to a saturated C-C bond by ERs, resulting in the formation of an acyl chain (C_{n+2}) still bound to the ACP. This acyl-ACP can then serve as a substrate for further elongation by the addition of an extender unit via KS, resulting in long fatty acid chains of typically C_6 - C_{18} in length (Burgard, 2017; Herbst et al., 2018; Théâtre et al., 2021). The long chain fatty acid-ACP is produced after additional cycles, and fatty acid precursors are released from ACP. Additional modifications may then occur, such as the transamination (addition of amino groups to the keto-acid) of the fatty acyl chain by the aminotransferases (AmT) (Théâtre et al., 2021). The fatty acids are then transferred onto the peptidyl carrier protein (PCP) and condensed with the starting amino acid through the condensation (C) domain in the first NRPS module (Kraas et al., 2010; Yang et al., 2020).

The NRPSs are thus multimodular enzymes that consist of repeated modules that catalyse the synthesis of peptide products from both proteinogenic and non-proteinogenic amino acids (Miller and Gulick, 2016; Kunakom and Eustáquio, 2019). A single module is comprised of a set of conserved catalytic domains responsible for incorporating a single residue into the peptide backbone (Miller and Gulick, 2016). The adenylation (A) domain typically recognises, selects and activates (using ATP) a specific

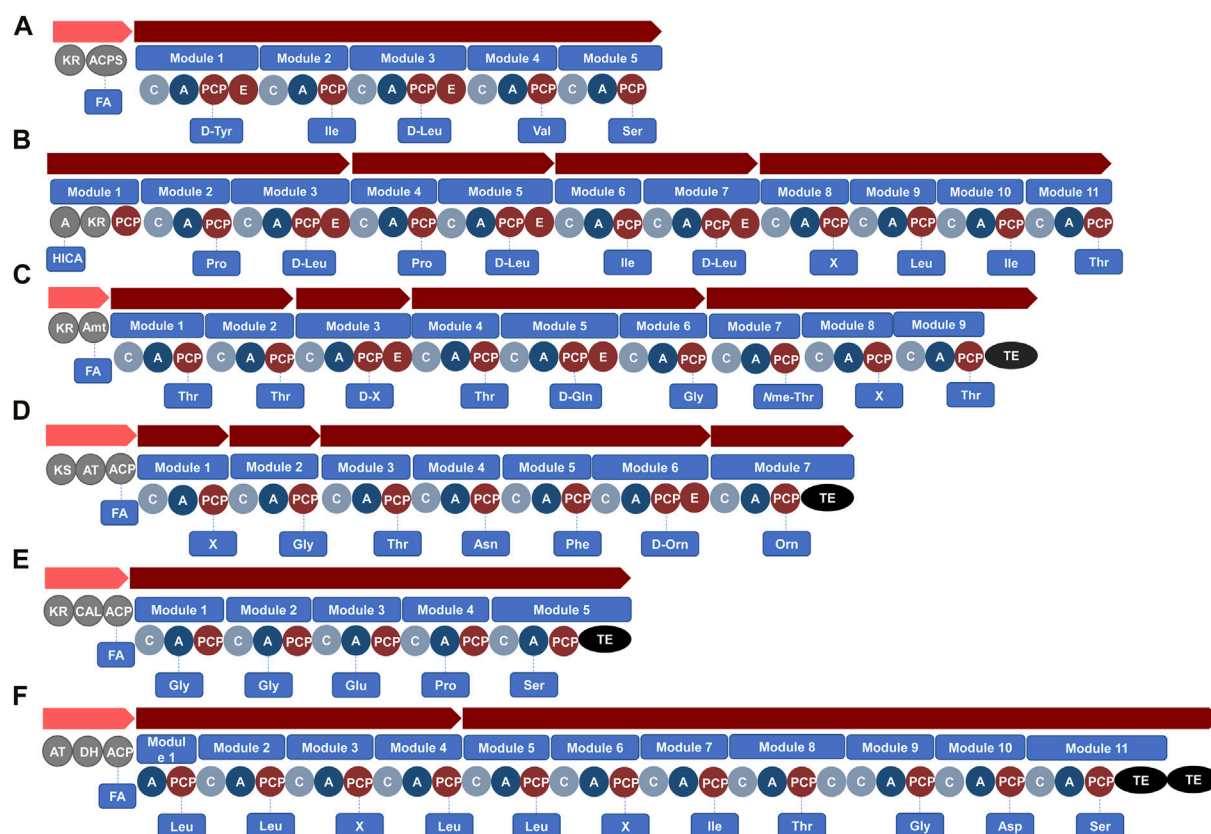
amino acid to form an aminoacyl-adenylate intermediate (Kunakom and Eustáquio, 2019). The aminoacyl-adenylate intermediate is then covalently attached to a 4'-phosphopanthetheine prosthetic group on the thiolation (T) domain or PCP via a thioester linkage. Hereafter, the PCP delivers the amino acid intermediate to the adjacent C domain to form a peptide (amine) bond to the growing peptide chain (Baltz et al., 2005; Kunakom and Eustáquio, 2019). Finally, the lipopeptide is synthesised as a linear molecule, which can be cyclised by the thioesterase (TE) domain at the end of the assembly line (in the final module within the BGC) (Baltz et al., 2005). Additional domains, such as the epimerase (E) domain, may be present in some modules to affect the conversion of L- to D-stereochemistry (Baltz et al., 2005). The order of modules is generally co-linear to the peptide sequence of the lipopeptide that is produced and the BGC can thus be used to predict the putative structure of the product (Baltz et al., 2005). Biosynthetic web-based tools, such as antiSMASH, have subsequently been developed to aid in the detection and annotation of BGCs and predict the structures of the PKS-NRPS products (Kunakom and Eustáquio, 2019).

Genome mining for prospective lipopeptides

The NCBI has an abundance of genome sequences available (at: <https://www.ncbi.nlm.nih.gov/genome/>) within its database that can be used in combination with antiSMASH to determine the potential of a strain to produce various natural products, and in particular, putatively predict lipopeptides. In this review, genome data available (a total of 378 bacterial genomes) on NCBI for members of the *Serratia* ($n = 197$ strains), *Brevibacillus* ($n = 24$ strains), *Burkholderia* ($n = 116$ strains), *Myxococcus* ($n = 16$ strains), *Cystobacter* ($n = 2$ strains) and *Lysobacter* ($n = 23$ strains) genera was analysed using antiSMASH as a prediction tool to identify typical PKS-NRPS BGCs (i.e., putatively predicted to encode for lipopeptides). It is important to note that further production and structural elucidation of the natural products encoded by the newly identified BGCs is required to confirm that the hybrid PKS-NRPS clusters produce lipopeptides, and thus only putative identification and predictions of novel BGCs will be made in this review.

Serratia

Genome mining revealed that 16 different *Serratia* species had at least one BGC encoding for PKS-NRPSs (Supplementary Table S1), while no BGC encoding for PKS-NRPSs was observed in *Serratia odorifera* ($n = 1$) or *Serratia entomophila* ($n = 1$). Moreover, the biosynthesis of serratamolides, serrawettin W2 and stephensolides by *Serratia* species has been previously elucidated (Li et al., 2005; Su et al., 2016; Ganley et al., 2018). The gene cluster involved in the biosynthesis of



The gene cluster involved in the biosynthesis of serrawettin W2 contains a PKS region, named *swrEFG* (incorporates a fatty acyl chain), and one NRPS-related gene, namely *swrA*, with five modules (predicted peptide sequence of Leu-Ser-Thr-Phe-X-

frontiersin.org

genomes of strains from four different *Serratia* species analysed in this review, including *S. fonticola*, *Serratia ficaria* (*S. ficaria*), *S. marcescens* and *S. ureilytica* (Supplementary Table S1).

A total of 18 unknown BGCs, with a hybrid PKS-NRPS system that did not correspond to previously characterised lipopeptide gene clusters, were then identified within *Serratia* species using genome mining. For instance, antiSMASH revealed a BGC that putatively encodes for a novel linear (no TE domain in the BGC) lipopeptide with the structure FA-Tyr-Ile-Leu-Val-Ser that was detected within genomes of *S. fonticola* ($n = 6$ strains) (Figure 4A; Supplementary Table S1), while the same gene (without the PKSs incorporating a fatty acid) was also detected in a *S. bockelmannii* strain (Supplementary Table S1). Moreover, antiSMASH analysis conducted in this review putatively identified 12 species (such as *S. bockelmannii*, *S. ficaria*, *S. fonticola*, *Serratia grimesii*, *Serratia inhibens* and *Serratia symbiotica*) as new lipopeptide producers (not previously reported to produce lipopeptides) as they contain at least one BGC that putatively encodes for a lipopeptide (hybrid PKS-NRPS system) (Supplementary Table S1).

Brevibacillus

Genome mining conducted for this review revealed that six different *Brevibacillus* species had at least one BGC encoding for PKS-NRPSs (Supplementary Table S2), while no BGC encoding for PKS-NRPSs was observed in *Brevibacillus choshinensis* ($n = 1$) and *Brevibacillus marinus* ($n = 1$). Moreover, the biosynthesis of tauramamide, bogorol, brevibacillin, brevilaterin, brevicidine, laterocidine and relacidine by *Brevibacillus* species has previously been elucidated (Table 1). The gene cluster involved in the biosynthesis of tauramamide contains a PKS region and one NRPS gene of five modules (predicted peptide sequence of Phe-Ser-Leu-Trp-Arg-TE) and was named *tau* (Table 1) (Desjardine et al., 2007; Dejong et al., 2016). The varying amino acid moiety of the elucidated tauramamide analogues suggests that the A domain of modules 1, 4 and 5 in *tau* have reduced amino acid specificity (Dejong et al., 2016). This BGC has been detected in *B. laterosporus* strains (Dejong et al., 2016) and was similarly detected in this species during genome mining conducted for this review (Supplementary Table S2).

Similar gene clusters have previously been identified for the synthesis of bogorol, brevibacillin and brevilaterin (Li et al., 2020a). The BGCs contain a PKS region and five NRPS-related genes in the BGCs of bogorol (named *bogA - bogF*) and brevilaterin (named *bre265 - bre270*), while brevibacillin has four NRPS-related genes (named *brvB - brvE*). All three NRPS-related genes contain 13 modules, with the predicted peptide sequence for bogorol as Dhb-Leu/Val-Orn/Lys-Ile/Val-Val/Ile-Val-Lys-Val-Leu-Lys-Tyr-Leu-Val, brevilaterin as Dhb-Leu-Orn-Val/Ile-Val/Ile-Val-Lys-Val/Ile-Val-Lys-Tyr-Leu-Val, and for brevibacillin as Dhb-Leu-

Orn-X-X-Val-Lys-X-Val-Lys-Tyr-Leu-Val, where the final amino acid (Val) is converted into valinol (Table 1) (Li et al., 2020a). For bogorol, variation in the peptide moiety suggests that the A domain in modules 2 – 5 and 9 had reduced specificity (Li et al., 2020a). Similarly, the A domain in modules 2, 3, 4, and 6 for brevilaterin and modules 4, 5 and 8 for brevibacillin likely have reduced amino acid specificity (Ning et al., 2021; Zhao et al., 2021; Chen et al., 2022). These three BGC have been detected in *B. laterosporus* strains, while only the bogorol BGC was detected in *B. laterosporus* strains using the genome mining analysis conducted for this review (Supplementary Table S2).

The gene cluster involved in the biosynthesis of brevicidine contains a PKS region and two NRPS-related genes of 12 modules (named *breC - breD*) with a predicted peptide sequence of Asn-X-Tyr-Orn-Orn-Gly-Orn-Tyr-Thr-Ile-Gly-Ser (Table 1) (Li et al., 2018). The variation in the peptide moiety of brevicidine suggests that the A domain in module 2 has reduced amino acid specificity (Zhao and Kuipers, 2021). The brevicidine gene cluster has been detected in *B. laterosporus* strains (Li et al., 2018) and was similarly detected in strains of this species using the genome mining analysis (of the 24 *Brevibacillus* strains available on NCBI) (Supplementary Table S2).

Similar gene clusters have previously been identified for the biosynthesis of laterocidine and relacidine (Li et al., 2020b). A PKS region and two NRPS-related genes were detected in the BGCs of laterocidine (named *latC - latD*) and relacidine (named *rlcC - rlcD*). Both BGCs contain 13 modules, with a predicted peptide sequence for laterocidine as Ser-Tyr-Trp-Orn-Orn-Gly-Orn-Trp-Thr-Ile-Asn-Gly-Gly and relacidine as Ser-Tyr-Trp-Orn-Orn-Gly-Orn-Trp-Thr-Ile-Gly-Ser-Gly (Table 1) (Li et al., 2020b). The variation in the peptide moiety of relacidine suggests that the A domain in module 13 has reduced amino acid specificity (Li et al., 2020b), while no variation in the peptide moiety of laterocidine has been described. Both BGCs have been detected in *B. laterosporus* strains (Li et al., 2020b) and were similarly detected in strains of this species using the genome mining analysis conducted (Supplementary Table S2).

It was, however, interesting to note that a total of 9 unknown BGCs with a hybrid PKS-NRPS system, were identified in *Brevibacillus* species through genome mining, which did not correspond to previously characterised lipopeptides. For instance, antiSMASH conducted in this review revealed a BGC that putatively encodes for a novel linear lipopeptide with a PKS region and four NRPS-related gene clusters containing 11 modules (with a putative sequence of α -hydroxy-isocaproic-acid-Pro-Leu-Pro-Leu-Ile-Leu-X-Leu-Ile-Thr, with variation in the module 8) (Figure 4B), with this BGC detected within genomes of *B. laterosporus* strains (Supplementary Table S2). Moreover, antiSMASH analysis putatively identified four species (i.e., *Brevibacillus agri*, *Brevibacillus composti*, *Brevibacillus formosus* and *Brevibacillus parabrevis*) as new lipopeptide producers containing at least one BGC that

putatively encodes for a lipopeptide (hybrid PKS-NRPS system) (Supplementary Table S2).

Burkholderia

Genome mining conducted for this review revealed that 21 different *Burkholderia* species had at least one BGC encoding for PKS-NRPSs (Supplementary Table S3), while no BGC encoding for PKS-NRPSs was observed in *B. humptydooensis* ($n = 2$), *B. anthina* ($n = 3$), *B. dolosa* ($n = 6$), *B. territorii* ($n = 2$), *B. diiffusa* ($n = 1$), *B. pseudomultivorans* ($n = 1$), *B. aenigmatica* ($n = 1$), *B. latens* ($n = 3$), *B. multivorans* ($n = 9$) and *B. metallica* ($n = 1$). Moreover, the biosynthesis of icosalides, malleipeptin/burkhomycin, glidopeptin, haereogladin, burriogladin, haereoglumins, burrioglumins, haereogladiodins and burriogladiodin A has been elucidated in literature (Table 1). Although the BGC for burkholdines was identified, the biosynthetic pathway was not described (Mullins et al., 2019).

The gene cluster involved in the biosynthesis of icosalides has previously been described to contain two PKS regions (incorporates two fatty acids) and one NRPS-related gene of four modules (with a predicted peptide sequence of Leu-Ser-Ser-Leu-TE), which was named *icoS* (Table 1) (Dose et al., 2018; Jenner et al., 2019). The icosalide gene cluster has been detected in *B. gladioli* strains (Dose et al., 2018; Jenner et al., 2019), while the genome mining analysis (of the 116 *Burkholderia* strains available on NCBI) conducted for this review detected the gene cluster in *B. gladioli* and *Burkholderia stagnalis* (*B. stagnalis*) strains (Supplementary Table S3).

Similar gene clusters have previously been identified for the synthesis of malleipeptin/burkhomycin and glidopeptin (Biggins et al., 2014; Wang et al., 2018). The BGCs contain a PKS region and three NRPS-related genes in the BGCs of malleipeptin/burkhomycin (named *mpnB-mpnD*) and glidopeptin (named *glpC-glpE*). Both BGCs contain 12 modules, with a predicted peptide sequence of malleipeptin as Ser-Glu-Ser-Lys-Thr-Leu-Dab-Thr-Thr-Glu-Gly-X and glidopeptin as Ser-Glu-Dab-Lys-X-Leu-Dab-Ser-X-Asn-Gly-X (Table 1) (Biggins et al., 2014; Wang et al., 2018). The variation in the peptide moiety of malleipeptin/burkhomycin suggests that the A domain in module 12 has reduced specificity (Wang et al., 2018). The variation in the peptide moiety of glidopeptin suggests that the A domain in modules 5, 9, and 12 has reduced amino acid specificity (Biggins et al., 2014). The malleipeptin/burkhomycin BGC has been detected in *B. pseudomallei*, *B. mallei* and *B. thailandensis* strains (Biggins et al., 2014), while the genome mining analysis conducted for this review detected the malleipeptin/burkhomycin gene cluster in *B. pseudomallei* (Supplementary Table S3). In comparison, the glidopeptin BGC has been detected in a *Burkholderia* DSM7029 strain (Wang et al., 2018).

Similar gene clusters have previously been identified for the synthesis of haereogladin, haereoglumins and haereogladiodins (Thongkongkaew et al., 2018; Chen et al., 2021). The BGCs contain a PKS region and one NRPS-related gene in the BGCs of haereogladin (named *hgdA*), haereoglumins (named *hgmC*) and haereogladiodins (named *hgddC*) (Table 1). All three BGCs contain 6 modules, with predicted peptide sequences of haereogladin as Dhb-Dhb-(β -Htyr/Tyr)-pHpg-PABA-Thr/H₂O, haereoglumins as Dhb-Dhb-Leu-Leu-PABA-Thr/H₂O, and haereogladiodins as Dhb-Dhb-Tyr-Leu-PABA-Thr/H₂O (Thongkongkaew et al., 2018; Chen et al., 2021). The variation in the peptide moiety of haereogladin suggests that the A domain in module 4 and 6, modules 4 – 6 for haereogladiodins, and modules 5 and 6 for haereoglumins have reduced amino acid specificity (Thongkongkaew et al., 2018; Chen et al., 2021). The haereogladin, haereoglumins and haereogladiodins BGCs have been detected in *B. gladioli*, *B. plantarii* and/or *B. glumae* strains (Thongkongkaew et al., 2018; Chen et al., 2021), while the genome mining analysis conducted for this review detected the haereogladin gene cluster in *B. gladioli*, *B. plantarii* and *Burkholderia perseverans* (Supplementary Table S3).

Similar gene clusters have previously been identified for the synthesis of burriogladin, burrioglumins and burriogladiodin (Thongkongkaew et al., 2018; Chen et al., 2021). The BGCs contain a PKS region and one or two NRPS-related genes in the BGCs of burriogladin (named *bgdA* and *bgdB*), burrioglumins (named *bgmA*) and burriogladiodin (named *bgddA*) (Table 1). Despite the three BGCs differing in the number of modules, similarity was observed between the peptide sequences of Dhb-Pro-Glu-Ala-pHpg-Phe-Pro (i.e., 6 modules) for the BGC of burriogladin, Dhb-Pro-Ser-Ala-Val/Leu-Phe-Pro-Thr (i.e., 8 modules) for the BGC of burrioglumins, and Dhb-Pro-Glu-Ala-Val/Ala/Ile/Leu-Phe-Pro (i.e., 7 modules) for the BGC of burriogladiodin (Table 1) (Thongkongkaew et al., 2018). The variation in the peptide moiety of burrioglumins suggests that the A domain in module 5 and modules 5–7 for burriogladiodin exhibited reduced amino acid specificity. The haereogladin, haereoglumins and haereogladiodins BGCs have been detected in *B. gladioli*, *B. plantarii* and/or *B. glumae* strains (Thongkongkaew et al., 2018; Chen et al., 2021), while the genome mining analysis conducted for this review detected the burriogladin gene cluster in *B. gladioli* and burrioglumin in *B. glumae* and *B. plantarii* (Supplementary Table S3).

A total of 19 unknown BGCs with a hybrid PKS-NRPS system were identified that did not correspond to lipopeptides previously characterised in *Burkholderia* species. For instance, antiSMASH analysis conducted in this review revealed a BGC that putatively encodes for a novel cyclic lipopeptide with a PKS region and four NRPS-related gene clusters containing nine modules (with a putative sequence of FA-Thr-Thr-X-Thr-Gln-Gly-(Nme-Thr)-X-Thr-TE, with variation in modules 3 and 8) (Figure 4C) and this BGC was detected within genomes of

TABLE 2 Summary of the known PKS-NRPS BGCs identified from *Myxococcus*, *Cystobacter* and *Lysobacter* species.

Lipopeptide	Producing genus	Gene name	No. of NRPS modules	NRPS domains	Peptide sequence	Reference(s)
Myxochromide A-type	<i>Myxococcus</i>	<i>mchA-C</i>	6	(C-A-MT-PCP) ₁ -(C-A-PCP-E) ₂ -(C-A-PCP) ₃₋₅ -(C-A-PCP-TE) ₆	Thr-Pro/Ala-Leu-Pro-Ala/Phe-Gln	Wenzel et al. (2005), Burgard et al. (2017)
Myxochromide B-type	<i>Myxococcus</i>	<i>mchA-C</i>	7	(C-A-MT-PCP) ₁ -(C-A-PCP-E) ₂ -(C-A-PCP) ₃₋₆ -(C-A-PCP-TE) ₇	Thr-Ala/Pro-Leu-Leu-Pro-Ala/Phe-Gln	Burgard et al. (2017)
Myxochromide C-type	<i>Myxococcus</i>	<i>mchA-C</i>	5	(C-A-MT-PCP) ₁ -(C-A-PCP-E) ₂ -(C-A-PCP) ₃₋₄ -(C-A-PCP-TE) ₅	Thr-Pro/Ala-Leu-Pro-Gln	Burgard et al. (2017)
Cystomanamide	<i>Cystobacter</i>	<i>cymA-D</i>	5	(C-A-PCP-E) ₁ -(C-C-A-PCP) ₂ -(C-A-PCP-E) ₃ -(C-flkH-PCP) ₄ -(C-A-PCP-E-TE) ₅	Asn-Asn-Phe-GA-Tyr	Etzbach et al. (2014)
WAP-8294A	<i>Lysobacter</i>	<i>wapA-B</i>	12	(C-A-PCP) ₁ -(C-A-PCP-E) ₂ -(C-A-PCP) ₃₋₄ -(C-A-PCP-MT-E) ₅ -(C-A-PCP) ₆ -(C-A-PCP-E) ₇ -(C-A-PCP) ₈ -(C-A-PCP-E) ₉₋₁₁ -(C-A-PCP-MT) ₁₂ -TE	Ser-Asn-Ser-Gly-(Nme-Phe)-Leu-Orn-Glu-Asn-Trp-Orn-(Nme-Val)	Zhang et al. (2011)
WBP-28479A1	<i>Lysobacter</i>	<i>wbpA-B</i>	11	(C-A-PCP) ₁ -(C-A-PCP-E) ₂ -(C-A-PCP) ₃₋₄ -(C-A-PCP-MT-E) ₅ -(C-A-PCP) ₆ -(C-A-PCP-E) ₇ -(C-A-PCP) ₈ -(C-A-PCP-E) ₉₋₁₀ -(C-A-PCP-TE) ₁₁	Val-Arg-Ser-Gly-(Nme-Phe)-Leu-Arg-Glu-Val-Trp-Aba	Sang et al. (2019)
Lysocin	<i>Lysobacter</i>	<i>lesA-B</i>	12	(C-A-PCP) ₁ -(C-A-PCP-E) ₂ -(C-A-PCP) ₃₋₄ -(C-A-PCP-MT-E) ₅ -(C-A-PCP) ₆ -(C-A-PCP-E) ₇ -(C-A-PCP) ₈ -(C-A-PCP-E) ₉₋₁₀ -(C-A-PCP) ₁₁ -(C-A-PCP-TE) ₁₂	Thr-Arg-Ser-Gly-Phe-Leu-Arg-Glu-Gln-Trp-Val/Ile-Thr	Panthee et al. (2016)

GA, glyceric acid; MT, methyltransferase.

Burkholderia mayonis (*B. mayonis*), *Burkholderia oklahomensis*, *B. stagnalis* and *Burkholderia ubonensis* (Supplementary Table S3). Moreover, antiSMASH analysis putatively identified 16 species (such as *B. cepacia*, *Burkholderia lata*, *Burkholderia pyrrocinia*, *Burkholderia stabilis* and *Burkholderia vietnamiensis*, etc.) as new lipopeptide producers containing at least one BGC that putatively encodes for a lipopeptide (hybrid PKS-NRPS system) (Supplementary Table S3).

Myxococcus

All 16 of the *Myxococcus* genomes (four different species) from the NCBI database that were analysed using antiSMASH were found to contain at least one BGC encoding for a hybrid PKS-NRPS system (Supplementary Table S4). The BGC involved in the production of myxochromide A, B and C has previously been identified and elucidated (Table 2). The BGCs for all three contain a PKS region (named *mchA*) and two NRPS-related genes in the BGCs (named *mchB* and *mchC*). Despite the three BGCs differing in the number of modules, similarity was observed between the peptide sequences of Thr-Pro/Ala-Leu-Pro-Ala/Phe-Gln (i.e., 6 modules) for the BGC of myxochromide A, Thr-Ala/Pro-Leu-Leu-Pro-Ala/Phe-Gln (i.e., 7 modules) for the BGC of myxochromide B, and Thr-Pro/Ala-Leu-Pro-Gln (i.e., 5 modules) for the BGC of myxochromide C (Table 2) (Wenzel et al., 2005; Burgard et al., 2017; Yan et al., 2018). The

variation in the peptide moiety of myxochromides suggests that the A domain in module 2 and 5 for myxochromide A, modules 2 and 6 for myxochromide B, and module 2 for myxochromide C exhibited reduced amino acid specificity. The myxochromide A, B or C BGCs have been detected in *M. xanthus*, *M. virescens*, *Myxococcus hansupus* (*M. hansupus*) and/or *Myxococcus fulvus* (Burgard et al., 2017), while genome mining analysis in this review detected the myxochromide A BGC in *M. xanthus* and myxochromide C in *M. xanthus* and *M. hansupus* (Supplementary Table S4).

During the genome mining conducted in the current review, 20 unknown BGCs with a hybrid PKS-NRPS system were identified that did not correspond to lipopeptides previously characterised in *Myxococcus* sp. For example, antiSMASH analysis showed a BGC present in *M. xanthus* and *M. hansupus*, that encodes for a lipopeptide with the structure FA-X-Gly-Thr-Asn-Phe-Orn-Orn-TE (Figure 4D; Supplementary Table S4). Moreover, antiSMASH analysis conducted in this review revealed that one species (*Myxococcus stipitatus*) may be a newly identified lipopeptide producer containing at least one BGC that putatively encodes for a lipopeptide (hybrid PKS-NRPS system).

Cystobacter

Two *C. fuscus* strains were available on the NCBI database for genome mining analysis in the current study and seven BGCs encoding for a PKS-NRPS hybrid system were detected within

this species. Additionally, the BGC involved in the biosynthesis of the cystomanamides was amongst these seven BGCs detected (Supplementary Table S4). The *ctm* BGC has been identified to encode for the production of the cystomanamides, where the *ctmA* gene in particular was found to encode for the complex protein that contain functional domains belonging to the fatty acid synthesis (Etzbach et al., 2014). The *ctmB*, *ctmC* and *ctmD* genes encode for NRPSs, with a predicted peptide sequence of Asn-Asn-Phe-GA-Tyr (where GA refers to glyceric acid) (Etzbach et al., 2014) (Table 2). The remaining six BGCs with a hybrid PKS-NRPS system did not correspond to lipopeptides previously characterised. For example, antiSMASH analysis conducted for this review showed a BGC present in *C. fuscus* DSM 52655 that putatively encodes for a lipopeptide with a NRPS gene cluster containing five modules. This unknown BGC putatively encodes for the sequence: FA-Gly-Gly-Glu-Pro-Ser-TE (Figure 4E).

Lysobacter

A total of 36 genomes (10 different species) from the NCBI were analysed using antiSMASH and all species were found to contain at least one BGC encoding for a hybrid PKS-NRPS system (Supplementary Table S5). The BGCs for the WAP-8294A, WBP-28479A1, lysocins and tripropeptins compounds have been described in literature (Table 2). The BGC for the WAP-8294A compounds, is reported to contain a PKS region with three structural genes, where *wapC* encodes for the NRPS-associated protein MbtH, and *wap2* and *wap3* encode for two multi-module NRPSs. The latter two NRPSs are comprised of 12 modules [predicted peptide sequence of Ser-Asn-Ser-Gly-(Nme-Phe)-X-X-X-Asn-X-X-(Nme-Val)] in the WAP-8294A compounds (Table 2) (Zhang et al., 2011; Yue et al., 2022). The WAP-8294A BGC has been detected in *L. enzymogenes* (Zhang et al., 2011), while genome mining analysis in this review detected the WAP-8294A BGC in *L. capsica* (Supplementary Table S5). Recently, Sang et al. (2019) identified and reported on the cryptic BGC for WBP-28479A1. The *wbp* BGC was identified to encode for two large NRPS genes with a total of 11 modules [predicted peptide structure of Val-Arg-Ser-Gly-(Nme-Phe)-Leu-Arg-Glu-Val-Trp-Abal] (Table 2). The WBP-28479A1 BGC has been detected in *L. antibioticus* (Zhang et al., 2011), and was similarly detected in strains of this species using the genome mining analysis conducted for this review (Supplementary Table S5).

For the lysocins, Panthee et al. (2016) sequenced the genome of *Lysobacter* sp. RH2180-5 and analysed the putative lysocin BGC. The study indicated that too large multi-modular NRPSs named *lesA* and *lesB*, containing 12 modules, were involved in the biosynthesis of lysocin E, where the predicted peptide sequence was Thr-Arg-Ser-Gly-Phe-Leu-Arg-Glu-Gln-Trp-Val/Ile-Thr (Table 2). The

biosynthetic genes involved in tripropeptin biosynthesis have not been reported in *Lysobacter*; however, the tripropeptin BGC was reported in *Collimonas* (Yue et al., 2022). The tripropeptins BGC was identified in *Collimonas fungivorans* Ter331 and Ter6 genomes by Song et al. (2015) and contained three NRPS-related genes (*trpA*, *trpB*, and *trpC*) in the BGC comprised of 8 modules.

During the genome mining conducted in the current review, 16 unknown BGCs with a hybrid PKS-NRPS system were identified that did not correspond to lipopeptides previously characterised in *Lysobacter* species. For example, antiSMASH analysis indicated a BGC that putatively encodes for a novel lipopeptide with a PKS and four NRPSs gene clusters, comprising 11 modules in *Lysobacter gummosus* (Figure 4F). The predicted peptide structure of this lipopeptide is FA-Leu-Leu-X-Leu-Leu-X-Ile-Thr-Gly-Asp-Ser-TE (Figure 4F; Supplementary Table S5). Moreover, antiSMASH analysis also putatively identified seven species (such as *Lysobacter alkalisoli*, *Lysobacter soli* and *Lysobacter solisilvae* etc.) as new lipopeptide producers containing at least one BGC that putatively encodes for a lipopeptide (hybrid PKS-NRPS system).

Discussion and conclusion

This review provided insight into the classification and chemical diversity of lipopeptides isolated from members of the underexplored *Serratia*, *Brevibacillus*, *Burkholderia*, *Myxococcus*, *Cystobacter*, and *Lysobacter* genera. Each family of lipopeptides generally contains numerous homologues and analogues, with differing antimicrobial properties. Apart from the unknown antimicrobial activities of the myxochromides, cystomanamides, malleipeptins/burkhomycin, “haereo” and “burrio” families, the majority of the lipopeptides from these bacterial genera exhibit potent activity and are thus valuable sources of clinically useful antibiotics or lead compounds. However, despite prominent antimicrobial activity exhibited by several lipopeptides from *Burkholderia* and *Serratia* species, limited information regarding the mode of action of these lipopeptides currently exists and further investigation is recommended. Moreover, apart from laterocidine and relacidines, the majority of the lipopeptides from *Brevibacillus* and *Lysobacter* have a general cell membrane disruption mechanism of action (in a menaquinone-dependent manner for lipopeptides from *Lysobacter*), which is considered advantageous as the development of resistance to lipopeptides is likely to be slow and limited (Cochrane and Vederas, 2016).

Based on the genome mining conducted within this review, it is apparent that many undiscovered BGCs with a hybrid PKS-NRPS system are present within the genomes of *Serratia*, *Brevibacillus*, *Burkholderia*, *Myxococcus*, *Cystobacter*, and

Lysobacter species, suggesting that they are underexplored sources of novel lipopeptide families with potentially potent antimicrobial activity. Therefore, future lipopeptide research should focus on either prospecting for these bacterial species from their respective environmental habitats to isolate and characterise these novel lipopeptide families or utilise the genome mining data from this review for genetic engineering and heterologous expression to biosynthesise these novel lipopeptide families (circumventing the need for culture-based prospecting methods).

Author contributions

Compiled the manuscript: TC-D and MK. Edited the manuscript: WK and SK.

Funding

Global Excellence Stature Fellowship 4.0 was provided in support of postdoctoral research within the Faculty of Health Sciences at the University of Johannesburg.

References

- Akbar, S., Dowd, S. E., and Stevens, D. C. (2017). Draft genome sequence of *Cystobacter ferrugineus* strain Cbfe23. *Genome Announc.* 5 (6), e01601-16–e01616. doi:10.1128/genomeA.01601-16
- Aleti, G., Sessitsch, A., and Brader, G. (2015). Genome mining: Prediction of lipopeptides and polyketides from *Bacillus* and related firmicutes. *Comput. Struct. Biotechnol. J.* 13, 192–203. doi:10.1016/j.csbj.2015.03.003
- Arlt, P., Hashizume, H., Igarashi, M., and Gross, H. (2021). Genome sequence of *Lysobacter* sp. strain BMK333-48F3, the producer strain of potent lipopeptide antibiotics of the tripropeptin family. *Microbiol. Resour. Announc.* 10 (49), e0096921. doi:10.1128/MRA.00969-21
- Atterbury, R. J., and Tyson, J. (2021). Predatory bacteria as living antibiotics—where are we now? *Microbiology* 167 (1), 001025. doi:10.1099/mic.0.001025
- Balleza, D., Alessandrini, A., and Beltrán García, M. J. (2019). Role of lipid composition, physicochemical interactions, and membrane mechanics in the molecular actions of microbial cyclic lipopeptides. *J. Membr. Biol.* 252 (2), 131–157. doi:10.1007/s00232-019-00067-4
- Baltz, R. H., Miao, V., and Wrigley, S. K. (2005). Natural products to drugs: Daptomycin and related lipopeptide antibiotics. *Nat. Prod. Rep.* 22 (6), 717–741. doi:10.1039/B416648P
- Barsby, T., Kelly, M. T., Gagné, S. M., and Andersen, R. J. (2001). Bogorol A produced in culture by a marine *Bacillus* sp. reveals a novel template for cationic peptide antibiotics. *Org. Lett.* 3 (3), 437–440. doi:10.1021/ol006942q
- Barsby, T., Warabi, K., Sørensen, D., Zimmerman, W. T., Kelly, M. T., and Andersen, R. J. (2006). The bogorol family of antibiotics: Template-based structure elucidation and a new approach to positioning enantiomeric pairs of amino acids. *J. Org. Chem.* 71 (16), 6031–6037. doi:10.1021/jo060667p
- Biggins, J. B., Kang, H. S., Ternei, M. A., DeShazer, D., and Brady, S. F. (2014). The chemical arsenal of *Burkholderia pseudomallei* is essential for pathogenicity. *J. Am. Chem. Soc.* 136 (26), 9484–9490. doi:10.1021/ja504617n
- Boros, C., Smith, C. J., Vasina, Y., Che, Y., Dix, A. B., Darveaux, B., et al. (2006). Isolation and identification of the icosalides-cyclic peptolides with selective antibiotic and cytotoxic activities. *J. Antibiot.* 59 (8), 486–494. doi:10.1038/ja.2006.68
- Burgard, C. (2017). “Exploitation and engineering of lipopeptide biosynthesis in *Myxobacteria*.” Dissertation (Saarbrücken, Germany: Universität des Saarlandes). doi:10.22028/D291-26983
- Burgard, C., Zaburannyi, N., Nadmid, S., Maier, J., Jenke-Kodama, H., Luxenburger, E., et al. (2017). Genomics-guided exploitation of lipopeptide diversity in *Myxobacteria*. *ACS Chem. Biol.* 12 (3), 779–786. doi:10.1021/acscchembio.6b00953
- Carrero, P., Garrote, J. A., Pacheco, S., García, A. I., Gil, R., and Carbajosa, S. G. (1995). Report of six cases of human infection by *Serratia plymuthica*. *J. Clin. Microbiol.* 33 (2), 275–276. doi:10.1128/jcm.33.2.275-276.1995
- Challinor, V. L., and Bode, H. B. (2015). Bioactive natural products from novel microbial sources. *Ann. N. Y. Acad. Sci.* 1354 (1), 82–97. doi:10.1111/nyas.12954
- Chambers, J., Sparks, N., Sydney, N., Livingstone, P. G., Cookson, A. R., and Whitworth, D. E. (2020). Comparative genomics and pan-genomics of the Myxococcaceae, including a description of five novel species: *Myxococcus eversor* sp. nov., *Myxococcus llanfairpwllgwyngyllgogerychwymdrobwlllantysiliogogochensis* sp. nov., *Myxococcus vastator* sp. nov., *Pyxidicoccus caerfyrddinensis* sp. nov., and *Pyxidicoccus truncator* sp. nov. *Genome Biol. Evol.* 12 (12), 2289–2302. doi:10.1093/gbe/evaa212
- Chang, K., Luo, J., Xu, H., Li, M., Zhang, F., Li, J., et al. (2017). Human infection with *Burkholderia thailandensis*, China, 2013. *Emerg. Infect. Dis.* 23 (8), 1416–1418. doi:10.3201/eid2308.170048
- Chen, H., Sun, T., Bai, X., Yang, J., Yan, F., Yu, L., et al. (2021). Genomics-driven activation of silent biosynthetic gene clusters in *Burkholderia gladioli* by screening recombineering system. *Molecules* 26 (3), 700. doi:10.3390/molecules26030700
- Chen, X., Li, S., Yu, L., Miller, A., and Du, L. (2019). Systematic optimization for production of the anti-MRSA antibiotics WAP-8294A in an engineered strain of *Lysobacter enzymogenes*. *Microb. Biotechnol.* 12 (6), 1430–1440. doi:10.1111/1751-7915.13484
- Chen, Z., Wang, X., Han, P., Liu, Y., Hong, D., Li, S., et al. (2022). Discovery of novel antimicrobial peptides, Brevilaterin V, from *Brevibacillus laterosporus* S62-9 after regulated by exogenously-added L-valine. *LWT* 155, 112962. doi:10.1016/j.lwt.2021.112962
- Chowdhury, T., Baindara, P., and Mandal, S. M. (2021). LPD-12: A promising lipopeptide to control COVID-19. *Int. J. Antimicrob. Agents* 57 (1), 106218. doi:10.1016/j.ijantimicag.2020.106218
- Christensen, P., and Cook, F. D. (1978). *Lysobacter*, a new genus of nonfruiting, gliding bacteria with a high base ratio. *Int. J. Syst. Bacteriol.* 28 (3), 367–393. doi:10.1099/00207713-28-3-367

Conflict of interest

The authors declare that the research was conducted in the absence of any commercial or financial relationships that could be construed as a potential conflict of interest.

Publisher's note

All claims expressed in this article are solely those of the authors and do not necessarily represent those of their affiliated organizations, or those of the publisher, the editors and the reviewers. Any product that may be evaluated in this article, or claim that may be made by its manufacturer, is not guaranteed or endorsed by the publisher.

Supplementary material

The Supplementary Material for this article can be found online at: <https://www.frontiersin.org/articles/10.3389/fchem.2022.1025979/full#supplementary-material>.

- Clements, T., Ndlovu, T., Khan, S., and Khan, W. (2019). Biosurfactants produced by *Serratia* species: Classification, biosynthesis, production and application. *Appl. Microbiol. Biotechnol.* 103 (2), 589–602. doi:10.1007/s00253-018-9520-5
- Clements, T., Rautenbach, M., Ndlovu, T., Khan, S., and Khan, W. (2021). A metabolomics and molecular networking approach to elucidate the structures of secondary metabolites produced by *Serratia marcescens* strains. *Front. Chem.* 9, 633870. doi:10.3389/fchem.2021.633870
- Clements-Decker, T., Rautenbach, M., Khan, S., and Khan, W. (2022). Metabolomics and genomics approach for the discovery of serrawettin W2 lipopeptides from *Serratia marcescens* NP2. *J. Nat. Prod.* 85 (5), 1256–1266. doi:10.1021/acs.jnatprod.1c01186
- Cochrane, S. A., and Vederas, J. C. (2016). Lipopeptides from *Bacillus* and *Paenibacillus* spp.: A gold mine of antibiotic candidates. *Med. Res. Rev.* 36 (1), 4–31. doi:10.1002/med.21321
- Coenye, T., and Vandamme, P. (2003). Diversity and significance of *Burkholderia* species occupying diverse ecological niches. *Environ. Microbiol.* 5 (9), 719–729. doi:10.1046/j.1462-2920.2003.00471.x
- Cristina, M. L., Sartini, M., and Spagnolo, A. M. (2019). *Serratia marcescens* infections in neonatal intensive care units (NICUs). *Int. J. Environ. Res. Public Health* 16 (4), 610. doi:10.3390/ijerph16040610
- Curtis, A. K., Lamb, C., Hassan, W. M., and Foxworth, J. (2020). *Brevibacillus laterosporus* bacteremia in an adult. *Cureus* 12 (9), e10481. doi:10.7759/cureus.10481
- De Bruijn, I., Cheng, X., de Jager, V., Exposito, R. G., Watrous, J., Patel, N., et al. (2015). Comparative genomics and metabolic profiling of the genus *Lysobacter*. *BMC Genomics* 16, 991–1016. doi:10.1186/s12864-015-2191-z/
- De Vos, P., Ludwig, W., Schleifer, K. H., and Whitman, W. B. (2011). Family IV. *Paenibacillaceae* fam. nov. *Bergey's Man. Syst. Bacteriol.* 3, 269.
- De Vries, R. D., Schmitz, K. S., Bovier, F. T., Predella, C., Khao, J., Noack, D., et al. (2021). Intranasal fusion inhibitory lipopeptide prevents direct-contact SARS-CoV-2 transmission in ferrets. *Science* 371 (6536), 1379–1382. doi:10.1126/science.abf4896
- Dejong, C. A., Chen, G. M., Li, H., Johnston, C. W., Edwards, M. R., Rees, P. N., et al. (2016). Polyketide and nonribosomal peptide retro-biosynthesis and global gene cluster matching. *Nat. Chem. Biol.* 12 (12), 1007–1014. doi:10.1038/nchembio.2188
- Deol, B. S., Bermingham, M. A., Still, J. L., Haydon, D. A., and Gale, E. F. (1973). The action of serratomolide on ion movement in lipid bilayers and biomembranes. *Biochimica Biophysica Acta - Biomembr.* 330 (2), 192–195. doi:10.1016/0005-2736(73)90224-1
- Desjardine, K., Pereira, A., Wright, H., Matainaho, T., Kelly, M., and Andersen, R. J. (2007). Tauramamide, a lipopeptide antibiotic produced in culture by *Brevibacillus laterosporus* isolated from a marine habitat: Structure elucidation and synthesis. *J. Nat. Prod.* 70 (12), 1850–1853. doi:10.1021/np070209r
- Dijksteelt, G. S., Ulrich, M. M. W., Middelkoop, E., and Boekema, B. K. H. L. (2021). Review: Lessons learned from clinical trials using antimicrobial peptides (AMPs). *Front. Microbiol.* 12, 616979. doi:10.3389/fmicb.2021.616979
- Dose, B., Niehs, S. P., Scherlach, K., Flórez, L. V., Kaltenpoth, M., and Hertweck, C. (2018). Unexpected bacterial origin of the antibiotic icosalide: Two-tailed desipeptide assembly in multifarious *Burkholderia* symbionts. *ACS Chem. Biol.* 13 (9), 2414–2420. doi:10.1021/acschembio.8b00600
- Dwivedi, D., Jansen, R., Molinari, G., Nimtz, M., Johri, B. N., and Wray, V. (2008). Antimycobacterial serratomolides and diacyl peptidoglycosamine derivatives from *Serratia* sp. *J. Nat. Prod.* 71 (4), 637–641. doi:10.1021/np7007126
- Eberl, L., Molin, S., and Givskov, M. (1999). Surface motility of *Serratia liquefaciens* MG1. *J. Bacteriol.* 181 (6), 1703–1712. doi:10.1128/JB.181.6.1703-1712.1999
- Ellis, D., Gosai, J., Emrick, C., Heintz, R., Romans, L., Gordon, D., et al. (2012). Occidiofungin's chemical stability and *in vitro* potency against *Candida* species. *Antimicrob. Agents Chemother.* 56 (2), 765–769. doi:10.1128/AAC.05231-11
- Esmael, Q., Pupin, M., Kieu, N. P., Chataigné, G., Béchet, M., Deravel, J., et al. (2016). *Burkholderia* genome mining for nonribosomal peptide synthetases reveals a great potential for novel siderophores and lipopeptides synthesis. *MicrobiologyOpen* 5 (3), 512–526. doi:10.1002/mbo3.347
- Etzbach, L. (2015). “Exploring the biosynthetic potential of *Cystobacter fuscus* – characterization of new structures and studies on their biosynthesis.” Dissertation (Saarbrücken, Germany: Universität des Saarlandes). doi:10.22028/D291-23048
- Etzbach, L., Plaza, A., Garcia, R., Baumann, S., and Müller, R. (2014). Cystomanamides: Structure and biosynthetic pathway of a family of glycosylated lipopeptides from myxobacteria. *Org. Lett.* 16, 2414–2417. doi:10.1021/ol500779s
- Fernández, C., Wilhelmi, I., Andradás, E., Gaspar, C., Gomez, J., Romero, J., et al. (1996). Nosocomial outbreak of *Burkholderia pickettii* infection due to a manufactured intravenous product used in three hospitals. *Clin. Infect. Dis.* 22 (6), 1092–1095. doi:10.1093/clinids/22.6.1092
- Garney, J. G., Carr, G., Ioerger, T. R., Sacchetti, J. C., Clardy, J., and Derbyshire, E. R. (2018). Discovery of antimicrobial lipodepsipeptides produced by a *Serratia* sp. within mosquito microbiomes. *ChemBioChem* 19 (15), 1590–1594. doi:10.1002/cbic.201800124
- Garrity, G. M., Bell, J. A., and Lilburn, T. (2005). Family I. Burkholderiaceae fam. nov. *Bergey's Man. Syst. Bacteriol.* 2, 575.
- Genilloud, O. (2014). The re-emerging role of microbial natural products in antibiotic discovery. *Ant. Van Leeuwenhoek* 106 (1), 173–188. doi:10.1007/s10482-014-0204-6
- Gómez Expósito, R., Postma, J., Raaijmakers, J. M., and De Bruijn, I. (2015). Diversity and activity of *Lysobacter* species from disease suppressive soils. *Front. Microbiol.* 6, 1243. doi:10.3389/fmicb.2015.01243
- Graves, M., Robin, T., Chipman, A. M., Wong, J., Khashe, S., and Janda, J. M. (1997). Four additional cases of *Burkholderia gladioli* infection with microbiological correlates and review. *Clin. Infect. Dis.* 25 (4), 838–842. doi:10.1086/515551
- Grimont, F., and Grimont, P. A. (2015). “*Serratia*,” in *Bergey's manual of systematics of archaea and bacteria* (New Jersey, US: Wiley), 1–22. doi:10.1002/9781118960608.gbm01167
- Hai, P. D., Hoa, L. T. V., Tot, N. H., Phuong, L. L., Quang, V. V., Thuyet, B. T., et al. (2020). First report of biliary tract infection caused by multidrug-resistant *Serratia fonticola*. *New Microbes New Infect.* 36, 100692. doi:10.1016/j.nmni.2020.100692
- Hamamoto, H., Urai, M., Ishii, K., Yasukawa, J., Paudel, A., Murai, M., et al. (2015). Lysozin E is a new antibiotic that targets menaquinone in the bacterial membrane. *Nat. Chem. Biol.* 11, 127–133. doi:10.1038/nchembio.1710
- Han, P., Chen, Z., Liu, Y., Ma, A., Li, S., and Jia, Y. (2022). Structural organization of brevilaterin biosynthesis in *Brevibacillus laterosporus* S62-9: A novel MbTH-independent cationic antimicrobial peptide synthetase system. *J. Agric. Food Chem.* 70 (24), 7471–7478. doi:10.1021/acs.jafc.2c01143
- Harada, K. I., Suzuki, M., Kato, A., Fujii, K., Oka, H., and Ito, Y. (2001). Separation of WAP-8294A components, a novel anti-methicillin-resistant *Staphylococcus aureus* antibiotic, using high-speed counter-current chromatography. *J. Chromatogr. A* 6, 75–81. doi:10.1016/S0021-9673(01)01235-3
- Hashizume, H., Sawa, R., Harada, S., Igarashi, M., Adachi, H., Nishimura, Y., et al. (2011). Tripropeptin C blocks the lipid cycle of cell wall biosynthesis by complex formation with undecaprenyl pyrophosphate. *Antimicrob. Agents Chemother.* 55 (8), 3821–3828. doi:10.1128/AAC.00443-11
- Hashizume, H., Takahashi, Y., Harada, S., and Nomoto, A. (2015). Natural lipopeptide antibiotic tripropeptin C revitalizes and synergistically potentiates the activity of beta-lactams against methicillin-resistant *Staphylococcus aureus*. *J. Antibiot. (Tokyo)*. 68 (6), 373–378. doi:10.1038/ja.2014.169
- Hayward, A. C., Fegan, N., Fegan, M., and Stirling, G. R. (2010). *Stenotrophomonas* and *lysobacter*: Ubiquitous plant-associated gamma-proteobacteria of developing significance in applied microbiology. *J. Appl. Microbiol.* 108 (3), 756–770. doi:10.1111/j.1365-2672.2009.04471.x
- Heinemann, B., Kaplan, M. A., Muir, R. D., and Hooper, I. R. (1953). Amphomycin, a new antibiotic. *Antibiot. Chemother.* 3 (12), 1239–1242.
- Heise, P., Liu, Y., Degenkolb, T., Vogel, H., Schäberle, T. F., and Vilcinskis, A. (2019). Antibiotic-producing beneficial bacteria in the gut of the burying beetle *Nicrophorus vespilloides*. *Front. Microbiol.* 10, 1178. doi:10.3389/fmicb.2019.01178
- Herbst, D. A., Huitt-Roehl, C. R., Jakob, R. P., Kravetz, J. M., Storm, P. A., Alley, J. R., et al. (2018). The structural organization of substrate loading in iterative polyketide synthases. *Nat. Chem. Biol.* 14 (5), 474–479. doi:10.1038/s41589-018-0026-3
- Herencias, C., Salgado-Briegas, S., Prieto, M. A., and Nogales, J. (2020). Providing new insights on the biphasic lifestyle of the predatory bacterium *Bdellovibrio bacteriovorus* through genome-scale metabolic modeling. *PLoS Comput. Biol.* 16 (9), e1007646. doi:10.1371/journal.pcbi.1007646
- Hermant, Y., Palpal-Latoc, D., Kovalenko, N., Cameron, A. J., Brimble, M. A., and Harris, P. W. (2021). The total chemical synthesis and biological evaluation of the cationic antimicrobial peptides, laterocidine and brevicidine. *J. Nat. Prod.* 84 (8), 2165–2174. doi:10.1021/acs.jnatprod.1c00222
- Herrmann, J., Fayad, A. A., and Müller, R. (2017). Natural products from myxobacteria: Novel metabolites and bioactivities. *Nat. Prod. Rep.* 34, 135–160. doi:10.1039/c6np00106h
- Hu, W., Niu, L., Yue, X., Zhu, L., Hu, W., Li, Y., et al. (2021). Characterization of constitutive promoters for the elicitation of secondary metabolites in Myxobacteria. *ACS Synth. Biol.* 10 (11), 2904–2909. doi:10.1021/acssynbio.1c00444
- Hubrich, F., Bösch, N. M., Chepkirui, C., Morinaka, B. I., Rust, M., Guggler, M., et al. (2022). Ribosomally derived lipopeptides containing distinct fatty acyl moieties. *Proc. Natl. Acad. Sci. U. S. A.* 119 (3), e2113120119. doi:10.1073/pnas.2113120119

- Itoh, H., Tokumoto, K., Kaji, T., Paudel, A., Panthee, S., Hamamoto, H., et al. (2018). Total synthesis and biological mode of action of WAP-8294A2: A menaquinone-targeting antibiotic. *J. Org. Chem.* 83, 6924–6935. doi:10.1021/acs.joc.7b02318
- Jenner, M., Jian, X., Dashti, Y., Masschelein, J., Hobson, C., Roberts, D. M., et al. (2019). An unusual *Burkholderia gladioli* double chain-initiating nonribosomal peptide synthetase assembles 'fungal' icosalide antibiotics. *Chem. Sci.* 10 (21), 5489–5494. doi:10.1039/C8SC04897E
- Jiang, H., Ji, C., Sui, J., Sa, R., Wang, X., Liu, X., et al. (2017). Antibacterial and antitumor activity of Bogorol B-JX isolated from *Brevibacillus laterosporus* JX-5. *World J. Microbiol. Biotechnol.* 33 (10), 177–211. doi:10.1007/s11274-017-2337-z
- Kadouri, D. E., and Shanks, R. M. (2013). Identification of a methicillin-resistant *Staphylococcus aureus* inhibitory compound isolated from *Serratia marcescens*. *Res. Microbiol.* 164 (8), 821–826. doi:10.1016/j.resmic.2013.06.002
- Kato, A., Nakaya, S., Ohashi, Y., Hirata, H., Fujii, K., and Harada, K. (1997). WAP-8294A2, a novel anti-MRSA antibiotic produced by *Lysobacter* sp. *J. Am. Chem. Soc.* 119 (28), 6680–6681. doi:10.1021/ja970895o
- Kraas, F. I., Helmetag, V., Wittmann, M., Strieker, M., and Marahiel, M. A. (2010). Functional dissection of surfactin synthetase initiation module reveals insights into the mechanism of lipoinitiation. *Chem. Biol.* 17 (8), 872–880. doi:10.1016/j.chembiol.2010.06.015
- Kreutzer, M. F., and Nett, M. (2012). Genomics-driven discovery of taiwachelin, a lipopeptide siderophore from *Cupriavidus taiwanensis*. *Org. Biomol. Chem.* 10 (47), 9338–9343. doi:10.1039/c2ob26296g
- Kunakom, S., and Eustáquio, A. S. (2019). *Burkholderia* as a source of natural products. *J. Nat. Prod.* 82 (7), 2018–2037. doi:10.1021/acs.jnatprod.8b01068
- Kuo, Y. H., Hsu, H. C., Chen, Y. C., Liang, T. W., and Wang, S. L. (2012). A novel compound with antioxidant activity produced by *Serratia ureilytica* TKU013. *J. Agric. Food Chem.* 60 (36), 9043–9047. doi:10.1021/jf302481n
- Labbate, M., Zhu, H., Thung, L., Bandara, R., Larsen, M. R., Willcox, M. D. P., et al. (2007). Quorum-sensing regulation of adhesion in *Serratia marcescens* MG1 is surface dependent. *J. Bacteriol.* 189 (7), 2702–2711. doi:10.1128/JB.01582-06
- Li, H., Tanikawa, T., Sato, Y., Nakagawa, Y., and Matsuyama, T. (2005). *Serratia marcescens* gene required for surfactant serrawettin W1 production encodes putative aminolipid synthetase belonging to nonribosomal peptide synthetase family. *Microbiol. Immunol.* 49 (4), 303–310. doi:10.1111/j.1348-0421.2005.tb03734.x
- Li, J.-Y., Wang, L., Liu, Y.-F., Zhou, L., Gang, H.-Z., Liu, J.-F., et al. (2021a). Microbial lipopeptide-producing strains and their metabolic roles under anaerobic conditions. *Microorganisms* 9, 2030. doi:10.3390/microorganisms9102030
- Li, R., Shi, H., Zhao, X., Liu, X., Duan, Q., Song, C., et al. (2021b). Development and application of an efficient recombinering system for *Burkholderia glumae* and *Burkholderia plantarii*. *Microb. Biotechnol.* 14 (4), 1809–1826. doi:10.1111/1751-7915.13840
- Li, Y. X., Zhong, Z., Zhang, W. P., and Qian, P. Y. (2018). Discovery of cationic nonribosomal peptides as Gram-negative antibiotics through global genome mining. *Nat. Commun.* 9 (1), 3273–3279. doi:10.1038/s41467-018-05781-6
- Li, Z., Chakraborty, P., de Vries, R. H., Song, C., Zhao, X., Roelfes, G., et al. (2020b). Characterization of two relacidines belonging to a novel class of circular lipopeptides that act against Gram-negative bacterial pathogens. *Environ. Microbiol.* 22 (12), 5125–5136. doi:10.1111/1462-2920.15145
- Li, Z., de Vries, R. H., Chakraborty, P., Song, C., Zhao, X., Scheffers, D. J., et al. (2020a). Novel modifications of nonribosomal peptides from *Brevibacillus laterosporus* MG64 and investigation of their mode of action. *Appl. Environ. Microbiol.* 86 (24), 019811–e2020. doi:10.1128/AEM.01981-20
- Lin, Z., Falkinham, J. O., III, Tawfik, K. A., Jeffs, P., Bray, B., Dubay, G., et al. (2012). *Burkholderia* from *Burkholderia ambifaria*: Antifungal agents and possible virulence factors. *J. Nat. Prod.* 75 (9), 1518–1523. doi:10.1021/np300108u
- Liu, Y., Ma, A., Han, P., Chen, Z., and Jia, Y. (2020). Antibacterial mechanism of brevilaterin B: An amphiphilic lipopeptide targeting the membrane of *Listeria monocytogenes*. *Appl. Microbiol. Biotechnol.* 104 (24), 10531–10539. doi:10.1007/s00253-020-10993-2
- Lu, S. E., Novak, J., Austin, F. W., Gu, G., Ellis, D., Kirk, M., et al. (2009). Occidiofungin, a unique antifungal glycopeptide produced by a strain of *Burkholderia contaminans*. *Biochemistry* 48 (35), 8312–8321. doi:10.1021/bi900814c
- Matsuyama, T., Fujita, M., and Yano, I. (1985). Wetting agent produced by *Serratia marcescens*. *FEMS Microbiol. Lett.* 28 (1), 125–129. doi:10.1111/j.1574-6968.1985.tb00777.x
- Matsuyama, T., Murakami, T., Fujita, M., Fujita, S., and Yano, I. (1986). Extracellular vesicle formation and biosurfactant production by *Serratia marcescens*. *Microbiology* 132 (4), 865–875. doi:10.1099/00221287-132-4-865
- Menezes, R. C., Piechulla, B., Warber, D., Svatoš, A., and Kai, M. (2021). Metabolic profiling of rhizobacteria *Serratia plymuthica* and *Bacillus subtilis* revealed intra- and interspecific differences and elicitation of lipastatins and short peptides due to co-cultivation. *Front. Microbiol.* 1207, 685224. doi:10.3389/fmicb.2021.685224
- Miller, B. R., and Gulick, A. M. (2016). "Structural biology of nonribosomal peptide synthetases," in *Nonribosomal peptide and polyketide biosynthesis* (New York, NY: Humana Press), 3–29.
- Mohr, K. I. (2018). Diversity of Myxobacteria - we only see the tip of the iceberg. *Microorganisms* 6 (3), 84. doi:10.3390/microorganisms6030084
- Mullins, A. J., Murray, J. A., Bull, M. J., Jenner, M., Jones, C., Webster, G., et al. (2019). Genome mining identifies cepacin as a plant-protective metabolite of the biopesticidal bacterium *Burkholderia ambifaria*. *Nat. Microbiol.* 4 (6), 996–1005. doi:10.1038/s41564-019-0383-z
- Murray, C. J., Ikuta, K. S., Sharara, F., Swetschinski, L., Aguilar, G. R., Gray, A., et al. (2022). Global burden of bacterial antimicrobial resistance in 2019: A systematic analysis. *Lancet* 399 (10325), 629–655. doi:10.1016/S0140-6736(21)02724-0
- Niehs, S. P., Scherlach, K., and Hertweck, C. (2018). Genomics-driven discovery of a linear lipopeptide promoting host colonization by endofungal bacteria. *Org. Biomol. Chem.* 16 (37), 8345–8352. doi:10.1039/C8OB01515E
- Ning, Y., Han, P., Ma, J., Liu, Y., Fu, Y., Wang, Z., et al. (2021). Characterization of brevilaterins, multiple antimicrobial peptides simultaneously produced by *Brevibacillus laterosporus* S62-9, and their application in real food system. *Food Biosci.* 42, 101091. doi:10.1016/j.fbio.2021.101091
- Ohlendorf, B., Kehraus, S., and König, G. M. (2008). Myxochromide B3, a new member of the myxochromide family of secondary metabolites. *J. Nat. Prod. (Gorakhpur)* 71 (10), 1708–1713. doi:10.1021/np800319v
- Panda, A. K., Bisht, S. S., DeMondal, S., Senthil Kumar, N., Gurusubramanian, G., and Panigrahi, A. K. (2014). *Brevibacillus* as a biological tool: A short review. *Ant. Van Leeuwenhoek* 105 (4), 623–639. doi:10.1007/s10482-013-0099-7
- Panthee, S., Hamamoto, H., Paudel, A., and Sekimizu, K. (2016). *Lysobacter* species: A potential source of novel antibiotics. *Arch. Microbiol.* 198, 839–845. doi:10.1007/s00203-016-1278-5
- Parvez, N., Cornelius, L. K., and Fader, R. (2009). *Brevibacillus brevis* peritonitis. *Am. J. Med. Sci.* 337 (4), 297–299. doi:10.1097/MAJ.0b013e3181891626
- Patel, S., Ahmed, S., and Eswari, J. S. (2015). Therapeutic cyclic lipopeptides mining from microbes: Latest strides and hurdles. *World J. Microbiol. Biotechnol.* 31 (8), 1177–1193. doi:10.1007/s11274-015-1880-8
- Ray, S., Patel, N., and Amin, D. (2020). "Brevibacillus," in *Beneficial microbes in agro-ecology* (Massachusetts, United States: Academic Press), 149–167. doi:10.1016/B978-0-12-823414-3.00009-5
- Reynolds, K. A., Luhavaya, H., Li, J., Dahesh, S., Nizet, V., Yamanaka, K., et al. (2018). Isolation and structure elucidation of lipopeptide antibiotic taromycin B from the activated taromycin biosynthetic gene cluster. *J. Antibiot.* 71 (2), 333–338. doi:10.1038/ja.2017.146
- Rosenberg, E., and Varon, M. (1984). "Antibiotics and lytic enzymes," in *Myxobacteria: Development and cell interactions*. Editor E. Rosenberg (New York: Springer), 109–125.
- Saadatpour, F., and Mohammadpanah, F. (2020). Bioprospecting of indigenous myxobacteria from Iran and potential of *Cystobacter* as a source of anti-MDR compounds. *Folia Microbiol. (Praha)* 65 (4), 639–648. doi:10.1007/s12223-019-00768-2
- Sang, M., Wang, H., Shen, Y., Rodrigues de Almeida, N., Conda-Sheridan, M., Li, S., et al. (2019). Identification of an anti-MRSA cyclic lipopeptide, WBP-29479A1, by genome mining of *Lysobacter antibioticus*. *Org. Lett.* 21 (16), 6432–6436. doi:10.1021/acs.orglett.9b02333
- Sester, A., Korp, J., and Nett, M. (2020). "Secondary metabolism of predatory bacteria," in *The ecology of predation at the microscale*. Editors E. Jurkevitch and R. Mitchell (New York: Springer), 127–153.
- Shoji, J. I., Sakazaki, R., Wakisaka, Y., Koizumi, K., Mayama, M., Matsuura, S., et al. (1976). Isolation of Brevistin, a new peptide antibiotic studies on antibiotics from the genus *Bacillus*. *J. Antibiot. (Tokyo)* 29 (4), 375–379. doi:10.7164/antibiotics.29.375
- Singh, S. S., Sharma, D., Baidara, P., Choksket, S., HarshvardhanMandal, S. M., Grover, V., et al. (2021). Characterization and antimicrobial studies of iturin-like and bogorol-like lipopeptides from *Brevibacillus* spp. strains GI9 and SKDU10. *Front. Microbiol.* 12, 729026. doi:10.3389/fmicb.2021.729026
- Song, C., Schmidt, R., de Jager, V., Krzyzanowska, D., Jongedijk, E., Cankar, K., et al. (2015). Exploring the genomic traits of fungus-feeding bacterial genus *Collimonas*. *BMC Genomics* 16 (1103). doi:10.1186/s12864-015-2289-3

- Srinivasan, A., Kraus, C. N., DeShazer, D., Becker, P. M., Dick, J. D., Spacek, L., et al. (2001). Glanders in a military research microbiologist. *N. Engl. J. Med.* 345 (4), 256–258. doi:10.1056/NEJM200107263450404
- Strieker, M., and Marahiel, M. A. (2009). The structural diversity of acidic lipopeptide antibiotics. *ChemBioChem* 10 (4), 607–616. doi:10.1002/cbic.200800546
- Su, C., Xiang, Z., Liu, Y., Zhao, X., Sun, Y., Li, Z., et al. (2016). Analysis of the genomic sequences and metabolites of *Serratia surfactantifaciens* sp. nov. YD25T that simultaneously produces prodigiosin and serrawettin W2. *BMC genomics* 17 (1), 865–919. doi:10.1186/s12864-016-3171-7
- Tawfik, K. A., Jeffs, P., Bray, B., Dubay, G., Falkinham, J. O., III, Mesbah, M., et al. (2010). Burkholdines 1097 and 1229, potent antifungal peptides from *Burkholderia ambifaria* 2.2 N. *Org. Lett.* 12 (4), 664–666. doi:10.1021/ol9029269
- Théâtre, A., Cano-Prieto, C., Bartolini, M., Laurin, Y., Deleu, M., Niehren, J., et al. (2021). The surfactin-like lipopeptides from *Bacillus* spp.: Natural biodiversity and synthetic biology for a broader application range. *Front. Bioeng. Biotechnol.* 9, 623701. doi:10.3389/fbioe.2021.623701
- Thongkongkaew, T., Ding, W., Bratovanov, E., Oueis, E., Garci'a-Altares, M., Zaburannyi, N., et al. (2018). Two types of threonine-tagged lipopeptides synergize in host colonization by pathogenic *Burkholderia* species. *ACS Chem. Biol.* 13 (5), 1370–1379. doi:10.1021/acscchembio.8b00221
- Treuner-Lange, A., Bruckskotten, M., Rupp, O., Goesmann, A., and Søgaard-Andersen, L. (2017). Whole-genome sequence of the fruiting myxobacterium *Cystobacter fuscus* DSM 52655. *Genome Announc.* 5 (43), 011966–17–e1217. doi:10.1128/genomeA.01196-17
- Waite, D. W., Chuvochina, M., Pelikan, C., Parks, D. P., Yilmaz, P., Wagner, M., et al. (2020). Proposal to reclassify the proteobacterial classes Deltaproteobacteria and Oligoflexia, and the phylum Thermodesulfobacteria into four phyla reflecting major functional capabilities. *Int. J. Syst. Evol. Microbiol.* 70, 5972–6016. doi:10.1099/ijsem.0.004213
- Wang, J., Haddad, N. I., Yang, S. Z., and Mu, B. Z. (2010). Structural characterization of lipopeptides from *Brevibacillus brevis* HOB1. *Appl. Biochem. Biotechnol.* 160 (3), 812–821. doi:10.1007/s12010-009-8536-9
- Wang, X., Zhou, H., Chen, H., Jing, X., Zheng, W., Li, R., et al. (2018). Discovery of recombinases enables genome mining of cryptic biosynthetic gene clusters in *Burkholderiales* species. *Proc. Natl. Acad. Sci. U. S. A.* 115 (18), E4255–E4263. doi:10.1073/pnas.1720941115
- Wasserman, H. H., Keggi, J. J., and McKeon, J. E. (1961). Serratamolide, a metabolic product of *Serratia*. *J. Am. Chem. Soc.* 83 (19), 4107–4108. doi:10.1021/ja01480a046
- Wenzel, S. C., Gross, F., Zhang, Y., Fu, J., Stewart, A. F., and Müller, R. (2005). Heterologous expression of a myxobacterial natural products assembly line in pseudomonads via red/ET recombineering. *Chem. Biol.* 12 (3), 349–356. doi:10.1016/j.chembiol.2004.12.012
- Wenzel, S. C., Meiser, P., Binz, T. M., Mahmud, T., and Müller, R. (2006). Nonribosomal peptide biosynthesis: Point mutations and module skipping lead to chemical diversity. *Angew. Chem. Int. Ed.* 45, 2296–2301. doi:10.1002/anie.200503737
- Wu, Y., Nie, T., Meng, F., Zhou, L., Chen, M., Sun, J., et al. (2021). The determination of antibacterial mode for cationic lipopeptides brevibacillins against *Salmonella typhimurium* by quantum chemistry calculation. *Appl. Microbiol. Biotechnol.* 105 (13), 5643–5655. doi:10.1007/s00253-021-11398-5
- Wu, Y., Zhou, L., Lu, F., Bie, X., Zhao, H., Zhang, C., et al. (2019). Discovery of a novel antimicrobial lipopeptide, brevibacillin V, from *Brevibacillus laterosporus* fmb70 and its application on the preservation of skim milk. *J. Agric. Food Chem.* 67 (45), 12452–12460. doi:10.1021/acs.jafc.9b04113
- Yan, F., Burgard, C., Popoff, A., Zaburannyi, N., Zipf, G., Maier, J., et al. (2018). Synthetic biology approaches and combinatorial biosynthesis towards heterologous lipopeptide production. *Chem. Sci.* 9, 7510–7519. doi:10.1039/c8sc02046a
- Yang, R., Lei, S., Xu, X., Jin, H., Sun, H., Zhao, X., et al. (2020). Key elements and regulation strategies of NRPSs for biosynthesis of lipopeptides by *Bacillus*. *Appl. Microbiol. Biotechnol.* 104 (19), 8077–8087. doi:10.1007/s00253-020-10801-x
- Yang, X., Huang, E., and Yousef, A. E. (2017). Brevibacillin, a cationic lipopeptide that binds to lipoteichoic acid and subsequently disrupts cytoplasmic membrane of *Staphylococcus aureus*. *Microbiol. Res.* 195, 18–23. doi:10.1016/j.micres.2016.11.002
- Yang, X., Huang, E., Yuan, C., Zhang, L., and Yousef, A. E. (2016). Isolation and structural elucidation of brevibacillin, an antimicrobial lipopeptide from *Brevibacillus laterosporus* that combats drug-resistant Gram-positive bacteria. *Appl. Environ. Microbiol.* 82 (9), 2763–2772. doi:10.1128/AEM.00315-16
- Yang, X., and Yousef, A. E. (2018). Antimicrobial peptides produced by *Brevibacillus* spp.: Structure, classification and bioactivity: A mini review. *World J. Microbiol. Biotechnol.* 34 (4), 57–10. doi:10.1007/s11274-018-2437-4
- Yoshimura, A., Covington, B. C., Gallant, É., Zhang, C., Li, A., and Seyedsayamdost, M. R. (2020). Unlocking cryptic metabolites with mass spectrometry-guided transposon mutant selection. *ACS Chem. Biol.* 15 (10), 2766–2774. doi:10.1021/acscchembio.0c00558
- Yue, H., Miller, A. L., Khetrapal, V., Jayaseker, V., Wright, S., and Du, L. (2022). Biosynthesis, regulation, and engineering of natural products from *Lysobacter*. *Nat. Prod. Rep.* 39 (4), 842–874. doi:10.1039/d1np00063b
- Zhang, W., Li, Y., Qian, G., Wang, Y., Chen, H., Li, Y. Z., et al. (2011). Identification and characterization of the anti-methicillin-resistant *Staphylococcus aureus* WAP-8294A2 biosynthetic gene cluster from *Lysobacter enzymogenes* OH11. *Antimicrob. Agents Chemother.* 55 (12), 5581–5589. doi:10.1128/AAC.05370-11
- Zhao, X., Kuipers, O. P., Shukla, R., Kumar, R., Weingarth, M., Breukink, E., et al. (2021). Brevibacillin 2V, a novel antimicrobial lipopeptide with an exceptionally low hemolytic activity. *Front. Microbiol.* 12, 693725. doi:10.3389/fmicb.2021.693725
- Zhao, X., Wang, X., Shukla, R., Kumar, R., Weingarth, M., Breukink, E., et al. (2021). Brevibacillin 2V, a novel antimicrobial lipopeptide with an exceptionally low hemolytic activity. *Front. Microbiol.* 12, 693725. doi:10.3389/fmicb.2021.693725
- Zhu, Y., Han, Y., Liu, G., Bian, Z., Yan, X., Li, Y., et al. (2022). Novel indole-mediated potassium ion import system confers a survival advantage to the Xanthomonadaceae family. *ISME J.* 16, 1717–1729. doi:10.1038/s41396-022-01219-6



OPEN ACCESS

EDITED BY

Gildardo Rivera,
Instituto Politécnico Nacional (IPN),
Mexico

REVIEWED BY

Anik Banik,
Sylhet Agricultural University,
Bangladesh
Haibing Zhou,
Wuhan University, China
Serena Massari,
University of Perugia, Italy
Andre Torres,
Federal University of Rio de Janeiro,
Brazil

*CORRESPONDENCE

Hong-Bin Zhang,
zhanghb@ynu.edu.cn
Yan-Ping He,
yphe@ynu.edu.cn
Yong-Tang Zheng,
zhengyt@mail.kiz.ac.cn

*These authors have contributed equally
to this work and share first authorship

SPECIALTY SECTION

This article was submitted to Medicinal
and Pharmaceutical Chemistry,
a section of the journal
Frontiers in Chemistry

RECEIVED 03 August 2022

ACCEPTED 22 September 2022

PUBLISHED 12 October 2022

CITATION

Zhou G-F, Xie C-Q, Xue J-X, Wang J-B,
Yang Y-Z, Zheng C-B, Luo R-H,
Yang R-H, Chen W, Yang L-M,
Wang Y-P, Zhang H-B, He Y-P and
Zheng Y-T (2022), Identification of 6 ω -
cyclohexyl-2-(phenylamino
carbonylmethylthio)pyrimidin-4(3H)-
ones targeting the ZIKV NS5 RNA
dependent RNA polymerase.
Front. Chem. 10:1010547.
doi: 10.3389/fchem.2022.1010547

COPYRIGHT

© 2022 Zhou, Xie, Xue, Wang, Yang,
Zheng, Luo, Yang, Chen, Wang,
Zhang, He and Zheng. This is an open-
access article distributed under the
terms of the [Creative Commons
Attribution License \(CC BY\)](#). The use,
distribution or reproduction in other
forums is permitted, provided the
original author(s) and the copyright
owner(s) are credited and that the
original publication in this journal is
cited, in accordance with accepted

Identification of 6 ω -cyclohexyl-2-(phenylamino carbonylmethylthio) pyrimidin-4(3H)-ones targeting the ZIKV NS5 RNA dependent RNA polymerase

Guang-Feng Zhou^{1,2†}, Cong-Qiang Xie^{3†}, Jian-Xia Xue^{1,4},
Jing-Bo Wang³, Yu-Zhuo Yang³, Chang-Bo Zheng⁵,
Rong-Hua Luo¹, Ren-Hua Yang⁵, Wen Chen³, Liu-Meng Yang¹,
Yue-Ping Wang³, Hong-Bin Zhang^{3*}, Yan-Ping He^{3*} and
Yong-Tang Zheng^{1*}

¹Key Laboratory of Bioactive Peptides of Yunnan Province/Key Laboratory of Animal Models and Human Disease Mechanisms of the Chinese Academy of Sciences, KIZ-CUHK Joint Laboratory of Bioresources and Molecular Research in Common Diseases, Kunming Institute of Zoology, Chinese Academy of Sciences, Kunming, Yunnan, China, ²College of Pharmacy, Soochow University, Suzhou, China, ³Key Laboratory of Medicinal Chemistry for Natural Resource, Yunnan Provincial Center for Research and Development of Natural Products, Ministry of Education, School of Pharmacy, Yunnan University, Kunming, China, ⁴Medical College, Kunming University of Science and Technology, Kunming, Yunnan, China, ⁵Yunnan Key Laboratory of Pharmacology for Natural Products, School of Pharmaceutical Science, Kunming Medical University, Kunming, China

Zika virus (ZIKV), a mosquito-borne flavivirus, is a global health concern because of its association with severe neurological disorders such as neonatal microcephaly and adult Guillain-Barre syndrome. Although many efforts have been made to combat ZIKV infection, there is currently no approved vaccines or antiviral drugs available and there is an urgent need to develop effective anti-ZIKV agents. In this study, 26 acetylarlyamine-S-DACOs derivatives were prepared, and eight of them were found to have inhibitory activity against Zika virus. Among these substances, 2-[(4-cyclohexyl-5-ethyl-6-oxo-1,6-dihydropyrimidin-2-yl)thio]-N-(3,5-difluorophenyl)acetamide (**4w**) with the best anti-ZIKV activity was selected for in-depth study of antiviral activity and mechanism of action. Here, we discovered **4w** targeted on the ZIKV NS5 RNA -dependent RNA polymerase (RdRp), which exhibited good *in vitro* antiviral activity without cell species specificity, both at the protein level and at the RNA level can significantly inhibit ZIKV replication. Preliminary molecular docking studies showed that **4w** preferentially binds to the palm region of NS5A RdRp through hydrogen bonding with residues such as LYS468, PHE466, GLU465, and GLY467. ZIKV NS5 RdRp enzyme activity experiment showed that **4w** could directly inhibit ZIKV RdRp activity with $EC_{50} = 11.38 \pm 0.51 \mu M$. In antiviral activity studies, **4w** was found to inhibit ZIKV RNA replication with $EC_{50} = 6.87 \pm 1.21 \mu M$. ZIKV-induced plaque formation was inhibited with $EC_{50} = 7.65 \pm 0.31 \mu M$. In conclusion, our study disclosed that

acetylarylamine-S-DACOs is a new active scaffolds against ZIKV, among which compound **4w** was proved to be a potent novel anti-ZIKV compound target ZIKV RdRp protein. These promising results provide a future prospective for the development of ZIKV RdRp inhibitors.

KEYWORDS

ZIKV, RdRp, acetylarylamine-S-DACOs, anti-ZIKV agent, NS5

1 Introduction

Zika virus (ZIKV) is an important member of genus *Flavivirus* which includes dengue virus (DENV), West Nile virus, yellow fever virus (YFV), hepatitis C virus (HCV) and Japanese encephalitis virus (Dick G et al., 1952; Barrows et al., 2018). ZIKV is transmitted primarily by mosquito bites, however vertical, sexual, transfusion, and transplantation transmissions have been also related (Li et al., 2012; Gregory et al., 2017). Since the worldwide outbreak of ZIKV in 2015, it has caused a serious threat to human health due to its clinical symptoms that are different from other flaviviruses, such as neonatal microcephaly, adult Guillain-Barre syndrome, and other serious neurological diseases (Petersen et al., 2016; Cumberworth et al., 2017; Bhagat et al., 2021). ZIKV is not a new type of virus, and its spread in human populations has a long history. However, the research on vaccines and antiviral drugs in recent years has not really prevented its spread, but the development of some vaccines and drugs has always stayed in the stage of drug clinical research. At present, there are no reliable vaccines and drugs that can be clearly used for the treatment and prevention of ZIKV infection (Boldescu et al., 2017; Kraemer et al., 2019). Therefore, the development of effective antiviral drugs is one of the most important strategies to inhibit ZIKV infection.

ZIKV is a single-stranded positive-stranded RNA virus with spherical virions, with a diameter of about 40 nm and an envelope (Guo et al., 2021). The viral core consists of viral genomic RNA and capsid proteins, and its surface proteins are arranged in icosahedral symmetry (Hu and Sun, 2019). The ZIKV genome is about 11 kb in length, including two flanking noncoding regions and one open reading frame. The ZIKV genome consists of three structural proteins (capsid protein, envelope protein, and prM protein) and seven non-structural proteins (NS1, NS2A, NS2B, NS3, NS4A, NS4B, and NS5) (Sirohi and Kuhn, 2017). NS5 is essential for the replication of the ZIKV RNA genome. The N-terminal portion of NS5 contains a methyltransferase (MTase), followed by a short linker that connects to the RNA-dependent RNA polymerase (RdRp), an enzyme that plays an important role in viral RNA replication, acting metalloproteinases (Lim et al., 2013). Regarding the function of the ZIKV RdRp subdomain, it was found that the palm subdomain mainly acts as a catalytic center (Züst et al., 2013) and mediates RNA template binding, translocation, and nucleoside triphosphate (NTP) specificity, as

well as nucleotide transfer and priming Alignment of Nucleotide ATP (Selisko et al., 2012; Duan et al., 2017; Shu and Gong, 2017). In addition, the thumb domain has an initiation loop, which is primarily responsible for facilitating the initiation of ATP-specific RNAs and regulating the transition of subsequent elongation steps (Bartholomeusz and Thompson, 1999). The finger domain is involved in the formation of the active site and NTP entry channel by controlling the *de novo* synthesis of RdRp (Akiyama et al., 2021; Li and Kang, 2022). Finally, alanine substitutions have demonstrated that several N-pocket residues are critical for NS5 polymerase *de novo* activity as well as viral replication (Ackermann and Padmanabhan, 2001; Malet et al., 2008). Due to its pivotal role in viral replication, RdRp is a promising drug target for ZIKV infection (Malet et al., 2008; Lim et al., 2015; Ferrero et al., 2019).

5-Alkyl-6-aryl-2-(phenylaminocarbonylmethylthio)pyrimidin-4(3H)-ones (acetylarylamine-S-DABOs general structure **1**, Figure 1) are a class of excellent non-nucleoside reverse transcriptase inhibitors (NNRTIs) with high broad-spectrum HIV-1 inhibitory activity (Yu et al., 2009; Yu et al., 2011). In our previous antiviral studies, starting from compounds of general structure **1**, we replaced the aromatic ring at the C-6 position of the pyrimidine by a cyclohexyl moiety, obtaining a series of 5-Alkyl-6-cyclohex-yl-2-(phenylaminocarbonylmethylthio)pyrimidin-4(3H)-ones (acetylarylamine-S-DACOs general structure **2**, Figure 1) which can inhibit HIV replication in the low nanomolar range (He et al., 2011), while compounds of general structure **3** showed good anti-HCV activity (He et al., 2015). In recent years, we have launched our search of new active scaffolds against flaviviruses such as HCV, DENV and ZIKV (Wu et al., 2017; Qian et al., 2022; Rui et al., 2022). Given the success of drug development against HCV infection and the presence of HCV homologs with ZIKV, the repurposing of HCV inhibitors for ZIKV is an attractive starting point for the discovery of a novel skeleton of anti-ZIKV drugs. By comparing the structures of the **2** and **3** series compounds, it can be seen that the compounds with F or OCH₃ substituent on the benzene ring at the end of C-2 side chain have good anti-HIV or HCV activity. Therefore, in the design of target molecules, fluoro-containing substituents such as F, CF₃, OCF₃ and OCH₃ were selected and introduced into different positions on the benzene ring. In addition, the C-6 substituent also had a significant effect on the antiviral activity of the compounds. For example, C-6 cyclohexylmethyl substituted compounds **2** have anti-HIV

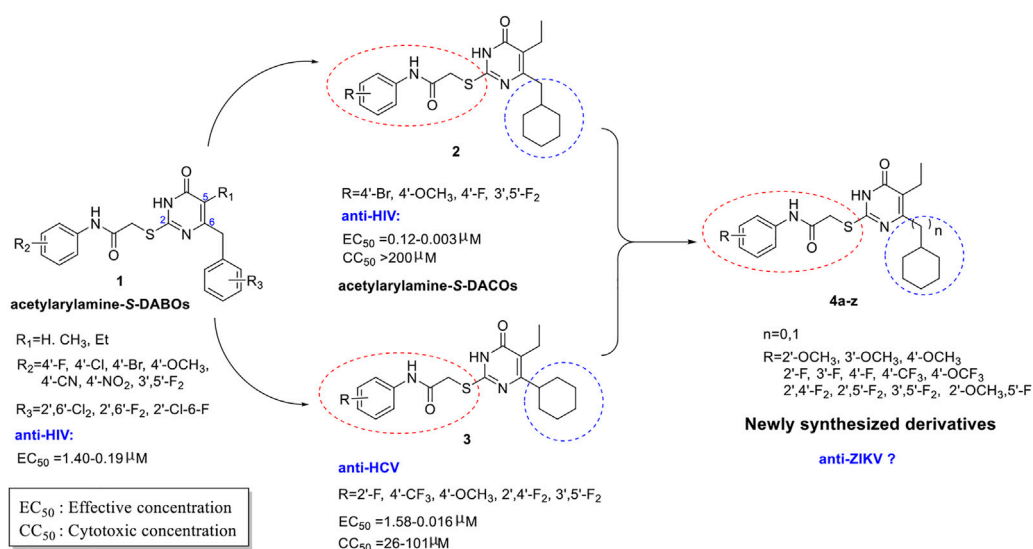
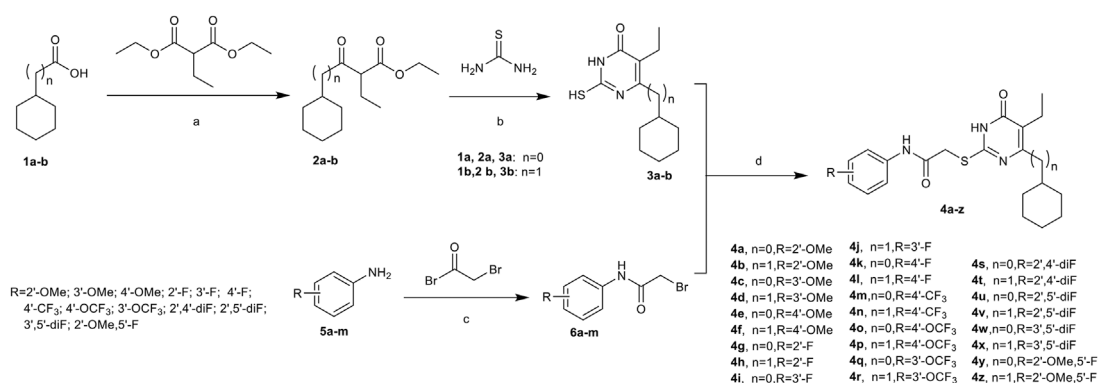


FIGURE 1

The chemical structure of the acetylarlyamine-S-DABOs compounds.



activity, while C-6 cyclohexyl substituted compounds **3** have anti-HCV activity. Therefore, we intend to synthesize C-6 cyclohexyl or C-6 cyclohexylmethyl substituted acetylarlyamine-S-DACOs target molecules simultaneously. Therefore, using compounds of general structures **2** and **3** as lead compounds, a series of new acetylarlyamine-S-DACO derivatives **4a-z** (Figure 1) were designed by introducing selective substituents (R) on the ω -phenyl group of the pyrimidine ring C-2 side chain and a cyclohexyl or cyclohexyl methyl at the C-6 position. In this paper, we describe the synthesis, cell-based and target-based activity

evaluation of the series of acetylarlyamine-S-DACOs derivatives against ZIKV infection.

2 Results and discussion

2.1 Chemistry

A series of acetylarlyamine-S-DACOs **4a-z** was synthesized as illustrated in Scheme 1. Following the procedure described previously (He et al., 2004; He et al.,

TABLE 1 Structures, EC₅₀^a, CC₅₀^b, and SI of titled compounds.

Compd.	R	n	EC ₅₀ (μM)	CC ₅₀ (μM)	SI
4a	2'-OMe	0	NA ^c	>200 ^d	/ ^e
4b	2'-OMe	1	NA	>200	/
4c	3'-OMe	0	NA	109.32 ± 3.19	/
4d	3'-OMe	1	NA	130.66 ± 5.49	/
4e	4'-OMe	0	NA	>200	/
4f	4'-OMe	1	NA	>200	/
4g	2'-F	0	16.29 ± 1.31	>200	>12.27
4h	2'-F	1	10.77 ± 1.67	136.8 ± 2.41	12.70
4i	3'-F	0	19.37 ± 0.38	>200	>10.33
4j	3'-F	1	7.48 ± 0.67	146.9 ± 1.01	19.64
4k	4'-F	0	NA	>200	/
4l	4'-F	1	NA	122.5 ± 5.19	/
4m	4'-CF ₃	0	NA	>200	/
4n	4'-CF ₃	1	7.75 ± 1.35	89.98 ± 1.35	11.62
4o	4'-OCF ₃	0	NA	>200	/
4p	4'-OCF ₃	1	NA	163.5 ± 7.34	/
4q	3'-OCF ₃	0	NA	>200	/
4r	3'-OCF ₃	1	8.84 ± 0.72	165.5 ± 2.38	18.73
4s	2',4'-diF	0	NA	>200	/
4t	2',4'-diF	1	10.51 ± 1.70	163.0 ± 5.76	15.51
4u	2',5'-diF	0	NA	>200	/
4v	2',5'-diF	1	NA	100.9 ± 5.03	/
4w	3',5'-diF	0	7.65 ± 0.31	>200	>26
4x	3',5'-diF	1	NA	60.25 ± 2.02	/
4y	2'-OMe,5'-F	0	NA	150.0 ± 0.86	/
4z	2'-OMe,5'-F	1	NA	>200	/
Ribavirin			48.88 ± 3.42	>200	>4.09

^aPlaque assay result conducted independently in triplicate.^bMTT result conducted independently in triplicate.^c"NA" represents "not active by the plaque assay that 50 μM of testing compound expresses less than 50% inhibition of ZIKV replication."^dIndicated concentration is the highest soluble concentration which does not reach 50% cytotoxicity.^e"/" means "not available."

2011; Wu et al., 2020; Li et al., 2021), the key intermediates β-Ketoesters **2a/b** were prepared by exposure of each commercially available cyclohexanecarboxylic acid **1a** or 2-cyclohexylacetic acid **1b** to 1,1'-carbonyl-diimidazole (CDI) followed by treatment with ethyl potassium malonates in the presence of anhydrous MgCl₂ and Et₃N. Subsequent condensation of **2a/b** with thiourea in the presence of EtONa in refluxing EtOH afforded 5,6-disubstituted thiouracils **3a/b**. Next by selective S-alkylation of **3a/b** with the appropriate N-phenylacetamide halides **6a-m** in the presence of anhydrous K₂CO₃ in anhydrous DMF afforded the desired target compounds **4a-z**. These compounds were characterized by ¹H NMR and HRMS for their structural accuracy.

2.2 Anti-ZIKV activity evaluation

Initially, the novel acetylarylamine-S-DACOs **4a-z** were tested for their cytotoxicity and anti-ZIKV activity in Vero cells by plaque formation according to previously detailed procedure (Xu et al., 2017). The activity data was interpreted in CC₅₀ values (cytotoxicity), EC₅₀ (anti-ZIKV activity) and SI (selectivity index, given by the CC₅₀/EC₅₀ ratio) (Table 1). As show in Table 1, the preliminary plaque results revealed that there are eight active compounds against ZIKV replication with EC₅₀ < 20 μM and CC₅₀ > 90 μM, ensuring that antiviral effect of these compounds is not related to their toxicity. The most potent compounds were **4j**, **4n**, and **4w** with EC₅₀ values of 7.48, 7.75, and 7.65 μM, respectively. They were about 6 times more potent than the reference drug Ribavirin (EC₅₀ = 48.88 μM). From Table 1, we can make a preliminary summary of this series of compounds: First, the type of substituent R on benzene ring has a significant impact on the anti-ZIKV activity of these compounds. For example, the R of the above eight compounds showing anti-ZIKV were all fluorine substituents, while the compounds **4a-f**, **4y**, and **4z** obtained by introducing methoxyl onto benzene ring did not show activity. In addition, the position of the substituent R on the benzene ring also has an important influence on the activity. For example, the activity of the 3'-F-substituted compound **4j** (EC₅₀ = 7.48 μM) is better than that of the 2'-F-substituted analog **4h** (EC₅₀ = 10.77 μM), while the 4'-F-substituted analog **4l** becomes inactive compound. The 3'-OCF₃-substituted compound **4r** can inhibit ZIKV with EC₅₀ value of 8.84 μM, while its 4'-OCF₃-substituted counterpart **4p** is inactive against ZIKV. At last, the length (n) of the connecting carbon chain between the C-6 site of the pyrimidine ring and cyclohexane also affects the activity of the compound, and there may be a synergistic relationship between n and substituent R. For example, compound **4j** (R = 3'-F, n = 1), **4n** (R = 4'-CF₃, n = 1), and **4r** (R = 3'-OCF₃, n = 1) are more active than their counterpart **4i** (R = 3'-F, n = 0), **4m** (R = 4'-CF₃, n = 0), and **4q** (R = 3'-OCF₃, n = 0), respectively, showing cyclohexylmethyl (n = 1) is more favorable for activity. Unlike SAR of 3'-F or 3'-OCF₃ series, **4x** (R = 3',5'-diF, n = 1) is less active than **4w** (R = 3',5'-diF, n = 0), showing cyclohexyl (n = 0) is more favorable for activity.

The strongest plaque inhibition by compound **4w** is shown in Figure 2. As we can see from Figure 2A, **4w** significantly inhibited the plaque formation of ZIKV, and this inhibitory effect was positively correlated with the concentration of **4w**. It inhibited ZIKV plaque formation with EC₅₀ = 7.65 ± 0.31 μM (Figure 2B). We tested its cytotoxicity to A549, Huh7 and Vero cells by MTT method, and found that it had no obvious toxicity to these three different cell lines, the CC₅₀ was greater than 200 μM (Figure 2C), and its SI value was greater than 26, which suggested that **4w** could be used as a new type of anti-ZIKV active compound for further development and research. Subsequently, compound **4w**, as a novel anti-ZIKV skeleton, was subjected to further analysis

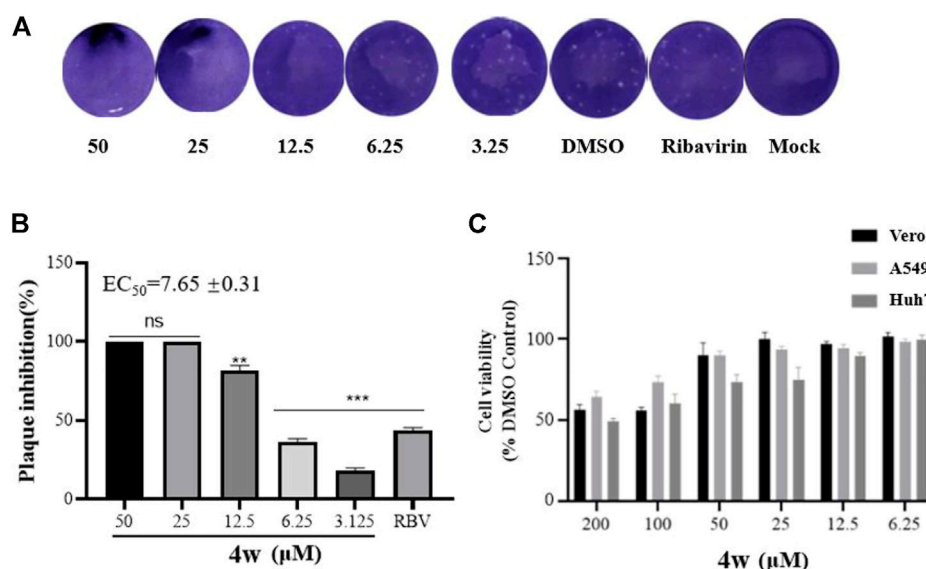


FIGURE 2

Compounds **4w** inhibited the plaque formation caused by ZIKV infection, Vero cells were infected with ZIKV (MOI = 0.1) at 37°C for 2 h. (A) Original graph of **4w** inhibiting ZIKV plaque formation; (B) **4w** inhibition rate of ZIKV-induced plaque formation; (C) **4w** cytotoxicity to Vero, Huh7, and A549 cells, data is the mean (\pm SD) of three experiments, with DMSO as a positive control, and Ribavirin = 50 μ M as a positive drug control. * p < 0.05; ** p < 0.01; *** p < 0.001.

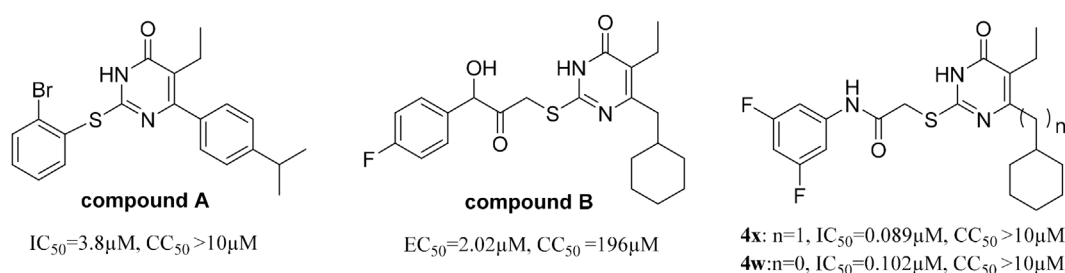


FIGURE 3

Pyrimidones analogues active against HCV targeting NS5B RdRp.

to detect the antiviral effects and elucidate the drug target and the mode of drug action.

2.3 Compound 4w interacts with ZIKV RdRp directly

Among the viral targets, NS5 polymerase is one of the most promising and exploited targets, being highly conserved among flaviviruses. Previously, some related pyrimidones have been identified as potential HCV inhibitors targeting NS5 RdRp. For example, Ding et al. have reported 5-cyano-6-aryl-2-thiouracil

(compound A, Figure 3) as a potent inhibitor of HCV NS5B RdRp (IC_{50} = 3.8 μ M) (Ding et al., 2006). Wu et al. (2017) identified 2-hydroxyphenethyl sulfanyl-oxypyrimidines derivatives as potential anti-HCV agent targeting HCV NS5B RdRp (e.g., compound B, Figure 3). After our research group revealed the potent anti-HCV activity of acetylarylamine-S-DACO derivatives (general structure 3, Figure 1), Shen (2015) further determined that this series of compounds targeted HCV NS5B RdRp. For example, compound **4x** and **4w** (Figure 3) as a potent inhibitor of HCV NS5B RdRp have IC_{50} of 0.089 μ M and 0.102 μ M. Since compound **4w** has already been shown to be a HCV RdRp inhibitor, we speculated compound **4w** may also act on ZIKV

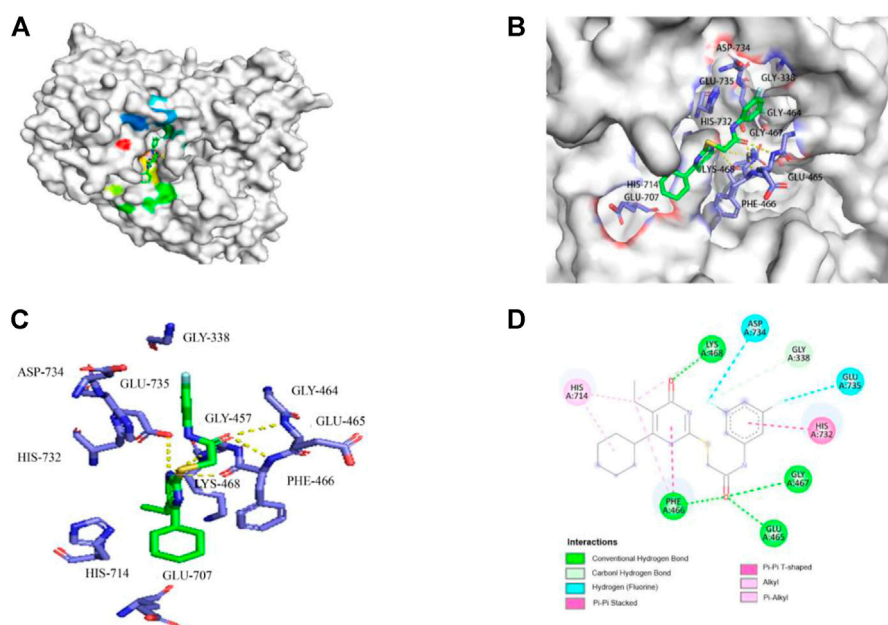


FIGURE 4

Molecular docking model of **4w** and ZIKV RdRp. (A) **4w** binds to ZIKV RdRp with lower free energy, the compound is shown in stick form, and the amino acid interaction site is shown as surface structure; (B) **4w** binds to ZIKV RdRp, the compound is shown in green, interacts amino acids are shown in purple; (C) The three-dimensional structure of the interaction between **4w** and ZIKV RdRp is magnified, **4w** is shown in green, the interacting amino acids are shown in purple, and the intermolecular hydrogen bond force is marked with a yellow dotted line; (D) The interaction map between **4w** and each amino acid of ZIKV RdRp protein, the intermolecular hydrogen bond force is shown in green.

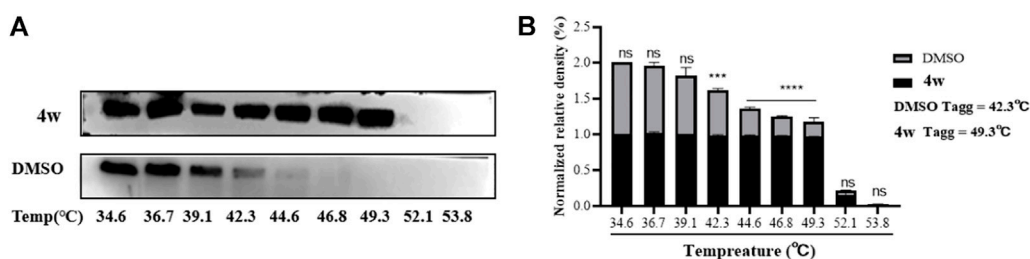


FIGURE 5

The interaction between **4w** and ZIKV NS5 protein. (A) WB detection of ZIKV NS5 protein expression under different temperature gradients after **4w** treatment; (B) NS5 protein grayscale analysis and ZIKV NS5 protein expression after **4w** treatment observed changes in aggregation temperature; data is the mean (\pm SD) of three experiments. * $p < 0.05$; ** $p < 0.01$; *** $p < 0.001$; **** $p < 0.0001$.

RdRp. We first detected whether **4w** could interact with ZIKV RdRp by molecular docking method, and found that **4w** can bind to ZIKV RdRp domain with low free energy (Figures 4A,B). ZIKV RdRp is mainly composed of three domains, namely palm domain (amino acid regions 321–488 and 542–608), finger domain (amino acid regions 489–541 and 609–714) and thumb (amino acid regions 715–903) (Chen et al., 2021). In the docking results, it was found that **4w** mainly binds to the palm domain of ZIKV RdRp, and preferentially binds to LYS468, PHE466, GLU465, and GLY467 amino acids in the palm region by hydrogen bonding

force (Figures 4C,D). Details are as follows: 1) The pyrimidine ring of compound **4w** is immobilized in the binding cavity by hydrogen bonding between its C-4 carbonyl group and LYS468 and π - π interaction with the benzene ring of PHE466. 2) The C-2 β -Carbonyl of **4w** formed triple hydrogen bonds with GLU465, PHE466 and GLY467, thus facilitating stable binding of the inhibitor to ZIKV RdRp; 3) The C-2 terminal 3, 5-2F-phenyl group of **4w** points to the region surrounded by the side chains of HIS732, GLU735, and ASP734. In addition to the π - π interaction between the benzene ring and the imidazole ring of HIS732, the two

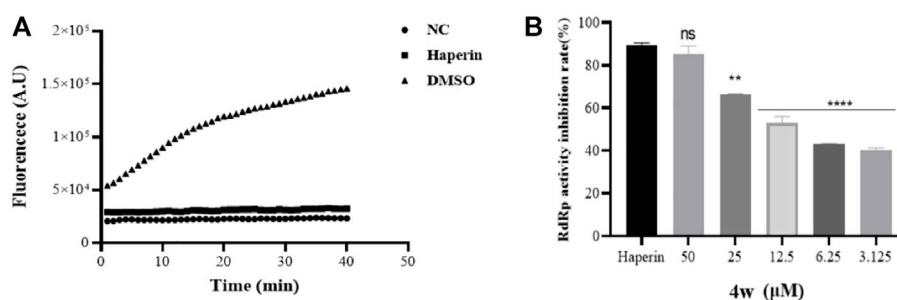


FIGURE 6

Compound **4w** inhibits ZIKV RdRp activity. (A) ZIKV RdRp activity assay, NC is the negative control with substrate only; DMSO is the compound solvent control, Heparin is the positive drug control; (B) **4w** concentration gradient inhibition of ZIKV RdRp protein. Data is the mean (\pm SD) of three experiments, with DMSO as a positive control, and Heparin = 5 μ M as a positive drug control. * p < 0.05; ** p < 0.01; *** p < 0.001; **** p < 0.0001.

F atoms on the benzene ring also form the F-H interaction with the two polarized CH groups on GLU735 and ASP734, respectively, which further strengthens the combination of **4w** and ZIKV RdRp.

2.4 Compound **4w** interacts with ZIKV NS5 protein

Cell thermal shift assay (CETSA) experiments are often used to detect the binding of intracellular drugs to target proteins. The assay was based on the principle of ligand-induced changes in protein thermal stability. The stability of the protein is evaluated by comparing the melting curves between the control group and the experimental group, thus assessing the interaction of the compound with the target protein.

Molecular docking experiments, suggested that **4w** interacts with ZIKV RdRp domain, and ZIKV RdRp domain is the C-terminal subdomain of ZIKV NS5 protein. Therefore, in order to further verify the interaction between **4w** and ZIKV NS5, ZIKV-infected cell were treated with **4w** (at 50 μ M concentration), then total protein was incubation for 60 min at room temperature, and it was divided into nine equal parts. The same volume of DMSO was added as a control, and the treated protein was heated in a temperature gradient and then detected ZIKV NS5 protein by WB assay (Figure 5A). It was found that **4w** can bind to ZIKV NS5 protein in cells, thereby improving the thermal stability of ZIKV NS5 protein and preventing its aggregation and precipitation at high temperature. The apparent aggregation temperature (Tagg) of ZIKV NS5 protein was increased from 42.3°C to 49.3°C (Figure 5B).

2.5 Compound **4w** inhibits ZIKV RdRp activity

Through molecular docking experiments and cell thermal shift analysis, we suppose that **4w** may have a direct interaction

with ZIKV RdRp. In order to verify whether the binding of **4w** and NS5 protein is directly related to ZIKV RdRp, we expressed and purified ZIKV RdRp domain, and detected its activity according to the method described in the literature (Qian et al., 2022) (Figure 6A). Through RdRp activity assay results, we found that **4w** inhibited ZIKV RdRp activity with EC_{50} = 11.38 \pm 0.51 μ M (Figure 6B). Heparin is a protein chelating agent. According to the literature (Sáez-Álvarez et al., 2019), it can significantly inhibited the activity of ZIKV RdRp. Heparin was selected as the positive control drug in this experiment, and the syto9-only group was used as the negative control, the same volume of DMSO as a positive control.

2.6 Compound **4w** inhibits ZIKV RNA synthesis

Through above experiments, we demonstrated that **4w** inhibits ZIKV RdRp activity in a dose-dependent manner. ZIKV RdRp was a important domain in the C-terminal of ZIKV NS5, and plays a crucial role in the replication and synthesis of RNA in the life cycle of ZIKV. In order to further verify that **4w** activity is related to RdRp domain inhibition, we examined the effect of **4w** on the replication cycle of ZIKV using four different drug treatments and time-sharing withdrawal experiments (Figure 7A). Through four different treatments with **4w**, we found that **4w** mainly acts on the post-entry stage of the virus, and it has a significant inhibitory effect on the viral load in cells after virus infection (Figure 7B). In the time of drug withdrawal experiment (Figure 7C), we found that drug withdrawal 4–6 h after dosing could significantly inhibit the release of progeny virus in the supernatant of ZIKV infected cells. From the results of drug treatment, we found that **4w** may mainly act on the ZIKV RNA synthesis stage (Figure 7D), which once again suggesting that **4w** binds into the ZIKV RdRp domain inhibition.

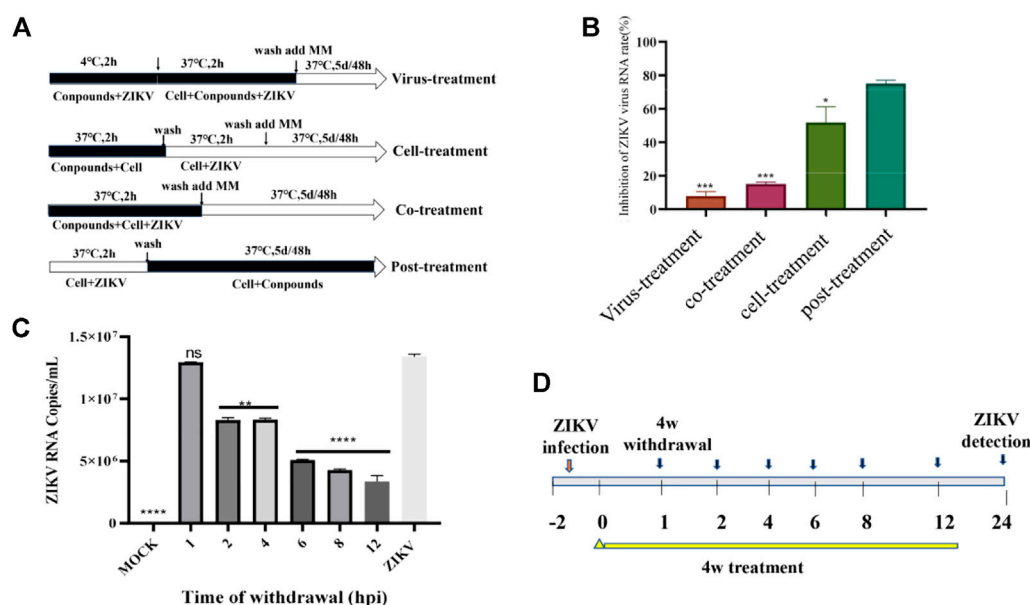


FIGURE 7

Compound **4w** inhibits the synthesis of ZIKV RNA. (A) Flow chart of four different drug treatments; (B) Determination of viral load in cell supernatants after four different drug treatments, VS. post-treatment, * $p < 0.05$; ** $p < 0.01$; *** $p < 0.001$; **** $p < 0.0001$; (C) experimental procedure of time-sharing withdrawal. (D) After drug withdrawal at different time points, the virus load in the cells was measured for 24 h after drug withdrawal.

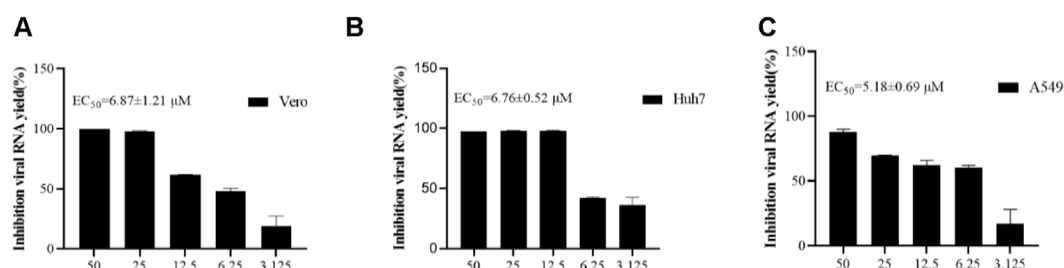


FIGURE 8

Compound **4w** inhibits virus release of ZIKV progeny in different cell lines. (A) Vero cells; (B) Huh7 cells; (C) A549 cells.

2.7 Compound 4w inhibits progeny virus release in different cell lines

In order to re-verify the inhibitory effect of **4w** on ZIKV at the molecular level, we used ZIKV to infect cell lines of different origins (A549, Vero, Huh7 cells) and then treated with **4w** in a concentration gradient. The change of viral load in the supernatant of cells after treatment was detected by qRT-PCR method. It was found that **4w** could significantly inhibit the replication of viral RNA in different cell lines infected with ZIKV (Figure 8). In Vero, A549 and Huh7 cells, **4w** inhibited the replication of ZIKV RNA with EC_{50} values 6.871 ± 1.21 , 5.18 ± 0.69 , and $6.76 \pm 0.52 \mu M$, respectively.

These results indicate that the inhibitory effect of **4w** on ZIKV is not dependent on cell species specificity.

2.8 Compound 4w inhibits the expression of ZIKV E and NS5 protein

ZIKV E protein is one of the most important structural proteins of ZIKV, which plays an important role in the correct assembly of the virus and evasion of the host's innate immunity (Jaimipuk et al., 2022). We have verified that **4w** has a significant inhibitory effect on ZIKV-infected cell lines from different sources at the molecular level, but it is unknown whether it

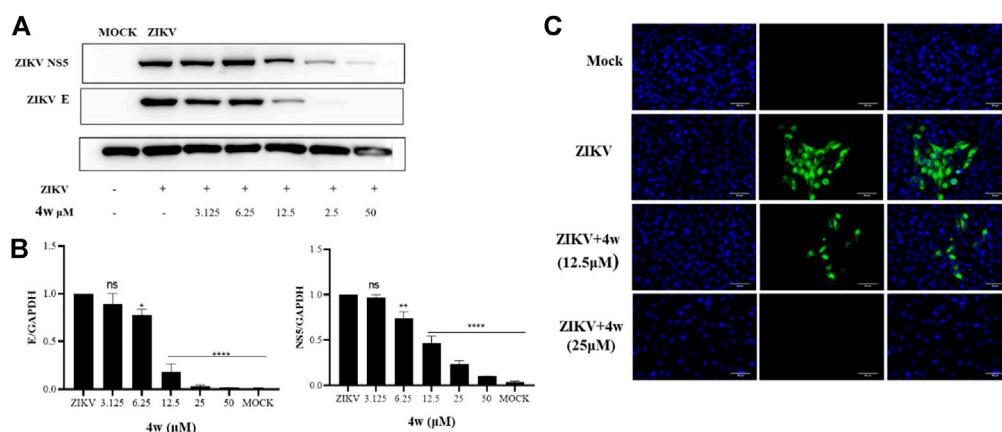


FIGURE 9

Compound **4w** inhibited the expression of ZIKV E and NS5 protein. (A) Western blot detected the inhibitory effect of **4w** on ZIKV E and NS5 protein under the concentration gradient of **4w**; (B) Grayscale analysis and statistics of the inhibition of **4w** on ZIKV E and NS5 protein under the concentration gradient of WB detection; Data is the mean (\pm SD) of three experiments, with DMSO as a positive control * $p < 0.05$; ** $p < 0.01$; *** $p < 0.001$; **** $p < 0.0001$. (C) Detected the inhibitory effect of **4w** on ZIKV E protein by immunofluorescence.

has the same antiviral effect at the protein level. Therefore, in order to explore the inhibitory effect of **4w** on ZIKV protein level, we added serially diluted **4w** to ZIKV-infected Vero cells for 48 h, collected the total protein for WB experiments, and then detected the effect of **4w** on ZIKV E and NS5 protein. At the same time, the inhibitory effect of **4w** on ZIKV E protein was verified again by immunofluorescence experiment. Through WB experiment (Figure 9A), we found that **4w** can still well inhibit the expression of ZIKV E and NS5 protein at the viral protein level, and its 12.5 μ M can significantly inhibit the expression of ZIKV E and NS5 protein (Figure 9B). Immunofluorescence results showed that **4w** 25 μ M completely inhibited the expression of ZIKV E protein (Figure 9C).

3 Materials and methods

3.1 Chemical general information

Melting points were determined on a WRS-1 digital melting point apparatus and are calibrated. ^1H NMR and ^{13}C NMR spectra were obtained on a Bruker AM 400 MHz spectrometer in the indicated solvents. Chemical shifts are expressed in δ units and TMS as internal reference. Mass spectra were taken on an Agilent LC/MSD TOF mass spectrometer. Solvents were reagent quality and, when necessary, were purified and dried by typical methods. Concentration of the reaction solutions involved the use of rotary evaporator (Heidolph) at reduced pressure. TLC was performed on silica gel GF254 for TLC (Shanghai Haohong Biopharmaceutical Technology Co., Ltd., Shanghai, China) and spots were visualized by iodine vapors or by irradiation with UV light (254 nm).

3.2 Chemistry synthesis

General procedure A: To a well stirred solution of diethyl ethylmalonate (100 mmol) in anhydrous EtOH (250 ml) was added a solution of KOH (100 mmol) in anhydrous EtOH (250 ml) at room temperature overnight. After removing the solvent, the residue was washed with a small amount of ethyl acetate and suspended in anhydrous CH_3CN (250 ml), Et_3N (120 mmol) and MgCl_2 (120 mmol) were added and the mixtures were stirred at room temperature for 1 h. Then were added the solutions of cyclohexyl acetyl imidazoline, prepared 30 min before by reaction between **1a/b** (100 mmol) and N,N-carbonyldiimidazole (CDI, 50 mmol) in CH_3CN (200 ml). The reaction mixtures were refluxed for 8–12 h. After the mixture was cooled to rt. Then the CH_3CN was removed in vacuo and the residues were dissolved in H_2O and subsequent acidification to pH 6 with 5% aq HCl. The aqueous layer was extracted with EtOAc (3×100 ml), and the combined organic layers were washed with saturated NaHCO_3 (3×200 ml) and brine (3×200 ml), dried (Na_2SO_4), filtered and concentrated to give the crude products **2a** and **2b**, respectively, which were precisely used in the following process without further purification.

General procedure B: Sodium metal (102 mmol) was dissolved in 250 ml of absolute ethanol, and thiourea (102 mmol) and β -Ketoesters **2a**, **2b** (85 mmol) were added to the clear solution at room temperature. The reaction mixture was refluxed for 8–12 h. After completion of the reaction, the solvent was removed in vacuo and the residues were dissolved in water and were precipitated addition of conc. HCl until pH = 4. The resulting precipitate was filtered off, washed with EtOH, then dried to give **3a**, **3b**, which is directly used in the next step without further purification.

General procedure C: To a solution of **5a-m** (40 mmol) in dichloroethane (150 ml) was added Et₃N (48 mmol) at 0°C, then bromoacetyl bromide (48 mmol) was added dropwise to the well-stirred mixture over a period of 45 min. The reaction solution was extracted with CH₂Cl₂ (50 ml × 3), and the combined organic layers were dried with Na₂SO₄. The residue was purified by recrystallization (CH₂Cl₂/petroleum ether) to give **4a-d**.

General procedure D: Compound **3a/b** (1.2 mmol) were dissolved in DMF (30 ml), and K₂CO₃ (1.32 mmol) was added. And then, **6a-m** (1.32 mmol) were added to the reaction solution. The reaction mixture was stirred at room temperature for 6–10 h. After the reaction was completed, the mixture was filtered under reduced pressure and H₂O (200 ml) was added, then the solution was extracted with EtOAc (50 ml × 3). The combined organic layers were dried with Na₂SO₄, filtered, and concentrated. The residue was purified by column chromatography on silica gel using EtOAc/petroleum ether as an eluent to give **4a-z**. Purity of final compounds was verified to be >95% by HPLC analysis.

3.2.1 2-[(4-cyclohexyl-5-ethyl-6-oxo-1,6-dihydropyrimidin-2-yl)thio]-N-(2-methoxyphenyl)acetamide (**4a**)

General procedure D. White solid; yield: 87%; m.p. 187–188°C; ¹H NMR (400 MHz, DMSO-*d*₆, ppm) δ 0.87–0.91 (m, 1H, cyclohexyl-H), 0.93–0.97 (t, 3H, *J* = 7.4 Hz, –CH₂CH₃), 1.17–1.26 (m, 2H, cyclohexyl-H), 1.34–1.42 (m, 2H, cyclohexyl-H), 1.45–1.60 (m, 5H, cyclohexyl-H), 2.33–2.39 (q, 2H, *J* = 7.4 Hz, –CH₂CH₃), 2.52–2.60 (m, 1H, cyclohexyl-H), 3.80 (s, 3H, –OCH₃), 4.06 (s, 2H, S-CH₂), 6.85–6.90 (m, 1H, Ph-H), 7.00–7.06 (m, 2H, Ph-H), 8.04–8.08 (m, 1H, Ph-H), 9.33 (s, 1H, NH); ESI-MS: *m/z* [M + H]⁺, 402.1846. C₂₁H₂₇N₃O₃S (401.18).

3.2.2 2-[(4-(cyclohexylmethyl)-5-ethyl-6-oxo-1,6-dihydropyrimidin-2-yl)thio]-N-(2-methoxyphenyl)acetamide (**4b**)

General procedure D. White solid; yield: 85%; m.p. 204–205°C; ¹H NMR (400 MHz, DMSO-*d*₆, ppm) δ 0.81–1.00 (m, 5H, cyclohexyl-H), 0.95–0.99 (t, 3H, *J* = 6.6 Hz, –CH₂CH₃), 1.40–1.50 (m, 5H, cyclohexyl-H), 1.59–1.68 (m, 1H, cyclohexyl-H), 2.29–2.33 (d, 2H, *J* = 6.7 Hz, cyclohexyl-CH₂), 2.34–2.39 (q, 2H, *J* = 6.4 Hz, –CH₂CH₃), 3.78 (s, 3H, –OCH₃), 4.03 (s, 2H, S-CH₂), 6.85–6.92 (m, 1H, Ph-H), 6.98–7.06 (m, 2H, Ph-H), 8.03–8.08 (m, 1H, Ph-H), 9.33 (s, 1H, NH); ESI-MS: *m/z* [M + H]⁺, 416.2002. C₂₂H₂₉N₃O₃S (415.19)

3.2.3 2-[(4-cyclohexyl-5-ethyl-6-oxo-1,6-dihydropyrimidin-2-yl)thio]-N-(3-methoxyphenyl)acetamide (**4c**)

General procedure D. White solid; yield: 88%; m.p. 207–209°C; ¹H NMR (400 MHz, DMSO-*d*₆, ppm) δ

0.86–0.90 (m, 1H, cyclohexyl-H), 0.91–0.95 (t, 3H, *J* = 7.4 Hz, –CH₂CH₃), 1.12–1.25 (m, 2H, cyclohexyl-H), 1.30–1.38 (m, 2H, cyclohexyl-H), 1.40–1.60 (m, 5H, cyclohexyl-H), 2.31–2.37 (q, 2H, *J* = 7.5 Hz, –CH₂CH₃), 2.51–2.57 (m, 1H, cyclohexyl-H), 3.70 (s, 3H, –OCH₃), 3.97 (s, 2H, S-CH₂), 6.58–6.62 (m, 1H, Ph-H), 7.10–7.14 (m, 1H, Ph-H), 7.16–7.20 (m, 1H, Ph-H), 7.31–7.32 (m, 1H, Ph-H), 10.26 (s, 1H, NH), 12.54 (s, 1H, NH); ESI-MS: *m/z* [M + H]⁺, 402.1846. C₂₁H₂₇N₃O₃S (401.18)

3.2.4 2-[(4-(cyclohexylmethyl)-5-ethyl-6-oxo-1,6-dihydropyrimidin-2-yl)thio]-N-(3-methoxyphenyl)acetamide (**4d**)

General procedure D. White solid; yield: 85%; m.p. 190–193°C; ¹H NMR (400 MHz, DMSO-*d*₆, ppm) δ 0.74–0.91 (m, 5H, cyclohexyl-H), 0.92–0.96 (t, 3H, *J* = 7.3 Hz, –CH₂CH₃), 1.35–1.45 (m, 5H, cyclohexyl-H), 1.57–1.68 (m, 1H, cyclohexyl-H), 2.23–2.27 (d, 2H, *J* = 6.7 Hz, cyclohexyl-CH₂), 2.29–2.35 (q, 2H, *J* = 7.7 Hz, –CH₂CH₃), 3.70 (s, 3H, –OCH₃), 3.97 (s, 2H, S-CH₂), 6.60–6.63 (m, 1H, Ph-H), 7.10–7.14 (m, 1H, Ph-H), 7.16–7.22 (m, 1H, Ph-H), 7.31–7.33 (m, 1H, Ph-H), 10.20 (s, 1H, NH), 12.58 (s, 1H, NH); ESI-MS: *m/z* [M + H]⁺, 416.2002. C₂₂H₂₉N₃O₃S (415.19).

3.2.5 2-[(4-cyclohexyl-5-ethyl-6-oxo-1,6-dihydropyrimidin-2-yl)thio]-N-(4-methoxyphenyl)acetamide (**4e**)

General procedure D. White solid; yield: 86%; m.p. 264–266°C; ¹H NMR (400 MHz, DMSO-*d*₆, ppm) δ 0.92–0.94 (t, 3H, *J* = 7.1 Hz, –CH₂CH₃), 0.95–1.00 (m, 1H, cyclohexyl-H), 1.12–1.27 (m, 2H, cyclohexyl-H), 1.32–1.42 (m, 2H, cyclohexyl-H), 1.43–1.63 (m, 5H, cyclohexyl-H), 2.32–2.38 (q, 2H, *J* = 7.4 Hz, –CH₂CH₃), 2.52–2.58 (m, 1H, cyclohexyl-H), 3.70 (s, 3H, –OCH₃), 3.96 (s, 2H, S-CH₂), 6.85–6.87 (m, 2H, Ph-H), 7.49–7.51 (m, 2H, Ph-H), 10.10 (s, 1H, NH); ESI-MS: *m/z* [M + H]⁺, 402.1846. C₂₁H₂₇N₃O₃S (401.18).

3.2.6 2-[(4-(cyclohexylmethyl)-5-ethyl-6-oxo-1,6-dihydropyrimidin-2-yl)thio]-N-(4-methoxyphenyl)acetamide (**4f**)

General procedure D. White solid; yield: 84%; m.p. 212–214°C; ¹H NMR (400 MHz, DMSO-*d*₆, ppm) δ 0.75–0.90 (m, 2H, cyclohexyl-H), 0.90–0.95 (m, 3H, cyclohexyl-H), 0.94–0.96 (t, 3H, *J* = 7.1 Hz, –CH₂CH₃), 1.35–1.52 (m, 5H, cyclohexyl-H), 1.61–1.72 (m, 1H, cyclohexyl-H), 2.27–2.28 (d, 2H, *J* = 7.1 Hz, cyclohexyl-CH₂), 2.31–2.35 (q, 2H, *J* = 7.4 Hz, –CH₂CH₃), 3.70 (s, 3H, –OCH₃), 3.96 (s, 2H, S-CH₂), 6.85–6.87 (m, 2H, Ph-H), 7.49–7.51 (m, 2H, Ph-H), 10.06 (s, 1H, NH); ESI-MS: *m/z* [M + H]⁺, 416.2002. C₂₂H₂₉N₃O₃S (415.19)

3.2.7 2-[(4-cyclohexyl-5-ethyl-6-oxo-1,6-dihydropyrimidin-2-yl)thio]-N-(2-fluorophenyl)acetamide (**4g**)

General procedure D. White solid; yield: 86%; m.p. 206–208°C; ¹H NMR (400 MHz, DMSO-*d*₆, ppm) δ 0.83–0.90 (m, 1H, cyclohexyl-H), 0.92–0.96 (t, 3H, *J* = 7.4 Hz, –CH₂CH₃), 1.13–1.26 (m, 2H, cyclohexyl-H), 1.34–1.42 (m, 2H, cyclohexyl-H), 1.43–1.61 (m, 5H, cyclohexyl-H), 2.32–2.38 (q, 2H, *J* = 7.3 Hz, –CH₂CH₃), 2.52–2.58 (m, 1H, cyclohexyl-H), 4.09 (s, 2H, S-CH₂), 7.06–7.16 (m, 2H, Ph-H), 7.27–7.28 (m, 1H, Ph-H), 8.02–8.08 (m, 1H, Ph-H), 10.06 (s, 1H, NH), 12.54 (s, 1H, NH); ESI-MS: *m/z* [M + H]⁺, 390.1647. C₂₀H₂₄FN₃O₂S (389.16).

3.2.8 2-[[4-(cyclohexylmethyl)-5-ethyl-6-oxo-1,6-dihydropyrimidin-2-yl]thio]-N-(2-fluorophenyl)acetamide (**4h**)

General procedure D. White solid; yield: 86%; m.p. 180–181°C; ¹H NMR (400 MHz, DMSO-*d*₆, ppm) δ 0.77–0.93 (m, 5H, cyclohexyl-H), 0.93–0.97 (t, 3H, *J* = 7.3 Hz, –CH₂CH₃), 1.39–1.49 (m, 5H, cyclohexyl-H), 1.61–1.70 (m, 1H, cyclohexyl-H), 2.27–2.31 (d, 2H, *J* = 7.3 Hz, cyclohexyl-CH₂), 2.31–2.36 (q, 2H, *J* = 7.3 Hz, –CH₂CH₃), 4.07 (s, 2H, S-CH₂), 7.08–7.16 (m, 2H, Ph-H), 7.22–7.28 (m, 1H, Ph-H), 7.98–8.03 (m, 1H, Ph-H), 9.98 (s, 1H, NH), 12.58 (s, 1H, NH); ESI-MS: *m/z* [M + H]⁺, 404.1800. C₂₁H₂₆FN₃O₂S (403.17).

3.2.9 2-[(4-cyclohexyl-5-ethyl-6-oxo-1,6-dihydropyrimidin-2-yl)thio]-N-(3-fluorophenyl)acetamide (**4i**)

General procedure D. White solid; yield: 86%; m.p. 184–187°C; ¹H NMR (400 MHz, DMSO-*d*₆, ppm) δ 0.78–0.88 (m, 1H, cyclohexyl-H), 0.90–0.94 (t, 3H, *J* = 7.1 Hz, –CH₂CH₃), 1.10–1.23 (m, 2H, cyclohexyl-H), 1.30–1.45 (m, 5H, cyclohexyl-H), 1.46–1.58 (m, 2H, cyclohexyl-H), 2.31–2.37 (q, 2H, *J* = 7.1 Hz, –CH₂CH₃), 2.50–2.55 (m, 1H, cyclohexyl-H), 3.98 (s, 2H, S-CH₂), 6.81–6.89 (m, 1H, Ph-H), 7.28–7.34 (m, 2H, Ph-H), 7.56–7.63 (m, 1H, Ph-H), 10.50 (s, 1H, NH), 12.54 (s, 1H, NH); ESI-MS: *m/z* [M + H]⁺, 390.1645. C₂₀H₂₄FN₃O₂S (389.16).

3.2.10 2-[[4-(cyclohexylmethyl)-5-ethyl-6-oxo-1,6-dihydropyrimidin-2-yl]thio]-N-(3-fluorophenyl)acetamide (**4j**)

General procedure D. White solid; yield: 86%; m.p. 216–218°C; ¹H NMR (400 MHz, DMSO-*d*₆, ppm) δ 0.73–0.91 (m, 5H, cyclohexyl-H), 0.92–0.96 (t, 3H, *J* = 7.3 Hz, –CH₂CH₃), 1.34–1.44 (m, 5H, cyclohexyl-H), 1.55–1.64 (m, 1H, cyclohexyl-H), 2.22–2.26 (d, 2H, *J* = 6.9 Hz, cyclohexyl-CH₂), 2.28–2.35 (q, 2H, *J* = 7.6 Hz, –CH₂CH₃), 3.98 (s, 2H, S-CH₂), 6.83–6.89 (m, 1H, Ph-H), 7.28–7.36 (m, 2H, Ph-H), 7.58–7.63 (m, 1H, Ph-H), 10.44 (s, 1H, NH), 12.59 (s, 1H, NH); ESI-MS: *m/z* [M + H]⁺, 404.1802. C₂₁H₂₆FN₃O₂S (403.17).

3.2.11 2-[(4-cyclohexyl-5-ethyl-6-oxo-1,6-dihydropyrimidin-2-yl)thio]-N-(4-fluorophenyl)acetamide (**4k**)

General procedure D. White solid; yield: 85%; m.p. 273–274°C; ¹H NMR (400 MHz, DMSO-*d*₆, ppm) δ 0.81–0.91 (m, 1H, cyclohexyl-H), 0.91–0.95 (t, 3H, *J* = 7.4 Hz, –CH₂CH₃), 1.12–1.23 (m, 2H, cyclohexyl-H), 1.31–1.38 (m, 2H, cyclohexyl-H), 1.41–1.60 (m, 5H, cyclohexyl-H), 2.32–2.37 (q, 2H, *J* = 7.3 Hz, –CH₂CH₃), 2.51–2.56 (m, 1H, cyclohexyl-H), 3.97 (s, 2H, S-CH₂), 7.11–7.15 (m, 2H, Ph-H), 7.61–7.64 (m, 2H, Ph-H), 10.35 (s, 1H, NH), 12.52 (s, 1H, NH); ESI-MS: *m/z* [M + H]⁺, 390.1646. C₂₀H₂₄FN₃O₂S (389.16).

3.2.12 2-[[4-(cyclohexylmethyl)-5-ethyl-6-oxo-1,6-dihydropyrimidin-2-yl]thio]-N-(4-fluorophenyl)acetamide (**4l**)

General procedure D. White solid; yield: 85%; m.p. 261–262°C; ¹H NMR (400 MHz, Pyr-*d*₅, ppm) δ 0.87–0.98 (m, 2H, cyclohexyl-H), 1.00–1.10 (m, 3H, cyclohexyl-H), 1.20–1.24 (t, 3H, *J* = 7.3 Hz, –CH₂CH₃), 1.47–1.67 (m, 5H, cyclohexyl-H), 1.85–1.96 (m, 1H, cyclohexyl-H), 2.45–2.48 (d, 2H, *J* = 7.3 Hz, cyclohexyl-CH₂), 2.63–2.68 (q, 2H, *J* = 7.4 Hz, –CH₂CH₃), 4.39 (s, 2H, S-CH₂), 7.14–7.18 (m, 2H, Ph-H), 7.95–7.98 (m, 2H, Ph-H), 11.12 (s, 1H, NH); ESI-MS: *m/z* [M + H]⁺, 404.1803. C₂₁H₂₆FN₃O₂S (403.17).

3.2.13 2-[(4-cyclohexyl-5-ethyl-6-oxo-1,6-dihydropyrimidin-2-yl)thio]-N-(4-(trifluoromethyl)phenyl)acetamide (**4m**)

General procedure D. White solid; yield: 88%; m.p. 257–259°C; ¹H NMR (400 MHz, DMSO-*d*₆, ppm) δ 0.72–0.83 (m, 1H, cyclohexyl-H), 0.91–0.94 (t, 3H, *J* = 7.3 Hz, –CH₂CH₃), 1.12–1.18 (m, 2H, cyclohexyl-H), 1.29–1.42 (m, 5H, cyclohexyl-H), 1.44–1.55 (m, 2H, cyclohexyl-H), 2.31–2.37 (q, 2H, *J* = 7.2 Hz, –CH₂CH₃), 2.51–2.55 (m, 1H, cyclohexyl-H), 4.03 (s, 2H, S-CH₂), 7.65–7.68 (d, 2H, *J* = 8.3 Hz, Ph-H), 7.81–7.83 (d, 2H, *J* = 8.3 Hz, Ph-H), 10.66 (s, 1H, NH); ESI-MS: *m/z* [M + H]⁺, 440.1614. C₂₁H₂₄F₃N₃O₂S (439.15).

3.2.14 2-[[4-(cyclohexylmethyl)-5-ethyl-6-oxo-1,6-dihydropyrimidin-2-yl]thio]-N-[4-(trifluoromethyl)phenyl]acetamide (**4n**)

General procedure D. White solid; yield: 89%; m.p. 206–207°C; ¹H NMR (400 MHz, DMSO-*d*₆, ppm) δ 0.67–0.88 (m, 5H, cyclohexyl-H), 0.92–0.95 (t, 3H, *J* = 7.1 Hz, –CH₂CH₃), 1.27–1.40 (m, 5H, cyclohexyl-H), 1.48–1.60 (m, 1H, cyclohexyl-H), 2.20–2.25 (d, 2H, *J* = 6.5 Hz, cyclohexyl-CH₂), 2.28–2.34 (q, 2H, *J* = 6.9 Hz, –CH₂CH₃), 4.01 (s, 2H, S-CH₂), 7.65–7.68 (d, 2H, *J* = 8.2 Hz, Ph-H), 7.82–7.84 (d, 2H, *J* = 8.4 Hz, Ph-H), 10.61 (s, 1H, NH), 12.59 (s, 1H, NH); ESI-MS: *m/z* [M + H]⁺, 454.1767. C₂₂H₂₆F₃N₃O₂S (453.17).

3.2.15 2-[(4-cyclohexyl-5-ethyl-6-oxo-1,6-dihydropyrimidin-2-yl)thio]-N-[4-(trifluoromethoxy)phenyl] acetamide (**4o**)

General procedure D. White solid; yield: 86%; m.p. 252–254°C; ¹H NMR (400 MHz, DMSO-*d*₆, ppm) δ 0.70–0.82 (m, 1H, cyclohexyl-H), 0.91–0.95 (t, 3H, *J* = 7.4 Hz, –CH₂CH₃), 1.10–1.25 (m, 2H, cyclohexyl-H), 1.30–1.44 (m, 5H, cyclohexyl-H), 1.45–1.55 (m, 2H, cyclohexyl-H), 2.30–2.38 (q, 2H, *J* = 7.2 Hz, –CH₂CH₃), 2.50–2.58 (m, 1H, cyclohexyl-H), 3.99 (s, 2H, S-CH₂), 7.29–7.34 (d, 2H, *J* = 8.8 Hz, Ph-H), 7.71–7.75 (d, 2H, *J* = 8.9 Hz, Ph-H), 10.52 (s, 1H, NH), 12.50 (s, 1H, NH); ESI-MS: *m/z* [M + H]⁺, 456.1563. C₂₁H₂₄F₃N₃O₃S (455.15).

3.2.16 2-[(4-(cyclohexylmethyl)-5-ethyl-6-oxo-1,6-dihydropyrimidin-2-yl)thio]-N-[4-(trifluoromethoxy)phenyl] acetamide (**4p**)

General procedure D. White solid; yield: 86%; m.p. 193–195°C; ¹H NMR (400 MHz, DMSO-*d*₆, ppm) δ 0.70–0.87 (m, 5H, cyclohexyl-H), 0.92–0.96 (t, 3H, *J* = 7.1 Hz, –CH₂CH₃), 1.28–1.42 (m, 5H, cyclohexyl-H), 1.51–1.60 (m, 1H, cyclohexyl-H), 2.21–2.27 (d, 2H, *J* = 6.6 Hz, cyclohexyl-CH₂), 2.28–2.35 (q, 2H, *J* = 7.4 Hz, –CH₂CH₃), 3.98 (s, 2H, S-CH₂), 7.28–7.34 (d, 2H, *J* = 8.4 Hz, Ph-H), 7.70–7.75 (d, 2H, *J* = 8.7 Hz, Ph-H), 10.44 (s, 1H, NH), 12.58 (s, 1H, NH); ESI-MS: *m/z* [M + H]⁺, 470.1720. C₂₂H₂₆F₃N₃O₃S (469.16).

3.2.17 2-[(4-cyclohexyl-5-ethyl-6-oxo-1,6-dihydropyrimidin-2-yl)thio]-N-[3-(trifluoromethoxy)phenyl] acetamide (**4q**)

General procedure D. White solid; yield: 85%; m.p. 219–221°C; ¹H NMR (400 MHz, DMSO-*d*₆, ppm) δ 0.70–0.82 (m, 1H, cyclohexyl-H), 0.90–0.94 (t, 3H, *J* = 7.3 Hz, –CH₂CH₃), 1.07–1.21 (m, 2H, cyclohexyl-H), 1.28–1.42 (m, 5H, cyclohexyl-H), 1.43–1.55 (m, 2H, cyclohexyl-H), 2.31–2.36 (q, 2H, *J* = 7.3 Hz, –CH₂CH₃), 2.51–2.55 (m, 1H, cyclohexyl-H), 3.99 (s, 2H, S-CH₂), 6.98–7.03 (m, 1H, Ph-H), 7.39–7.45 (m, 1H, Ph-H), 7.50–7.54 (m, 1H, Ph-H), 7.78–7.79 (m, 1H, Ph-H), 10.60 (s, 1H, NH), 12.56 (s, 1H, NH); ESI-MS: *m/z* [M + H]⁺, 456.1563. C₂₁H₂₄F₃N₃O₃S (455.15).

3.2.18 2-[(4-(cyclohexylmethyl)-5-ethyl-6-oxo-1,6-dihydropyrimidin-2-yl)thio]-N-[3-(trifluoromethoxy)phenyl] acetamide (**4r**)

General procedure D. White solid; yield: 86%; m.p. 180–182°C; ¹H NMR (400 MHz, DMSO-*d*₆, ppm) δ 0.70–0.88 (m, 5H, cyclohexyl-H), 0.92–0.96 (t, 3H, *J* = 7.0 Hz, –CH₂CH₃), 1.28–1.41 (m, 5H, cyclohexyl-H), 1.52–1.63 (m, 1H, cyclohexyl-H), 2.21–2.27 (d, 2H, *J* = 6.5 Hz, cyclohexyl-CH₂), 2.27–2.34 (q, 2H, *J* = 7.3 Hz, –CH₂CH₃), 3.99 (s, 2H, S-CH₂), 6.99–7.04 (m, 1H, Ph-H), 7.39–7.45 (m, 1H, Ph-H), 7.49–7.54 (m, 1H, Ph-H), 7.79–7.80 (m, 1H, Ph-H), 10.54 (s,

1H, NH), 12.60 (s, 1H, NH); ESI-MS: *m/z* [M + H]⁺, 470.1720. C₂₂H₂₆F₃N₃O₃S (469.16).

3.2.19 2-[(4-cyclohexyl-5-ethyl-6-oxo-1,6-dihydropyrimidin-2-yl)thio]-N-(2,4-difluorophenyl) acetamide (**4s**)

General procedure D. White solid; yield: 84%; m.p. 227–229°C; ¹H NMR (400 MHz, DMSO-*d*₆, ppm) δ 0.82–0.91 (m, 1H, cyclohexyl-H), 0.92–0.95 (t, 3H, *J* = 7.1 Hz, –CH₂CH₃), 1.15–1.29 (m, 2H, cyclohexyl-H), 1.36–1.43 (m, 2H, cyclohexyl-H), 1.45–1.60 (m, 5H, cyclohexyl-H), 2.31–2.39 (q, 2H, *J* = 7.6 Hz, –CH₂CH₃), 2.53–2.61 (m, 1H, cyclohexyl-H), 4.08 (s, 2H, S-CH₂), 7.01–7.09 (m, 1H, Ph-H), 7.28–7.38 (m, 1H, Ph-H), 7.96–8.04 (m, 1H, Ph-H), 10.10 (s, 1H, NH), 12.57 (s, 1H, NH); ESI-MS: *m/z* [M + H]⁺, 408.1552. C₂₀H₂₃F₂N₃O₂S (407.15).

3.2.20 2-[(4-(cyclohexylmethyl)-5-ethyl-6-oxo-1,6-dihydropyrimidin-2-yl)thio]-N-(2,4-difluorophenyl) acetamide (**4t**)

General procedure D. White solid; yield: 85%; m.p. 192–194°C; ¹H NMR (400 MHz, DMSO-*d*₆, ppm) δ 0.78–0.89 (m, 2H, cyclohexyl-H), 0.90–1.02 (m, 3H, cyclohexyl-H), 0.93–0.97 (t, 3H, *J* = 7.0 Hz, –CH₂CH₃), 1.41–1.52 (m, 5H, cyclohexyl-H), 1.60–1.70 (m, 1H, cyclohexyl-H), 2.27–2.30 (d, 2H, *J* = 6.9 Hz, cyclohexyl-CH₂), 2.31–2.36 (q, 2H, *J* = 7.3 Hz, –CH₂CH₃), 4.06 (s, 2H, S-CH₂), 7.01–7.09 (m, 1H, Ph-H), 7.28–7.37 (m, 1H, Ph-H), 7.91–8.00 (m, 1H, Ph-H), 10.01 (s, 1H, NH), 12.57 (s, 1H, NH); ESI-MS: *m/z* [M + H]⁺, 422.1703. C₂₁H₂₅F₂N₃O₂S (421.16).

3.2.21 2-[(4-cyclohexyl-5-ethyl-6-oxo-1,6-dihydropyrimidin-2-yl)thio]-N-(2,5-difluorophenyl) acetamide (**4u**)

General procedure D. White solid; yield: 83%; m.p. 190–192°C; ¹H NMR (400 MHz, DMSO-*d*₆, ppm) δ 0.85–0.91 (m, 1H, cyclohexyl-H), 0.92–0.96 (t, 3H, *J* = 7.4 Hz, –CH₂CH₃), 1.16–1.28 (m, 2H, cyclohexyl-H), 1.36–1.43 (m, 2H, cyclohexyl-H), 1.46–1.61 (m, 5H, cyclohexyl-H), 2.32–2.39 (q, 2H, *J* = 7.3 Hz, –CH₂CH₃), 2.52–2.61 (m, 1H, cyclohexyl-H), 4.08 (s, 2H, S-CH₂), 7.02–7.08 (m, 1H, Ph-H), 7.29–7.36 (m, 1H, Ph-H), 7.96–8.03 (m, 1H, Ph-H), 10.10 (s, 1H, NH), 12.51 (s, 1H, NH); ESI-MS: *m/z* [M + H]⁺, 408.1552. C₂₀H₂₃F₂N₃O₂S (407.15).

3.2.22 2-[(4-(cyclohexylmethyl)-5-ethyl-6-oxo-1,6-dihydropyrimidin-2-yl)thio]-N-(2,5-difluorophenyl) acetamide (**4v**)

General procedure D. White solid; yield: 82%; m.p. 186–188°C; ¹H NMR (400 MHz, DMSO-*d*₆, ppm) δ 0.79–1.00 (m, 5H, cyclohexyl-H), 0.93–0.97 (t, 3H, *J* = 7.3 Hz, –CH₂CH₃), 1.40–1.51 (m, 5H, cyclohexyl-H),

1.60–1.71 (m, 1H, cyclohexyl-H), 2.26–2.30 (d, 2H, $J = 6.8$ Hz, cyclohexyl-CH₂), 2.31–2.36 (q, 2H, $J = 7.3$ Hz, –CH₂CH₃), 4.05 (s, 2H, S-CH₂), 7.03–7.08 (m, 1H, Ph-H), 7.31–7.36 (m, 1H, Ph-H), 7.91–7.99 (m, 1H, Ph-H), 10.01 (s, 1H, NH), 12.59 (s, 1H, NH); ESI-MS: m/z [M + H]⁺, 422.1708. C₂₁H₂₅F₂N₃O₂S (421.16).

3.2.23 2-([4-cyclohexyl-5-ethyl-6-oxo-1,6-dihydropyrimidin-2-yl]thio)-N-(3,5-difluorophenyl)acetamide (**4w**)

General procedure D. White solid; yield:86%; m.p. 238–240°C; ¹H NMR (400 MHz, Pyr-*d*₅, ppm) δ 1.00–1.10 (m, 1H, cyclohexyl-H), 1.15–1.19 (t, 3H, $J = 7.4$ Hz, –CH₂CH₃), 1.22–1.34 (m, 2H, cyclohexyl-H), 1.54–1.68 (m, 5H, cyclohexyl-H), 1.75–1.87 (m, 2H, cyclohexyl-H), 2.64–2.69 (q, 2H, $J = 7.4$ Hz, –CH₂CH₃), 2.70–2.78 (m, 1H, cyclohexyl-H), 4.38 (s, 2H, S-CH₂), 6.79–6.86 (m, 1H, Ph-H), 7.68–7.75 (m, 2H, Ph-H), 11.64 (s, 1H, NH); ESI-MS: m/z [M + H]⁺, 408.1549. C₂₀H₂₃F₂N₃O₂S (407.15).

3.2.24 2-([4-(cyclohexylmethyl)-5-ethyl-6-oxo-1,6-dihydropyrimidin-2-yl]thio)-N-(3,5-difluorophenyl)acetamide (**4x**)

General procedure D. White solid; yield:86%; m.p. 214–216°C; ¹H NMR (400 MHz, DMSO-*d*₆, ppm) δ 0.71–0.89 (m, 5H, cyclohexyl-H), 0.92–0.96 (t, 3H, $J = 7.3$ Hz, –CH₂CH₃), 1.34–1.45 (m, 5H, cyclohexyl-H), 1.51–1.60 (m, 1H, cyclohexyl-H), 2.21–2.26 (d, 2H, $J = 7.2$ Hz, cyclohexyl-CH₂), 2.28–2.34 (q, 2H, $J = 7.5$ Hz, –CH₂CH₃), 3.98 (s, 2H, S-CH₂), 6.87–6.93 (m, 1H, Ph-H), 7.31–7.34 (m, 2H, Ph-H), 10.62 (s, 1H, NH); ESI-MS: m/z [M + H]⁺, 422.1708. C₂₁H₂₅F₂N₃O₂S (421.16).

3.2.25 2-([4-cyclohexyl-5-ethyl-6-oxo-1,6-dihydropyrimidin-2-yl]thio)-N-(5-fluoro-2-methoxyphenyl)acetamide (**4y**)

General procedure D. White solid; yield:87%; m.p. 166–167°C; ¹H NMR (400 MHz, DMSO-*d*₆, ppm) δ 0.79–0.89 (m, 1H, cyclohexyl-H), 0.92–0.95 (t, 3H, $J = 7.3$ Hz, –CH₂CH₃), 1.13–1.25 (m, 2H, cyclohexyl-H), 1.32–1.40 (m, 2H, cyclohexyl-H), 1.42–1.55 (m, 5H, cyclohexyl-H), 2.32–2.38 (q, 2H, $J = 7.6$ Hz, –CH₂CH₃), 2.52–2.58 (m, 1H, cyclohexyl-H), 4.08 (s, 2H, S-CH₂), 6.82–6.87 (m, 1H, Ph-H), 6.99–7.04 (m, 1H, Ph-H), 8.00–8.04 (m, 1H, Ph-H), 9.55 (s, 1H, NH), 12.57 (s, 1H, NH); ESI-MS: m/z [M + H]⁺, 420.1752. C₂₁H₂₆FN₃O₃S (419.17).

3.2.26 2-([4-(cyclohexylmethyl)-5-ethyl-6-oxo-1,6-dihydropyrimidin-2-yl]thio)-N-(5-fluoro-2-methoxyphenyl)acetamide (**4z**)

General procedure D. White solid; yield:88%; m.p. 182–183°C; ¹H NMR (400 MHz, DMSO-*d*₆, ppm) δ 0.77–0.93 (m, 5H, cyclohexyl-H), 0.95–0.99 (t, 3H, $J =$

7.3 Hz, –CH₂CH₃), 1.38–1.49 (m, 5H, cyclohexyl-H), 1.56–1.66 (m, 1H, cyclohexyl-H), 2.28–2.31 (d, 2H, $J = 6.7$ Hz, cyclohexyl-CH₂), 2.32–2.38 (q, 2H, $J = 7.3$ Hz, –CH₂CH₃), 3.80 (s, 3H, –OCH₃), 4.06 (s, 2H, S-CH₂), 6.83–6.90 (m, 1H, Ph-H), 7.00–7.06 (m, 1H, Ph-H), 7.99–8.04 (m, 1H, Ph-H), 9.51 (s, 1H, NH), 12.63 (s, 1H, NH); ESI-MS: m/z [M + H]⁺, 434.1908. C₂₂H₂₈FN₃O₃S (433.18).

4 Biology assay

4.1 Biological experimental materials

African green monkey kidney (Vero) cells, human hepatoma (Huh-7) cells and human alveolar basal epithelial (A549) cells were cultured in Dulbecco's modified Eagle's medium (DMEM; Thermo Fisher, United States) supplemented with 10% fetal bovine serum (FBS; Thermo Fisher, United States) at 37°C in 5% CO₂ incubator. *Aedes albopictus* (C6/36) cells was used to amplify ZIKV and cells were cultured in Roswell Park Memorial Institute medium (RPMI1640; Thermo Fisher, United States) contain 10% FBS. The ZIKV SZ-WIV01 strain (GenBank: KU963796) was kindly donated by Prof. Bo Zhang (Wuhan Institute of Virology, Chinese Academy of Sciences, Wuhan, China).

ZIKV NS5 RdRp Plasmid was a kindly gift from Prof. Shi Yi (Institute of Microbiology, Chinese Academy of Sciences, Beijing, China). Electro-competent *Escherichia coli* BL21 (DE3)-April cells were obtained from Tsingke Biotechnology. The following reagents were purchased from Sigma: NaCl, MgCl₂, ZnCl₂, glycerol, imidazole, isopropyl- β -D-1-thiogalactopyranoside (IPTG), 1,4-dithiothreitol (DTT), LB medium (powder), ampicillin (used at 100 μ g/ml) and MnCl₂, ammonium acetate, Tris base. SYTOTM nine green fluorescent dye was obtained from Thermo Fisher and His Pur TM Ni-NTA resin was purchased from GE. Tween 20, heparin, EDTA and oligonucleotides were also purchased from Sigma. ssRNA polyuridylic acid (poly-U) was obtained from Shanghai Yuanye Bio-Technology, ATP were purchased from Armresco. EDTA and oligonucleotides were also purchased from Sigma-Aldrich.

4.2 Plaque assay

Vero cells were inoculated in a 12-well plate at 3×10^5 cells/ml and cultured overnight, the medium was discarded and cells were washed with PBS, then the ZIKV (MOI = 0.5) was added to infect at 37°C for 2 h. The cells were washed with PBS, and then a mixture of DMEM supplemented with 4% FBS and 2% low-melting agarose (Amresco, United States) was overlaid on the cells. Next, the cells were fixed with 4% paraformaldehyde for 15 min at 5d post-infection (hpi), washed twice with PBS and

stained with 0.8% crystal violet for 10 min. Finally, an enzyme-linked fluorescence spot spectrometer (CTL, United States) was used for image acquisition. The compounds exhibiting more than 50% plaque inhibition at $50 \mu\text{mol L}^{-1}$ concentration were considered to have anti-ZIKV activity and will be submitted for further anti-ZIKV testing.

4.3 Cytotoxicity assay

MTT assay was used to detect the toxicity of the compound. Cells were seeded in 96-well plates and cultured overnight. Compounds with different concentrations were added and incubated for 96 h. Then, 20 μl of 5 mg/ml MTT (Sigma-Aldrich, United States) solution was added to each well and kept at 37°C for 4 h. Subsequently, 100 μl of 12% SDS-50% DMF (Sigma-Aldrich, United States) solution was added and incubated overnight at 37°C . After the crystalline formamidinium was completely dissolved, the optical density (OD) value was measured using a microplate reader (BioTek, United States) with a wavelength of 570 nm and a reference wavelength of 630 nm.

4.4 Cell thermal shift assay

Vero cells were inoculated in a 10 cm cell culture dish and cultured overnight, and after infection with ZIKV ($\text{MOI} \approx 2$), maintenance medium was added to continue culturing for 3 days. Detergent-free protein lysis buffer (25 mM HEPES, 20 mM MgCl_2 , 2 mM DTT) was added, and cells were lysed by sonication. The cell supernatant was collected by centrifugation at 20,000 g for 20 min at 4°C , and the supernatant was divided into two parts, one was added with 50 μM **4w**, and the other was added with the same volume of DMSO as a control. After mixing, the reaction was carried out at room temperature for 60 min. Divide the reacted samples into nine equal aliquots into PCR tubes, 50 μl per tube. The protein was heated in a temperature gradient for 3 min on the PCR machine, and immediately cooled on ice for 3 min. Then centrifuged at $20,000 \times g$ at 4°C for 20 min. The supernatants were collected to prepare the samples, and the binding of **4w** and ZIKV NS5 was analyzed by Western blotting (Chen et al., 2020; Chen et al., 2021).

4.5 Four different methods of drug treatment

As mentioned above (Duan et al., 2019; Zou et al., 2020), according to the different life cycles of the ZIKV, four different drug treatment methods are set: virus treatment, co-treatment, pre-treatment, post-treatment. For virus treatment, the ZIKV and **4w** were pre-treated in a 4°C refrigerator for 1 h, then the

treated virus was added to the cells for 2 h of infection, and the virus was discarded, washed twice with PBS, and added to maintenance medium (containing 2% FBS DMEM high sugar medium), continue to culture at 37°C , 5% CO_2 incubator for 3 days, collect the cell supernatant for RT-PCR and plaque experiments. For co-treatment: add **4w** and ZIKV to the cells at the same time, incubate at 37°C , 5% CO_2 for 2 h, then remove the virus and compounds, add maintenance medium for 3 days. Pre-treatment: Compound **4w** and cells were treated at 4°C for 1 h, then **4w** was removed, ZIKV was added for 2 h, remove virus and the maintenance medium was added to continue culturing for 3 days. Post-treatment: The virus was added to the cells to infect for 2 h, remove the virus and **4w** was added to continue culturing for 3 days.

4.6 Time of drug withdrawal

The virus was added to the cells and adsorbed for 2 h at 4°C , then the unabsorbed virus was washed away with pre-cooled PBS, and 50 μM **4w** was added at the same time. Withdraw the drug at 1, 2, 4, 6, 8, and 12 h after dosing. The cell supernatant was collected for viral load detection after the maintenance medium continued to culture for 24 h.

4.7 *In vitro* ZIKV RdRp activity assay

The ZIKV RdRp was expressed and purified, and the protein expression and purification method was as described before (Xu et al., 2017; Sáez-Álvarez et al., 2019). **4w** was diluted with protein dialysis buffer to 1,500 nM and stored for later use. *In vitro* RdRp polymerase activity assay was described previously (Qian et al., 2022), 1,500 ng of purified RdRp protein, gradient diluted **4w** and positive control drug 5 μM , 2 mg/ml Poly-U, 20mM ATP, 1M Tris-HCl, 100 mg/ml BSA, 100mM MnCl_2 was added to a 96-well PCR plate. After mixing, the reaction was performed at 30°C in the dark for 60 min. The reaction was terminated with 25 mM EDTA, and then 10 μM Syto9 was added to react at room temperature for 5 min. RdRp protein activity was detected on a real-time fluorescence quantitative PCR instrument.

4.8 Quantitative real-time polymerase chain reaction

Cells were infected with ZIKV SZ-WIV01 and then treated with **4w**. The viral load in the supernatant was detected by Quantitative real-time polymerase chain reaction (qRT-PCR) at in different time periods after infection. Then the RNA from culture supernatant was extracted using the EasyPure[®] Viral DNA/RNA Kit (TransGen Biotech, China) following the manufacturer's

instructions. Intracellular RNA extraction was according to trizol method. A one-step qRT-PCR kit RNA-direct™ Realtime PCR Master Mix (TOYOBO, Japan) and TaqMan probe were used to quantify the viral RNA produced. The primers (NS5 ZIKV 1086F: 5'-CCGCTGCCCAACACAAG-3' and NS5 ZIKV 1086R: 3'-TACAGACGTTTCTTGCAATCAC C-5') and probe (5'-FAM-AGCCTACCTTGACAAGCAGTCAGACACTCAA-TAMRA-3') were used for amplification of the ZIKV NS5 region. A standard curve of the serial dilutions was used to quantify the viral RNA yield.

4.9 Western blot analysis

Vero cells were infected with ZIKV (MOI = 1) at 37°C for 2 h. Next, the different amounts of **4w** were added to continue culturing for 48 h to extract the total protein in the cells. The total protein was separated in sodium dodecyl sulfate polyacrylamide gel electrophoresis (SDS-PAGE). Subsequently, the protein was transferred to a polyvinylidene fluoride (PVDF) membrane and incubated with ZIKV E (1:2,000) and NS5 antibody (1:2,000) overnight at 4°C (Sino Biological, China) then add the corresponding secondary antibody and incubate at room temperature for 2 h. A specific signal was presented with a chemiluminescent substrate. The antibody signal was recorded and quantified using the Tanon-5200 Multi Imaging System.

4.10 Immunofluorescence assay

Vero cells were seeded at 2×10^5 cells/ml in a 24-well plate with cell slides, and 500 μ l/well was cultured overnight in a 37°C, 5% CO₂ incubator. ZIKV (MOI = 1) was added to infect at 37°C for 2 h, and then discarded the virus. The cells were washed twice with PBS and then added to 500 μ l of **4w** diluted in concentration gradients. At the same time, virus-only as a positive control and a medium-only as negative control were set. After culturing at 37°C for 72 h, the cell culture supernatant was discarded, and 4% paraformaldehyde was added to fix the cells for 15 min at room temperature. Cells were washed twice with PBS, PBS containing 0.1% TritonX-100 was added to permeabilize cells at 4°C for 5 min, then the cells were washed with PBS for 5 min, and 5% BSA was added to block for 30 min at room temperature. The cells were stained overnight at 4°C using ZIKV E antibody (Sino Biological, China). Then, the Alexa Fluor®CY5 was added for 1 h in the dark. DAPI staining was used to delineate the nucleus of cells. Microscopic examinations were performed on a Leica DMI4000B Microsystem (Wetzlar, Germany), and an image was recorded using the system.

4.11 Statistical analysis

The 50% effective concentration (EC₅₀) and 50% cytotoxic concentration (CC₅₀) of the compound were calculated according to the Reed and Muench method, inhibition rate of ZIKV RNA yield- [(1-drug treatment/positive control) \times 100]. The data and graphs were processed using GraphPad Prism8 software, expressed as mean \pm standard deviation (Mean \pm SD), comparison between groups using ANOVA, $p < 0.05$ was considered statistically significant.

4.12 Molecular docking

Molecular docking method was used to detect the interaction between **4w** and ZIKV RdRp protein. Download the ZIKV NS5 RdRp protein from the PDB database (PDB ID: 5U0C) (Zhao et al., 2017), and save the protein structure file in pdb format for later use. The **4w** structure was drawn with ChemDraw, converted to 3D format with Chem3D, and saved as mol2 format for future use. Autodock vina1.2.0 was used for molecular docking of compound and protein. The protein and ligand were prepared using the utilities implemented by AutoDockTools1.5.4. The protein was added to polar hydrogen atoms. Gasteiger charges were assigned to both protein and ligand. The region of interest used by Autodock Vina was defined by considering the Zinc ion as the center of a grid box of 10 Å in the x , y , and z directions. The exhaustiveness parameter was set to 10 and the Energy_range to 4, whereas for all other parameters, Autodock Vina defaults were used. Only top-score binding pose was used in subsequent analyses. Subsequent visualization was performed with Pymol.

5 Conclusion

The ZIKV RdRp domain was in the C-terminal of ZIKV NS5, which has become an attractive target in anti-ZIKV virus research in recent years due to its conserved sequence and no human homologue. The development of antiviral drugs targeting ZIKV RdRp provides a new idea for the development of effective anti-ZIKV drugs. In this study, 26 acetylarlyamine-S-DABOs derivatives were designed, synthesized and evaluated against ZIKV replication and infection. It is discovered that eight compounds exhibit potent anti-ZIKV activity. Preliminary SAR analysis showed that the anti-ZIKV activity of these compounds was related to the type, and substitution position of substituent R on C-2 terminal benzene ring. Moreover, the length (n) of the connecting carbon chain between the C-6 site of the pyrimidine ring and cyclohexyl also affects the activity of the compounds, and there may be a synergistic relationship between n and substituent R. Furthermore, compound **4w** with the best anti-ZIKV activity was subjected to further analysis to detect the

antiviral effects and elucidate the target and the mode of action. The results discovered that **4w** targeting ZIKV RdRp, and verified its potent anti-ZIKV activity at the molecular and protein levels. In the process of protein target verification, the accuracy of using ZIKV RdRp as the main drug target was confirmed from many aspects. In order to verify that this antiviral effect has nothing to do with the specificity of cell species, we used cell lines from different sources such as A549, Huh7, Vero to verify its antiviral activity and cytotoxicity, and finally proved that **4w** is a new and has a good antiviral effect compound targeting the ZIKV NS5 RdRp. Although it has not been studied whether it has the same antiviral effect *in vivo*, this study also confirmed that **4w** is a valuable lead for anti-ZIKV drug discovery targeting ZIKV RdRp. On the basis of the current promising structural core element of the active acetylarylamine-S-DABOs derivatives, we will further optimize their structures through rational drug design to discover highly potent ZIKV inhibitors.

Data availability statement

The datasets presented in this study can be found in online repositories. The names of the repository/repositories and accession number(s) can be found in the article/[Supplementary Material](#).

Author contributions

Y-TZ, Y-PH, and H-BZ conceived and designed the experiments; G-FZ, C-QX, J-XX, J-BW, Y-ZY, C-BZ, R-HL, and R-HY performed the experiments; G-FZ, L-MY, Y-PW, and WC analyzed the data; and G-FZ, C-QX, Y-PH, and Y-TZ wrote the article.

References

- Ackermann, M., and Padmanabhan, R. (2001). De novo synthesis of RNA by the dengue virus RNA-dependent RNA polymerase exhibits temperature dependence at the initiation but not elongation phase. *J. Biol. Chem.* 276 (43), 39926–39937. doi:10.1074/jbc.M104248200
- Akiyama, B. M., Graham, M. E., Donoghue, Z. O., Beckham, J. D., and Kieft, J. (2021). Three-dimensional structure of a flavivirus dumbbell RNA reveals molecular details of an RNA regulator of replication. *Nucleic Acids Res.* 49 (12), 7122–7138. doi:10.1093/nar/gkab462
- Barrows, N. J., Campos, R. K., Liao, K. C., Kambham, R., Soto-Acosta, R., Yeh, S. C., et al. (2018). Biochemistry and molecular biology of Flaviviruses. *Chem. Rev.* 118 (8), 4448–4482. doi:10.1021/acs.chemrev.7b00719
- Bartholomeusz, A., and Thompson, P. (1999). Flaviviridae polymerase and RNA replication. *J. Viral Hepat.* 6 (4), 261–270. doi:10.1046/j.1365-2893.1999.00173.x
- Bhagat, R., Kaur, G., and Seth, P. (2021). Molecular mechanisms of zika virus pathogenesis: An update. *Indian J. Med. Res.* 154 (3), 433–445. doi:10.4103/ijmr.IJMR_169_20
- Boldescu, V., Behnam, M. A. M., Vasilakis, N., and Klein, C. D. (2017). Broad-spectrum agents for flaviviral infections: Dengue, Zika and beyond. *Nat. Rev. Drug Discov.* 16 (8), 565–586. doi:10.1038/nrd.2017.33
- Chen, H. N., Lao, Z. Z., Xu, J. T., Li, Z. X., Long, H. S., Li, D. T., et al. (2020). Antiviral activity of lycorine against Zika virus *in vivo* and *in vitro*. *Virology* 546, 88–97. doi:10.1016/j.virol.2020.04.009
- Chen, Y. T., Li, Z. X., Pan, P., Lao, Z. Z., Xu, J. T., Li, Z. H., et al. (2021). Cinnamic acid inhibits Zika virus by inhibiting RdRp activity. *Antivir. Res.* 192, 105117. doi:10.1016/j.antiviral.2021.105117
- Cumberworth, S. L., Barrie, J. A., Cunningham, M. E., Figueiredo, D. P. G., Schultz, V., Wilder-Smith, A. J., et al. (2017). Zika virus tropism and interactions in myelinating neural cell cultures: CNS cells and myelin are preferentially affected. *Acta Neuropathol. Commun.* 5 (1), 50. doi:10.1186/s40478-017-0450-8
- Dick, G. W., Kitchen, S. F., and Haddock, A. J. (1952). Zika virus. I. Isolations and serological specificity. *Trans. R. Soc. Trop. Med. Hyg.* 46, 509–520. doi:10.1016/0035-9203(52)90042-4
- Ding, Y. L., Girardet, J. L., Smith, K. L., Larson, G., Prigaro, B., Wu, J. Z., et al. (2006). Parallel synthesis of 5-cyano-6-aryl-2-thiouracil derivatives as inhibitors for hepatitis C viral NS5B RNA-dependent RNA polymerase. *Bioorg. Chem.* 34 (1), 26–38. doi:10.1016/j.bioorg.2005.10.001
- Duan, W. Q., Song, H., Wang, H. Y., Chai, Y., Su, C., Qi, J. X., et al. (2017). The crystal structure of Zika virus NS 5 reveals conserved drug targets. *EMBO J* 36 (7), 919–933. doi:10.15252/emboj.201696241

Funding

This work was supported by National Natural Science Foundation of China (21967020, 82273820, U1702286), the grants of Yunnan Applicative and Basic Research Program (2017ZF007), and the Program for Changjiang Scholars and Innovative Research Team in University (IRT_17R94), and Project of Innovative Research Team of Yunnan Province (202005AE160005), and National Key R and D Program of China (2019YFE0109200, 202103AC100005, 202103AQ100001).

Conflict of interest

The authors declare that the research was conducted in the absence of any commercial or financial relationships that could be construed as a potential conflict of interest.

Publisher's note

All claims expressed in this article are solely those of the authors and do not necessarily represent those of their affiliated organizations, or those of the publisher, the editors and the reviewers. Any product that may be evaluated in this article, or claim that may be made by its manufacturer, is not guaranteed or endorsed by the publisher.

Supplementary material

The Supplementary Material for this article can be found online at: <https://www.frontiersin.org/articles/10.3389/fchem.2022.1010547/full#supplementary-material>

- Duan, Y. P., Zeng, M., Jiang, B. W., Zhang, W., Wang, M. S., Jia, R. Y., et al. (2019). Flavivirus RNA-dependent RNA polymerase interacts with genome UTRs and viral proteins to facilitate flavivirus RNA replication. *Viruses* 11 (10), 929. doi:10.3390/v11100929
- Ferrero, D. S., Ruiz-Arroyo, V. M., Soler, N., Uson, I., Guarne, A., and Verdaguer, N. (2019). Supramolecular arrangement of the fulllength Zika virus NS5. *PLoS Pathog.* 15 (4), 10076566–e1007726. doi:10.1371/journal.ppat.1007656
- Gregory, C. J., Oduyebo, T., Brault, A. C., Brooks, J. T., Chung, K. W., Hills, S., et al. (2017). Modes of transmission of Zika virus. *J. Infect. Dis.* 216, S875–S883. doi:10.1093/infdis/jix396
- Guo, M. J., Hui, L. X., Nie, Y. W., Tefsen, B., and Wu, Y. (2021). ZIKV viral proteins and their roles in virus-host interactions. *Sci. China Life Sci.* 64 (5), 709–719. doi:10.1007/s11427-020-1818-4
- He, Y. P., Chen, F. E., Sun, G. F., Wang, Y. P., Clercq, E. D., Balzarini, J., et al. (2004). 5-Alkyl-2-[[aryl and alkyloxycarbonylmethyl]thio]-6-(1-naphthylmethyl) pyrimidin-4(3H)-ones as an unique HIV reverse transcriptase inhibitors of S-DABO series. *Bioorg. Med. Chem. Lett.* 14 (12), 3173–3176. doi:10.1016/j.bmcl.2004.04.008
- He, Y. P., Long, J., Zhang, S. S., Li, C., Lai, C. C., Zhang, C. S., et al. (2011). Synthesis and biological evaluation of novel dihydro-aryl/alkylsulfanyl-cyclohexylmethyl-oxypyrimidines (S-DACOs) as high active anti-HIV agents. *Bioorg. Med. Chem. Lett.* 21 (2), 694–697. doi:10.1016/j.bmcl.2010.12.003
- He, Y. P., Xia, X. S., Wu, D. C., Feng, Y., Zhang, Y., and Li, C. (2015). *Polysubstituted 1, 6-dihydropyrimidines, their synthesis methods and applications*. CN 201510716835.1.
- He, Y. P., Zhuang, D. M., Cai, Q. Q., Li, J. Y., Li, C., and Wang, H. (2011). 2-[(substituted phenylamino) carbonyl methylmercapto]-6-cyclohexomethyl-3H-pyrimidine -4-one compounds, their synthesis method and application. ZL 201110163552.0.
- Hu, Y., and Sun, L. (2019). Systematic analysis of structure similarity between zika virus and other flaviviruses. *ACS Infect. Dis.* 5 (7), 1070–1080. doi:10.1021/acscinfdis.9b00047
- Jaimipuk, T., Sachdev, S., Yoksan, S., and Thepparit, C. (2022). A small-plaque isolate of the Zika virus with envelope domain III mutations affect viral entry and replication in mammalian but not mosquito cells. *Viruses* 14 (3), 480. doi:10.3390/v14030480
- Kraemer, M. U. G., Reiner, R. C., Brady, O. J., Messina, J. P., Gilbert, M., Pigott, D. M., et al. (2019). Past and future spread of the arbovirus vectors *Aedes aegypti* and *Aedes albopictus*. *Nat. Microbiol.* 4 (5), 854–863. doi:10.1038/s41564-019-0376-y
- Li, D. X., Zhang, C. S., Ding, W., Huang, S. M., Yu, L., Lu, N., et al. (2021). Structure-based linker optimization of 6-(2-cyclohexyl-1-alkyl)- 2-(2-oxo-2-phenylethylsulfanyl) pyrimidin-4(3H)-ones as potent non-nucleoside HIV-1 reverse transcriptase inhibitors. *Chin. Chem. Lett.* 32 (3), 1020–1024. doi:10.1016/j.ccllet.2020.09.035
- Li, M. Z. I., Wong, P. S. J., Ng, L. C., and Tan, C. H. (2012). Oral susceptibility of Singapore *Aedes (stegomyia) aegypti* (linnaeus) to zika virus. *PLoS Negl. Trop. Dis.* 6 (8), e1792. doi:10.1371/journal.pntd.0001792
- Li, Q., and Kang, C. (2022). Structures and dynamics of dengue virus nonstructural membrane proteins. *Membranes* 12 (2), 231. doi:10.3390/membranes12020231
- Lim, S. P., Koh, J. H. K., Seh, C. C., Liew, C. W., Davidson, A. D., Chua, L. S., et al. (2013). A crystal structure of the dengue virus non-structural protein 5 (NS5) polymerase delineates interdomain amino acid residues that enhance its thermostability and de novo initiation activities. *J. Biol. Chem.* 288 (43), 31105–31114. doi:10.1074/jbc.M113.508606
- Lim, S. P., Noble, C. G., and Shi, P. Y. (2015). The dengue virus NS5 protein as a target for drug discovery. *Antivir. Res.* 119, 57–67. doi:10.1016/j.antiviral.2015.04.010
- Malet, H., Massé, N., Selisko, B., Romette, J.-L., Alvarez, K., Guillemot, J. C., et al. (2008). The flavivirus polymerase as a target for drug discovery. *Antivir. Res.* 80 (1), 23–35. doi:10.1016/j.antiviral.2008.06.007
- Petersen, L. R., Jamieson, D. J., Powers, A. M., and Honein, M. A. (2016). Zika virus. *N. Engl. J. Med.* 374 (16), 1552–1563. doi:10.1056/NEJMra1602113
- Qian, W. Y., Xue, J. X., Xu, J. X., Li, F., Zhou, G.-F., Wang, F., et al. (2022). Design, synthesis, discovery and SAR of the fused tricyclic derivatives of indoline and imidazolidinone against DENV replication and infection. *Bioorg. Chem.* 120, 105639. doi:10.1016/j.bioorg.2022.105639
- Qian, W. Y., Xue, J. X., Xu, J. X., Li, F., Zhou, G. F., Wang, F., et al. (2022). Design, synthesis, discovery and SAR of the fused tricyclic derivatives of indoline and imidazolidinone against DENV replication and infection. *Bioorg. Chem.* 120, 105639. doi:10.1016/j.bioorg.2022.105639
- Rui, R. M., Tang, C. R., Zhang, C. T., Pan, W. K., Gan, K., Luo, R. H., et al. (2022). C6-structural optimizations of 2-aryl-1H-pyrazole-S-DABOs: From anti-HIV to anti-DENV activity. *Bioorg. Chem.* 119, 105494. doi:10.1016/j.bioorg.2021.105494
- Saez-Alvarez, Y., Arias, A., Aguila, C. D., and Agudo, R. (2019). Development of a fluorescence-based method for the rapid determination of Zika virus polymerase activity and the screening of antiviral drugs. *Sci. Rep.* 9, 5397. doi:10.1038/s41598-019-41998-1
- Selisko, B., Potisopon, S., Agred, R., Priet, S., Varlet, I., Thillier, Y., et al. (2012). Molecular basis for nucleotide conservation at the ends of the dengue virus genome. *PLoS Pathog.* 8 (9), e1002912. doi:10.1371/journal.ppat.1002912
- Shen, L. X. (2015). *Novel NS5B inhibitors and their uses*. Beijing: CN 106496190 A.
- Shu, B., and Gong, P. (2017). The uncoupling of catalysis and translocation in the viral RNA-dependent RNA polymerase. *RNA Biol.* 14 (10), 1314–1319. doi:10.1080/15476286.2017.1300221
- Sirohi, D., and Kuhn, R. J. (2017). Zika virus structure, maturation, and receptors. *J. Infect. Dis.* 216, S935–S944. doi:10.1093/infdis/jix515
- Wu, D. C., Feng, Y., Wang, H., Yang, J. F., Chen, X., Wang, Y. P., et al. (2017). Synthesis and biological evaluation of novel anti-hepatitis C virus (HCV) agents: 2-hydroxyphenethyl sulfanyl-oxypyrimidines: 2-hydroxyphenethyl sulfanyl-oxypyrimidines. *Med. Chem. Res.* 26, 1388–1396. doi:10.1007/s00044-017-1815-z
- Wu, Y. M., Tang, C. R., Rui, R. M., Yang, L. M., Ding, W., Wang, J. Y., et al. (2020). Synthesis and biological evaluation of a series of 2-((5-alkyl/aryl-1H-pyrazol-3-yl) methyl)thio)-5-alkyl-6-(cyclohexyl- methyl)- pyrimidin-4(3H)-Ones as potential HIV-1 Inhibitors. *Acta Pharm. Sin. B* 10 (3), 512–528. doi:10.1016/j.apsb.2019.08.009
- Xu, H. T., Hassounah, S. A., Colby-Germinario, S. P., Oliveira, M., Fogarty, C., Quan, Y. D., et al. (2017). Purification of Zika virus RNA-dependent RNA polymerase and its use to identify small-molecule Zika inhibitors. *J. Antimicrob. Chemother.* 72 (3), 727–734. doi:10.1093/jac/dkw514
- Yu, M. Y., Li, Z. Y., Liu, S., Fan, E. K., Pannecouque, C., Clercq, E. D., et al. (2011). Synthesis and biological evaluation of 6-substituted 5-Alkyl-2-(phenylaminocarbonylmethylthio)pyrimidin-4(3H)-ones as potent HIV-1 NNRTIs. *ChemMedChem* 6 (5), 826–833. doi:10.1002/cmdc.201000555
- Yu, M. Y., Liu, X. Y., Li, Z. Y., Liu, S., Pannecouque, C., Clercq, E. D., et al. (2009). Synthesis and biological evaluation of novel 2-(substituted phenylaminocarbonylmethylthio)-6-(2, 6-dichloro benzyl) -pyrimidin-4(3H)-ones as potent HIV-1 NNRTIs. *Bioorg. Med. Chem.* 17 (22), 7749–7754. doi:10.1016/j.bmc.2009.09.035
- Zhao, B., Yi, G., Du, F., Chuang, Y. C., Vaughan, R. C., Sankaran, B., et al. (2017). Structure and function of the Zika virus full-length NS5 protein. *Nat. Commun.* 8, 14762. doi:10.1038/ncomms14762
- Zou, M., Liu, H. M., Li, J. Y., Yao, X. G., Chen, Y., Ke, C. W., et al. (2020). Structure-activity relationship of flavonoid bifunctional inhibitors against Zika virus infection. *Biochem. Pharmacol.* 177, 113962. doi:10.1016/j.bcp.2020.113962
- Züst, R., Dong, H. P., Li, X.-F., Chang, D. C., Zhang, B., Balakrishnan, T., et al. (2013). Rational design of a live attenuated dengue vaccine: 2'-O-Methyltransferase mutants are highly attenuated and immunogenic in mice and macaques. *PLoS Pathog.* 9 (8), e1003521. doi:10.1371/journal.ppat.1003521



OPEN ACCESS

EDITED BY

Siva S. Panda,
Augusta University, United States

REVIEWED BY

Pankaj Khanna,
University of Delhi, India
Zhiyuan Chen,
Zhejiang University City College, China

*CORRESPONDENCE

Kai Wei,
✉ weikai1987@126.com
Hongbin Zhang,
✉ zhanghb@ynu.edu.cn

SPECIALTY SECTION

This article was submitted to Medicinal and Pharmaceutical Chemistry, a section of the journal Frontiers in Chemistry

RECEIVED 29 August 2022

ACCEPTED 01 December 2022

PUBLISHED 12 December 2022

CITATION

Wei K, Zheng X and Zhang H (2022), Recent applications of dioxinone derivatives for macrocyclic natural product and terpenoid synthesis. *Front. Chem.* 10:1030541. doi: 10.3389/fchem.2022.1030541

COPYRIGHT

© 2022 Wei, Zheng and Zhang. This is an open-access article distributed under the terms of the [Creative Commons Attribution License \(CC BY\)](#). The use, distribution or reproduction in other forums is permitted, provided the original author(s) and the copyright owner(s) are credited and that the original publication in this journal is cited, in accordance with accepted academic practice. No use, distribution or reproduction is permitted which does not comply with these terms.

Recent applications of dioxinone derivatives for macrocyclic natural product and terpenoid synthesis

Kai Wei^{1,2*}, Xinhua Zheng¹ and Hongbin Zhang^{2*}

¹Henan Engineering Research Center of Funiu Mountain's Medical Resources Utilization and Molecular Medicine, School of Medical Sciences, Pingdingshan University, Pingdingshan, Henan, China, ²Key Laboratory of Medicinal Chemistry for Natural Resource, Ministry of Education, Yunnan Provincial Center for Research and Development of Natural Products, School of Chemical Science and Technology, Yunnan University, Kunming, Yunnan, China

Dioxinone derivatives, a class of acetoacetate derivatives, have attracted widespread attention because of their multiple reactive sites, high reactivity, unique chemical properties, and potential synthetic applications. The dioxinone group is also stable under a wide range of reaction conditions, including strong acids, as well as a variety of transition-metal-catalysed processes, such as olefin metathesis and Pd-mediated cross-coupling. The inherent reactivity and diverse applications of dioxinones make them valuable reactive intermediates in organic synthesis. The conversion of dioxinones to acylketenes and their subsequent nucleophilic capture is also an excellent strategy for synthesising β -keto acid derivatives, which can be applied even in complex molecular synthesis. This review focuses on the recent advances in the application of dioxinones in synthetic method research and the total synthesis of natural products, highlighting the exceptional utility of these synthetic methodologies in the construction of macrocyclic cores and terpenoid skeletons. In particular, successful transformations of dioxinone fragments are discussed.

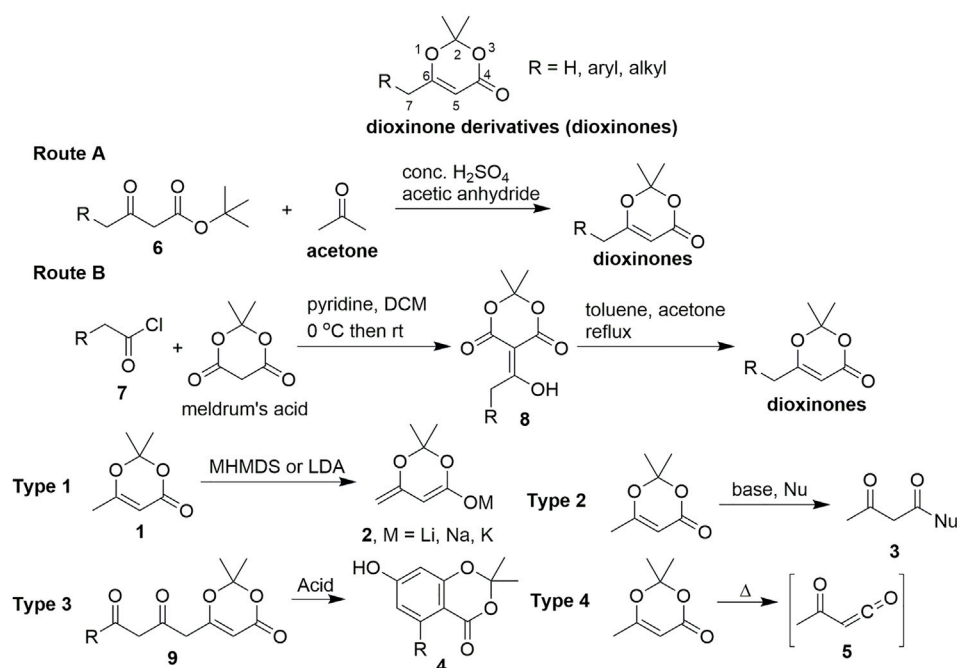
KEYWORDS

dioxinone, macrocyclic, macrolactam, terpenoid, macrolide

Introduction

Chemistry has developed rapidly since its inception as a field of study in the 17th century. Chemists have made outstanding progress in the development of new reagents, reactions, and strategies for selectively and efficiently transforming organic compounds. These advances have been so profound that many highly complex natural products have been obtained through chemical synthesis. The development and utilisation of new reagents remain an area of intense interest in organic chemistry to maximise efficiency and practicability in total synthesis.

Among the numerous reagents used in organic chemistry, dioxinone derivatives have received considerable attention from organic chemists because of their multiple reactive sites, high reactivity, unique chemical properties, and potential synthetic applications.



SCHEME 1

General sequence for the synthesis of dioxinone derivatives and their reactivity.

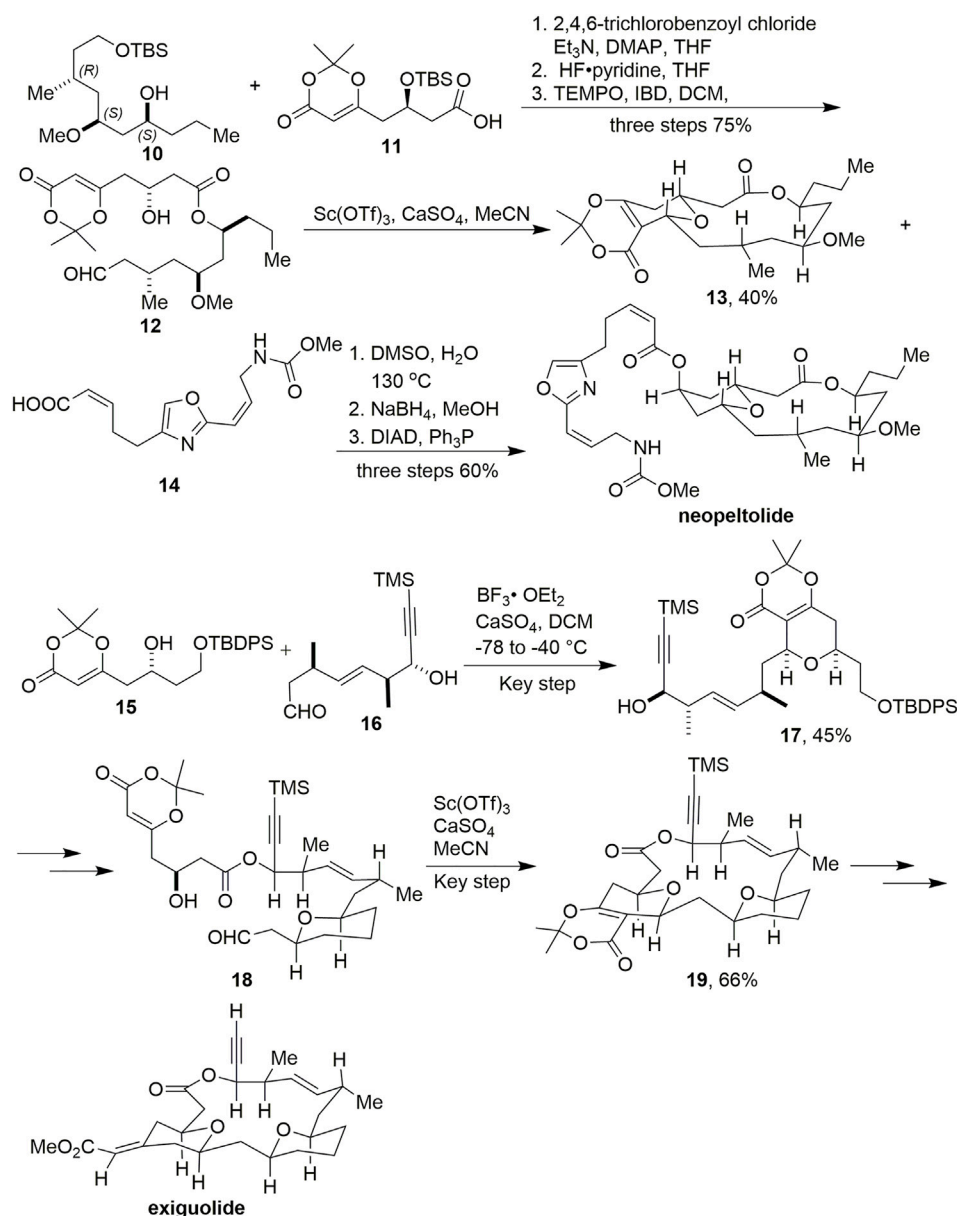
Moreover, dioxinone derivatives are increasingly being applied across a variety of research areas, including agrochemical development, natural product synthesis, and as chemical tools for a wide range of biological investigations.

Several factors have contributed to the popularity of dioxinone derivatives. Compound **1** is practical to use because it is inexpensive to prepare on a large scale using readily available commercial raw materials. Indeed, many chemical suppliers currently market **1** at reasonable prices (\$ 290/kg for bulk quantities). More importantly, the steps used to synthesize various organic synthetic building blocks from **1** are typically robust, straightforward, and broad in scope.

Various innovative methods have been developed for the preparation of dioxinone derivatives. Currently, two highly practical procedures (Scheme 1) are used by a large majority of chemical suppliers to produce **1**. The first method is a one-pot procedure using *tert*-butyl acetoacetate derivatives **6** as the starting materials in the presence of concentrated sulfuric acid, acetic anhydride, and acetone to obtain the dioxinone derivatives (route A) (Fuse et al., 2014). The other method uses meldrum's acid and acid chloride **7** by a practical two-step procedure (route B) (Aoki et al., 2015).

Dioxinone derivatives first entered the purview of chemists as organic synthetic building blocks in the 1950s and have gradually become widely used. In 1989, Winkler reported the asymmetric synthesis of perhydrohistrionicotoxin (Winkler Harshberger, 1989), which was the first application of dioxinone in the total synthesis of a

natural product. Dioxinone derivatives demonstrate multiple chemical properties because they can be considered a product of acetoacetate protected by acetone. There are several distinct types of this chemistry (using compound **1** as an example in Scheme 1): 1) The direct reaction of C-7 in **1** with a wide range of bases (e.g., MHMDS or LDA) proceeds to give **2** or enol silyl ethers (Scheme 1, type 1) in high yields. Kalesse reviewed the application of dioxinones in vinylogous aldol reactions in 2005 (Kalesse, 2005). 2) Compound **1** enables clean and high-yield additions of a very wide range of diverse nucleophiles, including organo-magnesium, lithium, and zinc reagents; stabilised carbanions exemplified by enolates; and numerous hydride reagents (Scheme 1, type 2). Compound **1** can also be converted to an acylketene reactive intermediate **5** under high-temperature conditions, exhibiting rich chemistry (Scheme 1, type 4). Reaction types 2 and 4, which provide direct access to β -keto lactones and β -keto lactams, respectively, have been effectively utilised in complex, target-directed synthesis. Intermolecular or intramolecular trapping of reactive acylketenes by nucleophiles gives rise to valuable structures and enables the execution of challenging and delicate bond formations that might be difficult to achieve using alternative synthetic strategies. Sorensen reviewed the application of dioxinones to bond formation by intermolecular and intramolecular trapings of acylketenes in the total synthesis of large-ring natural products in 2009 (Reber et al., 2009). 3) Moreover, a cyclisation–aromatisation cascade process can be accomplished by an acid-catalysed reaction with the dioxinone derivatives **9**, which serves as an electron-rich reagent widely used in the synthesis of resorcyate natural products (Scheme 1, type 3).



SCHEME 2

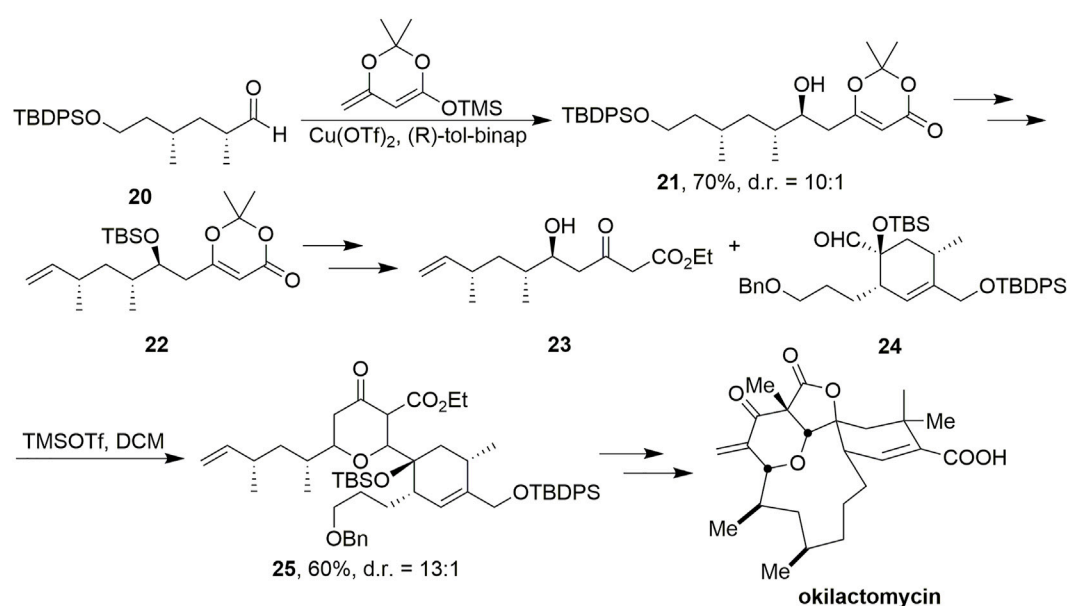
Scheidt's synthesis of neopeltolide and exiguolide.

This review aims to highlight recent strategic applications of dioxinone derivatives in natural product synthesis that were not covered in previous reviews (Kalesse, 2005; Reber et al., 2009), and emphasise the significant role they play in generating molecular skeletons. Only representative examples in which dioxinones are used as a crucial step in the construction of either the core structure or the key structural motif of the target molecule are presented. General applications of the selected examples of total synthesis are grouped based on the natural product types, including macrocyclic natural products,

terpenoids, and some applications in research on synthetic methods, with a particular focus on studies from the last decade.

Macrocyclic natural product synthesis

The most common application of acylketenes in organic synthesis is the preparation of β -keto acid derivatives for construction of macrocyclic natural product frameworks,



SCHEME 3

Scheidt's synthesis of okilactomycin.

which are widely used in the synthesis of macrolides and macrolactams. Boeckman and Pruitt were the first to use dioxinones as precursors to acylketenes in the synthesis of complex natural products featuring macrolactones and macrolactams, as reviewed by Sorensen (Reber et al., 2009). Here, we briefly introduce other studies. In this section, select recent examples are presented to illustrate contemporary solutions to problems involving dioxinones.

In 2009, Scheidt and coworkers reported the successful synthesis of neopeltolide (Scheme 2, Custar et al., 2008, 2009). Dioxinone **1** was used as an important functional block to construct intermediate **11** via a vinylogous aldol reaction. After condensation, deprotection of TBS, and oxidation, key intermediate **12** was obtained. Macrocyclic **13** was successfully acquired in 25% yield by cyclisation via an intramolecular Prins reaction promoted by $\text{Sc}(\text{OTf})_3$.

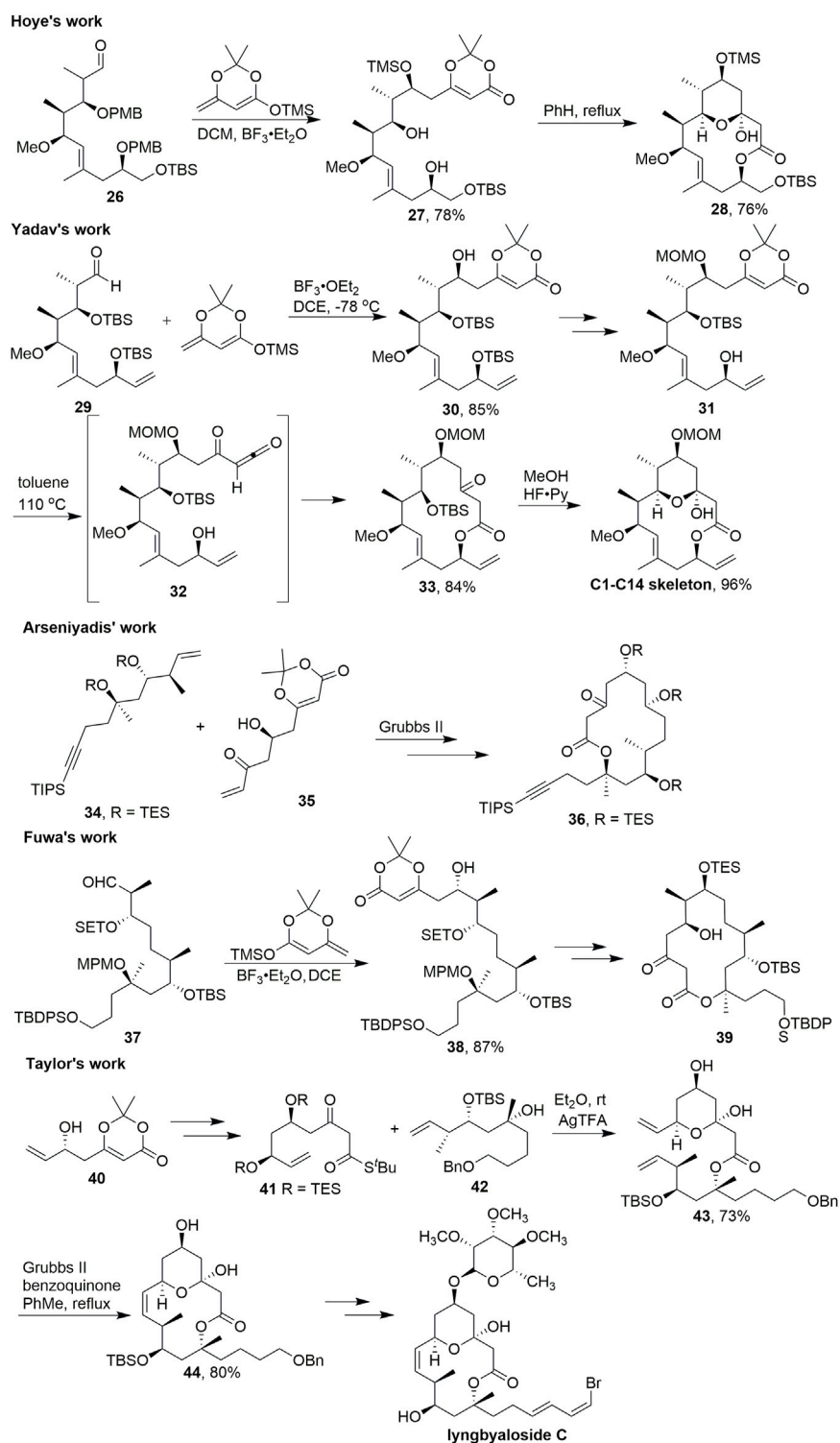
In 2011, This group constructed the exigulolide skeleton using the same strategy via two Prins cyclisations and ultimately completed the total synthesis of exigulolide (Scheme 2, Crane et al., 2011). The first Prins reaction was successfully mediated by $\text{BF}_3 \cdot \text{Et}_2\text{O}$ with compounds **15** and **16** to produce **17** in 45% yield. After multiple transformations, the second key Prins reaction was promoted by $\text{Sc}(\text{OTf})_3$ to construct macrocyclic intermediate **19** in 66% yield.

Dioxinone was also used as an important synthetic block to provide the skeleton in the synthesis of okilactomycin by Scheidt's group (Scheme 3, Tenenbaum et al., 2011). Using copper-catalyzed vinylogous aldol reaction conditions with dioxinone silyl enol ether and aldehyde **20**, β -hydroxy

dioxinone **21** was formed in 70% yield and 10:1 diastereomeric ratio favoring the desired product. After multistep transformations to obtain **22**, treatment of it with KOEt smoothly provided a β -ketoester, where the protecting group was removed with HFpy to afford **23** without any observed lactonization. The conditions of the stereoselective coupling of **23** and **24** were TMSOTf in DCM , and led to the desired **25** in 60% yield and as a 13:1 mixture of diastereomers favoring the desired 2,6-cis isomer. Ultimately, (–)-okilactomycin has been achieved successfully.

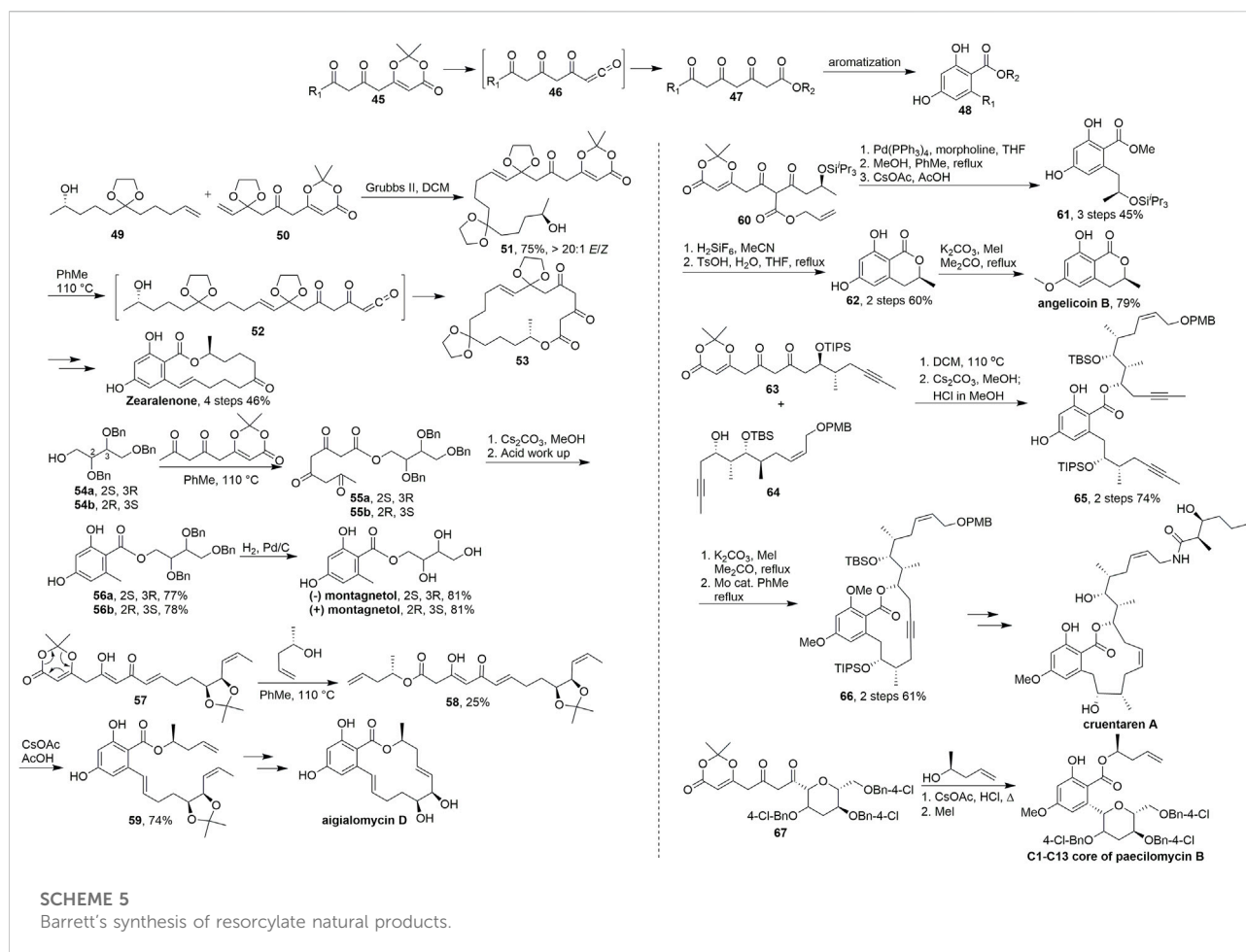
Callipeltoside is a popular target for total synthesis because of its complex architecture and promising anti-tumour bioactivity (Zampella et al., 1996). Like the related compounds lyngbouilloside and lyngbyaloside, these two natural products feature a 14-membered macrolactone with a transannular hemiketal. In 2010, Hoye et al. (2010) reported the asymmetric total synthesis of the macrolide natural product callipeltoside A (Scheme 4). After a vinylogous aldol reaction with **26**, acylketene macrolactonisation took place with a high degree of regioselectivity. Acylketene precursor **27** contains two unprotected hydroxyl groups, yet only the single constitutional isomer **28** was observed after heating this substrate in refluxing benzene.

In 2012, Yadav et al. (2012) used almost the same strategy to build the skeleton in the total synthesis of callipeltoside A (Scheme 4). By employing a diastereoselective aldol addition from the C5–C14 aldehyde segment **29** and dienyl silyl ether, afforded the adduct **30** as the only product in 85% yield. After several steps, compound **31** was received in good yield. Thus,



SCHEME 4

Synthesis of a 14-membered macrolactone central macrolide.



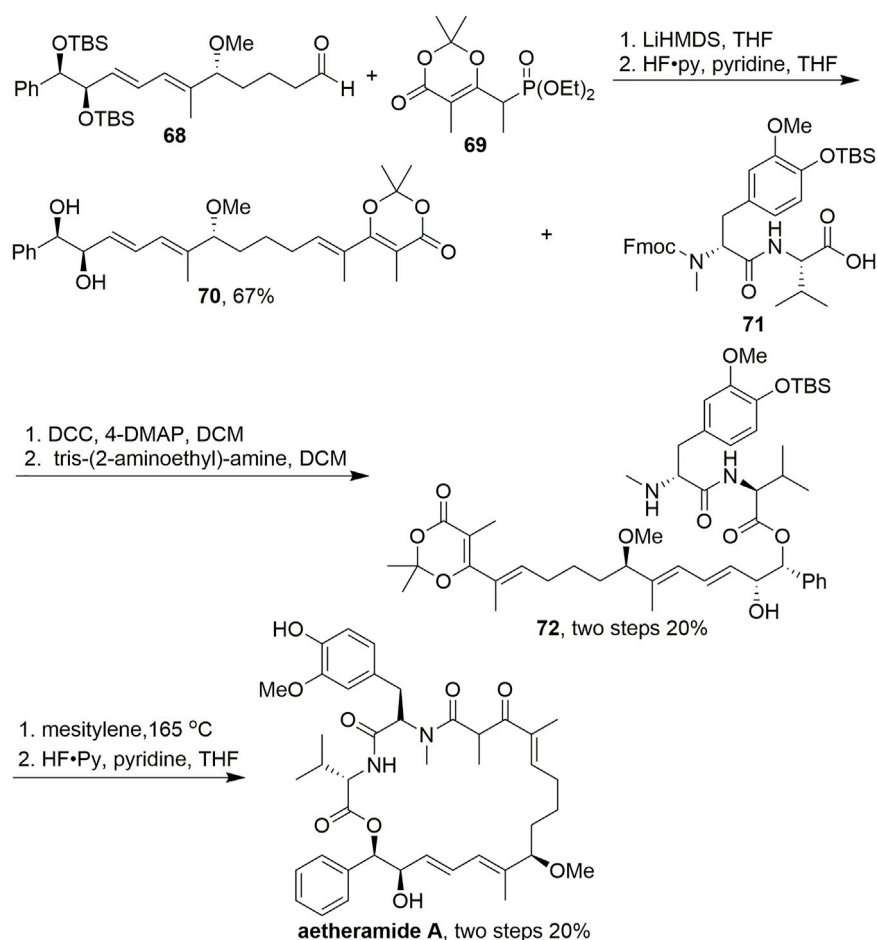
refluxing of a dilute solution of **31** in toluene induced the loss of acetone through thermal decomposition to evolve the acylketene intermediate **32**, which was then trapped intramolecularly by the secondary hydroxy at C13 to generate the 14-membered lactone **33** in 84% yield. The final synthetic operation was carried out by using HF·Py to transform **33** to the C1–C14 skeleton of (–) callipeltoside A by removing the silyl group to form the requisite tetrahydropyran ring.

Similar strategies targeting the central macrolide were reported by Arseniyadis (ElMarrouni et al. 2011), Fuwa (Fuwa et al., 2015), and Taylor (Chang et al., 2015) (Scheme 4). Arseniyadis successfully used C–C bond formation *via* olefin metathesis with key intermediates **34** and **35**; **36** was obtained by heating the dioxinone intermediate. Vinylogous aldol reaction was used to construct the key intermediate **38** to accomplish the subsequent 14-membered macrocyclic **39** in Fuwa's study. Taylor and coworkers prepared **41** from **40** to obtain key intermediate **43** using AgTFA; Then **43** served as the precursor for olefin metathesis. After the 14-membered macrocyclic **44** was obtained by olefin metathesis cyclization, linybyaloside C was synthesized multi-step functional group transformation.

In 2008, Barrett's group developed a new route (Navarro et al., 2008) to resorcyate natural products which was inspired by biosynthetic considerations and was based on macrocyclisation and transannular aromatisation of the dioxinone fragment (Scheme 5). The lactones **48** containing these units utilizing tandem late stage aromatization was obtained from 2,4,6-triketo-ester precursors **47**, which was prepared with the dioxinone derivatives **45** by efficient trapping of the resultant ketene **46** with alcohols.

In their research (Miyatake-ondoab and Barrett, 2010), key advanced intermediate **51** was obtained in 75% yield (E/Z > 20/1) *via* olefin metathesis using a Grubbs II catalyst. Then, **51** was converted into acyl ketene intermediate **52** under refluxing toluene, and intramolecular hydroxyl capture led to the formation of 18-membered macrocyclic lactone **53**. The synthesis was completed *via* multistep transformations and transannular aromatisation. Barrett et al. have used this strategy from 2010 to 2018 in some brilliant studies on the synthesis of resorcyate type natural products.

Thermolysis of dioxinone in the presence of benzyl-protected erithritols **54a** and **54b** gave the triketo-esters **55a** and **55b**,



SCHEME 6

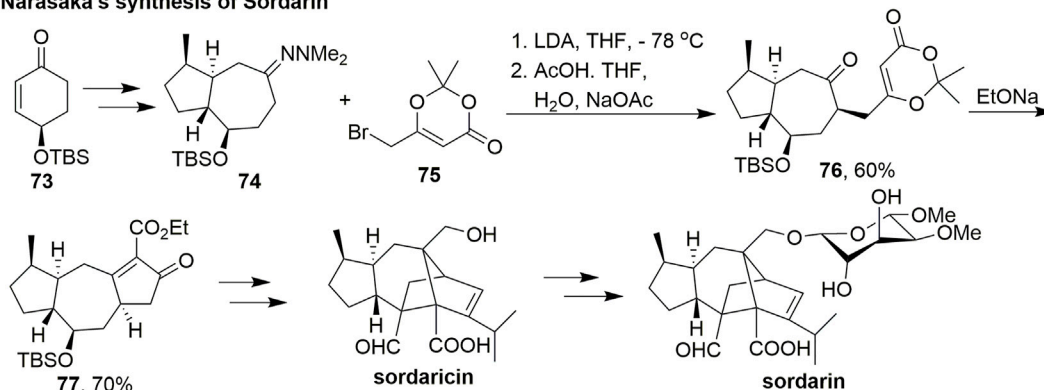
Kalesse's synthesis of aetheramide A.

respectively. Cyclisation and aromatisation followed by hydrogenolysis of the benzyl groups gave (+)-montagnitol. (+)-Erythrin also could be prepared based on the same route in this work (Scheme 5, Basset et al., 2010). Upon heating in toluene, the dioxinones 57 was trapped with chiral alcohol to generate the ketene 58 and directly aromatized by reaction with cesium acetate followed by acetic acid to give the resorcyates 59 respectively in 74% overall yields. After the key RCM and deprotection of the acetonide moiety, aigialomycin D was achieved successfully (Scheme 5, Calo et al., 2009). In 2011, Barrett and coworkers (Scheme 5, Anderson et al., 2011) used one pot palladium(0)-catalyzed deallylation-decarboxylation-ketene trapping-aromatization to give the desired resorcyate 61 in 45% yield over three steps. Deprotection of the silyl ether and acid catalyzed cyclisation gave lactone 62 in 60% yield over two steps. Finally, regioselective methylation of 62 provided angelicoic B. The core resorcyate unit 65 of cruentaren A was synthesized by thermolysis of diketo-dioxinone 63 afforded the corresponding highly reactive ketene, which was

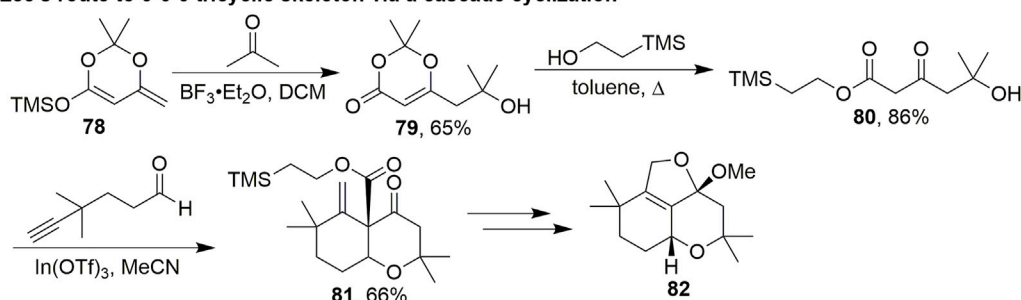
trapped with 64 in 74% yield over two steps. After the ring closing by alkyne metathesis and methylation, the key intermediate 66 was obtained and finally cruentaren A was achieved in several steps from 66 (Scheme 5, Fouché et al., 2012). The C1 to C13 tetrahydropyranyl-resorcyate core of paecilomycin B was also synthesized by this strategy in 2018 (Scheme 5, Cookson et al., 2018).

In addition to its usefulness for macrolide synthesis, dioxinone is also an excellent fragment for the nucleophilic addition of amines to form macrolactams. In 2016, Kalesse reported the synthesis of aetheramide A, which is a highly potent anti-HIV reagent (Scheme 6, Gerstmann and Kalesse, 2016). In their research, to access precursor 72, dioxinone 69 was used as a Horner–Wadsworth–Emmons (HWE) resource in an HWE reaction. The dioxinone moiety was introduced through this olefination, and the final TBS deprotection step completed the synthesis of polyketidic fragment 70 in 67% yield. After condensation with acid 71, mesitylene led to the formation of the acylketene intermediates, which were trapped intramolecularly

Narasaka's synthesis of Sordarin



Lee's route to 5-6-5 tricyclic skeleton via a cascade cyclization



SCHEME 7

Applications of dioxinones in Narasaka and Lee's studies.

by the secondary amine. Deprotection was then carried out using HF-pyridine to give aetheramide A. This synthesis is particularly interesting because although there are various well-established procedures for macrolactamisations using unsubstituted dioxinones, examples with dioxinones bearing a methyl group are rare, possibly because of the considerably higher temperatures necessary to initiate the retro Diels–Alder reaction.

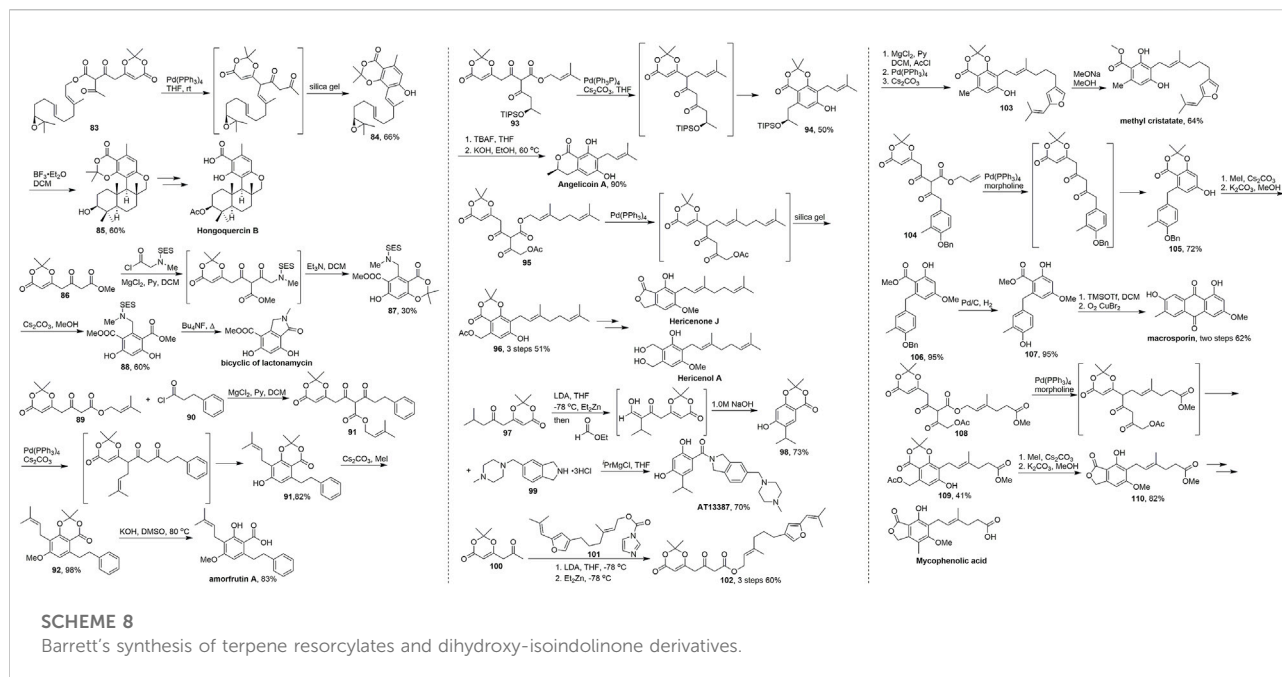
Captures of acylketenes are particularly useful in a synthetic context because sometimes medium and large rings can be formed, which are often difficult to synthesise using more typical methods. The diverse reactivities and applications of dioxinones make them valuable reactive synthetic blocks for macrocyclic natural products. Many similar synthetic studies have been reported (Rentsch and Kalesse, 2012; Dalby et al., 2013; Ogura et al., 2016), which will not be repeated here, in addition to those described earlier.

Terpenoid synthesis

Terpenoids are structurally intriguing natural products that have attracted extensive attention owing to their unique and complex structural characteristics and diverse biological activities. Dioxinone derivatives also play an important role in the total synthesis of some complex terpenoids.

In 2006, Narasaka et al. reported the asymmetric synthesis of sordarin and sordaricin (Scheme 7, Chiba et al., 2006). Sordarin has a tetracyclic cage-like structure with a glycosidic moiety which makes it particularly challenging to synthesize. They started with optically active 73, which could prepare 74 in five steps. Dioxinone 75 was used as an alkylation reagent and added dropwise to a mixture of 74 and LDA. After cleavage of *N,N*-dimethylhydrazone, the resulting ketone 76 was treated with sodium ethoxide in ethanol to give tricyclic keto ester 77 via deprotection of the acetonide group and subsequent condensation. Sordaricin was then obtained through multistep transformations, and glycosylation of sordaricin completed the synthesis of sordarin.

In 2011, Lee's group developed a novel route to construct the 5-6-5 tricyclic furanochroman skeleton of phomactin A via a Prins/Conia-ene cascade cyclisation (Scheme 7, Huang et al., 2011). Phomactins represent a new class of platelet-activating factor (PAF) antagonists isolated from the marine fungus *Phoma* sp. and inhibit PAF-induced platelet aggregation (Sugano et al., 1991, 1996). Dioxinone 79 was obtained via a vinylogous aldol reaction between 78 and acetone. The product was then heated in toluene with the appropriate alcohol to give β-ketoester 80. Subsequently, a variety of factors of this cascade approach, including Lewis acids, solvents, and temperature, were



examined. This multifunctional intermediate successfully underwent a Prins/Conia-ene cascade cyclisation with the alkynaldehyde facilitated by $\text{In}(\text{OTf})_3$ to give **81** in 66% yield. The desired tricyclic skeleton was obtained after several subsequent steps.

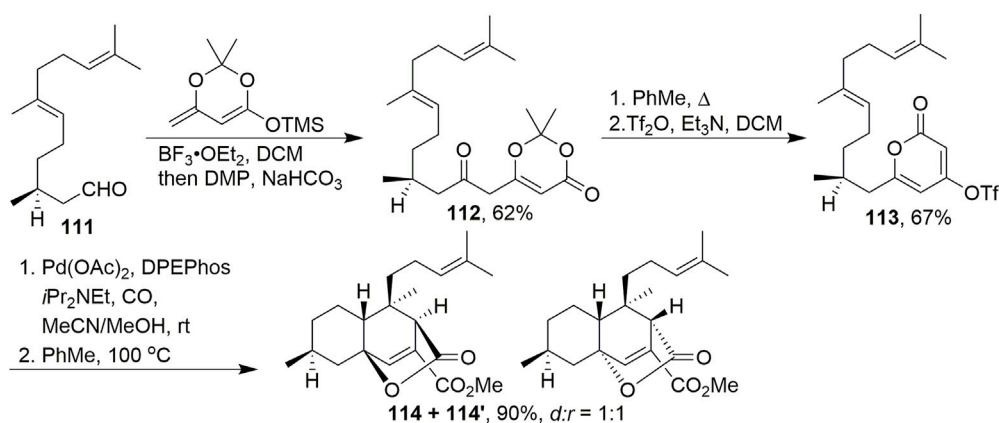
In 2014, Barrett and Barrett (2014) reported the total synthesis of the complex natural product hongoquercin B, which has been isolated from extracts of an unidentified terrestrial fungus and exhibits antibiotic activity against vancomycin-resistant *Enterococcus faecium* and methicillin-resistant *Staphylococcus aureus* (Scheme 8, Roll et al., 1998; Ma et al., 2018). The key advanced intermediate **84** was formed *via* a decarboxylation allylation tandem aromatization of **83**. Treatment of ester **83** with $\text{Pd}(\text{PPh}_3)_4$ at room temperature gave a diketo-dioxinone intermediate, which was readily aromatized over silica gel to give resorcyate **84** in 66% yield over three steps. Notably, only the desired linear *E,E*-isomer was obtained in this sequence. Subsequent addition of $\text{BF}_3 \cdot \text{Et}_2\text{O}$ in dichloromethane furnished pentacyclic skeleton **85** in 60% yield by cascade cyclisation. The total synthesis of hongoquercin B was completed in two steps through functional group modifications.

Since the first example reported by Barrett in 2011, more than ten molecules have been synthesized using this approach *via* the cascade cyclisation-aromatization, which is an efficient and concise method for constructing dioxinone-resorcyate especially the terpene resorcyates and dihydroxy-isoindolinone derivatives. Barrett's works (Scheme 8) were carried out using dioxinone derivatives as an important synthetic building block to achieve the diketo-dioxinone ester, palladium catalyzed migratory, decarboxylative prenylation-aromatization sequence as the key

cascade process to establish the core frameworks of natural products with the mild conditions, easy work-up, wide scopes and high yield.

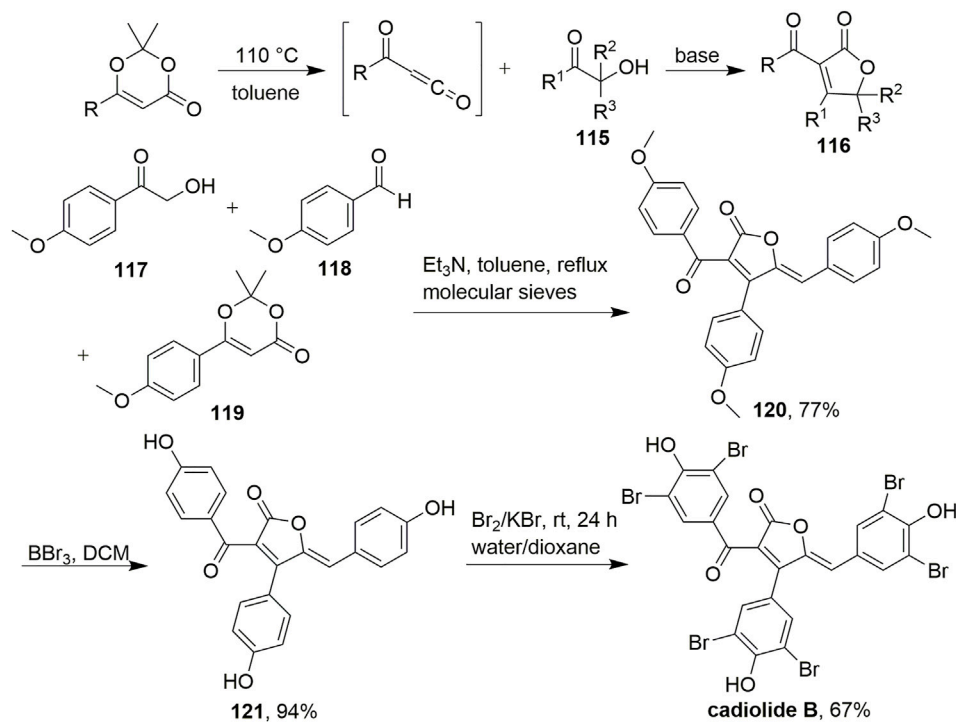
In 2011, they developed a concise five-step synthesis to the E, F-ring system of lactonamycin (Jacques et al., 2011). Dioxinone ketoester **89** and chloride **90** were used to provide the key in intermediate. Then subsequent reaction of diketoester-dioxinone **91** with $\text{Pd}(\text{PPh}_3)_4$ and cesium carbonate resulted in decarboxylative prenyl migration and formation of the resorcyate **92**. Amorfrutin A was obtained after the phenol methylation and saponification (Laclef et al., 2012). In 2012, Barrett and coworkers used different dioxinone-diketoesters **93** and **95** to provide the corresponding products **94** and **96** of the tandem process in good yields over several steps. Finally, they accomplished three terpene resorcyates angelicoin A, hericenone J and hericenol A in just five steps (Cordes et al., 2012). In 2012, Patel and Barrett (2012) completed the total synthesis of a Hsp90 inhibitor AT13387. They started with ketoester **97** and gave the dioxinone-resorcyate **98** in 73% yield and obtained AT13387 after the saponification and condensation in total 3 steps from **97**. Barrett's group finished the total synthesis of macrosporin (Cordes and Barrett, 2013), mycophenolic acid (Brookes et al., 2013) and methyl cristatate (George et al., 2013) utilizing this tandem strategy in 2013. In general, this conversion strategy has great advantages in the synthesis of natural products containing aryl-phenol structures and provides a new convenient route for this kind of natural product.

In 2015, Zhao and Maimone (2015) used dioxinone as a key building block to construct key intermediate **114** in the asymmetric total synthesis of chatancin (Scheme 9). A



SCHEME 9

Maimone's protocol to synthesise the tricyclic skeleton of chatancin.

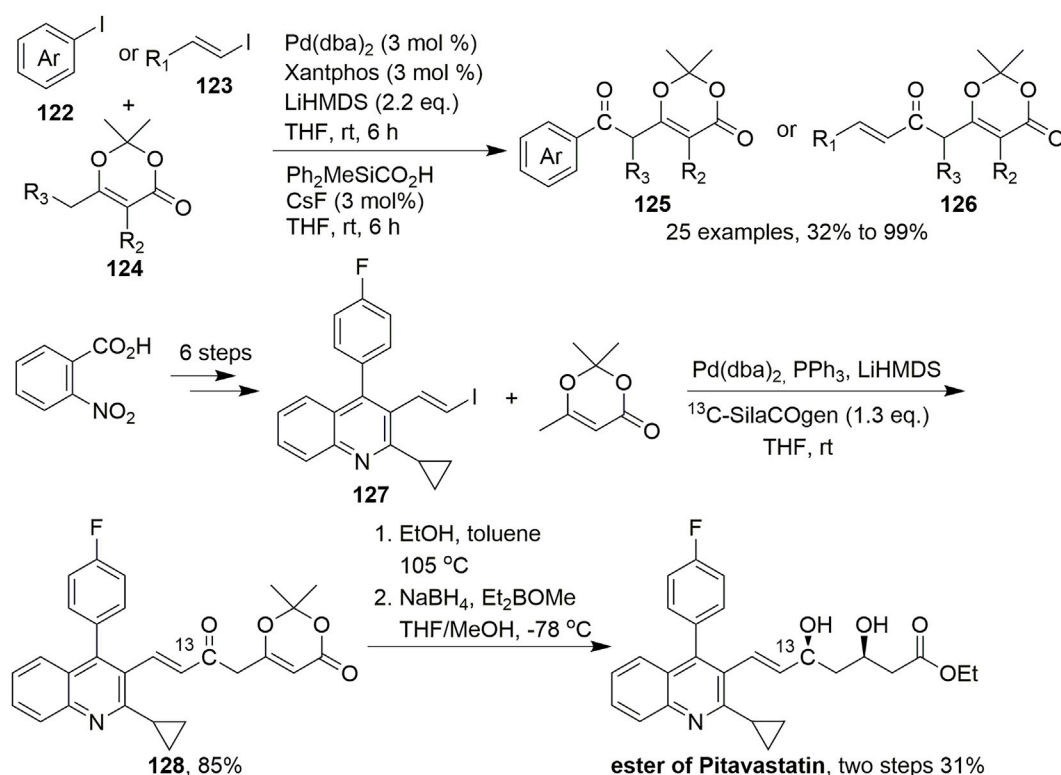


SCHEME 10

A new cycloaddition to prepare novel multisubstituted γ -butyrolactones.

vinylous adol reaction was employed to convert aldehyde **111** and an enol ether into a secondary alcohol, followed by treatment with DMP to furnish dioxinone **112**. After heating in toluene and the intramolecular capture of acylketenes, treatment of the product with TiF_2O successfully gave **113**. Pd-catalysed carbonylation of **113** dissolved in a mixture of acetonitrile and

methanol successfully provided desired product **114**. It was discovered that heating a toluene solution of the ester for 4 days smoothly elicited a [4 + 2] cycloaddition in high yield. This process forged four stereocentres in a single operation. Equimolar amounts of diastereomers **114** and **114'** were formed during this process.



SCHEME 11

Pd-catalysed carbonylative couplings.

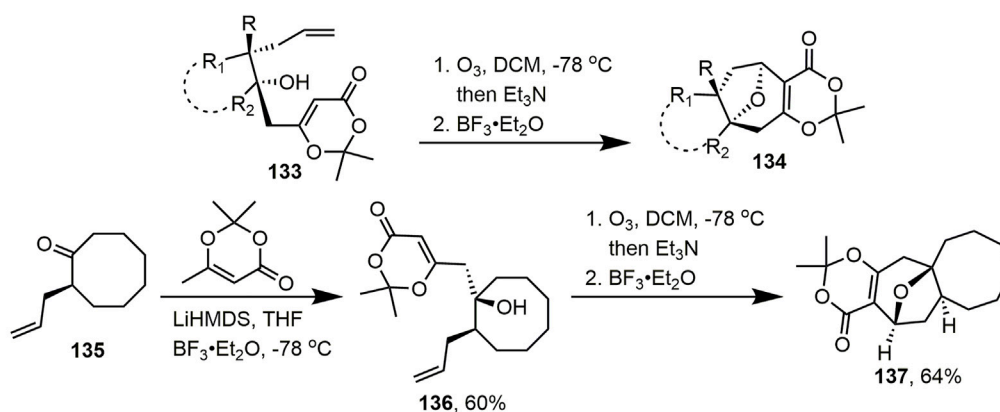
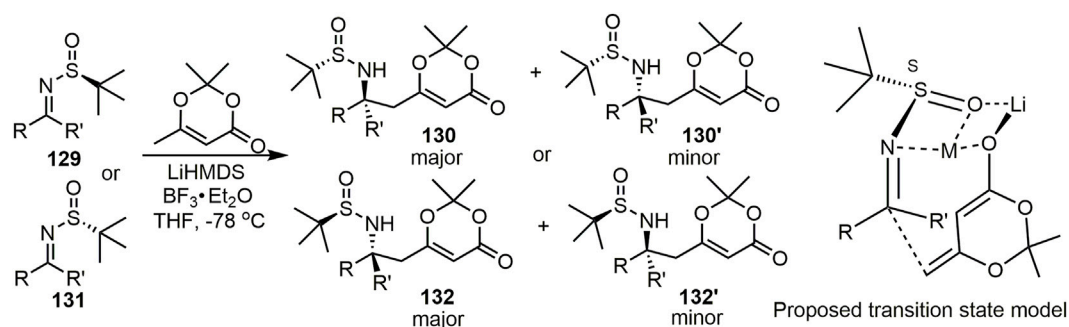
New synthetic methods research

Since early efforts on the synthesis of perhydrohistrionicotoxin in 1989, using dioxinone to build the β -keto acid derivatives used to access macrocyclic and terpenoid natural products has been investigated in many groups around the world. In this section, select recent examples illustrate contemporary methodologies for applications involving dioxinone derivatives.

In 2013, a new cycloaddition methodology to synthesise novel multisubstituted γ -butyrolactones was developed by Leleu et al. (Scheme 10, Peixoto et al., 2013). In this study, multisubstituted γ -butyrolactones **116** were prepared in a one-step procedure by capturing the thermal fragmentation of dioxinones in the presence of hydroxy ketones **115** under basic conditions. Various parameters were considered for the one-step synthesis of γ -butyrolactones, including the amount of base or dioxinone and the nature of the base. Ultimately, the use of 0.5 equiv. triethylamine and 1.5 equiv. dioxinone resulted in the highest yields. Under these conditions, acylfuranone **120** was prepared in one step from **117**, **118**, and **119** in 77% yield. This method was extended to the one-pot multicomponent synthesis of densely functionalized γ -butyrolactones. This diversity-oriented approach provided expeditious access to various

small-ring compounds with potentially high antimicrobial activities under mild conditions with easy handling procedures and a wide scope of substrates. This will most certainly find a broad range of applications in medicinal chemistry.

The palladium-catalysed arylation or vinylation of enolisable carbonyl and related compounds represents a viable and useful C–C bond-forming reaction, that is, widely applied in synthetic organic chemistry. In 2015, Lindhardt et al. developed a Pd-catalysed carbonylative coupling of aryl and vinyl halides with vinylogous enolates in which the C–C bond is formed exclusively at the γ -position (Scheme 11, Makarov et al., 2015). In this reaction, the conditions for the carbonylative coupling, including ligand, base, and solvent, were screened under Pd(dba)₂ catalysis. Ultimately, using Xantphos as the ligand and LiHMDS as the base, this reaction gave an 82% yield under 3 mol% Pd(dba)₂ catalysis in THF. The reaction was performed under mild conditions with various dioxinones and substituted aryl and alkenyl iodides to give aryl and alkenyl ketones **125** and **126**, respectively. Dioxinone was coupled to a range of aryl and vinyl iodides to provide 3,5-dicarbonyl acids with complete γ -selectivity. Furthermore, the carbonylation reactions were performed at room temperature with stoichiometric amounts of carbon monoxide. To apply this reaction to natural product



SCHEME 12

The application of dioxinone in Zhang's work.

synthesis, first, substituted quinoline **127** was readily prepared from 2-nitrobenzoic acid in six steps. Subsequently, ^{13}C -SilaCOgen produced ^{13}C -labeled dioxinone **128** according to the standard conditions for carbonylative coupling in an excellent isolated yield of 85%. Dioxinone opening was then accomplished using ethanol in toluene, which was followed by *syn*-diastereoselective reduction of the two ketones, ultimately affording the ^{13}C -labeled ethyl ester of (\pm)-pitavastatin in 31% isolated yield over two steps. The synthesis of this corresponding ^{13}C -labeled product was to indicate that this carbonylative coupling reaction could be used to synthesize drug molecules and also demonstrate the origin of carbonyl groups.

In 2017, Zhang et al. reported the full details of a general and practical diastereoselective approach towards the synthesis of δ -amino acid derivatives by vinylogous Mannich reactions between *N*-*tert*-butanesulfinyl imines and dioxinone lithium dienolate (Scheme 12, Li et al., 2017). In this study, systematic screening of the reaction conditions, especially the base and Lewis acid, was conducted to optimize the yield and diastereoselectivity of this reaction. It was clear that the base and Lewis acid had a major influence on the reaction. Notably, the corresponding product (**130**, **130'** and **132**, **132'**) was

isolated in up to 87% yield and 40:1 d.r. in the presence of 2 equiv. $\text{BF}_3\cdot\text{Et}_2\text{O}$. With the scope of the diastereoselective vinylogous Mannich reactions having been investigated, a variety of aryl, alkyl, and cyclic substituted *N*-*tert*-butanesulfinyl aldimines and ketimines (**129** and **131**) were obtained in mild to excellent diastereoselectivities (d.r. 1.2:1 to >40:1) and yields (20%–96%) under optimized conditions. Moreover, heterocyclic- and fused-ring-substituted imines gave moderate to excellent yields and diastereoselectivities. In the proposed transition state model, the author inferred that the imine was activated by coordination with BF_3 , and Si-face addition of the dioxinone-derived lithium dienolate led to major products with S-configuration for the newly formed stereocenter. This reaction provides a novel method for the synthesis of amino acids and chiral amines. Most importantly, the corresponding products can undergo many valuable transformations. Additionally, this method provides a foundation for the synthesis of natural products.

Two years later, Zhang's group developed a practical method for the construction of an oxa-bridged bicyclic ring system via an oxidative-cleavage/Prins-cyclisation approach towards the synthesis of highly functional oxa-bridged seven-, eight-, and nine-membered rings (Scheme 12, Wang et al., 2019). Zhang

et al. used various substituted aldehydes, ketones, and Weinreb amides as starting materials. Alcohol **133** was successfully obtained in two steps and set the stage for the proposed oxidative cleavage and Prins cyclisation. In the initial studies, oxidation by ozone provided a semiketal that formed an oxonium ion upon treatment with $\text{BF}_3 \cdot \text{Et}_2\text{O}$, and cyclisation gave the desired oxa-bridged compound. According to the established route, Zhang et al. extended the general utility of this process to synthesise ring systems of other sizes, including 7/8/9-membered oxa-bridged rings. Substrates bearing cyclopentane, cyclohexane, cycloheptane, and cyclooctane also reacted well and provided tetracyclic products. In addition, seven–eight fused, eight–eight fused, and nine-membered ring systems could be constructed using this methodology. Notably, **137** can also be obtained from ketone **135**, which is the core skeleton of neoabyssomicin D. This straightforward method for the synthesis of oxa-bridged bicyclic ring systems in many natural products is flexible and enables the entry of various highly functionalized fused carbocycles. Reactions are easy to handle, highly diastereoselective, and can be performed on the Gram scale. This process is applicable for the synthesis of natural products containing an oxa-bridged bicyclic core skeleton.

Conclusion

This review illustrates recent advances in the application of dioxinone derivatives to macrocyclic natural products, terpenoid synthesis, and new synthetic methods. Dioxinone derivatives have quickly become powerful, fascinating, and highly efficient tools in organic synthesis. Many researchers have contributed innovative and often practical methods that have established dioxinone derivatives as extremely versatile reagents for the robust and general synthesis of diverse classes of functional compounds, especially β -keto acid derivatives, even in complex natural products. The commercial availability in large quantities at low cost, the robustness and generality of its methods, and the prominence of macrocyclic and terpenoid natural products ensures that dioxinone-based strategies will continue to be some of the most extensively used methods in synthesis. Despite these achievements, new strategies and novel methodologies are both required and expected to facilitate the synthesis of complex molecules. However, due to the sensitivity of the dioxinone derivatives to strong base and high temperature,

the application in synthesis is restricted to a certain extent. It is necessary to develop more novel dioxinone derivatives with diverse structure to make up for its defects and adapt to more extensive reaction conditions. We hope that organic chemists will continue to utilise dioxinone derivatives in their endeavours and make use of these multifunctional intermediates in the synthesis of even more complex natural products.

Author contributions

KW conceived and wrote the manuscript. All other authors (XZ and HZ) provided comments and discussion on the manuscript to aid its preparation.

Funding

This work was supported by grants from the PhD Research Program of Pingdingshan University (Grant No. PXY-BSQD-2022038).

Acknowledgments

We would like to thank Dr Jiuling Li and Dr Jinxu Qi from Pingdingshan University for useful discussion on this topic.

Conflict of interest

The authors declare that the research was conducted in the absence of any commercial or financial relationships that could be construed as a potential conflict of interest.

Publisher's note

All claims expressed in this article are solely those of the authors and do not necessarily represent those of their affiliated organizations, or those of the publisher, the editors and the reviewers. Any product that may be evaluated in this article, or claim that may be made by its manufacturer, is not guaranteed or endorsed by the publisher.

References

- Anderson, K., Calo, F., Pfaffeneder, T., White, A. J. P., and Barrett, A. G. M. (2011). Biomimetic total synthesis of angelicoic acid and B via a palladium-catalyzed decarboxylative prenylation aromatization sequence. *Org. Lett.* 13, 5748–5750. doi:10.1021/ol202320m
- Aoki, Y., Ohmori, K., and Suzuki, K. (2015). Dioxinone-fused dienes enable highly *endo* – selective intramolecular diels–alder reactions. *Org. Lett.* 17, 2756–2759. doi:10.1021/acs.orglett.5b01172
- Barrett, T. N., and Barrett, A. G. M. (2014). Cascade polyketide and polyene cyclizations: Biomimetic total synthesis of hongoquercin B. *J. Am. Chem. Soc.* 136, 17013–17015. doi:10.1021/ja511534x
- Basset, J. F., Leslie, C., Hamprecht, D., White, A. J. P., and Barrett, A. G. M. (2010). Studies on the resorcyates: Biomimetic total syntheses of (+)-montagnitol and (+)-erythrin. *Tetrahedron Lett.* 51, 783–785. doi:10.1016/j.tetlet.2009.11.134

- Brookes, P. A., Cordes, J., White, A. J. P., and Barrett, A. G. M. (2013). Total synthesis of mycophenolic acid by a palladium-catalyzed decarboxylative allylation and biomimetic aromatization sequence. *Eur. J. Org. Chem.* 7313, 7313–7319. doi:10.1002/ejoc.201300974
- Calo, F., Richardson, J., and Barrett, A. G. M. (2009). Total synthesis of aigialomycin D using a one-pot ketene generation-trapping-aromatization sequence. *Org. Lett.* 11, 4910–4913. doi:10.1021/ol901979x
- Chang, C. F., Stefan, E., and Taylor, R. E. (2015). Total synthesis and structural reassignment of lyngbyaloside C highlighted by intermolecular ketene esterification. *Chem. Eur. J.* 21, 10681–10686. doi:10.1002/chem.201502132
- Chiba, S., Kitamura, M., and Narasaka, K. (2006). Synthesis of (-)-Sordarin. *J. Am. Chem. Soc.* 128, 6931–6937. doi:10.1021/ja060408h
- Cookson, R., White, A. J. P., and Barrett, A. G. M. (2018). Synthesis of the C1 to C13 tetrahydropyranyl-resorcyate core of paecilomycin B. *Tetrahedron* 74, 5040–5048. doi:10.1016/j.tet.2018.05.083
- Cordes, J., and Barrett, A. G. M. (2013). Synthesis of macrosporin and related 9, 10-anthraquinones by biomimetic polyketide aromatization and cyclization of 6-benzylresorcyates. *Eur. J. Org. Chem.* 1318, 1318–1326. doi:10.1002/ejoc.201201480
- Cordes, J., Calo, F., Anderson, K., Pfaffeneder, T., Laclef, S., White, A. J. P., et al. (2012). Total syntheses of angelicin A, hericenone J, and hericenol A via migratory prenyl- and geranylation-aromatization sequences. *J. Org. Chem.* 77, 652–657. doi:10.1021/jo202354j
- Crane, E. A., Zabawa, T. P., Farmer, R. L., and Scheidt, K. A. (2011). Enantioselective synthesis of (-)-Exiguolide by iterative stereoselective dioxinone-directed Prins cyclizations. *Angew. Chem. Int. Ed. Engl.* 50, 9278–9281. doi:10.1002/ange.201102790
- Custar, D. W., Zabawa, T. P., Hines, J., Crews, C. M., and Scheidt, K. A. (2009). Total synthesis and structure-activity investigation of the marine natural product neopeltolide. *J. Am. Chem. Soc.* 131, 12406–12414. doi:10.1021/ja904604x
- Custar, D. W., Zabawa, T. P., and Scheidt, K. A. (2008). Total synthesis and structural revision of the marine macrolide neopeltolide. *J. Am. Chem. Soc.* 130, 804–805. doi:10.1021/ja710080q
- Dalby, S. M., Tindall, J. G., and Paterson, I. (2013). Total synthesis of (-)-Rhizopodin. *Angew. Chem. Int. Ed. Engl.* 52, 6517–6521. doi:10.1002/anie.201301978
- ElMarrouni, A., Lebeuf, R., Gebauer, J., Heras, M., Arseniyadis, S., and Cossy, J. (2011). Total synthesis of nominal lyngbouilioside aglycon. *Org. Lett.* 14, 314–317. doi:10.1021/ol203064r
- Fouché, M., Rooney, L., and Barrett, A. G. M. (2012). Biomimetic total synthesis of cruentaren A via aromatization of diketodioxinones. *J. Org. Chem.* 77, 3060–3070. doi:10.1021/jo300225z
- Fuse, S., Yoshida, H., Oosumi, K., and Takahashi, T. (2014). Rapid and structurally diverse synthesis of multi-substituted β -keto amide derivatives based on a dioxinone scaffold. *Eur. J. Org. Chem.* 4854, 4854–4860. doi:10.1002/ejoc.201402478
- Fuwa, H., Okuaki, Y., Yamagata, N., and Sasaki, M. (2015). Total synthesis, stereochemical reassignment, and biological evaluation of (-)-Lyngbyaloside B. *Angew. Chem. Int. Ed. Engl.* 54, 882–887. doi:10.1002/ange.201409629
- George, N. S., Anderson, K. E., and Barrett, A. G. M. (2013). Total synthesis of cristic acid based on late-stage decarboxylative allylic migration and biomimetic aromatization of a diketo dioxinone. *Eur. J. Org. Chem.* 7604, 7604–7610. doi:10.1002/ejoc.201301102
- Gerstmann, L., and Kalesse, M. (2016). Total synthesis of aetheramide A. *Chem. Eur. J.* 22, 11210–11212. doi:10.1002/chem.201602682
- Hoye, T. R., Danielson, M. E., May, A. E., and Zhao, H. Y. (2010). Total synthesis of (-)-Callipeltoside A. *J. Org. Chem.* 75, 7052–7060. doi:10.1021/jo101598y
- Huang, S. P., Du, G. Y., and Lee, C. S. (2011). Construction of the tricyclic furanochroman skeleton of phomactin A via the prins/conia-ene cascade cyclization approach. *J. Org. Chem.* 76, 6534–6541. doi:10.1021/jo200644t
- Jacques, S. A., Patel, B. H., and Barrett, A. G. M. (2011). Biomimetic synthetic studies on lactonamycin: An expedient synthesis of dihydroxy-isoindolinone-carboxylates. *Tetrahedron Lett.* 52, 6072–6075. doi:10.1016/j.tetlet.2011.08.173
- Kalesse, M. (2005). Recent advances in vinylogous aldol reactions and their applications in the syntheses of natural products. *Top. Curr. Chem. (Cham)*. 244, 43–76. doi:10.1007/b96887
- Laclef, S., Anderson, K., White, A. J. P., and Barrett, A. G. M. (2012). Total synthesis of amorfrutin A via a palladium-catalyzed migratory prenylation-aromatization sequence. *Tetrahedron Lett.* 53, 225–227. doi:10.1016/j.tetlet.2011.11.019
- Li, G. J., Xu, X. L., Tian, H. C., Liu, X. T., Chen, W., Yang, X. D., et al. (2017). Asymmetric synthesis of δ -amino acid derivatives via diastereoselective vinylogous Mannich reactions between N-tert-butanesulfinyl imines and dioxinone-derived lithium dienolate. *RSC Adv.* 7, 50822–50828. doi:10.1039/c7ra10529k
- Ma, T. K., Elliott, D. C., Reid, S., White, A. J. P., Parsons, P. J., and Barrett, A. G. M. (2018). Meroterpenoid synthesis via sequential polyketide aromatization and cationic polyene cyclization: Total syntheses of (+)-Hongoquercin A and B and related meroterpenoids. *J. Org. Chem.* 83, 13276–13286. doi:10.1021/acs.joc.8b02095
- Makarov, I. S., Kuwahara, T., Jusseau, X., Ryu, I., Lindhardt, A. T., and Skrydstrup, T. (2015). Palladium-catalyzed carbonylative couplings of vinylogous enolates: Application to statin structures. *J. Am. Chem. Soc.* 137, 14043–14046. doi:10.1021/jacs.5b09342
- Miyatake-Ondozabal, H., and Barrett, A. G. M. (2010). A novel biomimetic synthesis of (S) (-)-zearenone: Via macrocyclization and transannular aromatization. *Tetrahedron* 66, 6331–6334. doi:10.1016/j.tet.2010.05.084
- Navarro, I., Basset, J. F., Hebbe, S., Major, S. M., Werner, T., Howsham, C., et al. (2008). Biomimetic synthesis of resorcyate natural products utilizing late stage aromatization: Concise total syntheses of the marine antifungal agents 15G256i and 15G256j. *J. Am. Chem. Soc.* 130, 10293–10298. doi:10.1021/ja803445u
- Ogura, Y., Sato, H., and Kuwahara, S. (2016). Total synthesis of amphirionin-4. *Org. Lett.* 18, 2399–2402. doi:10.1021/acs.orglett.6b00883
- Patel, B. H., and Barrett, A. G. M. (2012). Total synthesis of resorcinol amide Hsp90 inhibitor AT13387. *J. Org. Chem.* 77, 11296–11301. doi:10.1021/jo302406w
- Peixoto, P. A., Boulangé, A., Leleu, S., and Franck-Versatile, X. (2013). Versatile synthesis of acylfuranones by reaction of acylketenes with α -hydroxy ketones: Application to the one-step multicomponent synthesis of cadiolide B and its analogues. *Eur. J. Org. Chem.* 3316, 3316–3327. doi:10.1002/ejoc.201300166
- Reber, K. P., Tilley, S. D., and Sorensen, E. J. (2009). Bond formations by intermolecular and intramolecular trappings of acylketenes and their applications in natural product synthesis. *Chem. Soc. Rev.* 38, 3022–3034. doi:10.1039/b912599j
- Rentsch, A., and Kalesse, M. (2012). The total synthesis of coralopyronin A and myxopyronin B. *Angew. Chem. Int. Ed.* 51, 11381–11384. doi:10.1002/anie.201206560
- Roll, D. M., Manning, J. K., and Carter, G. T. (1998). Hongoquercins A and B, new sesquiterpenoid antibiotics: Isolation, structure elucidation, and antibacterial activity. *J. Antibiot.* 51, 635–639. doi:10.7164/antibiotics.51.635
- Sugano, M., Sato, A., Iijima, Y., Oshima, T., Furuya, K., Kuwano, H., et al. (1991). Phomactin A; a novel PAF antagonist from a marine fungus *Phoma* sp. *J. Am. Chem. Soc.* 113, 5463–5464. doi:10.1021/ja00014a053
- Sugano, M., Sato, A., Saito, K., Takaishi, S., Matsushita, Y., and Iijima, Y. (1996). Structure-Activity relationships of phomactin derivatives as platelet activating factor antagonists. *J. Med. Chem.* 39, 5281–5284. doi:10.1021/jm950640q
- Tenenbaum, J. M., Morris, W. J., Custar, D. W., and Scheidt, K. A. (2011). Synthesis of (-)-Okilactomycin by a prins-type fragment-assembly strategy. *Angew. Chem. Int. Ed. Engl.* 50, 5892–5895. doi:10.1002/anie.201102037
- Wang, M. S., Wang, Z., Chen, W., Yang, X. D., and Zhang, H. B. (2019). Synthesis of oxa-bridged medium-sized carbocyclic rings via Prins cyclization. *Org. Lett.* 21, 1881–1884. doi:10.1021/acs.orglett.9b00491
- Winkler, J. D., and Hershberger, P. M. (1989). A stereoselective synthesis of (-)-Perhydrohistrionicotoxin. *J. Am. Chem. Soc.* 111, 4852–4856. doi:10.1021/ja00195a042
- Yadav, J. S., Haldar, A., and Maity, T. (2012). Towards the synthesis of (-)-Callipeltoside A: Stereoselective synthesis of the C1-C14 macrolactone core. *Eur. J. Org. Chem.* 2012, 2062–2071. doi:10.1002/ejoc.201101635
- Zampella, A., D'Auria, M. V., Minale, L., Debitus, C., and Roussakis, C. (1996). Callipeltoside A: A cytotoxic aminodeoxy sugar-containing macrolide of a new type from the marine lithistida sponge *callipelta* sp. *J. Am. Chem. Soc.* 118, 11085–11088. doi:10.1021/ja9621004
- Zhao, Y. M., and Maimone, T. J. (2015). Short, enantioselective total synthesis of chatancin. *Angew. Chem. Int. Ed.* 54, 1223–1226. doi:10.1002/anie.201410443

Glossary

Ac Acetyl	KHMDS Potassium Hexamethyldisilazide
Ar Aryl	LDA Lithium diisopropylamide
Bn Benzyl	LHMDS Lithium Hexamethyldisilazide
Boc <i>tert</i> -Butyloxycarbonyl	<i>m</i>-CPBA <i>meta</i> -Chloroperbenzoic Acid
Bu Butyl	Me Methyl
Bz Benzoyl	MOM methoxymethyl acetal
Cbz Carbobenzoxyl	PCC Pyridinium chlorochromate
DBU 1,8-Diazabicyclo[5,4,0]undec-7-ene	PE Petroleum ether
DCC <i>N,N'</i> -Dicyclohexylcarbodiimide	Ph phenyl
DCE Dichloroethane	PMB <i>p</i> -methoxybenzyl
DCM Dichloromethane	PMBCl <i>para</i> -Methoxybenzyl
DDQ 2,3-Dicyano-5,6-dichlorobenzoquinone	PPTS Pyridinium toluene-4-sulphonate
DIBAL-H Diisobutyl aluminium hydride	<i>p</i>-TsOH <i>p</i> -Toluenesulfonic acid
DIPEA <i>N,N</i> -Diisopropylethylamine	Py pyridine
DMAP 4-Dimethylaminopyridine	rt Room temperature
DMF <i>N,N</i> -Dimethylformamide	TBAF Tetrabutylammonium fluoride
DMP Dess-Martin Periodinane	TBS <i>tert</i> -Butyldimethylsilyl
DMSO Dimethyl sulfoxide	TBDPS <i>tert</i> -Butyldiphenylchlorosilyl
dr Diastereomer ratio	TEA Triethylamine
EA Ethyl acetate	Tf trifluoromethanesulfonate
ee Enantiomeric excess	TFA Trifluoroacetic acid
eq. Equivalent	TFAA trifluoroacetic anhydride
Et Ethyl	THF Tetrahydrofuran
IBX 2-Iodoxybenzoic Acid	TLC Thin layer chromatography
im Imidazole	TIPS Triisopropylsilyl
<i>i</i>-Pr isopropyl	TMS Trimethylsilyl
	Ts <i>p</i> -toluenesulfonyl



OPEN ACCESS

EDITED BY

Jian-Wei Dong,
Qujing Normal University, China

REVIEWED BY

Keyume Ablajan,
Xinjiang University, China
Gopal Chandru Senadi,
SRM Institute of Science and
Technology, India

*CORRESPONDENCE

Guogang Deng,
✉ ggden@ynu.edu.cn
Xiaodong Yang,
✉ xdyang@ynu.edu.cn

[†]These authors have contributed equally
to this work

SPECIALTY SECTION

This article was submitted to Medicinal
and Pharmaceutical Chemistry,
a section of the journal
Frontiers in Chemistry

RECEIVED 07 November 2022

ACCEPTED 05 December 2022

PUBLISHED 15 December 2022

CITATION

Jiang Y, Wang B, Liu D, Xia D, Liu Z, Li L,
Deng G and Yang X (2022), Aryl
acrylonitriles synthesis enabled by
palladium-catalyzed α -alkenylation of
arylacetonitriles with vinyl halides/
triflates.
Front. Chem. 10:1091566.
doi: 10.3389/fchem.2022.1091566

COPYRIGHT

© 2022 Jiang, Wang, Liu, Xia, Liu, Li,
Deng and Yang. This is an open-access
article distributed under the terms of the
[Creative Commons Attribution License](#)
(CC BY). The use, distribution or
reproduction in other forums is
permitted, provided the original
author(s) and the copyright owner(s) are
credited and that the original
publication in this journal is cited, in
accordance with accepted academic
practice. No use, distribution or
reproduction is permitted which does
not comply with these terms.

Aryl acrylonitriles synthesis enabled by palladium-catalyzed α -alkenylation of arylacetonitriles with vinyl halides/triflates

Yonggang Jiang[†], Bijun Wang[†], Dongxiang Liu, Dazhen Xia,
Zhengfen Liu, Liang Li, Guogang Deng* and Xiaodong Yang*

Key Laboratory of Medicinal Chemistry for Natural Resource, Ministry of Education, Yunnan Provincial Center for Research & Development of Natural Products, School of Pharmacy, Yunnan University, Kunming, China

Aryl acrylonitriles are an important subclass of acrylonitriles in the medicinal chemistry and pharmaceutical industry. Herein, an efficient synthesis of aryl acrylonitrile derivatives using a Palladium/NIXANTPHOS-based catalyst system was developed. This approach furnishes a variety of substituted and functionalized aryl acrylonitriles (up to 95% yield). The scalability of the transformation and the synthetic versatility of aryl acrylonitrile were demonstrated.

KEYWORDS

arylacetonitrile, palladium catalysis, alkenylation, isomerization, aryl acrylonitrile

Introduction

Acrylonitriles, especially substituted acrylonitriles, are versatile building blocks widely occurring in the pharmaceutical industry, natural products and synthetic organic chemistry (Fringuelli et al., 1994; Fleming, 1999; Fleming et al., 2010; Carta et al., 2011; Shen et al., 2015; Baker et al., 2020; Sirim et al., 2020; Solangi et al., 2020; Baker et al., 2021). Among acrylonitrile-containing molecules, aryl acrylonitriles are an important subclass in the medicinal chemistry and pharmaceutical industry (ANI-7 (Tarleton et al., 2011), CDCPA (Baker et al., 2018), TPAT-AN-XF (Niu et al., 2019), CC-5079 (Zhang et al., 2006), Entacapone (Seeberger and Hauser, 2009), and Rilpivirine (Clercq, 2005) Figure 1). Therefore, the development of efficient and practical approaches for the synthesis of aryl acrylonitriles remains in demand.

Classical synthetic routes to acrylonitrile derivatives include the Wittig/Horner–Wadsworth–Emmons reaction (Zhang et al., 1998; Kojima et al., 2002; Fang et al., 2011; Ando et al., 2013) and Peterson type reactions (Kojima et al., 2004; Pabmo' et al., 1990; Palomo et al., 1990). However, these procedures suffer from limitations such as a poor substrate scope, low efficiency for the synthesis of polysubstituted acrylonitriles. During the past decade, organic chemists keep

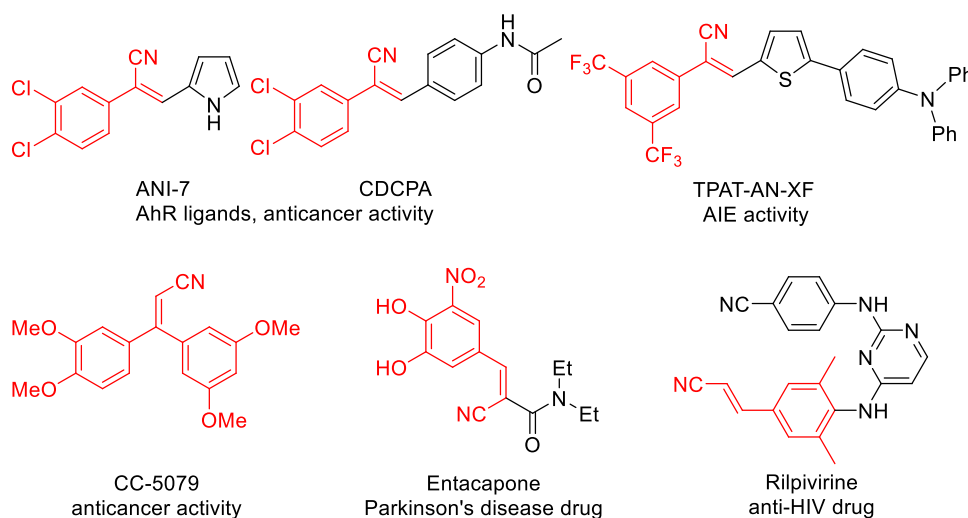
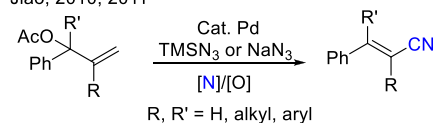


FIGURE 1

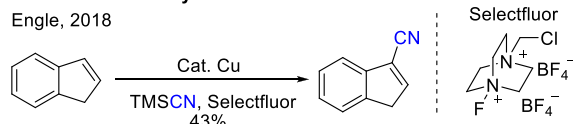
Representative examples of bioactive compounds with an aryl acrylonitrile.

A Tandem Pd-catalyzed azidation/oxidative rearrangement

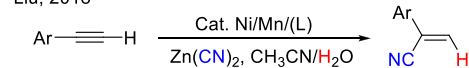
Jiao, 2010, 2011

**B Direct oxidative cyanation of alkenes**

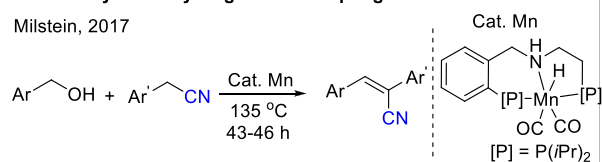
Engle, 2018

**C Ni/Mn-catalyzed hydrocyanation of terminal alkynes**

Liu, 2018

**D Mn-catalyzed dehydrogenative coupling**

Milstein, 2017



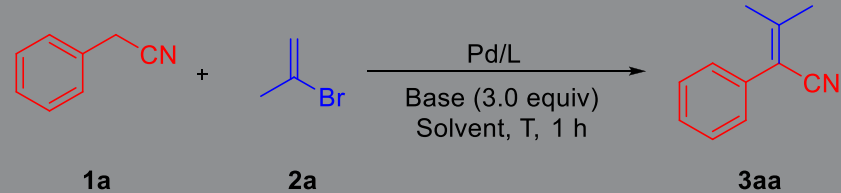
SCHEME 1

General strategies of aryl acrylonitriles.

searching new and efficient reactions, including oxidative Heck-type reactions (Zou et al., 2003; Zhang and Liebeskind, 2006), cyanation of alkenyl halides (Stuhl, 1985; Alterman and Hallberg, 2000; Pradal and Evano, 2014; Ahuja and Sudalai, 2015; Chaitanya and Anbarasan, 2015; Yang

et al., 2018), alcohols (Oishi et al., 2009; Rokade et al., 2012; Thiyagarajan and Gunanathan, 2018; Yadav et al., 2020), aldehydes (Tomioka et al., 2011; Laulhe et al., 2012; Del Fiandra et al., 2016; Wu et al., 2016), acrylamide/oxime dehydration (Yamaguchi et al., 2007; Zhou et al., 2009), carbocyanation of alkynes (Nakao et al., 2007; Cheng et al., 2008; Minami et al., 2013; Yang et al., 2013; He et al., 2016; Qi et al., 2017), cross-metathesis (Crowe and Goldberg, 1995; Randl et al., 2001; Mu et al., 2019), and direct conversion of allylic carbon to nitrile (Qin and Jiao, 2010; Zhou et al., 2010) have been developed and could be applied for the synthesis of acrylonitriles. For example, Jiao developed a series of powerful synthesis of substituted acrylonitriles, which used allyl esters or halides and NaN₃ or TMSN₃ by a tandem Pd-catalyzed azidation and the subsequent oxidative rearrangement process (Scheme 1A) (Qin and Jiao, 2010; Zhou et al., 2010; Jiao et al., 2011; Wang and Jiao, 2014). Engle reported a direct oxidative cyanation of terminal and internal alkenes to prepare substituted acrylonitriles using a homogeneous copper catalyst and a bystander N-F oxidant (Scheme 1B) (Gao et al., 2018). Recently, Liu reported an elegant synthesis of aryl substituted terminal acrylonitriles through Ni/Mn-catalyzed hydrocyanation of terminal alkynes with Zn(CN)₂ (Scheme 1C) (Zhang et al., 2018). Milstein reported an effective synthesis of aryl acrylonitriles through dehydrogenative coupling of alcohols with nitriles catalyzed by a pincer complex of manganese at 135°C for 43–60 h (Scheme 1D) (Chakraborty et al., 2017).

Despite these advances, these methods are generally restricted by the addition of dangerous reagents (cyanide reagents, azide reagents) and stoichiometric amount of

TABLE 1 Optimization of the reaction conditions^a.


Entry	Pd source	L	Base	Solvent	T (°C)	2a (equiv)	Pd/L (mol%)	AY (%) ^b
1	Pd(OAc) ₂	L1	B1	DME	65	1.5	10/20	10
2	PdCl ₂ (cod)	L1	B1	DME	65	1.5	10/20	9
3	[PdCl(allyl)] ₂	L1	B1	DME	65	1.5	10/20	10
4	Pd(NCPh) ₂ Cl ₂	L1	B1	DME	65	1.5	10/20	9
5	Pd(dba) ₂	L1	B1	DME	65	1.5	10/20	4
6	Pd ₂ (dba) ₃	L1	B1	DME	65	1.5	10/20	7
7	Pd(PPh ₃) ₄	L1	B1	DME	65	1.5	10/20	3
8	Pd(Cy ₃) ₂	L1	B1	DME	65	1.5	10/20	8
9	Pd(OAc) ₂	L2-L8	B1	DME	65	1.5	10/20	0–4
10	Pd(OAc) ₂	L1	B2-B6	DME	65	1.5	10/20	0–20
11	Pd(OAc) ₂	L1	B5	Dioxane	65	1.5	10/20	0
12	Pd(OAc) ₂	L1	B5	CPME	65	1.5	10/20	7
13	Pd(OAc) ₂	L1	B5	THF	65	1.5	10/20	3
14	Pd(OAc) ₂	L1	B5	Toluene	65	1.5	10/20	13
15	Pd(OAc) ₂	L1	B5	DME	80	1.5	10/20	57
16	Pd(OAc) ₂	L1	B5	DME	100	1.5	10/20	28
17	Pd(OAc) ₂	L1	B5	DME	80	2.0	10/20	73
18	Pd(OAc) ₂	L1	B5	DME	80	3.0	10/20	77 (75) ^c
19	Pd(OAc) ₂	L1	B5	DME	80	4.0	10/20	68
20	Pd(OAc) ₂	L1	B5	DME	80	3.0	5/10	57

^aReactions conducted on a 0.1 mmol scale using **1a** and **2a**.^bAssay yield determined by ¹H NMR spectroscopy of the crude reaction mixture.^cIsolated yield after chromatographic purification.

oxidants (DDQ, Selectfluor), high catalyst loading, tedious synthetic procedures, low yielding and high reaction temperatures. Therefore, an optional method for the efficient synthesis of aryl acrylonitrile derivatives under mild reaction conditions using simple, easily available substrates are very necessary. Herein, we report an efficient synthesis of aryl acrylonitrile derivatives using a Palladium/NIXANTPHOS-based catalyst system. This approach furnishes efficient access to a variety of substituted and functionalized aryl acrylonitriles (21 examples, up to 95%). The scalability of the transformation was demonstrated and the derivatizations of the aryl acrylonitrile were conducted.

Results and discussion

We initiated our reaction optimization by using phenylacetonitrile **1a** and 2-bromoprop-1-ene **2a** as the model substrates. At the outset, based on our experience with deprotonative cross-coupling processes of weakly acidic substrates (Yang et al., 2016; Duan et al., 2018; Liu et al., 2018), we have found that NIXANTPHOS can effectively implement these conversions. The high reactivity of the Pd/NIXANTPHOS-based system may be due to the presence of the main group metal and the deprotonation of the ligand N–H moiety under basic reaction conditions (Zhang et al., 2014). A

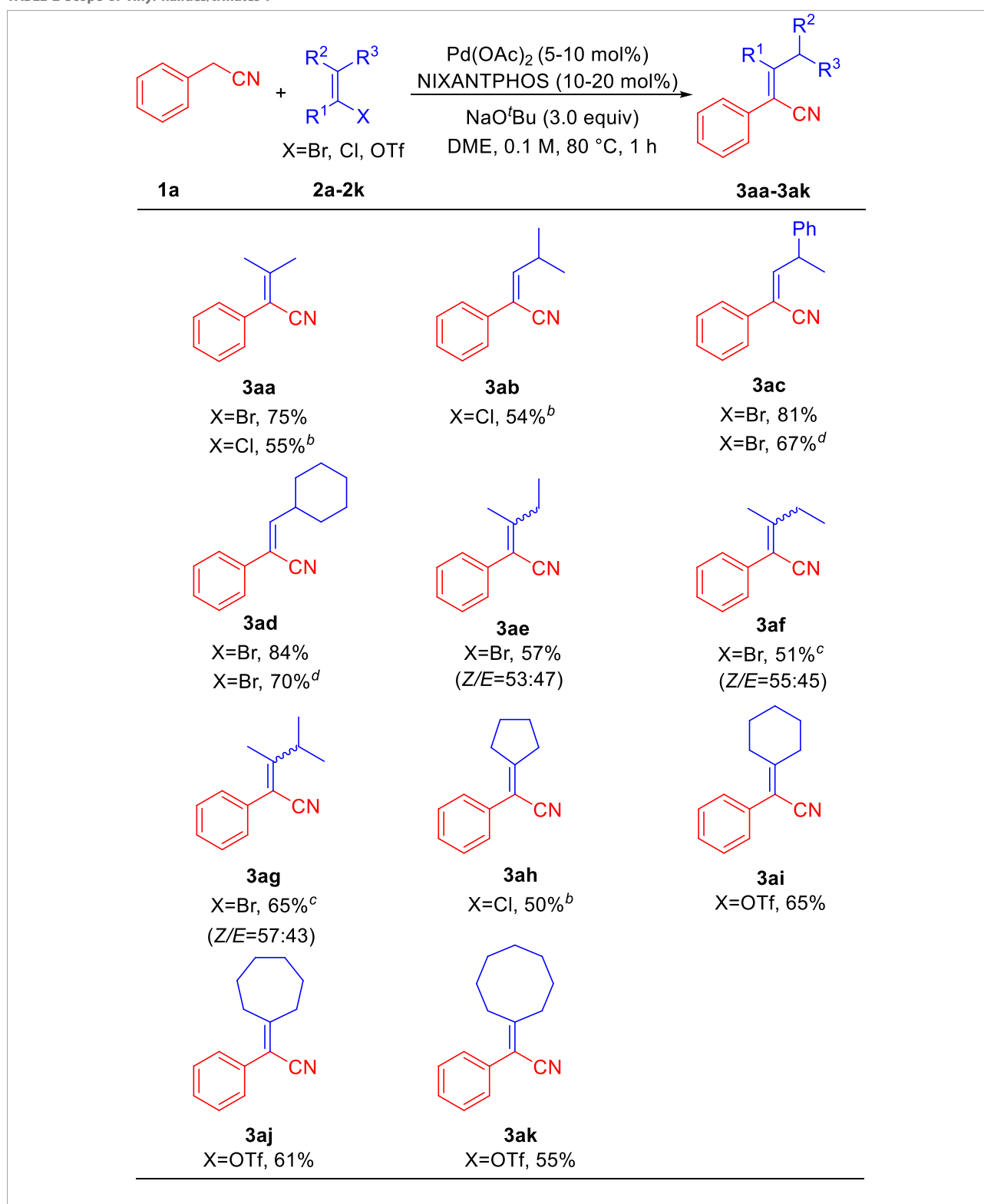
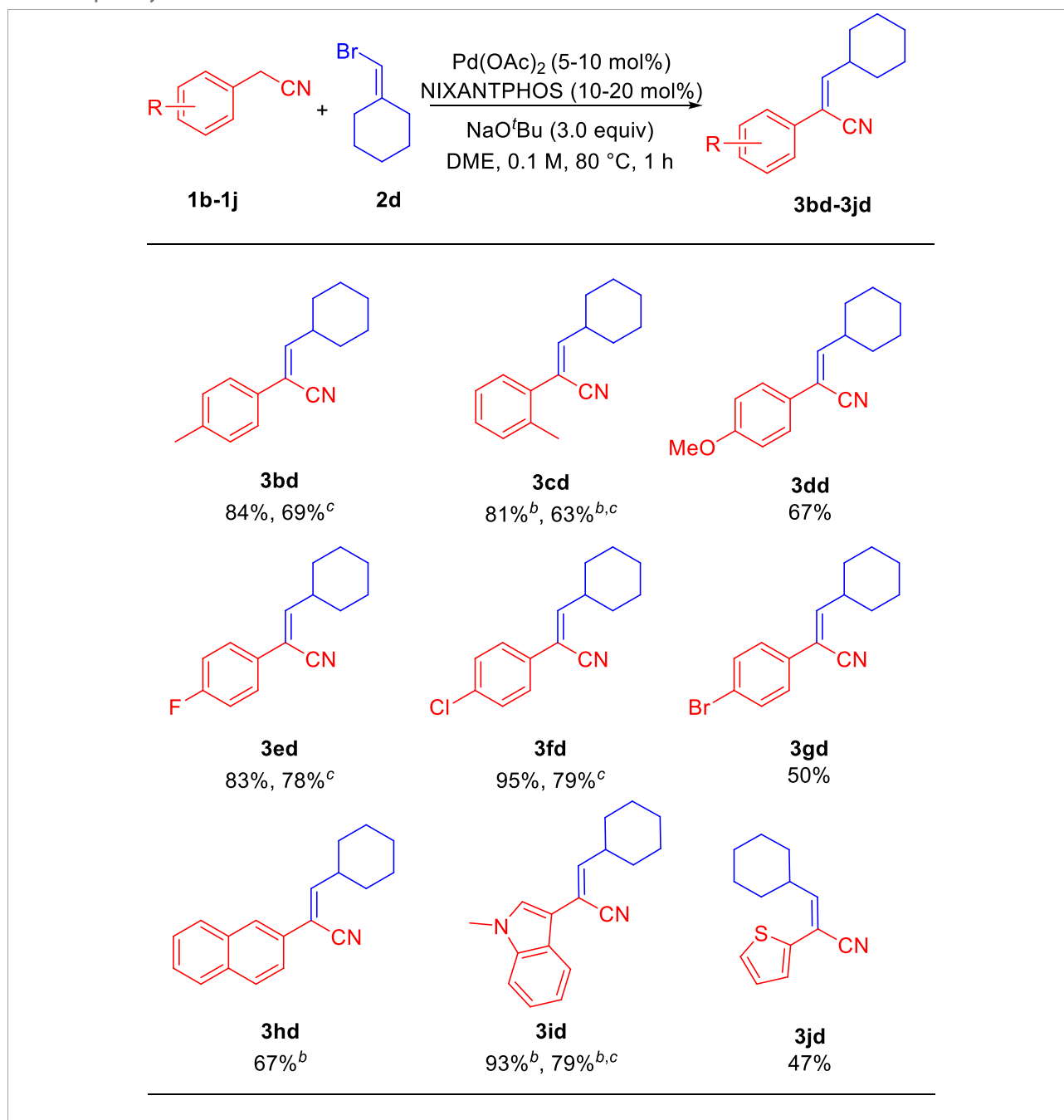
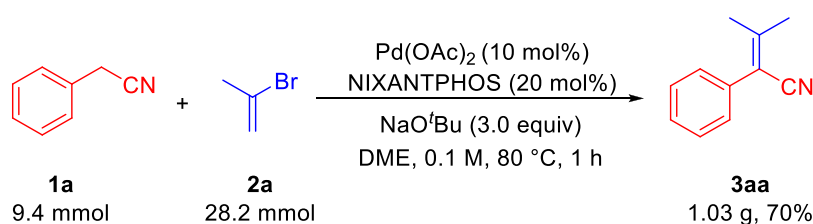
TABLE 2 Scope of vinyl halides/triflates^a.^aReactions conducted on 0.3 mmol scale using 1.0 equiv of **1a** and 3.0 equiv of **2a-2k**. Isolated yield after chromatographic purification.^b7 h reaction time.^c100°C reaction temperature, 7 h reaction time.^d5 mol% $\text{Pd}(\text{OAc})_2$ and 10 mol% NIXANTPHOS, for the reaction.

TABLE 3 Scope of arylacetonitriles^a.^aReactions conducted on 0.3 mmol scale using 1.0 equiv of **1b-1j** and 3.0 equiv of **2d**. Isolated yield after chromatographic purification.^b7 h reaction time.^c5 mol% Pd(OAc)₂ and 10 mol% NIXANTPHOS, for the reaction.

variety of palladium source including different Pd⁰ and Pd^{II} precursors, phosphine ligands and six bases (LiN(SiMe₃)₂, NaN(SiMe₃)₂, KN(SiMe₃)₂, LiO^tBu, NaO^tBu and KO^tBu) were examined the coupling of phenylacetonitrile **1a** and 2-bromoprop-1-ene **2a** in DME at 65°C for 1 h (Table 1, entries 1–10) (see the optimization of reaction conditions on page S2 in Supplementary Material). The top Pd/L/base combination from

this screen was Pd(OAc)₂/NIXANTPHOS/NaO^tBu resulted in 20% assay yield (AY, determined by ¹H NMR analysis). Other four solvents (dioxane, CPME, THF and Toluene) were tested, which only afforded trace amount of product (0%–13%) (entries 11–14). Raising the reaction temperature to 80 and 100°C led to increases to 57 and 28% AY, respectively (entries 15 and 16). Changing the equivalent of **2a** from 2 to 4 led to



SCHEME 2

Synthesis of aryl acrylonitrile **3aa** in gram scale.

increases of AY (entries 17–19). When a 3 equivalent was employed, the AY increased to 77% (75% isolated yield, entry 18). Reducing the Pd/ligand ratio to 5:10, AY dropped to 57% (entry 20).

L1: NIXANTPHOS, L2: XANTPHOS, L3: PPh_3 , L4: $\text{P}(o\text{-TOL})_3$, L5: $\text{P}(1\text{-NAP})_3$, L6: *rac*-BINAP, L7: JOHNPHOS, L8: PCy_3

B1: $\text{LiN}(\text{SiMe}_3)_2$, B2: $\text{NaN}(\text{SiMe}_3)_2$, B3: $\text{KN}(\text{SiMe}_3)_2$, B4: LiO^tBu , B5: NaO^tBu , B6: KO^tBu

With the optimized reaction conditions (Table 1, entry 18), we explored the structural diversity of vinyl halides/triflates using phenylacetonitrile **1a** as the model substrate. As shown in Table 2, 2-bromo-1-ene **2a** delivered aryl acrylonitrile **3aa** in 75% yield, while 2-chloro-1-ene **2a'** gave 55% yield. Vinyl chloride 1-chloro-2-methylprop-1-ene **2b** led to product **3ab** in 54% yield. (*E*)-(1-bromoprop-1-en-2-yl)benzene **2c** provided product **3ac** in 81% yield (67% yield for 5% Pd/10% L). Sterically hindered bromomethylenecyclohexane **2d** rendered product **3ad** with excellent yield of 84% yield (70% yield for 5% Pd/10% L). Trans- and cis-2-bromobut-2-ene (**2e** and **2f**) furnished products **3ae** and **3af** in overall 57% and 51% yields. 2-Bromo-3-methylbut-2-ene **2g** afforded product **3ag** in overall 65% yield. Cycloolefin halides/triflates were all suitable reaction partners in this transformation and provided a series of cycloalkane-functionalized aryl acrylonitriles in moderate yields. 1-Chlorocyclopent-1-ene **2h** led to product **3ah** in 50% yield. Six/seven/eight-membered cycloolefin triflates proceeded the corresponding products **3ai**, **3aj**, and **3ak** in 65%, 61% and 55% yields, respectively.

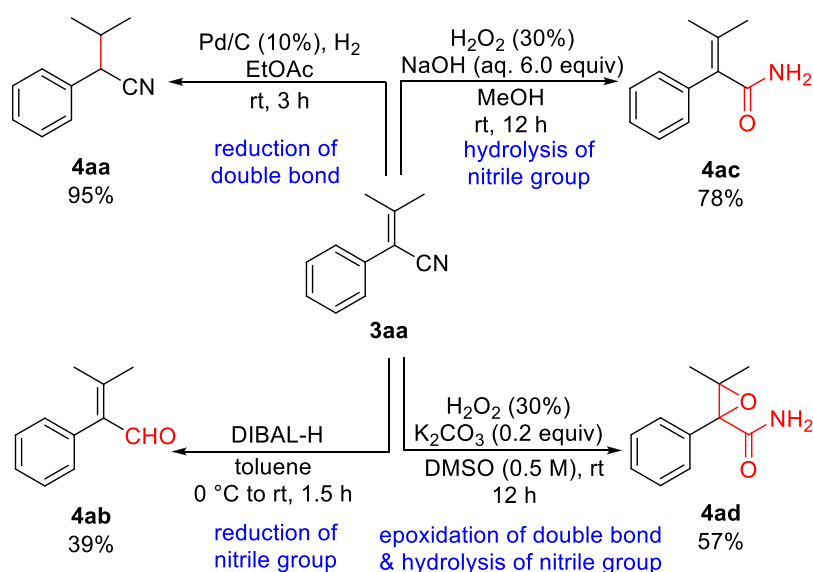
We next explored the scope of arylacetonitriles using sterically hindered bromomethylenecyclohexane **2d** as the model substrate. As shown in Table 3, in general, arylacetonitriles bearing electron-donating and electron-withdrawing Ar groups or heterocyclic rendered good to excellent yields under the standard conditions (Table 3). Arylacetonitriles possessing alkyl 4-Me (**1b**) and 2-Me (**1c**) reacted with bromomethylenecyclohexane **2d** to give aryl acrylonitriles **3bd** and **3cd** in 84% and 81% yields (69% and 63% yields for 5% Pd). Arylacetonitrile with electro-donating (4-OMe, **1d**) substituents provided product **3dd** in 67% yield.

Arylacetonitriles bearing electron-withdrawing 4-F (**1e**), 4-Cl (**1f**) and 4-Br (**1g**) generated the products **3ed**, **3fd** and **3gd** in 83% (78% yield for 5% Pd), 95% (79% yield for 5% Pd) and 50% yields, respectively. The sterically demanding 2-naphthyl acetonitrile (**1h**) was well tolerated, led to product **3hd** in 67% yield. Interesting, medicinally important heterocyclic-containing acetonitriles were suitable reaction partners. 2-(1-Methyl-1*H*-indol-3-yl)acetonitrile (**1i**) reacted with **2d** to generate the aryl acrylonitrile **3id** with excellent yield of 93% (79% yield for 5% Pd). 2-(Thiophen-2-yl)acetonitrile (**1j**) provided product **3jd** in 47% yield.

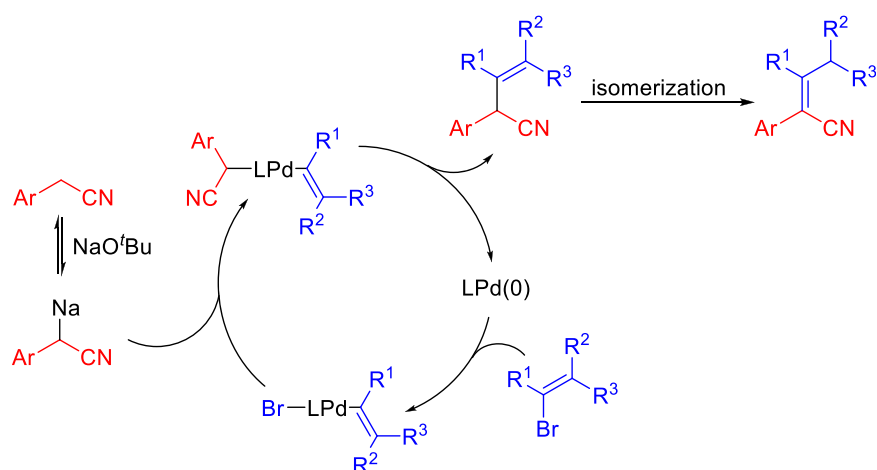
To evaluate the scalability of our transformation, we next carried out the reaction of phenylacetonitrile **1a** and 2-bromo-1-ene **2a** on a gram-scale under the optimal conditions (Scheme 2). The desired aryl acrylonitrile **3aa** was isolated in 1.03 g (70% yield), demonstrating the scalability of our method.

Finally, to illustrate further the synthetic versatility of the resulting aryl acrylonitrile, a series of derivatizations were performed on **3aa** (Scheme 3). Thus, the selective reduction of the carbon-carbon double bond of aryl acrylonitrile **3aa** using Pd/C and hydrogen led to the substituted saturated phenylacetonitrile **4aa** in 95% yield. Then, the selective reduction of the nitrile group of **3aa** employing DIBAL-H in toluene at 0°C generated the corresponding α,β -unsaturated aldehyde **4ab** in 39% yield (Chen et al., 2019). Meanwhile, the hydrolysis of the nitrile group of **3aa** using 30% H_2O_2 and NaOH in MeOH rendered the corresponding α,β -unsaturated amide **4ac** in 78% yield. Furthermore, the epoxidation of the carbon-carbon double bond and hydrolysis of the nitrile group of **3aa** using 30% H_2O_2 and K_2CO_3 in DMSO afforded the corresponding α,β -epoxy amide **4ad** in 57% yield.

A possible catalytic cycle is shown in Scheme 4 based on Walsh's work on the palladium-catalyzed deprotonative cross-coupling processes (Hussain et al., 2014; Jia et al., 2014; Mao et al., 2014; Jia et al., 2015). The deprotonation of aryl acetonitrile by NaO^tBu gives benzyl anions. After oxidative addition of the vinyl bromide to Pd (0), the vinyl palladium intermediate is proposed to bind the benzyl anions to form the palladium complex. Then, reductive elimination occurs to afford the



SCHEME 3
Derivatizations of aryl acrylonitrile **3aa**.



SCHEME 4
Plausible reaction mechanism.

enenitrile and regenerates Pd (0). Finally, enenitrile isomerizes to obtain aryl acrylonitrile.

Conclusion

In conclusion, we have successfully synthesized a series of aryl acrylonitrile derivatives employing a Pd/NIXANTPHOS-based catalyst system for the first time. In this protocol, commercially

available arylacetonitriles and vinyl bromides/chlorides/triflates underwent palladium-catalyzed α -alkenylation to furnish efficient access to a variety of substituted and functionalized aryl acrylonitriles. The scalability of the method was demonstrated by the gram-scale reaction. A series of derivatization of aryl acrylonitrile were performed, including the selective reduction of the double bond or nitrile group, the hydrolysis of the nitrile group, and the epoxidation of the double bond, which demonstrated the synthetic versatility of

aryl acrylonitrile. It is noteworthy that this approach does not require dangerous reagents and stoichiometric amount of oxidants, which enables the synthesis of a range of aryl acrylonitriles in an effective and straightforward means.

Data availability statement

The original contributions presented in the study are included in the article/Supplementary Material, further inquiries can be directed to the corresponding authors.

Author contributions

YJ and BW contributed equally to this work. XY conceived of the project. GD and XY supervised the project. DL, DX, ZL, and LL performed the research. GD and XY wrote the manuscript.

Funding

This work was supported by grants from the National Key R&D Program of China (2019YFE0109200), NSFC (21662043), NSF of Yunnan (202207AA110007, 202207AB110002), Yunnan Science and Technology Department and Yunnan University Joint Fund Project (2019FY003010), Ling-Jun Scholars Yunnan

Province (202005AB160003), Program for Xingdian Talents (Yun-Ling Scholars) and IRTSTYN.

Conflict of interest

The authors declare that the research was conducted in the absence of any commercial or financial relationships that could be construed as a potential conflict of interest.

The handling editor JD declared a past co-authorship with the author XY, YJ.

Publisher's note

All claims expressed in this article are solely those of the authors and do not necessarily represent those of their affiliated organizations, or those of the publisher, the editors and the reviewers. Any product that may be evaluated in this article, or claim that may be made by its manufacturer, is not guaranteed or endorsed by the publisher.

Supplementary material

The Supplementary Material for this article can be found online at: <https://www.frontiersin.org/articles/10.3389/fchem.2022.1091566/full#supplementary-material>

References

- Ahuja, B. B., and Sudalai, A. (2015). Cu-Catalyzed debrominative cyanation of gem-dibromoolefins: A facile access to α , β -unsaturated nitriles. *Org. Biomol. Chem.* 13, 5918–5923. doi:10.1039/c5ob00394f
- Alterman, M., and Hallberg, A. (2000). Fast microwave-assisted preparation of aryl and vinyl nitriles and the corresponding tetrazoles from organo-halides. *J. Org. Chem.* 65, 7984–7989. doi:10.1021/jo0009954
- Ando, K., Okumura, M., and Nagaya, S. (2013). Highly Z-selective synthesis of α , β -unsaturated nitriles using the Horner–Wadsworth–Emmons reaction. *Tetrahedron Lett.* 54, 2026–2028. doi:10.1016/j.tetlet.2013.02.020
- Baker, J. R., Gilbert, J., Paula, S., Zhu, X., Sakoff, J. A., and McCluskey, A. (2018). Dichlorophenylacrylonitriles as AhR ligands that display selective breast cancer cytotoxicity *in vitro*. *ChemMedChem* 13, 1447–1458. doi:10.1002/cmdc.201800256
- Baker, J. R., Russell, C. C., Gilbert, J., McCluskey, A., and Sakoff, J. A. (2021). Amino alcohol acrylonitriles as broad spectrum and tumour selective cytotoxic agents. *RSC Med. Chem.* 12, 929–942. doi:10.1039/d1md00021g
- Baker, J. R., Russell, C. C., Gilbert, J., Sakoff, J. A., and McCluskey, A. (2020). Amino alcohol acrylonitriles as activators of the aryl hydrocarbon receptor pathway: An unexpected MTT phenotypic screening outcome. *ChemMedChem* 15, 490–505. doi:10.1002/cmdc.201900643
- Carta, A., Briguglio, I., Piras, S., Boatto, G., La Colla, P., Loddo, R., et al. (2011). 3-Aryl-2-[1H-benzotriazol-1-yl]acrylonitriles: A novel class of potent tubulin inhibitors. *Eur. J. Med. Chem.* 46, 4151–4167. doi:10.1016/j.ejmech.2011.06.018
- Chaitanya, M., and Anbarasan, P. (2015). Rhodium-catalyzed cyanation of C(sp²)-H bond of alkenes. *Org. Lett.* 17, 3766–3769. doi:10.1021/acs.orglett.5b01746
- Chakraborty, S., Das, U. K., Ben-David, Y., and Milstein, D. (2017). Manganese catalyzed α -olefination of nitriles by primary alcohols. *J. Am. Chem. Soc.* 139, 11710–11713. doi:10.1021/jacs.7b06993
- Chen, L. L., Zhang, J. W., Chen, P., Zhang, S., Yang, W. W., Fu, J. Y., et al. (2019). Base-controlled divergent synthesis of 5-cyanobenzoxepines and benzofuro[2,3-b]pyridines from 2-bromophenylacetone nitriles and ynones. *Org. Lett.* 21, 5457–5461. doi:10.1021/acs.orglett.9b01700
- Cheng, Y., Duan, Z., Yu, L., Li, Z., Zhu, Y., and Wu, Y. (2008). Palladium-catalyzed three-component arylation of internal alkynes with aryl bromides and K₄[Fe(CN)₆]. *Org. Lett.* 10, 901–904. doi:10.1021/ol703018t
- Clercq, E. D. (2005). Emerging anti-HIV drugs. *Expert Opin. Emerg. Drugs* 10, 241–274. doi:10.1517/14728214.10.2.241
- Crowe, W. E., and Goldberg, D. R. (1995). Acrylonitrile cross-metathesis: Coaxing olefin metathesis reactivity from a reluctant substrate. *J. Am. Chem. Soc.* 117, 5162–5163. doi:10.1021/ja00123a023
- Del Fiandra, C., Moccia, M., Cerulli, V., and Adamo, M. F. (2016). Catalytic asymmetric conjugate addition of isocyanacetate to (Z)-3-substituted-2-(4-pyridyl)-acrylonitrile, a reactive class of Michael acceptor. *Chem. Commun.* 52, 1697–1700. doi:10.1039/c5cc08105j
- Duan, S., Li, M., Ma, X., Chen, W., Li, L., Zhang, H., et al. (2018). Palladium-catalyzed alkenylation of azaarylmethylamines with vinyl halides. *Adv. Synth. Catal.* 360, 4837–4842. doi:10.1002/adsc.201801045
- Fang, F., Li, Y., and Tian, S. K. (2011). Stereoselective olefination of N-sulfonyl imines with stabilized phosphonium ylides for the synthesis of electron-deficient alkenes. *Eur. J. Org. Chem.* 2011, 1084–1091. doi:10.1002/ejoc.201001379
- Fleming, F. F. (1999). Nitrile-containing natural products. *Nat. Prod. Rep.* 16, 597–606. doi:10.1039/A804370A
- Fleming, F. F., Yao, L., Ravikumar, P. C., Funk, L., and Shook, B. C. (2010). Nitrile-containing pharmaceuticals: Efficacious roles of the nitrile pharmacophore. *J. Med. Chem.* 53, 7902–7917. doi:10.1021/jm100762r

- Fringuelli, F., Pani, G., Piermatti, O., and Pizzo, F. (1994). Condensation reactions in water of active methylene compounds with arylaldehydes. One-pot synthesis of flavonols. *Tetrahedron* 50, 11499–11508. doi:10.1016/S0040-4020(01)89287-5
- Gao, D. W., Vinogradova, E. V., Nimmagadda, S. K., Medina, J. M., Xiao, Y., Suci, R. M., et al. (2018). Direct access to versatile electrophiles via catalytic oxidative cyanation of alkenes. *J. Am. Chem. Soc.* 140, 8069–8073. doi:10.1021/jacs.8b03704
- He, Y. T., Li, L. H., Wang, Q., Wu, W., and Liang, Y. M. (2016). Synthesis of β -difluoroalkylated acrylonitriles in the presence of copper powder. *Org. Lett.* 18, 5158–5161. doi:10.1021/acs.orglett.6b02627
- Hussain, N., Frensch, G., Zhang, J., and Walsh, P. J. (2014). Chemo- and regioselective C(sp³)-H arylation of unactivated allylarenes by deprotonative cross-coupling. *Angew. Chem. Int. Ed.* 53, 3693–3697. doi:10.1002/anie.201309084
- Jia, T., Bellomo, A., Montel, S., Zhang, M., El Baina, K., Zheng, B., et al. (2014). Diaryl sulfoxides from aryl benzyl sulfoxides: A single palladium-catalyzed triple relay process. *Angew. Chem. Int. Ed.* 53, 260–264. doi:10.1002/anie.201307172
- Jia, T., Zhang, M., Sagamanova, I. K., Wang, C. Y., and Walsh, P. J. (2015). Palladium catalyzed diaryl sulfoxide generation from aryl benzyl sulfoxides and aryl chlorides. *Org. Lett.* 17, 1168–1171. doi:10.1021/acs.orglett.5b00092
- Jiao, N., Zhou, W., Xu, J., and Zhang, L. (2011). An efficient approach to alkenyl nitriles from allyl esters. *Synlett* 2011, 887–890. doi:10.1055/s-0030-1259719
- Kojima, S., Fukuzaki, T., Yamakawa, A., and Murai, Y. (2004). Highly (Z)-selective synthesis of β -monosubstituted- α , β -unsaturated cyanides using the Peterson reaction. *Org. Lett.* 6, 3917–3920. doi:10.1021/ol0486728
- Kojima, S., Kawaguchi, K., Matsukawa, S., Uchida, K., and Akiba, K.-y. (2002). Highly Z-selective synthesis of disubstituted α , β -unsaturated cyanides and amides using 10-P-5 Wittig type reagents. *Chem. Lett.* 31, 170–171. doi:10.1246/cl.2002.170
- Laulhe, S., Gori, S. S., and Nantz, M. H. (2012). A chemoselective, one-pot transformation of aldehydes to nitriles. *J. Org. Chem.* 77, 9334–9337. doi:10.1021/jo301133y
- Liu, Z., Li, M., Wang, B., Deng, G., Chen, W., Kim, B.-S., et al. (2018). Chemoselective synthesis of aryl(pyridinyl)methanol derivatives through NiXANTPHOS catalyzed α -arylation and tandem arylation/rearrangement of pyridylmethyl ethers. *Org. Chem. Front.* 5, 1870–1876. doi:10.1039/c8qo00207j
- Mao, J., Jia, T., Frensch, G., and Walsh, P. J. (2014). Palladium-catalyzed debenzylative cross-coupling of aryl benzyl sulfides with aryl bromides: Synthesis of diaryl sulfides. *Org. Lett.* 16, 5304–5307. doi:10.1021/ol502470e
- Minami, Y., Yoshiyasu, H., Nakao, Y., and Hiyama, T. (2013). Highly chemoselective carbon-carbon sigma-bond activation: Nickel/Lewis acid catalyzed polyfluoroarylcyanation of alkynes. *Angew. Chem. Int. Ed.* 52, 883–887. doi:10.1002/anie.201207880
- Mu, Y., Nguyen, T. T., Koh, M. J., Schrock, R. R., and Hoveyda, A. H. (2019). E- and Z-di- and tri-substituted alkenyl nitriles through catalytic cross-metathesis. *Nat. Chem.* 11, 478–487. doi:10.1038/s41557-019-0233-x
- Nakao, Y., Yada, A., Ebata, S., and Hiyama, T. (2007). A dramatic effect of Lewis acid catalysts on nickel-catalyzed carbocyanation of alkynes. *J. Am. Chem. Soc.* 129, 2428–2429. doi:10.1021/ja067364x
- Niu, G., Zheng, X., Zhao, Z., Zhang, H., Wang, J., He, X., et al. (2019). Functionalized acrylonitriles with aggregation-induced emission: Structure tuning by simple reaction-condition variation, efficient red emission, and two-photon bioimaging. *J. Am. Chem. Soc.* 141, 15111–15120. doi:10.1021/jacs.9b06196
- Oishi, T., Yamaguchi, K., and Mizuno, N. (2009). Catalytic oxidative synthesis of nitriles directly from primary alcohols and ammonia. *Angew. Chem. Int. Ed.* 48, 6286–6288. doi:10.1002/anie.200900418
- Palomo, C., Aiipurua, J. M., and Aurrekoetxea, N. (1990). A stereoselective synthesis of cis-alkenenitriles through Reformatsky-Peterson reaction. *Tetrahedron Lett.* 31, 2209–2210. doi:10.1016/0040-4039(90)80110-8
- Palomo, C., Aizpurua, J. M., Garcia, J. M., Ganboa, I., Cossio, F. P., Lecea, B., et al. (1990). A new version of the Peterson Olefination using bis(trimethylsilyl)methyl derivatives and fluoride ion as catalyst. *J. Org. Chem.* 55, 2498–2503. doi:10.1021/jo00295a047
- Pradal, A., and Evano, G. (2014). A vinylic Rosenmund-von Braun reaction: Practical synthesis of acrylonitriles. *Chem. Commun.* 50, 11907–11910. doi:10.1039/c4cc05557h
- Qi, C., Peng, Y., Ouyang, L., Ren, Y., and Jiang, H. (2017). Base-promoted addition of arylacetonitriles to terminal alkynes: Regio- and stereoselective access to disubstituted acrylonitriles. *Adv. Synth. Catal.* 359, 1339–1350. doi:10.1002/adsc.201601024
- Qin, C., and Jiao, N. (2010). Iron-facilitated direct oxidative C-H transformation of allylarenes or alkenes to alkenyl nitriles. *J. Am. Chem. Soc.* 132, 15893–15895. doi:10.1021/ja1070202
- Randl, S., Gessler, S., Wakamatsu, H., and Blechert, S. (2001). ChemInform abstract: Highly selective cross metathesis with acrylonitrile using a phosphine free Ru-complex. *ChemInform* 32, 430–432. doi:10.1002/CHIN.200128080
- Rokade, B. V., Malekar, S. K., and Prabhu, K. R. (2012). A novel oxidative transformation of alcohols to nitriles: An efficient utility of azides as a nitrogen source. *Chem. Commun.* 48, 5506–5508. doi:10.1039/c2cc31256e
- Seeberger, L. C., and Hauser, R. A. (2009). Levodopa/carbidopa/entacapone in Parkinson's disease. *Expert Rev. Neurother.* 9, 929–940. doi:10.1586/ern.09.64
- Shen, Y., Zificsak, C. A., Shea, J. E., Lao, X., Bollt, O., Li, X., et al. (2015). Design, synthesis, and biological evaluation of sulfonyl acrylonitriles as novel inhibitors of cancer metastasis and spread. *J. Med. Chem.* 58, 1140–1158. doi:10.1021/jm501437v
- Sirim, M. M., Krishna, V. S., Sriram, D., and Unsal Tan, O. (2020). Novel benzimidazole-acrylonitrile hybrids and their derivatives: Design, synthesis and antimycobacterial activity. *Eur. J. Med. Chem.* 188, 112010. doi:10.1016/j.ejmech.2019.112010
- Solangi, M., Kanwal, Khan, K. M., Saleem, F., Hameed, S., Iqbal, J., et al. (2020). Indole acrylonitriles as potential anti-hyperglycemic agents: Synthesis, α -glucosidase inhibitory activity and molecular docking studies. *Bioorg. Med. Chem.* 28, 115605. doi:10.1016/j.bmc.2020.115605
- Stuhl, L. S. (1985). Reaction of [Co(CN)₅]³⁻ with alkenyl halides in an aprotic medium. *J. Org. Chem.* 50, 3934–3936. doi:10.1021/jo00220a055
- Tarleton, M., Gilbert, J., Robertson, M. J., McCluskey, A., and Sakoff, J. A. (2011). Library synthesis and cytotoxicity of a family of 2-phenylacrylonitriles and discovery of an estrogen dependent breast cancer lead compound. *Med. Chem. Commun.* 2, 31–37. doi:10.1039/c0md00147c
- Thiyagarajan, S., and Gunanathan, C. (2018). Ruthenium-catalyzed α -olefination of nitriles using secondary alcohols. *ACS Catal.* 8, 2473–2478. doi:10.1021/acscatal.7b04013
- Tomioka, T., Sankranti, R., Vaughan, T. G., Maejima, T., and Yanase, T. (2011). An α -diaminoboryl carbanion assisted stereoselective single-pot preparation of α , β -disubstituted acrylonitriles. *J. Org. Chem.* 76, 8053–8058. doi:10.1021/jo201280x
- Wang, T., and Jiao, N. (2014). Direct approaches to nitriles via highly efficient nitrogenation strategy through C-H or C-C bond cleavage. *Acc. Chem. Res.* 47, 1137–1145. doi:10.1021/ar400259e
- Wu, Q., Luo, Y., Lei, A., and You, J. (2016). Aerobic copper-promoted radical-type cleavage of coordinated cyanide anion: Nitrogen transfer to aldehydes to form nitriles. *J. Am. Chem. Soc.* 138, 2885–2888. doi:10.1021/jacs.5b10945
- Yadav, V., Landge, V. G., Subaramanian, M., and Balaraman, E. (2020). Manganese-catalyzed α -olefination of nitriles with secondary alcohols. *ACS Catal.* 10, 947–954. doi:10.1021/acscatal.9b02811
- Yamaguchi, K., Fujiwara, H., Ogasawara, Y., Kotani, M., and Mizuno, N. (2007). A tungsten-tin mixed hydroxide as an efficient heterogeneous catalyst for dehydration of aldioximes to nitriles. *Angew. Chem. Int. Ed.* 46, 3922–3925. doi:10.1002/anie.200605004
- Yang, J., Li, H., Qin, J., Song, F., Zhang, J., Qing, F.-L., et al. (2018). Ligand-accelerated, branch-selective oxidative cyanation of alkenes. *Sci. Bull. (Beijing)* 63, 1479–1484. doi:10.1016/j.scib.2018.09.005
- Yang, X., Arai, S., and Nishida, A. (2013). Catalytic cyanation of carbon-carbon triple bonds through a three-component cross-coupling reaction under nickel catalysis. *Adv. Synth. Catal.* 355, 2974–2981. doi:10.1002/adsc.201300553
- Yang, X., Kim, B. S., Li, M., and Walsh, P. J. (2016). Palladium-catalyzed selective α -alkenylation of pyridylmethyl ethers with vinyl bromides. *Org. Lett.* 18, 2371–2374. doi:10.1021/acs.orglett.6b00815
- Zhang, J., Bellomo, A., Trongsiwat, N., Jia, T., Carroll, P. J., Spencer, D., et al. (2014). NiXantphos: A deprotonatable ligand for room-temperature palladium-catalyzed cross-couplings of aryl chlorides. *J. Am. Chem. Soc.* 136, 6276–6287. doi:10.1021/ja411855d
- Zhang, L. H., Wu, L., Raymon, H. K., Chen, R. S., Corral, L., Shirley, M. A., et al. (2006). The synthetic compound CC-5079 is a potent inhibitor of tubulin polymerization and tumor necrosis factor- α production with antitumor activity. *Cancer Res.* 66, 951–959. doi:10.1158/0008-5472.CAN-05-2083

Zhang, T. Y., O'Toole, J. C., and Dunigan, J. M. (1998). An efficient and practical synthesis of diphenyl cyanomethylenephosphonate: Applications to the stereoselective synthesis of *cis*- α , β -unsaturated nitriles. *Tetrahedron Lett.* 39, 1461–1464. doi:10.1016/S0040-4039(97)10836-X

Zhang, X., Xie, X., and Liu, Y. (2018). Nickel-catalyzed highly regioselective hydrocyanation of terminal alkynes with $\text{Zn}(\text{CN})_2$ using water as the hydrogen source. *J. Am. Chem. Soc.* 140, 7385–7389. doi:10.1021/jacs.8b02542

Zhang, Z., and Liebeskind, L. S. (2006). Palladium-catalyzed, copper(I)-mediated coupling of boronic acids and benzylthiocyanate. A cyanide-free cyanation of boronic acids. *Org. Lett.* 8, 4331–4333. doi:10.1021/ol061741t

Zhou, S., Addis, D., Das, S., Junge, K., and Beller, M. (2009). New catalytic properties of iron complexes: Dehydration of amides to nitriles. *Chem. Commun.* 32, 4883–4885. doi:10.1039/b910145d

Zhou, W., Xu, J., Zhang, L., and Jiao, N. (2010). An efficient transformation from benzyl or allyl halides to aryl and alkenyl nitriles. *Org. Lett.* 12, 2888–2891. doi:10.1021/ol101094u

Zou, G., Wang, Z., Zhu, J., and Tang, J. (2003). Rhodium-catalyzed heck-type reaction of arylboronic acids with α , β -unsaturated esters: Tuning β -hydrogen elimination vs. hydrolysis of alkylrhodium species. *Chem. Commun.* 9, 2438–2439. doi:10.1039/b305771m



OPEN ACCESS

EDITED BY

Anton V. Dolzhenko,
Monash University, Australia

REVIEWED BY

Hoda Hamidi,
Alzahra University, Iran
Zhixiang Xie,
Lanzhou University, China

*CORRESPONDENCE

Wen Chen,
✉ wenchen@ynu.edu.cn
Hongbin Zhang,
✉ zhanghb@ynu.edu.cn

[†]These authors have contributed equally
to this work

SPECIALTY SECTION

This article was submitted to Medicinal
and Pharmaceutical Chemistry,
a section of the journal
Frontiers in Chemistry

RECEIVED 20 November 2022

ACCEPTED 09 December 2022

PUBLISHED 22 December 2022

CITATION

Wei K, Sun Y, Xu Y, Hu W, Ma Y, Lu Y,
Chen W and Zhang H (2022), Total
synthesis of justicidin B, justicidin E, and
taiwanin C: A general and flexible
approach toward the synthesis of
natural aryl-naphthalene lactone lignans.
Front. Chem. 10:1103554.
doi: 10.3389/fchem.2022.1103554

COPYRIGHT

© 2022 Wei, Sun, Xu, Hu, Ma, Lu, Chen
and Zhang. This is an open-access
article distributed under the terms of the
Creative Commons Attribution License
(CC BY). The use, distribution or
reproduction in other forums is
permitted, provided the original
author(s) and the copyright owner(s) are
credited and that the original
publication in this journal is cited, in
accordance with accepted academic
practice. No use, distribution or
reproduction is permitted which does
not comply with these terms.

Total synthesis of justicidin B, justicidin E, and taiwanin C: A general and flexible approach toward the synthesis of natural aryl-naphthalene lactone lignans

Kai Wei^{1,2†}, Yucui Sun^{1†}, Yiren Xu^{1†}, Wen Hu¹, Ying Ma¹, Yi Lu¹,
Wen Chen^{1*} and Hongbin Zhang^{1*}

¹Key Laboratory of Medicinal Chemistry for Natural Resource, Ministry of Education, Yunnan Provincial Center for Research and Development of Natural Products, Yunnan Characteristic Plant Extraction Laboratory, School of Pharmacy, Yunnan University, Kunming, China, ²Henan Engineering Research Center of Funiu Mountain's Medical Resources Utilization and Molecular Medicine, School of Medical Sciences, Pingdingshan University, Pingdingshan, China

Lignans are widely present in traditional medicinal plants. Many natural aryl-naphthalene lactone lignans (NALLs) isolated from the genera *Justicia*, *Haplophyllum*, and *Phyllanthus* possess interesting biological activities. Herein, we report a general strategy for the total synthesis of this kind of lignans. Features of this new approach are an aryl-alkyl Suzuki cross-coupling to introduce the dioxinone unit, a cation-induced cyclization to construct the aryl dihydronaphthalene, and base-mediated oxidative aromatization to furnish the aryl-naphthalene core. By incorporating these key transformations, the total syntheses of justicidins B and E and taiwanin C covered type I and type II NALLs were accomplished.

KEYWORDS

total synthesis, natural products, aryl-naphthalene lactone lignans, Suzuki cross-coupling, cation-induced cyclization

1 Introduction

Natural aryl-naphthalene lactone lignans (NALLs) are widely isolated from the plant family *Acanthaceae* (Day et al., 1999; Shen et al., 2004; Zhang et al., 2007; Jin et al., 2014; Jiang et al., 2017; Jin et al., 2017; Lv et al., 2021; Liu et al., 2022), *Euphorbiaceae* (Anjaneyulu et al., 1981; Wu et al., 2006) and *Rutaceae* (Gözler et al., 1984; Sheriha et al., 1984; Hesse et al., 1992; Ulubelen et al., 1994; Gözler et al., 1996), especially from the genera *Justicia*, *Haplophyllum*, and *Phyllanthus*. Many of these lignans possess a broad range of biological activities, including antimicrobial (Kawazoe et al., 2001), antifungal (Ashraf et al., 1995), anti-cancer (Wang et al., 2019), antiplatelet (Chen et al., 1996; Weng et al., 2004), antiprotozoal (Gertsch et al., 2003), antitumorigenic (Hajdu et al., 2014), antiviral (Sagar et al., 2004; Yeo et al., 2005; Janmanchi et al., 2010), cytotoxic (Day et al., 2002; Chang et al., 2003; Susplugas et al., 2005; Vasilev et al., 2006), and neuroprotective

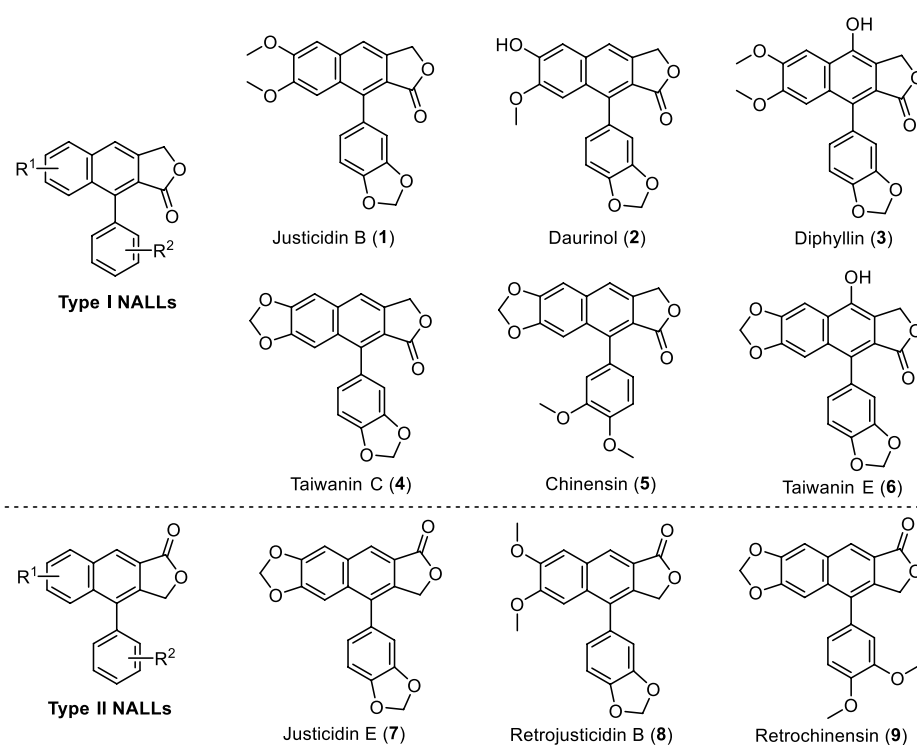


FIGURE 1
Representative NALLs.

activities (Chun et al., 2017) in cell-based assays or animal models. For instance, justicidin B exhibits powerful antimicrobial activity (El-Gendy et al., 2008) and inhibitory activity against the Sindbis virus (Charlton, 1998). Meanwhile, taiwanin C exhibits important antiplatelet activity (Daron et al., 2022) and was found to be a potent COX inhibitor (Ban et al., 2002). Some representative natural aryl-naphthalene lactone lignans (1–9) are shown in Figure 1.

Because of their important pharmacological properties, NALLs have attracted attention from the organic synthetic community since the pioneering synthetic work on these lignans in 1895 by Michael et al. (1895). Synthetic efforts have resulted in many impressive approaches toward these highly substituted 1-arylnaphthalenes and culminated in the total synthesis of a series of aryl-naphthalene lactone-type lignans (Chen et al., 2018; Zhao et al., 2018; Park et al., 2020). Methodologies for the construction of 1-arylnaphthalenes could be roughly classified into five categories: Diels–Alder type cycloaddition (Brown et al., 1964; Holmes et al., 1971; Klemm et al., 1971; Takano et al., 1985; Stevenson et al., 1989; Padwa et al., 1996; Xiong et al., 2012; Kudoh et al., 2013; Kocsis et al., 2014; Park et al., 2014; Meng et al., 2016), benzannulation (Ogiku et al., 1995; Flanagan et al., 2002; Nishii et al., 2005; Ishikawa et al., 2021; Moriguchi et al., 2021), Garratt–Braverman-type cyclization (Mondal et al., 2011; Mondal et al., 2012), transition metal-

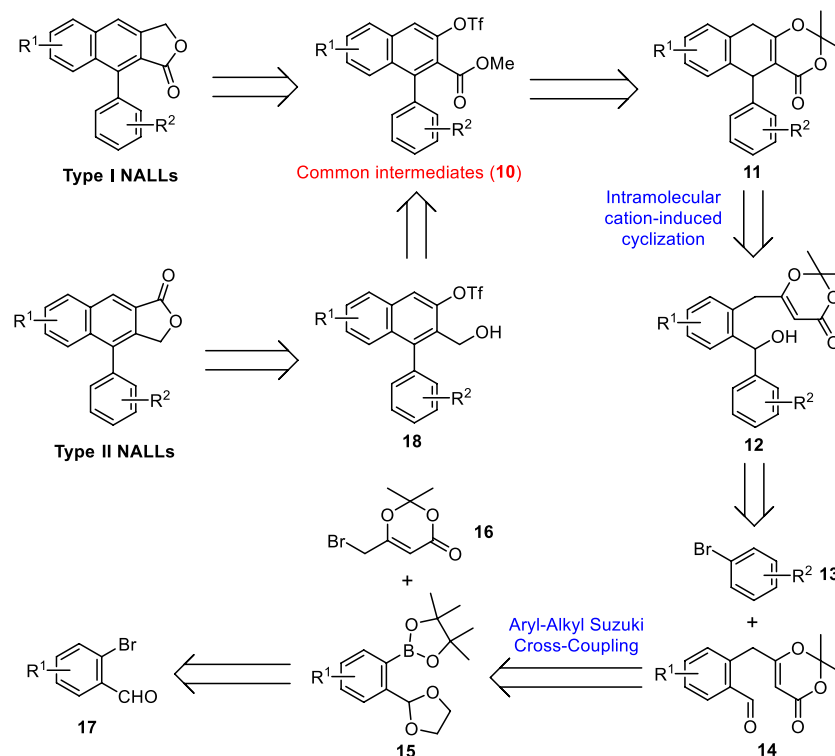
mediated cyclization (Murakami et al., 1998; Mizufune et al., 2001; Sato et al., 2004; Sato et al., 2007; Gudla et al., 2011; Patel et al., 2013; Wong et al., 2014; Kao et al., 2015; Naresh et al., 2015; Xiao et al., 2018), and other type of annulations (Ogiku et al., 1990; Kamal et al., 1994; Ogiku et al., 1995; Harrowven et al., 2001; Foley et al., 2010; He et al., 2014; Hayat et al., 2015; Yamamoto et al., 2015).

Inspired by these well-designed processes and our previous efforts on cation-induced cyclization (Chen et al., 2017; Chen et al., 2019; Wei et al., 2021; Chen et al., 2022; Li et al., 2022), we recently developed an intramolecular cation-induced reaction to synthesize the highly substituted 1-aryl dihydronaphthalene unit, an advanced precursor of natural aryl-naphthalene lactone lignans. In this paper, we report a general and flexible strategy toward the synthesis of justicidin E (type II NALLs), justicidin B, and taiwanin C (type I NALLs) based on this efficient cation-induced cyclization.

2 Results and discussion

2.1 Retrosynthetic analysis

Our retrosynthetic analysis for both type I and type II NALLs is shown in Scheme 1. Type I NALLs could be achieved



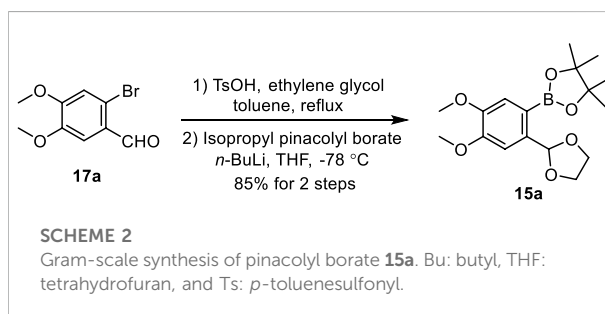
SCHEME 1

Retrosynthetic analysis for both type I and II NALLs.

by a Stille cross-coupling between common intermediates (**10**) and tributylstannyl methanol followed by lactonization (Zhang et al., 2019). Type II NALLs could be accessed *via* carbonylative lactonization (Crisp et al., 1995) of triflate **18**, which could be obtained *via* a reduction from common intermediates (**10**). Ring opening of dioxinone **11** followed by subsequent base-mediated oxidation (Zhao et al., 2020) and triflation would lead to methyl ester **10**. Dihydronaphthalene **11** could be accessed through the intramolecular cation-induced cyclization of alcohol **12**, which could be prepared by a selective nucleophilic addition of aryl lithium generated *in situ* from aryl bromide **13** to aldehyde **14**. Aldehyde **14** was expected to be formed by an aryl-alkyl Suzuki cross-coupling between pinacolyl borate **15** and commercially available alkyl bromide **16** followed by a deprotection of the ketal moiety. Borate **15** could be obtained from commercially available bromide **17** *via* functional group protection, halogen-lithium exchange reaction, and borylation.

2.2 Total synthesis of justicidin B

We chose justicidin B, a type I NALL, as the first target of our synthetic journey. Our synthesis began with the preparation of

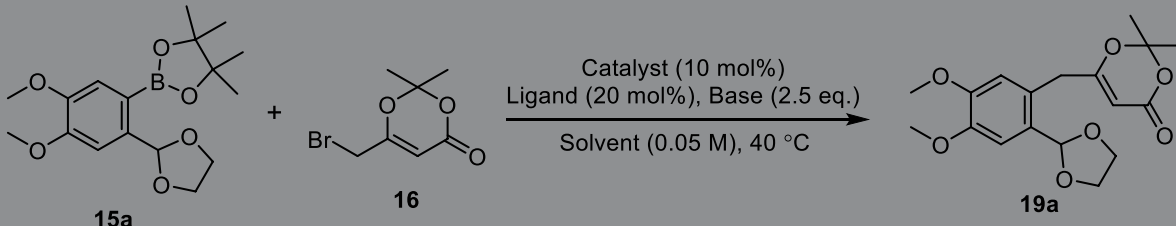


SCHEME 2

Gram-scale synthesis of pinacolyl borate **15a**. Bu: butyl, THF: tetrahydrofuran, and Ts: *p*-toluenesulfonyl.

pinacolyl borate **15a** (Scheme 2). Treatment of commercially available bromo-aldehyde **17a** with ethylene glycol provided its acetal, after subsequent halogen-lithium exchange by exposing it with *n*-butyllithium followed by borylation (Nagaki et al., 2012) provided **15a** in 85% yield.

With pinacolyl borate in hand, we next explored aryl-alkyl Suzuki cross-coupling between borate **15a** and commercially available alkyl bromide **16** (Table 1). Although numerous conditions for Suzuki cross-coupling reactions between alkyl halide and aryl boric acid or borate have been developed, using alkyl bromide **16** as a coupling partner to accomplish this cross-coupling reaction is still challenging due to the

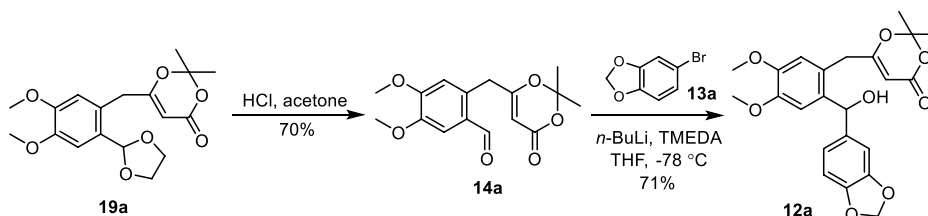
TABLE 1 Optimization for the aryl-alkyl Suzuki cross-coupling^a.


Entry	Catalyst	Ligand	Base	Solvent	Yield [%] ^b
1	Pd(PPh ₃) ₄	-	K ₃ PO ₄	1,4-Dioxane	Trace
2	Pd(OAc) ₂	PPh ₃	K ₃ PO ₄	1,4-Dioxane	2
3	Pd(dppf)Cl ₂	PPh ₃	K ₃ PO ₄	1,4-Dioxane	3
4	Pd ₂ (dba) ₃	PPh ₃	K ₃ PO ₄	1,4-Dioxane	4
5	Pd(dba) ₂	PPh ₃	K ₃ PO ₄	1,4-Dioxane	8
6	Pd(dba) ₂	PPh ₃	K ₂ CO ₃	1,4-Dioxane	3
7	Pd(dba) ₂	PPh ₃	Na ₂ CO ₃	1,4-Dioxane	0
8	Pd(dba) ₂	PPh ₃	Cs ₂ CO ₃	1,4-Dioxane	5
9	Pd(dba) ₂	PPh ₃	KOAc	1,4-Dioxane	2
10	Pd(dba) ₂	<i>t</i> -Bu ₃ P	K ₃ PO ₄	1,4-Dioxane	20
11	Pd(dba) ₂	PCy ₃	K ₃ PO ₄	1,4-Dioxane	26
12	Pd(dba) ₂	X-Phos	K ₃ PO ₄	1,4-Dioxane	Trace
13	Pd(dba) ₂	S-Phos	K ₃ PO ₄	1,4-Dioxane	51
14	Pd(dba) ₂	S-Phos	K ₃ PO ₄	DMF	Trace
15	Pd(dba) ₂	S-Phos	K ₃ PO ₄	THF	71
16	Pd(dba) ₂	S-Phos	K ₃ PO ₄	CPME	51
17	Pd(dba) ₂	S-Phos	K ₃ PO ₄	TBME	63
18	Pd(dba) ₂	S-Phos	K ₃ PO ₄	DME	77

^aThe reactions were performed with **15a** (0.2 mmol), **16** (0.26 mmol), catalyst (10 mol%), ligand (20 mol%), base (2.5 eq.), and solvent (3 ml) at 40°C for 7 h.

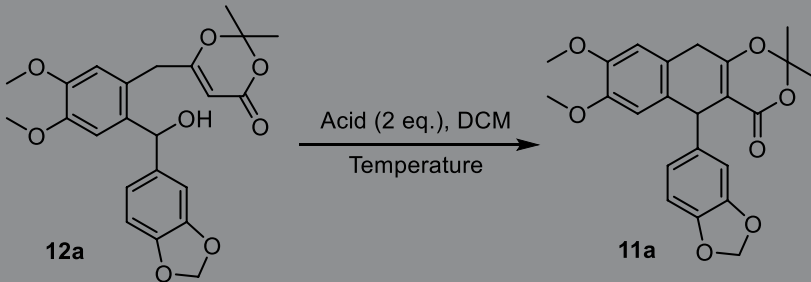
^bYields represent isolated yields. Ac: acetyl, Bu: butyl, CPME: cyclopentyl methyl ether, Cy: cyclohexyl, dba: dibenzylideneacetone, DME: 1,2-dimethoxyethane, DMF:

N,N-dimethylformamide, dppf: 1,1'-bis(diphenylphosphino)ferrocene, Ph: phenyl, S-Phos 2-dicyclohexylphosphino-2',6'-dimethoxybiphenyl, TBME: *tert*-butyl methyl ether, X-Phos 2-(dicyclohexylphosphino)-2',4',6'-tri-*i*-propyl-1,1'-biphenyl.

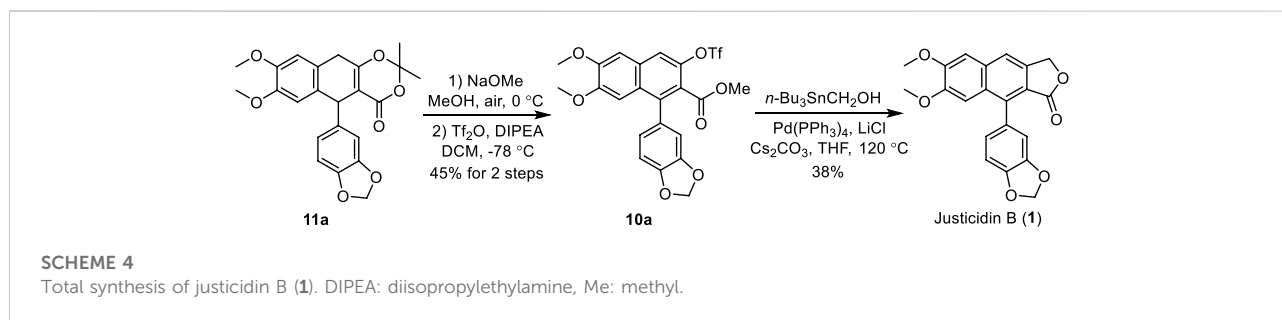


SCHEME 3

Synthesis of benzhydrol **12a**. TMEDA: *N,N,N',N'*-tetramethylethylenediamine.

TABLE 2 Optimization for the intramolecular cation-induced cyclization^a.


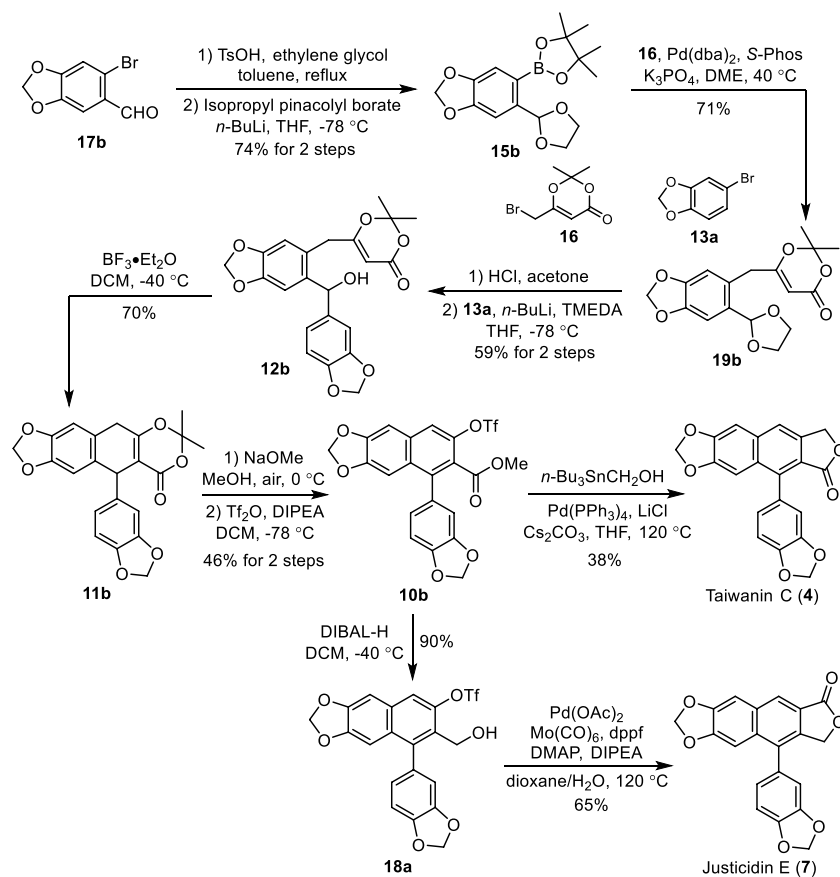
Entry	Acid	Temperature [°C]	Yield [%] ^b
1	TfOH	0	Trace
2	TFA	0	40
3	CSA	0	19
4	TsOH	0	43
5	TMSCl	0	46
6	BF ₃ ·Et ₂ O	0	50
7	BF ₃ ·Et ₂ O	-30	60
8	BF ₃ ·Et ₂ O	-40	69
9	BF ₃ ·Et ₂ O	-50	61
10	BF ₃ ·Et ₂ O	-40	68 ^c

^aThe reactions were performed with **12a** (0.2 mmol), acid (2.0 eq.), and solvent (3 ml) for 3 h.^bYields represent isolated yields.^cThe reaction was conducted at a 2.1-mmol scale. CSA: camphorsulfonic acid, DCM: dichloromethane, Et: ethyl, and TFA: trifluoroacetic acid.

thermosensitive and base-sensitive dioxinone unit present in substrate **16** (Reber et al., 2009; Katsuki et al., 2017).

In order to optimize the yield of this cross-coupling reaction, a systematic screening of reaction conditions was conducted (Table 1). Initially, we used the regular catalyst Pd(PPh₃)₄ employed in Suzuki cross-coupling (Miyaura et al., 1979). Not surprisingly, Pd(PPh₃)₄ was completely ineffective for the desired cross-coupling (Table 1, entry 1). Reactions were then conducted at a 0.2-mmol scale with several commercially available palladium catalysts (10 mol%) in the presence of PPh₃ (20 mol%) and K₃PO₄ in 1,4-dioxane (Table 1, entries 2–5). We found that Pd(dba)₂ served as an efficient Pd source

for this coupling process (Table 1, entry 5). Next, the bases were screened, and the yield of the desired product **19a** was not increased with a number of bases (Table 1, entries 5–9). A number of ligands were then used. We found that a ligand has a significant impact on the efficiency of this cross-coupling reaction (Table 1, entries 9–13). When the S-Phos ligand was used, the desired product **19a** could be obtained with 51% yield (Table 1, entry 9). With the catalytic system in hand, we next screened the solvents, and DME gave the best results (Table 1, entries 13–18). Finally, the optimum reaction conditions for this coupling reaction (Table 1, entry 18) were established.



SCHEME 5

Total synthesis of taiwanin C (4) and justicidin E (7). DMAP: 4-dimethylaminopyridine, dppf: 1,1'-bis(diphenylphosphino)ferrocene.

Next, the acetal protecting group of compound **19a** was removed with HCl in acetone to produce aldehyde **14a** (Scheme 3). The treatment of **13a** with *n*-BuLi followed by the addition of aldehyde **14a** unfortunately failed to yield the desired benzhydrol **12a**. To promote the desired reaction, a number of additives were used including hexamethylphosphoric acid triamide (HMPA), *N,N*-dimethyl propylene urea (DMPU), and *N,N,N',N'*-tetramethylethylenediamine (TMEDA). The addition of TMEDA provided benzhydrol **12a** at 71% yield.

With benzhydrol **12a** in hand, we next focused on the proposed cation-induced cyclization (Table 2). A number of Brønsted acids and Lewis acids (Table 2, entries 1–6) were used. Although the cyclization could be promoted by Brønsted acids, BF₃•Et₂O provided the best yield (Table 2, entry 6). The yield of the targeted product could be further improved when the reaction was conducted at a lower temperature (Table 2, entry 8). This cation-induced cyclization could be scaled up to 2.1 mmol (Table 2, entry 8, 0.90 g, and 68% yield).

Having established the procedure for advanced intermediate **11a**, research focus was then directed toward the total synthesis of justicidin B (**1**). The treatment of **11a** with sodium methoxide in MeOH under air followed by the addition of Tf₂O and DIPEA in DCM produced the first common intermediate **10a** in 45% yield (Scheme 4). It is noteworthy that an oxidative (by air) aromatization occurred under strong basic conditions. Next, a Pd-catalyzed Stille cross-coupling of triflate **10a** with tributylstannyl methanol in the presence of Pd(PPh₃)₄, Cs₂CO₃, and LiCl followed by spontaneous lactonization provided natural justicidin B (Zhang et al., 2019). The NMR spectra of our synthetic sample were in full agreement with those reported in the literature (Okigawa et al., 1970; Borges et al., 2018).

2.3 Total synthesis of taiwanin C and justicidin E

To demonstrate the generality and flexibility of our strategy, the total syntheses of naturally occurring arynaphthalene lignans taiwanin C (type I) and justicidin E (type II) were conducted

accordingly. Treatment of commercially available piperonyl bromide **17b** with ethylene glycol in the presence of TsOH followed by a halogen–lithium exchange and borylation afforded the pinacolyl borate **15b** in 74% yield (Scheme 5). Suzuki cross-coupling of bromide **16** with **15b** under the optimum reaction conditions afforded the corresponding dioxinone **19b**. Deprotection of the acetal of **19b** with HCl in acetone followed by a selective 1,2-addition with the 3,4-methylenedioxyphenyllithium, which was generated *in situ* from the halogen–lithium exchange between bromide **13a** and *n*-BuLi, yielded the benzhydrol **12b** in 59% for two steps.

Aryl dihydronaphthalene **11b** was obtained successfully in 70% yield through our intramolecular cation-induced cyclization from benzhydrol **12b**. The treatment of **11b** with NaOMe in MeOH under air followed by triflation with Tf₂O afforded the common intermediate **10b** in 46% yield for two steps. Reaction of **10b** with tributylstannyl methanol in the presence of Pd(PPh₃)₄, Cs₂CO₃, and LiCl produced the natural taiwanin C (**4**). Reduction of **10b** with DIBAL-H provided the alcohol **18a** in 90% yield. Natural justicidin E (**7**) was furnished in 38% isolated yield *via* an improved Pd-catalyzed carbonylative lactonization of triflate **18a** with Co(CO)₆. The NMR spectra of these two synthetic samples agree well with the reported literature (Anjaneyulu et al., 1981; Subbaraju et al., 1996; Flanagan et al., 2002).

3 Conclusion

We have developed a general and flexible strategy for the synthesis of justicidin B, taiwanin C, and justicidin E from commercially available materials. Key transformations to the success of the synthesis were an aryl–alkyl Suzuki cross-coupling, an intramolecular cation-induced cyclization, and a base-mediated oxidative aromatization. Our new approach paves the way toward the synthesis of biologically active natural aryl-naphthalene lactone lignans and could be used for the preparation of their analogues.

Data availability statement

The raw data supporting the conclusions of this article will be made available by the authors, without undue reservation.

References

- Anjaneyulu, A. S. R., Ramaiah, P. A., Row, L. R., Venkateswarlu, R., Pelter, A., and Ward, R. S. (1981). New lignans from the heartwood of *Cleistanthus collinus*. *Tetrahedron* 37, 3641–3652. doi:10.1016/S0040-4020(01)98893-3
- Atta-ur-Rahman, Ashraf, M., Choudhary, M. I., Habib-ur-Rehman and Kazmi, M. H. (1995). Antifungal aryltetralin lignans from leaves of *Podophyllum hexandrum*. *Phytochemistry* 40 (2), 427–431. doi:10.1016/0031-9422(95)00195-D

Author contributions

HZ conceived the synthetic design. WC and HZ supervised the project. KW, YS, YX, WH, YM, and YL conducted the experimental work and data analysis. WC and HZ wrote the manuscript.

Funding

This work was supported by grants from the Natural Science Foundation of China (U1702286, 21901224, 22261054, and 22271247), the Program for Changjiang Scholars and Innovative Research Team in University (IRT17R94), Ling-Jun Scholars of Yunnan Province (202005AB160003), YunLing Scholar Programs, Yunnan Fundamental Research Projects (202201AT070141 and 2019FI018), the Talent Plan of Yunnan Province (YNWR-QNBJ-2018-025), the Project of Yunnan Characteristic Plant Screening and R&D Service CXO Platform (2022YKZY001), and the National Key Research and Development Program of China (2019YFE0109200).

Conflict of interest

The authors declare that the research was conducted in the absence of any commercial or financial relationships that could be construed as a potential conflict of interest.

Publisher's note

All claims expressed in this article are solely those of the authors and do not necessarily represent those of their affiliated organizations, or those of the publisher, the editors, and the reviewers. Any product that may be evaluated in this article, or claim that may be made by its manufacturer, is not guaranteed or endorsed by the publisher.

Supplementary material

The Supplementary Material for this article can be found online at: <https://www.frontiersin.org/articles/10.3389/fchem.2022.1103554/full#supplementary-material>

- Ban, H. S., Lee, S., Kim, Y. P., Yamaki, K., Shin, K. H., and Ohuchi, K. (2002). Inhibition of prostaglandin E₂ production by taiwanin C isolated from the root of *Acanthopanax chiisanensis* and the mechanism of action. *Biochem. Pharmacol.* 64, 1345–1354. doi:10.1016/s0006-2952(02)01348-5

- Borges, L. D. C., Negrão-Neto, R., Pamplona, S., Fernandes, L., Barros, M., Fontes-Júnior, E., et al. (2018). Anti-inflammatory and antinociceptive studies of hydroalcoholic extract from the leaves of *Phyllanthus brasiliensis* (Aubl.) Poir. and

- isolation of 5-O- β -D-glucopyranosyljusticidin B and six other lignans. *Molecules* 23, 941. doi:10.3390/molecules23040941
- Brown, D., and Stevenson, R. (1964). Action of *N*, *N*-dicyclohexylcarbodiimide on phenylpropionic acids: Synthesis of dehydro-otobain. *Tetrahedron Lett.* 5, 3213–3216. doi:10.1016/0040-4039(64)83136-1
- Chang, W. L., Chiu, L. W., Lai, J. H., and Lin, H. C. (2003). Immunosuppressive flavones and lignans from *Bupleurum scorzoniferifolium*. *Phytochemistry* 64, 1375–1379. doi:10.1016/j.phytochem.2003.08.002
- Charlton, J. L. (1998). Antiviral activity of lignans. *J. Nat. Prod.* 61, 1447–1451. doi:10.1021/np980136z
- Chen, C. C., Hsin, W. C., Ko, F. N., Huang, Y. L., Ou, J. C., and Teng, C. M. (1996). Antiplatelet arylnaphthalide lignans from *Justicia procumbens*. *J. Nat. Prod.* 59, 1149–1150. doi:10.1021/np960443+
- Chen, W., Hu, D., Feng, Z., Lin, M., and Han, M. (2018). Progress in synthesis of α -aryl naphthalene lignan lactones. *Chem. Bull.* 81, 303–311. doi:10.14159/j.cnki.0441-3776.2018.04.003
- Chen, W., Ma, Y., He, W., Wu, Y., Huang, Y., Zhang, Y., et al. (2022). Structure units oriented approach towards collective synthesis of sarpagine-ajmaline-koumine type alkaloids. *Nat. Commun.* 13, 908. doi:10.1038/s41467-022-28535-x
- Chen, W., Tian, H., Tan, W., Liu, X., Yang, X., and Zhang, H. (2019). Total synthesis of (–)-vindoline. *Tetrahedron* 75, 1751–1759. doi:10.1016/j.tet.2018.11.046
- Chen, W., Yang, X.-D., Tan, W.-Y., Zhang, X.-Y., Liao, X.-L., and Zhang, H. (2017). Total synthesis of (–)-Vindorosine. *Angew. Chem. Int. Ed.* 56, 12327–12331. doi:10.1002/anie.201707249
- Chun, Y. S., Kim, J., Chung, S., Khorombi, E., Naidoo, D., Nthambeleni, R., et al. (2017). Protective roles of *Monsonia angustifolia* and its active compounds in experimental models of Alzheimer's disease. *J. Agric. Food Chem.* 65, 3133–3140. doi:10.1021/acs.jafc.6b04451
- Crisp, G. T., and Meyer, A. G. (1995). Synthesis of α , β -unsaturated lactams by palladium-catalysed intramolecular carbonylative coupling. *Tetrahedron* 51, 5585–5596. doi:10.1016/0040-4020(95)00219-X
- Daron, É. C. A. S., Negri, W. T., Borges, A., Lescano, C. H., Antunes, E., and Laurentiz, R. S. D. (2022). Design, synthesis, and *in vitro* antiplatelet aggregation activities of taiwanin C. *Nat. Prod. Res.*, 1–7. doi:10.1080/14786419.2022.2036145
- Day, S.-H., Chiu, N.-Y., Won, S.-J., and Lin, C.-N. (1999). Cytotoxic lignans of *Justicia ciliata*. *J. Nat. Prod.* 62, 1056–1058. doi:10.1021/np9900167
- Day, S. H., Lin, Y. C., Tsai, M. L., Tsao, L. T., Ko, H. H., Chung, M. I., et al. (2002). Potent cytotoxic lignans from *Justicia procumbens* and their effects on nitric oxide and tumor necrosis factor- α production in mouse macrophages. *J. Nat. Prod.* 65, 379–381. doi:10.1021/np0101651
- El-Gendy, M. M. A., Hawas, U. W., and Jaspars, M. (2008). Novel bioactive metabolites from a marine derived bacterium *Nocardia* sp. *ALAA 2000 J. Antibiot.* 61, 379–386. doi:10.1038/ja.2008.53
- Flanagan, S. R., Harrowven, D. C., and Bradley, M. (2002). A new benzannulation reaction and its application in the multiple parallel synthesis of aryl naphthalene lignans. *Tetrahedron* 58, 5989–6001. doi:10.1016/S0040-4020(02)00616-6
- Foley, P., Eghbali, N., and Anastas, P. T. (2010). Advances in the methodology of a multicomponent synthesis of aryl naphthalene lactones. *Green Chem.* 12, 888–892. doi:10.1039/B913685A
- Gertsch, J., Tobler, R. T., Brun, R., Sticher, O., and Heilmann, J. (2003). Antifungal, antiprotazoal, cytotoxic and piscicidal properties of Justicidin B and a new aryl naphthalide lignan from *Phyllanthus piscatorum*. *Planta Med.* 69, 420–424. doi:10.1055/s-2003-39706
- Gözler, B., Rentsch, D., Gözler, T., Ünver, N., and Hesse, M. (1996). Lignans, alkaloids and coumarins from *Haplophyllum vulcanicum*. *Phytochemistry* 42, 695–699. doi:10.1016/0031-9422(96)00062-3
- Gözler, T., Gözler, B., Patra, A., Leet, J. E., Freyer, A. J., and Shamma, M. (1984). Konyanin: A new lignan from *Haplophyllum vulcanicum*. *Tetrahedron* 40, 1145–1150. doi:10.1016/S0040-4020(01)99319-6
- Gudla, V., and Balamurugan, R. (2011). Synthesis of aryl naphthalene lignan scaffold by gold-catalyzed intramolecular sequential electrophilic addition and benzannulation. *J. Org. Chem.* 76, 9919–9933. doi:10.1021/jo201918d
- Hajdu, Z., Haskó, J., Krizbai, I. A., Wilhelm, I., Jedlinski, N., Fazakas, C., et al. (2014). Evaluation of lignans from *Heliopsis helianthoides* var. *scabra* for their potential antimetastatic effects in the brain. *J. Nat. Prod.* 77, 2641–2650. doi:10.1021/np500508y
- Harrowven, D. C., Bradley, M., Castro, J. L., and Flanagan, S. R. (2001). Total syntheses of justicidin B and retrojusticidin B using a tandem Horner–Emmons–Claisen condensation sequence. *Tetrahedron Lett.* 42, 6973–6975. doi:10.1016/S0040-4039(01)01436-8
- Hayat, F., Kang, L., Lee, C. Y., and Shin, D. (2015). Synthesis of aryl naphthalene lignan lactone using benzoin condensation, intramolecular thermal cyclization and Suzuki coupling. *Tetrahedron* 71, 2945–2950. doi:10.1016/j.tet.2015.03.023
- He, Y., Zhang, X., and Fan, X. (2014). Synthesis of naphthalene amino esters and aryl naphthalene lactone lignans through tandem reactions of 2-alkynylbenzonitriles. *Chem. Commun.* 50, 5641–5643. doi:10.1039/C4CC01738B
- Hesse, M., Gözler, B., Arar, G., and Gözler, T. (1992). Isodaurinol, an aryl naphthalene lignan from *Haplophyllum cappadocicum*. *Phytochemistry* 31, 2473–2475. doi:10.1016/0031-9422(92)83302-F
- Holmes, T. L., and Steveson, R. (1971). Aryl naphthalene lignans. Synthesis of justicidin E, taiwanin C, dehydromethylconidendrin, and dehydromethylretroendrin. *J. Org. Chem.* 36, 3450–3453. doi:10.1021/jo00821a037
- Ishikawa, S., Masuyama, Y., Adachi, T., Shimonishi, T., Morimoto, S., and Tanabe, Y. (2021). Synthesis of naphthaleman family utilizing regiocontrolled benzannulation: Unique molecules composed of multisubstituted naphthalenes. *ACS Omega* 6, 32682–32694. doi:10.1021/acsomega.1c04413
- Janmanchi, D., Tseng, Y. P., Wang, K. C., Huang, R. L., Lin, C. H., and Yeh, S. F. (2010). Synthesis and the biological evaluation of aryl naphthalene lignans as anti-hepatitis B virus agents. *Bioorg. Med. Chem.* 18, 1213–1226. doi:10.1016/j.bmc.2009.12.038
- Jiang, J., Dong, H., Wang, T., Zhao, R., Mu, Y., Geng, Y., et al. (2017). A strategy for preparative separation of 10 lignans from *Justicia procumbens* L. by high-speed counter-current chromatography. *Molecules* 22, 2024. doi:10.3390/molecules22122024
- Jin, H., Yang, S., and Dong, J.-X. (2017). New lignan glycosides from *Justicia procumbens*. *J. Asian Nat. Prod. Res.* 19, 1–8. doi:10.1080/10286020.2016.1241771
- Jin, H., Yin, H.-L., Liu, S.-J., Chen, L., Tian, Y., Li, B., et al. (2014). Cytotoxic activity of lignans from *Justicia procumbens*. *Fitoterapia* 94, 70–76. doi:10.1016/j.fitote.2014.01.025
- Kamal, A., Daneshalab, M., and Micetich, R. G. (1994). A rapid entry into podophyllotoxin congeners: Synthesis of justicidin B. *Tetrahedron Lett.* 35, 3879–3882. doi:10.1016/S0040-4039(00)76691-3
- Kao, T. T., Lin, C. C., and Shia, K. S. (2015). The total synthesis of retrojusticidin B, justicidin E, and helioxanthin. *J. Org. Chem.* 80, 6708–6714. doi:10.1021/acs.joc.5b00866
- Katsuki, N., Isshiki, S., Fukatsu, D., Okamura, J., Kuramochi, K., Kawabata, T., et al. (2017). Total synthesis of dendrochrysane through a frame rearrangement. *J. Org. Chem.* 82, 11573–11584. doi:10.1021/acs.joc.7b02223
- Kawazoe, K., Yutani, A., Tamemoto, K., Yuasa, S., Shibata, H., Higuti, T., et al. (2001). Phenyl naphthalene compounds from the subterranean part of *Vitex rotundifolia* and their antibacterial activity against methicillin-resistant *Staphylococcus aureus*. *J. Nat. Prod.* 64, 588–591. doi:10.1021/np000307b
- Klemm, L. H., Klemm, R. A., Santhanam, P. S., and White, D. V. (1971). Intramolecular Diels–Alder reactions. VI. Synthesis of 3-hydroxymethyl-2-naphthoic acid lactones. *J. Org. Chem.* 36, 2169–2172. doi:10.1021/jo00814a029
- Kocsis, L. S., and Brummond, K. M. (2014). Intramolecular dehydro-Diels–Alder reaction affords selective entry to aryl naphthalene or aryl dihydronaphthalene lignans. *Org. Lett.* 16, 4158–4161. doi:10.1021/ol501853y
- Kudoh, T., Shishido, A., Ikeda, K., Saito, S., and Ishikawa, T. (2013). Concise synthesis of aryl naphthalene lignans by regioselective intramolecular anionic Diels–Alder reactions of 1, 7-diaryl-1, 6-dienes. *Synlett* 24, 1509–1512. doi:10.1055/s-0033-1339184
- Li, R., Wei, K., Chen, W., Li, L., and Zhang, H. (2022). Carbon–sulfur bond formation: Tandem process for the synthesis of functionalized isothiazoles. *Org. Lett.* 24, 339–343. doi:10.1021/acs.orglett.1c03994
- Liu, B., Zhang, T., Xie, Z., Hong, Z., Lu, Y., Long, Y., et al. (2022). Effective components and mechanism analysis of anti-platelet aggregation effect of *Justicia procumbens* L. *J. Ethnopharmacol.* 294, 115392. doi:10.1016/j.jep.2022.115392
- Lv, J.-P., Yang, S., Dong, J.-X., and Jin, H. (2021). New cyclopeptide alkaloids from the whole plant of *Justicia procumbens* L. *Nat. Prod. Res.* 35, 4032–4040. doi:10.1080/14786419.2020.1758090
- Meng, J., Du, L., and Guo, L. (2016). Synthesis of aryl naphthalene lignan lactones. *Chin. J. Org. Chem.* 36, 2723–2728. doi:10.6023/cjoc201603007
- Michael, A., and Bucher, J. E. (1895). Ueber die einwirkung von essigsäureanhydrid auf säuren der acetylenreihe. *Ber. Dtsch. Chem. Ges.* 28, 2511–2512. doi:10.1002/cber.18950280337
- Miyaura, N., and Suzuki, A. (1979). Stereoselective synthesis of arylated (*E*)-alkenes by the reaction of alk-1-enylboranes with aryl halides in the presence of palladium catalyst. *J. Chem. Soc. Chem. Commun.*, 866–867. doi:10.1039/C39790000866

- Mizufune, H., Nakamura, M., and Mitsudera, H. (2001). The first regioselective synthesis of helioxanthin by novel palladium-catalyzed benzannulation reaction of α , β -bisbenzylidene- γ -lactone. *Tetrahedron Lett.* 42, 437–439. doi:10.1016/S0040-4039(00)01982-1
- Mondal, S., Maji, M., and Basak, A. (2011). A Garratt–Braverman route to aryl naphthalene lignans. *Tetrahedron Lett.* 52, 1183–1186. doi:10.1016/j.tetlet.2011.01.011
- Mondal, S., Mitra, T., Mukherjee, R., Addy, P. S., and Basak, A. (2012). Garratt–Braverman cyclization, a powerful tool for C–C bond formation. *Synlett* 23, 2582–2602. doi:10.1055/s-0032-1317321
- Moriguchi, K., Sasaki, R., Morita, J. I., Kamakura, Y., Tanaka, D., and Tanabe, Y. (2021). *Ipso*-Type regiocontrolled benzannulation for the synthesis of uniquely substituted α -arylnaphthalenes: Application to the first total synthesis of chaihunaphthone. *ACS Omega* 6, 18135–18156. doi:10.1021/acsomega.1c02000
- Murakami, M., Hoshino, Y., Ito, H., and Ito, Y. (1998). Palladium-catalyzed coupling reactions of *N*-methoxy-*N*-methylcarbamoyl chloride for the synthesis of *N*-methoxy-*N*-methylamides. *Chem. Lett.* 27, 163–164. doi:10.1246/cl.1998.163
- Nagaki, A., Moriawaki, Y., and Yoshida, J. I. (2012). Flow synthesis of arylboronic esters bearing electrophilic functional groups and space integration with Suzuki–Miyaura coupling without intentionally added base. *Chem. Commun.* 48, 11211–11213. doi:10.1039/C2CC36197C
- Nareish, G., Kant, R., and Narender, T. (2015). Silver(I)-catalyzed regioselective construction of highly substituted alpha-naphthols and its application toward expeditious synthesis of lignan natural products. *Org. Lett.* 17, 3446–3449. doi:10.1021/acs.orglett.5b01477
- Nishii, Y., Yoshida, T., Asano, H., Wakasugi, K., Morita, J. I., Aso, Y., et al. (2005). Regiocontrolled benzannulation of diaryl (*gem*-dichlorocyclopropyl) methanols for the synthesis of unsymmetrically substituted α -arylnaphthalenes: Application to total synthesis of natural lignan lactones. *J. Org. Chem.* 70, 2667–2678. doi:10.1021/jo047751u
- Ogiku, T., Seki, M., Takahashi, M., Ohmizu, H., and Iwasaki, T. (1990). A new two-step synthesis of 1-arylnaphthalene lignans from cyanohydrins. *Tetrahedron Lett.* 31, 5487–5490. doi:10.1016/S0040-4039(00)97879-1
- Ogiku, T., Yoshida, S. I., Ohmizu, H., and Iwasaki, T. (1995). Efficient syntheses of 1-arylnaphthalene lignan lactones and related compounds from cyanohydrins. *J. Org. Chem.* 60, 4585–4590. doi:10.1021/jo00119a041
- Okigawa, M., Maeda, T., and Kawano, N. (1970). The isolation and structure of three new lignans from *Justicia procumbens* Linn. var. *leucantha* Honda. *Tetrahedron* 26, 4301–4305. doi:10.1016/S0040-4020(01)93074-1
- Padwa, A., Cochran, J. E., and Kappe, C. O. (1996). Tandem Pummerer–Diels–Alder reaction sequence. A novel cascade process for the preparation of 1-arylnaphthalene lignans. *J. Org. Chem.* 61, 3706–3714. doi:10.1021/jo960295s
- Park, J. E., Lee, J., Seo, S. Y., and Shin, D. (2014). Regioselective route for aryl naphthalene lactones: Convenient synthesis of taiwanin C, justicidin E, and daurinol. *Tetrahedron Lett.* 55, 818–820. doi:10.1016/j.tetlet.2013.12.014
- Park, S., Kim, J.-H., Kim, S.-H., and Shin, D. (2020). Transition metal-mediated annulation approaches for synthesis of aryl naphthalene lignan lactones. *Front. Chem.* 8, 628. doi:10.3389/fchem.2020.00628
- Patel, R. M., and Argade, N. P. (2013). Palladium-promoted 2+2+2 cocyclization of arynes and unsymmetrical conjugated dienes: Synthesis of justicidin B and retrojusticidin B. *Org. Lett.* 15, 14–17. doi:10.1021/ol3028658
- Reber, K. P., Tilley, S. D., and Sorensen, E. J. (2009). Bond formations by intermolecular and intramolecular trappings of acylketenes and their applications in natural product synthesis. *Chem. Soc. Rev.* 38, 3022–3034. doi:10.1039/B912599J
- Sagar, K. S., Chang, C. C., Wang, W. K., Lin, J. Y., and Lee, S. S. (2004). Preparation and anti-HIV activities of retrojusticidin B analogs and azalignans. *Bioorg. Med. Chem.* 12, 4045–4054. doi:10.1016/j.bmc.2004.05.036
- Sato, Y., Tamura, T., Kinbara, A., and Mori, M. (2007). Synthesis of biaryls via palladium-catalyzed 2+2+2 cocyclization of arynes and diynes: Application to the synthesis of aryl naphthalene lignans. *Adv. Synth. Catal.* 349, 647–661. doi:10.1002/adsc.200600587
- Sato, Y., Tamura, T., and Mori, M. (2004). Arylnaphthalene lignans through Pd-catalyzed 2+2+2 cocyclization of arynes and diynes: Total synthesis of taiwanins C and E. *Angew. Chem. Int. Ed.* 43, 2436–2440. doi:10.1002/anie.200453809
- Shen, C.-C., Ni, C.-L., Huang, Y.-L., Huang, R.-L., and Chen, C. (2004). Furanolabdane diterpenes from *Hypoestes purpurea*. *J. Nat. Prod.* 67, 1947–1949. doi:10.1021/np0497402
- Sheriha, G. M., and Abou Amer, K. M. (1984). Lignans of *Haplophyllum tuberculatum*. *Phytochemistry* 23, 151–153. doi:10.1016/0031-9422(84)83096-4
- Stevenson, R., and Weber, J. V. (1989). Improved methods of synthesis of lignan aryl naphthalene lactones via arylpropargyl arylpropionate esters. *J. Nat. Prod.* 52, 367–375. doi:10.1021/np50062a024
- Subbaraju, G. V., and Pillai, K. R. (1996). Lignans from *Justicia diffusa* Willd. *Indian J. Chem. B* 35, 1233–1234.
- Susplugas, S., Hung, N. V., Bignon, J., Thoison, O., Kruczynski, A., Sévenet, T., et al. (2005). Cytotoxic aryl naphthalene lignans from a Vietnamese acanthaceae, *Justicia patentiflora*. *J. Nat. Prod.* 68, 734–738. doi:10.1021/np050028u
- Takano, S., Otaki, S., and Ogasawara, K. (1985). A new route to 1-phenylnaphthalenes by cycloaddition: A simple and selective synthesis of some naphthalene lignan lactones. *Tetrahedron Lett.* 26, 1659–1660. doi:10.1016/S0040-4039(00)98577-0
- Ulubelen, A., Meriçli, A. H., Meriçli, F., and Kaya, Ü. (1994). An alkaloid and lignans from *Haplophyllum telephoides*. *Phytochemistry* 35, 1600–1601. doi:10.1016/S0031-9422(00)86905-8
- Vasilev, N., Elfahmi, B., Bos, R., Kayser, O., Momkov, G., and Konstantinov, S. (2006). Production of justicidin B, a cytotoxic aryl naphthalene lignan from genetically transformed root cultures of *Linum leonii*. *Nat. Prod.* 69, 1014–1017. doi:10.1021/np060022k
- Wang, S.-H., Wu, H.-C., Badrealam, K. F., Kuo, Y.-H., Chao, Y.-P., Hsu, H.-H., et al. (2019). Taiwanin E induces cell cycle arrest and apoptosis in arecoline/4-NQO-induced oral cancer cells through modulation of the ERK signaling pathway. *Front. Oncol.* 9, 1309. doi:10.3389/fonc.2019.01309
- Wei, K., Sun, Y. C., Li, R., Zhao, J. F., Chen, W., and Zhang, H. (2021). Synthesis of highly functionalized pyridines: A metal-free cascade process. *Org. Lett.* 23, 6669–6673. doi:10.1021/acs.orglett.1c02234
- Weng, J. R., Ko, H. H., Yeh, T. L., Lin, H. C., and Lin, C. N. (2004). Two new aryl naphthalide lignans and antiplatelet constituents from *Justicia procumbens*. *Arch. Pharm.* 337, 207–212. doi:10.1002/ardp.200300841
- Wong, Y.-C., Kao, T.-T., Huang, J.-K., Jhang, Y.-W., Chou, M.-C., and Shia, K.-S. (2014). Manganese(III)-catalyzed oxidative cyclization of aryl 1-cyanoalk-5-ynyl ketone systems: A convenient and general approach to cyclopenta[b]naphthalene derivatives. *Adv. Synth. Catal.* 356, 3025–3038. doi:10.1002/adsc.201400257
- Wu, S.-J., and Wu, T.-S. (2006). Cytotoxic aryl naphthalene lignans from *Phyllanthus oligospermus*. *Chem. Pharm. Bull.* 54, 1223–1225. doi:10.1248/cpb.54.1223
- Xiao, J., Cong, X.-W., Yang, G.-Z., Wang, Y.-W., and Peng, Y. (2018). Divergent asymmetric syntheses of podophyllotoxin and related family members via stereoselective reductive Ni-catalysis. *Org. Lett.* 20, 1651–1654. doi:10.1021/acs.orglett.8b00408
- Xiong, L., Bi, M. G., Wu, S., and Tong, Y. F. (2012). Total synthesis of 6'-hydroxyjusticidin A. *J. Asian Nat. Prod. Res.* 14, 322–326. doi:10.1080/10286020.2011.653561
- Yamamoto, Y., Mori, S., and Shibuya, M. (2015). A combined transition metal-catalyzed and photopromoted process: Synthesis of 2, 3-fused 4-phenylnaphthalen-1-yl carboxylates from 1, 7-diaryl-1, 6-diynes. *Chem. Eur. J.* 21, 9093–9100. doi:10.1002/chem.201500978
- Yeo, H., Li, Y., Fu, L., Zhu, J. L., Gullen, E. A., Dutschman, G. E., et al. (2005). Synthesis and antiviral activity of helioxanthin analogues. *J. Med. Chem.* 48, 534–546. doi:10.1021/jm034265a
- Zhang, L., Zhang, Y., Li, W., and Qi, X. (2019). Total synthesis of (–)-alstofoline A through a furan oxidation/rearrangement and indole nucleophilic cyclization cascade. *Angew. Chem. Int. Ed.* 58, 4988–4991. doi:10.1002/anie.201900156
- Zhang, Y., Bao, F., Hu, J., Liang, S., Zhang, Y., Du, G., et al. (2007). Antibacterial lignans and triterpenoids from *Rostellularia procumbens*. *Planta Med.* 73, 1596–1599. doi:10.1055/s-2007-99374h
- Zhao, C., Rakesh, K. P., Mumtaz, S., Moku, B., Asiri, A. M., Marwani, H. M., et al. (2018). Arylnaphthalene lactone analogues: Synthesis and development as excellent biological candidates for future drug discovery. *RSC Adv.* 8, 9487–9502. doi:10.1039/c7ra13754k
- Zhao, Y., Li, Y., Wang, B., Zhao, J., Li, L., Luo, X. D., et al. (2020). Total synthesis of dactylicapnosines A and B. *J. Org. Chem.* 85, 13772–13778. doi:10.1021/acs.joc.0c01900



OPEN ACCESS

EDITED BY

Siva S. Panda,
Augusta University, United States

REVIEWED BY

Cheng-xue Pan,
Guangxi Normal University, China
Hongtao Xu,
ShanghaiTech University, China

*CORRESPONDENCE

Yan Li,
✉ yan.li@ynu.edu.cn
Jingfeng Zhao,
✉ jfzhao@ynu.edu.cn
Xiaodong Yang,
✉ xdyang@ynu.edu.cn

[†]These authors have contributed equally to this work

RECEIVED 22 March 2023

ACCEPTED 21 April 2023

PUBLISHED 10 May 2023

CITATION

Yin M, Fang Y, Sun X, Xue M, Zhang C, Zhu Z, Meng Y, Kong L, Myint YY, Li Y, Zhao J and Yang X (2023), Synthesis and anticancer activity of podophyllotoxin derivatives with nitrogen-containing heterocycles. *Front. Chem.* 11:1191498. doi: 10.3389/fchem.2023.1191498

COPYRIGHT

© 2023 Yin, Fang, Sun, Xue, Zhang, Zhu, Meng, Kong, Myint, Li, Zhao and Yang. This is an open-access article distributed under the terms of the [Creative Commons Attribution License \(CC BY\)](#). The use, distribution or reproduction in other forums is permitted, provided the original author(s) and the copyright owner(s) are credited and that the original publication in this journal is cited, in accordance with accepted academic practice. No use, distribution or reproduction is permitted which does not comply with these terms.

Synthesis and anticancer activity of podophyllotoxin derivatives with nitrogen-containing heterocycles

Meng Yin^{1†}, Yongsheng Fang^{1†}, Xiaotong Sun¹, Minggao Xue¹, Caimei Zhang¹, Zhiyun Zhu¹, Yamiao Meng¹, Lingmei Kong¹, Yi Yi Myint², Yan Li^{1*}, Jingfeng Zhao^{1*} and Xiaodong Yang^{1*}

¹Key Laboratory of Medicinal Chemistry for Natural Resource, Ministry of Education, Yunnan Provincial Center for Research & Development of Natural Products, School of Pharmacy, Yunnan University, Kunming, China, ²Department of Chemistry, University of Mandalay, Mandalay, Myanmar

Three series of podophyllotoxin derivatives with various nitrogen-containing heterocycles were designed and synthesized. The antitumor activity of these podophyllotoxin derivatives was evaluated *in vitro* against a panel of human tumor cell lines. The results showed that podophyllotoxin-imidazolium salts and podophyllotoxin-1,2,4-triazolium salts **a1–a20** exhibited excellent cytotoxic activity. Among them, **a6** was the most potent cytotoxic compound with IC₅₀ values of 0.04–0.29 μM. Podophyllotoxin-1,2,3-triazole derivatives **b1–b5** displayed medium cytotoxic activity, and podophyllotoxin-amine compounds **c1–c3** has good cytotoxic activity with IC₅₀ value of 0.04–0.58 μM. Furthermore, cell cycle and apoptosis experiments of compound **a6** were carried out and the results exhibited that **a6** could induce G2/M cell cycle arrest and apoptosis in HCT-116 cells.

KEYWORDS

podophyllotoxin, imidazolium salts, triazoles, antitumor activity, structure-activity relationships

1 Introduction

According to the data from the International Agency for Cancer Research (IARC), there would be around 19.3 million new cancer diagnoses and nearly 10 million cancer-related deaths in 2020 (Sung et al., 2021). Therefore, the development of innovative anticancer agents and therapeutic strategies is essential (Boshuizen and Peeper, 2020). Medicinal chemists have increasingly viewed natural products as valuable resources for developing anticancer drug (Choi et al., 2017). About 84% of antitumor small molecule drugs approved between 1981 and 2019 were derived from natural products or structural units containing natural products (Newman and Cragg, 2020). The design and rational synthesis of natural product-like libraries, from which lead compounds with high efficiency, high selectivity, and low toxicity can be screened and discovered for preclinical studies, is one of the significant approaches for developing new drugs (Liu et al., 2017).

Podophyllotoxin is a natural product with anticancer activity belonging to the lignans cyclo lignolide family (Dagenais et al., 2020). Podophyllotoxin and its semi-synthetic glycoside derivatives Etoposide, Teniposide and Etoposide Phosphate have

been proved to be highly active antitumor agents with excellent clinical effects and are essential drugs for the treatment of small cell lung cancer, leukemia, testicular cancer and other types of tumors (Zhang et al., 2018; Li et al., 2019; Guo and Jiang, 2021; Zhao et al., 2021). Numerous structural and pharmacological studies have demonstrated that C-4 derivatization could enhance the biological activity of this family of drugs (Xiao et al., 2020).

On the other side, nitrogen-containing heterocycles are widely used in drug design and discovery (Xu et al., 2014a; Vitaku et al., 2014). The unique structural features of imidazoles and triazoles possess desirable electron rich properties, which are more favorable for conjugation with other molecules, and the molecular activity could be improved after hybridization (Verma et al., 2013; Gaba and Mohan, 2015; Bozorov et al., 2019; Xu et al., 2019; Dixit et al., 2021; Sharma et al., 2021). Among them, imidazolium salts have attracted much attention for their important and extensive biological and pharmacological activities, especially antitumor activity (Cui et al., 2003; Yang et al., 2009). In this context, our group has devoted to the synthesis of novel imidazolium salt derivatives and found a series of promising compounds with antitumor activity (Chen et al., 2013; Wang et al., 2013; Xu et al., 2014b; Xu et al., 2015; Zhou et al., 2016a; Zhou et al., 2016b). Further mechanistic studies confirmed that these imidazolium salt derivatives can induce cell cycle arrest and apoptosis in tumor cells (Liu et al., 2013; Liu et al., 2015; Huang et al., 2019). The representative examples are an effective antitumor active diosgenin-imidazolium salt and a new mTOR pathway inhibitor B591 (Figure 1) (Deng et al., 2019; Zhou et al., 2019).

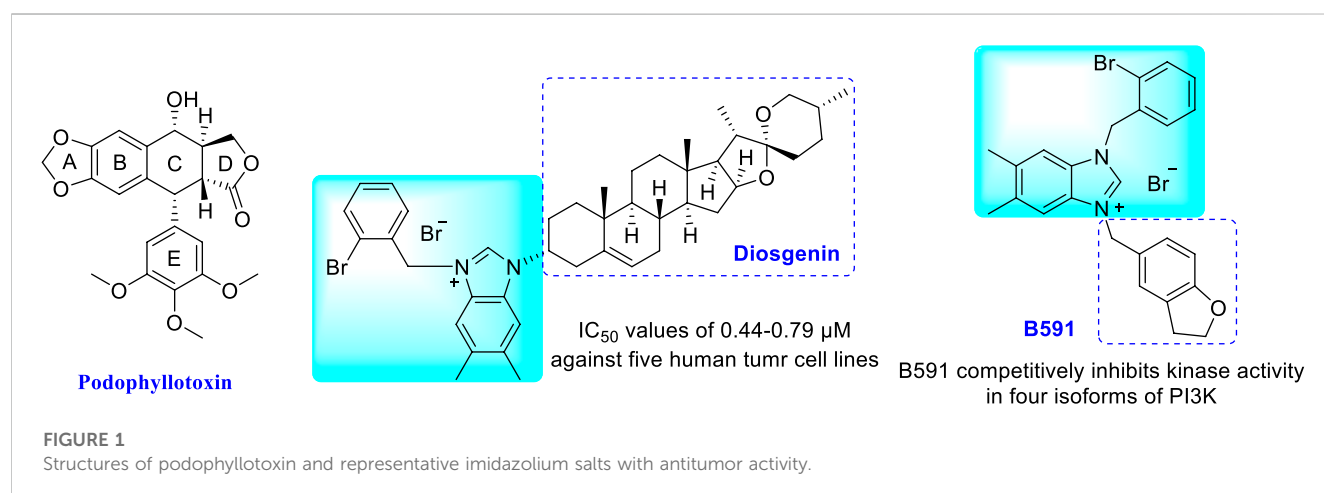
In the past three decades, molecular hybridization has played an important role in drug discovery (Zhang et al., 2017; Yang et al., 2021). In view of the potential anticancer activity of podophyllotoxin and nitrogen-containing heterocycles, we launched the synthesis of hybrid compounds of natural product podophyllotoxin and imidazolium/triazolium salts. Although some nitrogen-containing heterocycles-podophyllotoxin derivatives were prepared and found to possess anticancer and neuroactive activities (Chen et al., 2011; Shang et al., 2012;

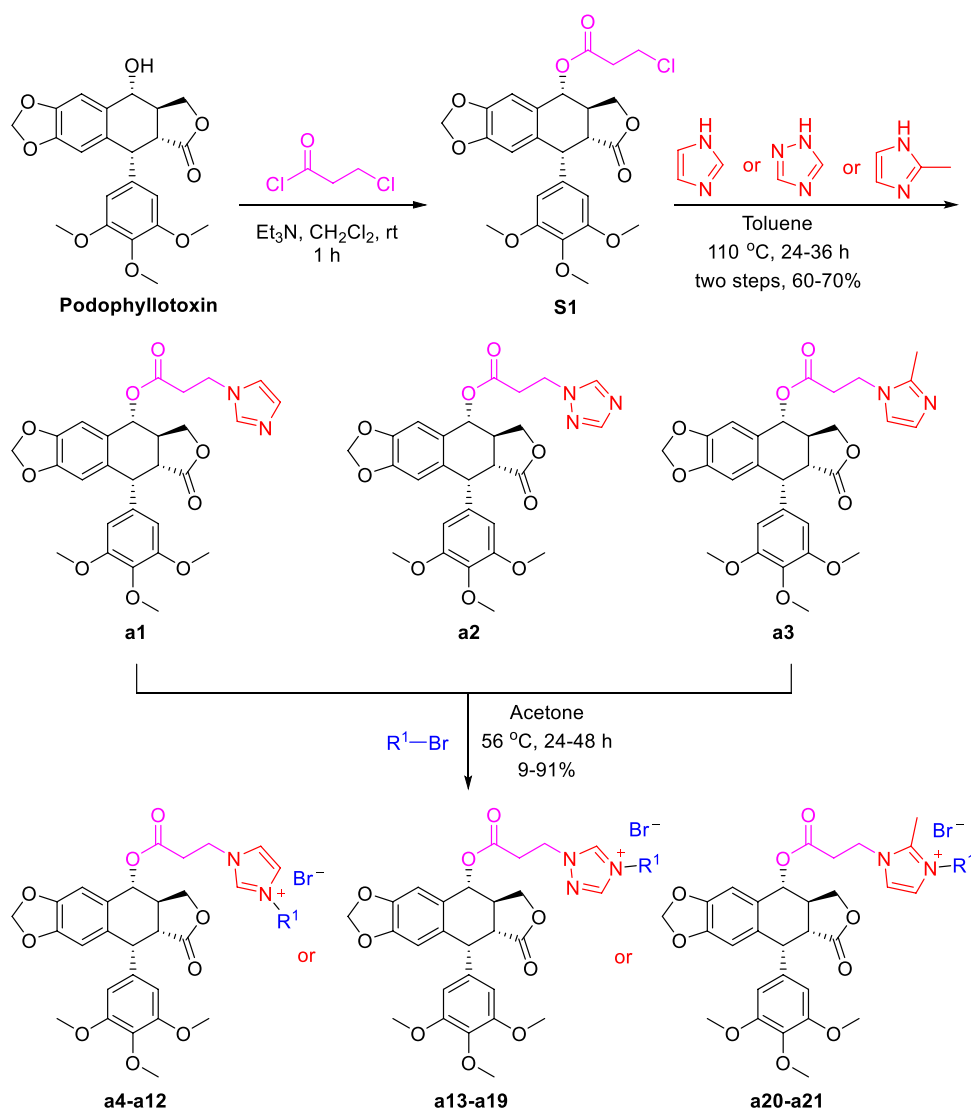
Vishnuvardhan et al., 2017; Hou et al., 2019), to the best of our knowledge, there are no reports on the synthesis and bioactivity of imidazolium/triazolium salt hybrids of podophyllotoxin. With this in mind, we turned our attention to the synthesis and antitumor activity of a series of novel podophyllotoxin nitrogen-containing heterocycles, especially imidazolium and triazolium salts.

2 Results and discussion

2.1 Chemistry

As shown in Scheme 1, firstly, to synthesize podophyllotoxin nitrogen-containing heterocycles, imidazole, 1,2,4-triazole, 2-methylimidazole, 1,2,3-triazole and amines were used for reaction. Using the commercial podophyllotoxin as starting material, the esterification reaction with 2-chloropropionyl chloride was carried out to obtain the ester S1. Next, S1 reacted with imidazole, 1,2,4-triazole and 2-methylimidazole to obtain the nitrogen-containing heterocycles a1–a3 (60%–70% yields, two steps). Then, treatment of a1–a3 with various bromides generated the podophyllotoxin imidazolium/triazolium salts a4–a21 (9%–91% yields). Secondly, as shown in Scheme 2, 4-chlorinated podophyllotoxin S2 was obtained by commercial podophyllotoxin reacting with thionyl chloride. Next, a nucleophilic substitution reaction with sodium azide was conducted to obtain compound S3 (46% yield, two steps). Then, azide S3 reacted with various terminal alkynes under Click reaction condition to get the podophyllotoxin-1,2,3-triazole derivatives b1–b5 (31%–47% yields). Finally, as shown in Scheme 3, using podophyllotoxin as the starting material, esterification reaction with 2-chloropropionyl chloride was performed to obtain the ester S1, which then underwent a nucleophilic substitution reaction with commercial cyclic amines (pyrrole, piperidine and morpholine) to furnish the podophyllotoxin-amines c1–c3 (48%–61% yields, two steps). To summarize, the structures and yields of all new podophyllotoxin nitrogen-containing heterocycle derivatives were shown in Table 1.





SCHEME 1
Synthesis of podophyllotoxin nitrogenous derivatives **a1**–**a21**.

2.2 Biological evaluation and structure-activity relationship analysis

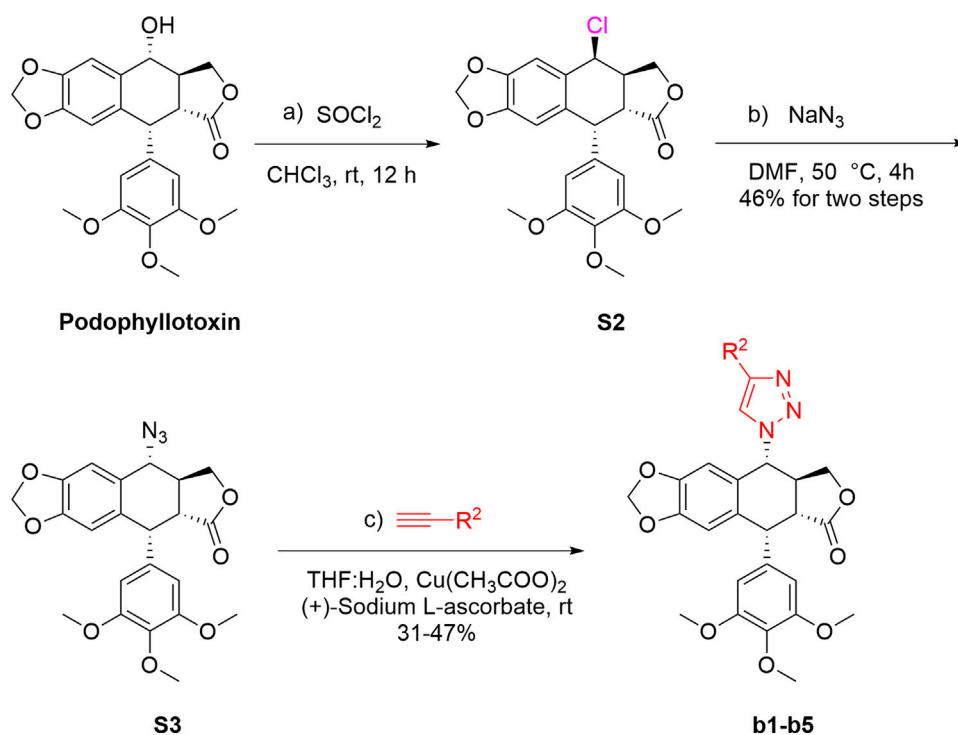
2.2.1 Biological assay procedures and results

The synthesized twenty-nine podophyllotoxin nitrogen-containing derivatives were evaluated *in vitro* antitumor cytotoxic activity screening by MTS method (Perchellet et al., 2005). Four human cancer cell lines including hepatocellular carcinoma cells (HepG-2), non-small cell lung cancer cells (A-549), breast cancer cells (MDA-MB-231) and colon cancer cells (HCT-116) were selected to determine *in vitro* cytotoxic activity. DDP (Cisplatin), Etoposide, and Paclitaxel were chosen as positive controls. The results were listed in Table 2.

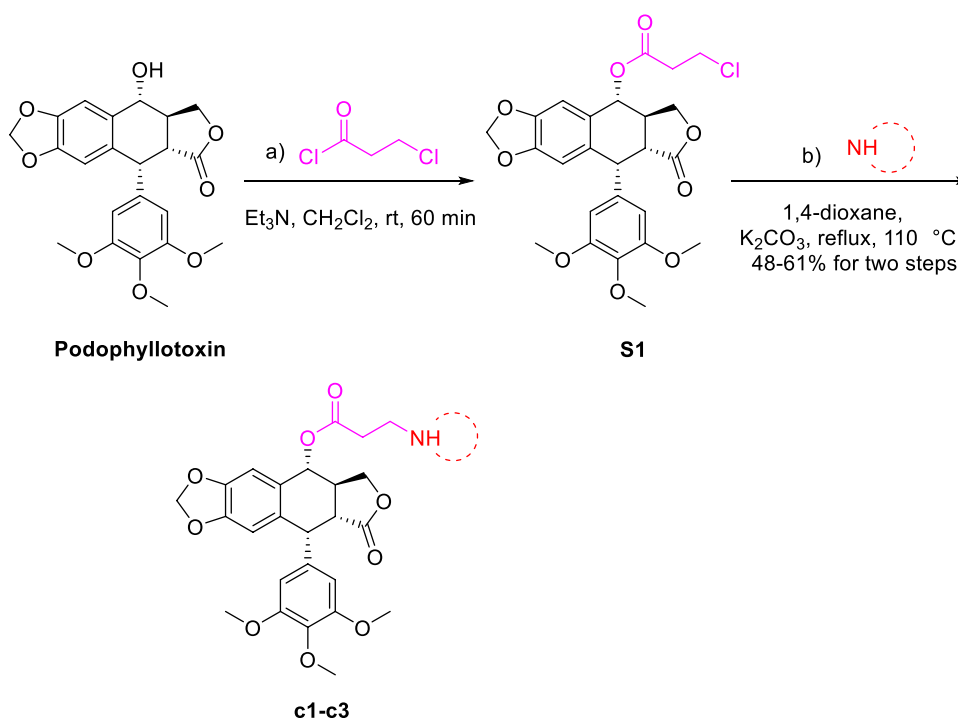
As presented in Table 2, the majority of podophyllotoxin nitrogen-containing heterocycles showed potent inhibitory activity than positive controls Etoposide and DDP. Notably, these

derivatives have obvious selective inhibitory against HCT-116 cell lines. The results showed that the structures of podophyllotoxin nitrogen-containing heterocycles plays a crucial role in regulating cytotoxic activity.

For pharmacophores of nitrogen-containing heterocycles, podophyllotoxin-imidazole and its salts (**a1/a3/a4-a12/a20/a21**) and podophyllotoxin-1,2,4-triazole and its salts (**a2/a13-a19**) exhibited excellent cytotoxic activity with IC_{50} values of 0.04–1.53 μM except **a20**. Among them, **a6** was the most potent cytotoxic compound and its IC_{50} values for HepG2, A-549, MDA-MB-231 and HCT-116 were 0.07, 0.29, 0.11 and 0.04 μM , respectively. Secondly, the introduction of 1,2,3-triazole derivatives **b1**–**b5** by Click reaction showed medium cytotoxic activity with IC_{50} values of 0.04–9.64 μM except **b5**. Finally, while compounds **c1**–**c3** introduced with cyclic amines also showed excellent cytotoxic activity with IC_{50} values of 0.04–0.58 μM .



SCHEME 2

Synthesis of podophyllotoxin nitrogenous derivatives **b1–b5**.

SCHEME 3

Synthesis of podophyllotoxin nitrogenous derivatives **c1–c3**.

TABLE 1 Structures and yields of podophyllotoxin nitrogen-containing heterocycles a1–a21/b1–b5/c1–c3.

Entry	Compound	R ¹	R ²	R ³	Yields (%)
1	a1	—	—	—	68
2	a2	—	—	—	70
3	a3	—	—	—	60
4	a4	2-naphthylacyl	—	—	38
5	a5	4-bromophenacyl	—	—	91
6	a6	2-naphthylmethyl	—	—	58
7	a7	phenacyl	—	—	44
8	a8	4-methoxyphenacyl	—	—	53
9	a9	4-bromobenzyl	—	—	82
10	a10	4-methylbenzyl	—	—	46
11	a11	2-bromobenzyl	—	—	81
12	a12	5-bromomethyl	—	—	78
13	a13	2-naphthylacyl	—	—	30
14	a14	4-bromophenacyl	—	—	34
15	a15	2-naphthylmethyl	—	—	63
16	a16	phenacyl	—	—	37
17	a17	4-methoxyphenacyl	—	—	80
18	a18	4-bromobenzyl	—	—	71
19	a19	4-methylbenzyl	—	—	9
20	a20	4-bromophenacyl	—	—	58
21	a21	phenacyl	—	—	50
22	b1	—	F	—	31
23	b2	—	Br	—	47
24	b3	—	OMe	—	33
25	b4	—	Pyridine	—	38
26	b5	—	Naphthalene	—	43
27	c1	—	—	Pyrrolidine	58
28	c2	—	—	Piperidine	61
29	c3	—	—	Morpholine	48

For the groups at position-3 of imidazolium and triazolium salts (**a4–a21**), the cytotoxic activities of most substituted benzyl groups were superior to those of substituted phenacyl groups. Among them, 2-naphthylmethyl substituent at position-3 of the imidazole ring (**a6** and **a15**) showed excellent cytotoxic activity with IC₅₀ values of 0.04–0.75 μ M and **a6** was the most powerful compound. Similarly, 4-bromobenzyl, 4-methylbenzyl, 4-methoxybenzyl and 2-bromobenzyl groups at position-3 of the imidazole ring exhibited good cytotoxic activity with IC₅₀ values of 0.04–0.65 μ M.

For the groups at position-4 of 1,2,3-triazole ring (**b1–b5**), when the substituent was replaced with electron donating groups

(R² = OMe), **b3** exhibits higher inhibitory activity with IC₅₀ values of 0.49–3.48 μ M. In contrast, when the substituent was charged with electron-withdrawing groups (R² = F, Br), **b1** and **b2** were decreased slightly with IC₅₀ values of 0.04–7.31 μ M. When the substituent group was pyridine, **b4** exhibited poor inhibitory activity with IC₅₀ values of 1.49–9.64 μ M, due to the electron-withdrawing effect of pyridine. When the substituent was a naphthalene ring, **b5** did not exhibit any inhibitory activity.

For the cyclic amines (**c1–c3**), piperidine derivative of podophyllotoxin (**c2**) displayed excellent cytotoxic activity with IC₅₀ values of 0.10–0.39 μ M, which was superior to pyrrole derivative (0.04–0.58 μ M) and morpholine derivative

TABLE 2 Cytotoxic activities of podophyllotoxin nitrogen-containing heterocycles **a1–a21/b1–b5/c1–c3** in *vitro*^a (IC₅₀, μM^b).

Entry	Compound No.	HepG-2	A-549	MDA-MB-231	HCT-116
1	a1	0.31 ± 0.02	0.76 ± 0.12	0.47 ± 0.01	0.04 ± 0.00
2	a2	0.23 ± 0.01	0.30 ± 0.02	0.45 ± 0.03	0.15 ± 0.01
3	a3	0.32 ± 0.06	0.65 ± 0.03	0.38 ± 0.04	0.31 ± 0.04
4	a4	0.33 ± 0.01	1.11 ± 0.04	0.53 ± 0.01	0.04 ± 0.00
5	a5	0.29 ± 0.00	0.76 ± 1.54	0.51 ± 0.05	0.04 ± 0.00
6	a6	0.07 ± 0.00	0.29 ± 0.04	0.11 ± 0.01	0.04 ± 0.00
7	a7	0.18 ± 0.01	1.08 ± 0.20	0.48 ± 0.02	0.04 ± 0.00
8	a8	0.26 ± 0.01	0.65 ± 0.39	0.55 ± 0.02	0.04 ± 0.00
9	a9	0.25 ± 0.01	0.44 ± 0.10	0.49 ± 0.02	0.29 ± 0.00
10	a10	0.25 ± 0.01	0.25 ± 0.00	0.45 ± 0.09	0.30 ± 0.05
11	a11	0.27 ± 0.00	0.42 ± 0.09	0.33 ± 0.06	0.30 ± 0.08
12	a12	0.26 ± 0.05	0.53 ± 0.10	0.51 ± 0.02	0.21 ± 0.01
13	a13	0.34 ± 0.02	1.10 ± 0.14	0.41 ± 0.06	0.10 ± 0.02
14	a14	0.42 ± 0.03	1.53 ± 0.23	0.33 ± 0.04	0.05 ± 0.02
15	a15	0.29 ± 0.01	0.75 ± 0.07	0.30 ± 0.00	0.27 ± 0.15
16	a16	0.28 ± 0.02	0.75 ± 0.07	0.25 ± 0.02	0.20 ± 0.06
17	a17	0.25 ± 0.02	0.74 ± 0.19	0.28 ± 0.05	0.04 ± 0.09
18	a18	0.28 ± 0.03	0.58 ± 0.01	0.23 ± 0.02	0.04 ± 0.00
19	a19	0.25 ± 0.00	0.65 ± 0.01	0.26 ± 0.00	0.04 ± 0.00
20	a20	7.98 ± 0.51	15.84 ± 0.04	>20	6.80 ± 0.11
21	a21	0.40 ± 0.03	0.28 ± 0.05	0.11 ± 0.03	0.07 ± 0.01
22	b1	1.86 ± 0.15	3.60 ± 0.56	2.03 ± 0.14	0.04 ± 0.33
23	b2	2.14 ± 0.04	7.31 ± 0.12	1.74 ± 0.47	6.58 ± 1.87
24	b3	1.60 ± 0.00	3.48 ± 0.03	0.49 ± 0.01	0.90 ± 0.42
25	b4	4.59 ± 0.37	9.64 ± 0.62	7.57 ± 0.62	1.49 ± 1.76
26	b5	>20	>20	>20	>20
27	c1	0.28 ± 0.01	0.58 ± 0.02	0.04 ± 0.03	0.05 ± 0.01
28	c2	0.10 ± 0.01	0.39 ± 0.03	0.10 ± 0.00	0.10 ± 0.02
29	c3	0.21 ± 0.03	0.39 ± 0.01	0.36 ± 0.11	0.06 ± 0.11
30	DDP	1.85 ± 0.34	5.52 ± 0.21	12.77 ± 2.71	10.92 ± 0.26
31	Etoposide	16.95 ± 2.00	14.77 ± 0.26	1.92 ± 0.96	14.19 ± 0.13
32	Paclitaxel	<0.008	<0.008	<0.008	<0.008

^aData represent the mean values of three independent determinations.^bCytotoxicity as IC₅₀ for each cell line, is the concentration of compound which reduced by 50% the optical density of treated cells with respect to untreated cells using the MTS assay.

(0.06–0.39 μM). Notably, compound **c1** has selective inhibitory against MDA-MB-231 cell lines with an IC₅₀ value of 0.04 μM.

The results demonstrated that the introduction of imidazole ring into podophyllotoxin and a 2-naphthyl methyl substituent at the imidazolium salt's 3-position play a critical role in enhancing cytotoxic activity. The preliminary structure activity relationships (SARs) of the derivatives were summarized in [Scheme 4](#).

2.2.2 Compound **a6** induced G2/M cell cycle arrest and apoptosis

To determine the possible mechanism of compound **a6** induced proliferation inhibition, cell cycle and apoptosis analysis were performed with flow cytometry. Firstly, HCT-116 cells were treated with indicated concentrations of compound **a6** for 24 h and the cell cycle phase distribution of **a6**-treated cells was



The compound **a6** induced cell apoptosis was also determined with Annexin V-FITC/PI staining. As shown in [Figure 3](#), after treated with compound **a6** at 25, 50 and 200 nM for 48 h, the apoptotic rate of HCT-116 cells remarkably elevated to $5.37 \pm 0.37\%$, $10.45 \pm 0.20\%$ and $64.98 \pm 2.40\%$, respectively. The results

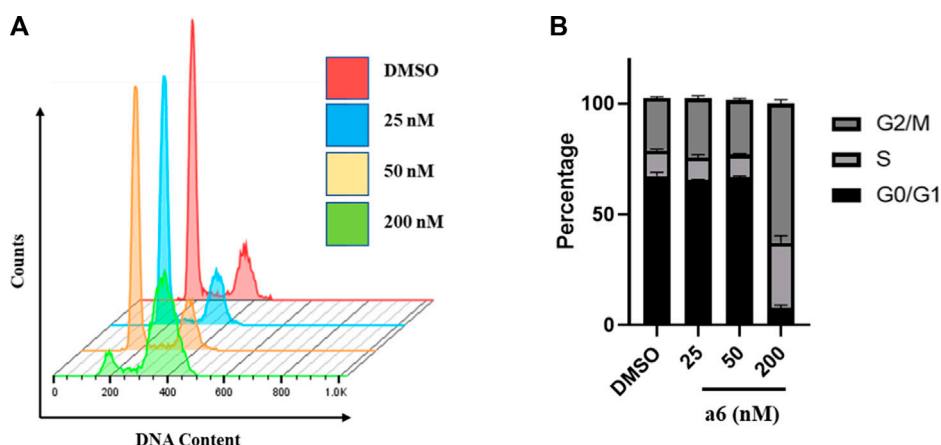


FIGURE 2

Compound **a6** induced G2/M phase arrest in HCT-116 cells. (A) Cells were treated with different concentrations of compound **a6** (25, 50 and 200 nM) for 24 h, and cell cycle was determined by cell cytometry with PI staining. (B) The percentages of cells in different phases were quantified.

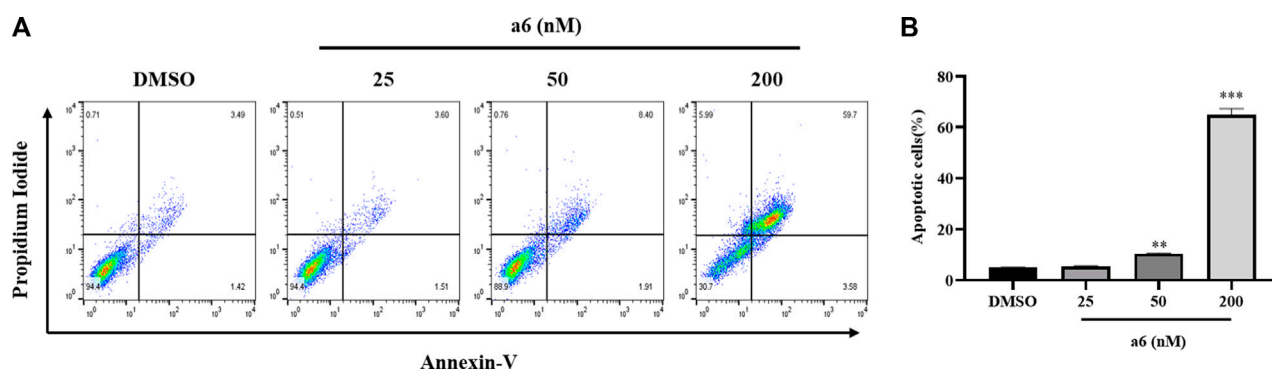


FIGURE 3

Compound **a6** induced apoptosis of HCT-116 cells. (A) Cells were treated with 25, 50 and 200 nM compound **a6** for 48 h. Cell apoptosis was determined by Annexin V-FITC/PI staining analysis. (B) The quantification of apoptotic cells.

suggested that compound **a6** inhibited cell proliferation through induction of G2/M cell cycle arrest and apoptosis of HCT-116 cells.

3 Conclusion

In conclusion, a series of novel podophyllotoxin nitrogen-containing heterocycle derivatives with potential antitumor activity were prepared using a straightforward synthetic approach. The results showed that the imidazole-substituted derivatives demonstrated more effective inhibitory activity than 1,2,4-triazole-substituted and 1,2,3-triazole-substituted equivalents. The biological activity was significantly improved when the imidazole or imidazolium salt group was introduced into the structure of podophyllotoxin. Among them, imidazolium salt **a6** was the most potent cytotoxic activity with IC_{50} values of 0.04–0.29 μ M. It has an obvious selective inhibitory against HCT-116 cell lines with an IC_{50} value of 0.04 μ M and could induce G2/M

cell cycle arrest and apoptosis in HCT-116 cells. Podophyllotoxin-imidazolium salt **a6** could be employed as a promising lead compound for further structural modification and in-depth activity research to identify new starting points for more effective anticancer agents.

Data availability statement

The original contributions presented in the study are included in the article/Supplementary Material, further inquiries can be directed to the corresponding authors.

Author contributions

XY, JZ, and YL conceived and designed the experiments. MY, YF, XS, MX, CZ, and YaM performed the experiments. MY, YF, ZZ, LK, and YiM analyzed the data. XY, YF, and LK wrote the article.

Funding

This work was supported by grants from the National Key R&D Program of China (2019YFE0109200), the Central Government Guides Local Science and Technology Development Fund (202207AA110007, 202207AB110002), Yunnan Science and Technology Department and Yunnan University Joint Fund Project (2019FY003010), Program for Xingdian Talents (Yun-Ling Scholars) and IRTSTYN, and the Project of Yunnan Characteristic Plant Screening and R&D Service CXO Platform (2022YKZY001).

Conflict of interest

The authors declare that the research was conducted in the absence of any commercial or financial relationships that could be construed as a potential conflict of interest.

References

- Boshuizen, J., and Peeper, D. S. (2020). Rational cancer treatment combinations: An urgent clinical need. *Mol. Cell.* 78 (6), 1002–1018. doi:10.1016/j.molcel.2020.05.031
- Bozorov, K., Zhao, J., and Aisa, H. A. (2019). 1,2,3-Triazole-containing hybrids as leads in medicinal chemistry: A recent overview. *Bioorg. Med. Chem.* 27 (16), 3511–3531. doi:10.1016/j.bmc.2019.07.005
- Chen, H., Zuo, S., Wang, X., Tang, X., Zhao, M., Lu, Y., et al. (2011). Synthesis of 4 β -triazole-podophyllotoxin derivatives by azide-alkyne cycloaddition and biological evaluation as potential antitumor agents. *Eur. J. Med. Chem.* 46 (9), 4709–4714. doi:10.1016/j.ejmech.2011.07.024
- Chen, W., Deng, X. Y., Li, Y., Yang, L. J., Wan, W. C., Wang, X. Q., et al. (2013). Synthesis and cytotoxic activities of novel hybrid 2-phenyl-3-alkylbenzofuran and imidazole/triazole compounds. *Bioorg. Med. Chem. Lett.* 23 (15), 4297–4302. doi:10.1016/j.bmcl.2013.06.001
- Choi, H., Cho, S. Y., Pak, H. J., Kim, Y., Choi, J.-y., Lee, Y. J., et al. (2017). Npcare: Database of natural products and fractional extracts for cancer regulation. *J. Cheminformatics* 9 (1), 2. doi:10.1186/s13321-016-0188-5
- Cui, B. L., Zheng, B. L., He, K., and Zheng, Q. Y. (2003). Imidazole alkaloids from lepidium meyenii. *J. Nat. Prod.* 66, 1101–1103. doi:10.1021/np030031i
- Dagenais, G. R., Leong, D. P., Rangarajan, S., Lanas, F., Lopez-Jaramillo, P., Gupta, R., et al. (2020). Variations in common diseases, hospital admissions, and deaths in middle-aged adults in 21 countries from five continents (PURE): A prospective cohort study. *Lancet* 395 (10226), 785–794. doi:10.1016/s0140-6736(19)32007-0
- Deng, G., Zhou, B., Wang, J., Chen, Z., Gong, L., Gong, Y., et al. (2019). Synthesis and antitumor activity of novel steroidal imidazolium salt derivatives. *Eur. J. Med. Chem.* 168, 232–252. doi:10.1016/j.ejmech.2019.02.025
- Dixit, D., Verma, P. K., and Marwaha, R. K. (2021). A review on 'triazoles': Their chemistry, synthesis and pharmacological potentials. *J. Iran. Chem. Soc.* 18 (10), 2535–2565. doi:10.1007/s13738-021-02231-x
- Gaba, M., and Mohan, C. (2015). Development of drugs based on imidazole and benzimidazole bioactive heterocycles: Recent advances and future directions. *Med. Chem. Res.* 25 (2), 173–210. doi:10.1007/s00044-015-1495-5
- Guo, Q., and Jiang, E. (2021). Recent advances in the application of podophyllotoxin derivatives to fight against multidrug-resistant cancer cells. *Curr. Top. Med. Chem.* 21 (19), 1712–1724. doi:10.2174/1568026621666210113163327
- Hou, W., Zhang, G., Luo, Z., Su, L., and Xu, H. (2019). Click chemistry-based synthesis and cytotoxic activity evaluation of 4a-triazole acetate podophyllotoxin derivatives. *Chem. Biol. Drug Des.* 93 (4), 473–483. doi:10.1111/cbdd.13436
- Huang, M., Duan, S., Ma, X., Cai, B., Wu, D., Li, Y., et al. (2019). Synthesis and antitumor activity of aza-brazilian derivatives containing imidazolium salt pharmacophores. *Med. Chem. Commun.* 10 (6), 1027–1036. doi:10.1039/c9md00112c
- Li, Y., Chen, M., Yao, B., Lu, X., Zhang, X., He, P., et al. (2019). Transferrin receptor-targeted redox/pH-sensitive podophyllotoxin prodrug micelles for multidrug-resistant breast cancer therapy. *J. Mat. Chem. B* 7 (38), 5814–5824. doi:10.1039/c9tb00651f
- Liu, L.-X., Wang, X.-Q., Yan, J.-M., Li, Y., Sun, C.-J., Chen, W., et al. (2013). Synthesis and antitumor activities of novel dibenzo[b,d]furan-imidazole hybrid compounds. *Eur. J. Med. Chem.* 66, 423–437. doi:10.1016/j.ejmech.2013.06.011
- Liu, L. X., Wang, X. Q., Zhou, B., Yang, L. J., Li, Y., Zhang, H. B., et al. (2015). Synthesis and antitumor activity of novel N-substituted carbazole imidazolium salt derivatives. *Sci. Rep.* 5, 13101. doi:10.1038/srep13101
- Liu, Z., Zhang, C., Duan, S., Liu, Y., Chen, W., Li, Y., et al. (2017). Synthesis and cytotoxic activity of novel hybrid compounds between indolo[b]tetrahydrofuran and imidazolium salts. *Chin. J. Org. Chem.* 37 (6), 1506–1515. doi:10.6023/cjoc201610043
- Newman, D. J., and Cragg, G. M. (2020). Natural products as sources of new drugs over the nearly four decades from 01/1981 to 09/2019. *J. Nat. Prod.* 83 (3), 770–803. doi:10.1021/acs.jnatprod.9b01285
- Perchellet, E. M., Perchellet, J.-P., and Baures, P. W. (2005). Imidazole-4,5-dicarboxamide derivatives with antiproliferative activity against HL-60 cells. *J. Med. Chem.* 48 (19), 5955–5965. doi:10.1021/jm050160r
- Shang, H., Chen, H., Zhao, D., Tang, X., Liu, Y., Pan, L., et al. (2012). Synthesis and biological evaluation of 4a/4 β -imidazolyl podophyllotoxin analogues as antitumor agents. *Arch. Pharm. Chem. Life Sci.* 345 (1), 43–48. doi:10.1002/ardp.201100094
- Sharma, P., LaRosa, C., Antwi, J., Govindarajan, R., and Werbovetz, K. A. (2021). Imidazoles as potential anticancer agents: An update on recent studies. *Molecules* 26 (14), 4213. doi:10.3390/molecules26144213
- Sung, H., Ferlay, J., Siegel, R. L., Laversanne, M., Soerjomataram, I., Jemal, A., et al. (2021). Global cancer statistics 2020: GLOBOCAN estimates of incidence and mortality worldwide for 36 cancers in 185 countries. *CA Cancer J. Clin.* 71 (3), 209–249. doi:10.3322/caac.21660
- Verma, A., Joshi, S., and Singh, D. (2013). Imidazole: Having versatile biological activities. *J. Chem.* 2013, 1–12. doi:10.1155/2013/329412
- Vishnuvardhan, M., V. S. R., Chandrasekhar, K., Lakshma Nayak, V., Sayeed, I. B., Alarifi, A., et al. (2017). Click chemistry-assisted synthesis of triazolo linked podophyllotoxin conjugates as tubulin polymerization inhibitors. *Med. Chem. Commun.* 8 (9), 1817–1823. doi:10.1039/c7md00273d
- Vitaku, E., Smith, D. T., and Njardarson, J. T. (2014). Analysis of the structural diversity, substitution patterns, and frequency of nitrogen heterocycles among U.S. FDA approved pharmaceuticals. *J. Med. Chem.* 57 (24), 10257–10274. doi:10.1021/jm501100b
- Wang, X. Q., Liu, L. X., Li, Y., Sun, C. J., Chen, W., Li, L., et al. (2013). Design, synthesis and biological evaluation of novel hybrid compounds of imidazole scaffold-based 2-benzylbenzofuran as potent anticancer agents. *Eur. J. Med. Chem.* 62, 111–121. doi:10.1016/j.ejmech.2012.12.040
- Xiao, J., Gao, M., Sun, Z., Diao, Q., Wang, P., and Gao, F. (2020). Recent advances of podophyllotoxin/epipodophyllotoxin hybrids in anticancer activity, mode of action, and structure-activity relationship: An update (2010–2020). *Eur. J. Med. Chem.* 208, 112830. doi:10.1016/j.ejmech.2020.112830
- Xu, H., Tang, H., Feng, H., and Li, Y. (2014a). Design, synthesis and anticancer activity evaluation of novel C14 heterocycle substituted epi-triptolide. *Eur. J. Med. Chem.* 73, 46–55. doi:10.1016/j.ejmech.2013.11.044
- Xu, X. L., Wang, J., Yu, C. L., Chen, W., Li, Y. C., Li, Y., et al. (2014b). Synthesis and cytotoxic activity of novel 1-(indol-3-yl)methyl-1H-imidazolium salts. *Bioorg. Med. Chem. Lett.* 24 (21), 4926–4930. doi:10.1016/j.bmcl.2014.09.045
- Xu, X. L., Yu, C. L., Chen, W., Li, Y. C., Yang, L. J., Li, Y., et al. (2015). Synthesis and antitumor activity of novel 2-substituted indoline imidazolium salt derivatives. *Org. Biomol. Chem.* 13 (5), 1550–1557. doi:10.1039/c4ob02385d

Publisher's note

All claims expressed in this article are solely those of the authors and do not necessarily represent those of their affiliated organizations, or those of the publisher, the editors and the reviewers. Any product that may be evaluated in this article, or claim that may be made by its manufacturer, is not guaranteed or endorsed by the publisher.

Supplementary material

The Supplementary Material for this article can be found online at: <https://www.frontiersin.org/articles/10.3389/fchem.2023.1191498/full#supplementary-material>

- Xu, Z., Zhao, S. J., and Liu, Y. (2019). 1,2,3-Triazole-containing hybrids as potential anticancer agents: Current developments, action mechanisms and structure-activity relationships. *Eur. J. Med. Chem.* 183, 111700. doi:10.1016/j.ejmech.2019.111700
- Yang, X. D., Zeng, X. H., Zhang, Y. L., Qing, C., Song, W. J., Li, L., et al. (2009). Synthesis and cytotoxic activities of novel phenacylimidazolium bromides. *Bioorg. Med. Chem. Lett.* 19 (7), 1892–1895. doi:10.1016/j.bmcl.2009.02.065
- Yang, Z., Zhou, Z., Luo, X., Luo, X., Luo, H., Luo, L., et al. (2021). Design and synthesis of novel podophyllotoxins hybrids and the effects of different functional groups on cytotoxicity. *Molecules* 27 (1), 220. doi:10.3390/molecules27010220
- Zhang, H., Tian, Y., Kang, D., Huo, Z., Zhou, Z., Liu, H., et al. (2017). Discovery of uracil-bearing DAPY's derivatives as novel HIV-1 NNRTIs via crystallographic overlay-based molecular hybridization. *Eur. J. Med. Chem.* 130, 209–222. doi:10.1016/j.ejmech.2017.02.047
- Zhang, X., Rakesh, K. P., Shantharam, C. S., Manukumar, H. M., Asiri, A. M., Marwani, H. M., et al. (2018). Podophyllotoxin derivatives as an excellent anticancer aspirant for future chemotherapy: A key current imminent needs. *Bioorg. Med. Chem.* 26 (2), 340–355. doi:10.1016/j.bmc.2017.11.026
- Zhao, W., Cong, Y., Li, H. M., Li, S., Shen, Y., Qi, Q., et al. (2021). Challenges and potential for improving the druggability of podophyllotoxin-derived drugs in cancer chemotherapy. *Nat. Prod. Rep.* 38 (3), 470–488. doi:10.1039/d0np00041h
- Zhou, B., Liu, Z. F., Deng, G. G., Chen, W., Li, M. Y., Yang, L. J., et al. (2016a). Synthesis and antitumor activity of novel N-substituted tetrahydro-beta-carboline-imidazolium salt derivatives. *Org. Biomol. Chem.* 14 (39), 9423–9430. doi:10.1039/c6ob01495j
- Zhou, H., Yu, C., Kong, L., Xu, X., Yan, J., Li, Y., et al. (2019). B591, a novel specific pan-PI3K inhibitor, preferentially targets cancer stem cells. *Oncogene* 38 (18), 3371–3386. doi:10.1038/s41388-018-0674-5
- Zhou, Y., Duan, K., Zhu, L., Liu, Z., Zhang, C., Yang, L., et al. (2016b). Synthesis and cytotoxic activity of novel hexahydropyrrolo[2,3-b]indole imidazolium salts. *Bioorg. Med. Chem. Lett.* 26 (2), 460–465. doi:10.1016/j.bmcl.2015.11.092

Frontiers in Chemistry

Explores all fields of chemical science across the periodic table

Advances our understanding of how atoms, ions, and molecules come together and come apart. It explores the role of chemistry in our everyday lives - from electronic devices to health and wellbeing.

Discover the latest Research Topics

[See more →](#)

Frontiers

Avenue du Tribunal-Fédéral 34
1005 Lausanne, Switzerland
frontiersin.org

Contact us

+41 (0)21 510 17 00
frontiersin.org/about/contact

